Complexes of polyelectrolytes with defined charge distance and different dendrimer counterions

Dissertation
zur Erlangung des Grades
"Doktor der Naturwissenschaften"
am Fachbereich Chemie und Pharmazie
der Johannes-Gutenberg-Universität in Mainz

Magdalena Chelmecka

Mainz 2004

Dekan:

1.Berichterstatter:

2.Berichterstatter:

Tag der mündlichen Prüfung:

"If we knew what it was we were doing,
it would not be called research, would it?"
Albert Einstein

CONTENTS

A: BACKGROUND

B: RESULTS

A: BACKGROUND

I. Introduction

Close spatial arrangement of small compounds gives rise for new properties of living organisms. Aggregation of enzymes is responsible for a series of consecutive transformation which occurs continuously in living bodies. "One of the most interesting properties evolving from the intricate interplay of thousands of subcellular components on the length scale of about one micron is life itself."[1]

Due to this inspiration it is of interest to be able to design supramolecular assemblies and hierarchical structures. The conventional way by which compounds are synthesized in the laboratory -and to a large extent in vivo, bases on the stepwise formation of covalent bonds. However such a process is burdened with several inherent limitations when applied to the construction of extremely large and complex biological molecules. Each synthetic step would have to proceed with absolute fidelity, since one mistake could jeopardize the functional integrity of the target species. Nature first encountered these limitations during protobiogenesis. How were primordial cells created from relatively simple building blocks when these cells did not contain the necessary machinery, catalytic, genetic, or otherwise directed their own synthesis? A possibility is that these building block molecules could spontaneously assemble into an intact cell, i.e. each building block molecule contained all the necessary information to recognize and interact with other appropriate molecules. Today so-called self-assembly has been recognized to be both a crucial component in the molecular events that comprised the evolution of life and an essential participant in the biosynthesis of contemporary biological systems.[2]

Self-assembly may be defined as a highly convergent synthesis protocol that is exclusively driven by noncovalent interactions. As a consequence the same noncovalent interaction are responsible for preserving the structural integrity of the end product.[2] Classically, such non-covalent interactions are "hydrophobic interactions" and self-assembly refers to the association of amphiphilic molecules such as lipids and surfactants. Depending on the architecture of the building block, well-defined aggregates of a wide variety of geometry's can be formed, such as spatial and cylindrical micelles, bilayers etc. Recently, other concepts for self assembly are investigated, e.g. based on hydrogen bonds and based on electrostatic interactions.[4]

Self assembly structures also occur in the field of polyelectrolyte complexes. Polyelectrolytes are macromolecules that have many charged or chargeable groups, when dissolved in polar solvents, especially in water. The polyelctrolyte dissociates into a macroion and many small counterions in aqueous solution.[3] Two types of polyelectrolyte complexes have been widely investigated. The first type: (PECs) are complexes of cationic and anionic polyelectrolytes. The second type (PE-surfs) are complexes of polyelectrolytes and oppositely charged surfactants. In its most simple form complex formation is observed when the two oppositely charged species- polyelectrolyte and polyelectrolyte or polyelectrolyte and surfactant are mixed in an aqueous solution. But a number of different procedures to form PECs and PE-surfs have been developed. For example, multilayer films of PECs on solid surfaces were prepared by chemisorption from solution. This is well-known as the "layer-by-layer" technique and sometimes synonymously as electrostatic self assembly. The "layer-by-layer" method meanwhile has been extended to other compounds as proteins and colloids. Moreover, hollow nano- and microspheres are obtained via "layer-by-layer" adsorption of oppositely charged polyelectrolytes on template nano- and micropatricles. The formation of polyelectrolyte-polyelectrolyte complexes and polyelectrolyte-surfactant complexes is closely related to self assembly processes. A major difference between PECs and PE-surfs can be found in their solid state structures. PE-surfs typically show highly ordered mesophases in the

solid state which is in contrast to the less defined ladder and scrambled-egg structures of PECs which will be explained later. Reasons for the high ordering of PE-surfs are: i) cooperative binding phenomena of the surfactant molecules onto the polyelectrolyte chain and ii) the amphiphilicity of the surfactant molecules. A further result of the cooperative zipper mechanism between a polyelectrolyte and oppositely charged surfactant molecules is a 1:1 stiochiometry.[5] The amphiphilicity of surfactants favors a microphase separation in PE-surfs that results in periodic nanostructures with repeat units of 1 to 10 nm. In contrast, structures of PECs normally display no such periodic nanostructure. In many practical uses PECs formation takes place under conditions, where structure formation is mainly determined by the fast kinetics of this process, concealing the effects of different parameters of influence such as the mixing regime, medium conditions macromolecular characteristics of polyelectrolytes. The investigation of PECs formation in highly diluted aqueous solutions offers a much better chance of elucidating the general features of this process and to examine the consequences by varying the combination of polyelectrolytes and the formation conditions.[5] Further the study of complexes in solution is of interest to investigate whether the formation of well-defined assemblies like in classical surfactant systems is possible.

Aim of this thesis is to investigate the electrostatic self-assembly of linear polycations of varying charge distance with "large" counterions of varying architecture. We especially investigate the morphology of objects formed, but also their stability under salt free condition and after low molecular mass salt addition. As polycations, Poly(dialkylimino)-alkylene salts (Ionenes) I65MeBr and I25MeBr were chosen. Ionenes are synthesized via Menschutkin reaction and characterized by standard methods. Counterions are Polyamidoamine (PAMAM) dendrimers of generations G2.5, G5.5, G7.5 with -COONa surface groups and shape-persistent, Polyphenylene dendrimers of generation G1 with surface -COOH groups. A complex interplay of interactions is expected to direct the self assembly via electrostatic interaction, geometric factors, hydrophobic interaction or hydrogen bonds. Methods used for the investigation of complexes are: UV-spectroscopy, pH-metric techniques, dynamic and static light scattering, small angle neutron scattering, ζ potential measurements and potentiometric titration.

II. Self-assembly Systems

1. Linear polyelectrolytes with counterions

There are several interaction modes between the polyion and the small ions. One may distinguish three different modes of counterion binding: unspecific electrostatic binding (A), specific binding (B) and hydrophobic binding (C)(adsorption).[6]

   A. Counterions are nonspecifically electrostatically attracted by the polyion. This is caused by the opposite charge and is dependent of the counterion nature, sometimes named "territorial binding". The tightness of binding depends on the nature of the polyion, the solvent, and the counterion species. At one extreme a "territorially bound" counterion is dehydrated and localized near a polyion group, but it is not associated with the group. At the other extreme the counterion is delocalized. It retains the fully hydrated state while moving in an unrestricted and random way along the axis of the polyion chain. There are a number of theoretical approaches on this electrostatic binding. These include counterion condensation theory[7], analysis of the Poisson-Boltzmann equation[8],
and Monte Carlo computer simulation[9,10]. Most of these theoretical approaches have reached qualitatively similar conclusions and found reasonable agreement with experiments. However, there are still two problems that are not fully solved. First, there is no general accepted theoretical expression for the territory of a certain bound counterion V_p. Second, most theories have been primarily concerned with the long-range interactions between the counterions and the polyion. That is why, in most cases, it is assumed that the counterions are bound

delocalized. Short-range, site specific interactions (B) were given much less consideration although they are dominant very often. For instance, the binding constant of Eu^{3+} -binding on DNA based on purely long-range electrostatic interactions is found[11] to be nearly two orders of magnitude smaller then the experimental value.[6] Electrostatic (nonspecific) counterion binding and counterion distribution can be explained by a continuous competition between thermal and electrostatic potential energy which regulate the counterion dissociation in the solution. Electrical work has to be performed to move charged objects in the vicinity of like-charged surfaces in response to the field. To simplify calculations the ion is treated as a point charge. Energies in moving aside other ions or creating a hole in the solvent and local effects are neglected. The change in potential in the vicinity of charged surface is described by the Poisson-Boltzmann (P-B) equation *(1)*.[12]

$$\nabla^2 \boldsymbol{y} = \frac{-1}{\boldsymbol{e}_0 \boldsymbol{e}_r} \sum_i n_i^0 z_i e \exp\left(\frac{-z_i e \boldsymbol{y}}{kT} \right) \tag{1}$$

$\boldsymbol{y}$ - potential

∇^2 - Laplace operator

$\boldsymbol{e}_r$ - relative permittivity

$\boldsymbol{e}_0$ - dielectric permittivity of a vacuum (8.85 10^{-12} Fm^{-1})

n_i^0 - bulk concentration of ions type i

z_i - charge of ions type i

e - elemental charge

k – Boltzmann constant

T - temperature (K)

If the electrical energy is small compared to the thermal energy $\left(|z_i e \boldsymbol{y}| < kT\right)$ it is possible to linearize the Poisson-Boltzmann equation. Such approximation is called Debye-Hückel approximation, the solution is:

$$\boldsymbol{y} = const \exp(-\boldsymbol{k}x) \tag{2}$$

κ is the Debye-Hückel parameter, has a dimension of (length^{-1}) and plays a prominent role in the double layer theory. The extent of the double layer is measured by the size $1/\kappa$. $1/\kappa$ is called "Debye-Hückel screening length". Debye-Hückel parameter κ is defined as:

$$\boldsymbol{k}^2 = 4\boldsymbol{p}l_B I \tag{3}$$

where I is the ionic strength, a parameter that estimates the interaction between ions in solution. It is calculated as one-half the sum of the products of ionic concentration and the square of ionic charge for all the charged species in a solution:

$$I = \frac{1}{2} \sum_i n_i^0 z_i^2 \tag{4}$$

l_B is the Bjerrum length characteristic for the solvent. l_B is defined as a distance over which the electrostatic energy between two elementary charges e in a solvent of dielectric permittivity $\boldsymbol{e}$ is compensated by the thermal energy kT.

$$l_B = \frac{e^2}{\boldsymbol{e}kT} \tag{5}$$

The Bjerrum length for pure water at 20°C is ~ 7.12 Å.

The Debye-Hückle constant κ depends on the temperature and the bulk electrolyte concentration. With increasing salt concentration κ^{-1} (measure of an extent of the double layer) decreases, leading to the shorter range of the potential (screening).[12]

Polyelectrolytes and counterions in the solution are in the balance. The degree of dissociation of counterions may be described by the Manning's theory:

$$V = \frac{q^2}{\varepsilon kTB} \qquad (6)$$

ζ –linear charge density of the polyion, Manning's reduced charge density

q - protonic charge

B – distance between neighboring charges on the polymer molecule (for maximal extention).

When the parameter ζ is equal 1 according to Manning's theory, "counterion condensation occurs". $1/\zeta$ defines the degree of dissociation of the counterions. The distance B between charges is proportional to the degree of dissociation $1/\zeta$.[12]

Apart from the territorial binding one can also distinguish two other types of binding. So called site and hydrophobic binding.

B. Site binding (counterion association): If short range, site –specific interactions are strong, the counterions may bind on specific sites of the polyion. To the short-range forces belongs i.e. electrostatic interactions between a counterion and its own binding site which may additionally involve more than one charged group of the polyion near the binding site. The counterion is directly coordinated or associated to one or more charged groups on the polyion. Additional effects like excluded volume effects or ion size effect belong to a short-range interactions as well. The hydration number of the bound ion may change. All these interactions constitute the origins of short-range forces. The main difference between the long-range (electrostatic) and short range (specific) interactions is that the former strongly depend on the ionic strength while the latter do not. The affinity of a counterion species for a polyion may be covalent, ionic, or non-ionic. Tight localized binding is also expected when the nearest-neighborhood charge spacing on the polyion is sufficiently close, so that two or more groups can cooperate in holding the counterion. The larger the association constant, the larger will be both the number of associated counterions and the stability of each binding.

Specific and nonspecific counterion binding occurs simultaneously while one mode is the dominant one. Experimentally, it is difficult to separate the effects of the two modes. Most techniques, such as dialysis, dilatometry yield the total extent of counterion binding, i.e. the sum of the counterions that are bound territorially and by association.[6]

C. Hydrophobic binding: The hydrocarbon nature of polyions makes itself felt in the interactions of organic counterions. This is seen when one examines the selective uptake of organic ions of different configuration by polyions having different charge density. For instance, the binding of aromatic counterions by polyions containing aromatic rings, is particularly strong. Comparisons can be made with the oleophilic ion-exchange polymers[13] by altering the length of the aliphatic substituent chain. These polymers swell strongly or weakly depending upon the degree of such substitution and the kind of the solvent. However, the theories of association and territorial binding of an inorganic counterions are more elaborated.[6]

The changes in system energy translate thermodynamically in enthalpy changes. The explanation of the competition between thermal and electrostatic potential energy as a reason for counterion binding given in the paragraph *A* suggests then enthalpic character of the binding.

In contrast Sinn et al. describe isothermal titration calorimetry (ITC) study for the systems of poly(sodium acrylate) (NaPAA) and poly(sodium styrenesulfonate) (NaPSS).[14] These systems are compared to the corresponding low molecular mass salts, sodium acetate and sodium sulfate measured also by ITC. In a first set of experiments, determination of the heat of dilution of two standard polyelectrolytes poly(sodium acrylate) and poly(sodium styrenesulfonate) has been performed. As the dilution of PSS and PAA are partially athermal, this justifies their use as model polyelectrolytes. Afterward the enthalpic effects of counterion exchange of monovalent Na^+ with divalent Ca^{2+} for three carboxylate carrying polymers has

been characterized. Contrary to simple expectation the heat of exchange is strongly endothermic. Because heat can be regarded as liberated potential energy, it becomes obvious that the description of the Ca^{2+} binding to polyelectrolytes by screened Coulomb potentials is insufficient (as this would always lead to an exothermic process). Instead, binding has to be described as a counterion exchange, which is at best energetically neutral with respect to the electrostatic forces involved. The real reason for the stronger binding of multivalent ions onto polylelectrolytes is therefore not the stronger electrostatic force, but it is due to entropic effects which keep the free energy of this process negative (as it occurs spontaneously) but which remain unseen in calorimetric experiments. This is in good agreement with the binding of ions onto other colloidal objects, such as the binding of earth alkaline ions and La^{3+} onto lipid vesicles or the binding of earth alkaline cations onto low molecular mass compounds. Therefore, the observed effects seem to be the rule rather than the exception. The total amount of released water molecules is given by the dehydration of Ca^{2+} and COO- minus the partial rehydration of Na^+ As the final effect e.g. Ca-PAA precipitates from water. This process generates the minimal number of six water molecules required to counterbalance the endothermic binding heat. A quantitative estimate on the base of the binding measurements with a Ca^{2+}- sensitive electrode revealed the equivalent of 10+/-2 water molecules leaving enough gain of free energy for strong and spontaneous binding. As the heat of dilution of all species involved is about athermal, one can exclude a relevance of long-range water structure effects onto the binding process. The scenario may also imply altered target structures for the development of optimized scale inhibitors: it is not the charge or charge density which is decisive, but the induction of a transition from a very hydrated to a rather unhydrated polymer state by ion binding. The potential of this model is to prescribe additional features like ion selectivity of binding, which is found in a number of cases, but cannot be explained by electrostatic models.[14-19]

Not only theoretical and experimental investigations are performed but also a number of computer simulations on polyelectrolyte systems e.g. by Klos and Pakula.[20] It is of interest to simulate the behavior of synthetic PEC systems and compare with real systems e.g. in the living cell, RNA-complexes and DNA-complexes. In the cell these molecules can interact both with smaller ions and with other charged objects such as macroions and membranes. This, in turn, might lead to a variety of effects that, among others, are believed to be useful in modern medicine. For instance, charge inversion might take place, a phenomenon that simplifies gene transfer to the cell. The DNA helix immersed in a "sea" of positive particle, passes the negatively charged cell membrane more easily.[20] Klos and Pakula, carried out Monte Carlo simulations of neutral solutions of strongly charged chains and counterions at various temperatures and monomer concentrations. The calculations have shown that in the limit of very high temperatures the electrostatic interactions are effectively weak. Chain behavior is dominated by the entropy itself. Under such conditions the polyelectrolytes and counterions are distributed uniformly throughout the space without revealing any properties of collectivity. Subsequently, at intermediate temperatures, the former are relatively more outstretched because of still being strongly charged and the Coulomb interactions are already comparable with thermal fluctuations. Below a certain temperature the counterions condense on the polymers which causes them to drastically decrease the size and become collapsed. Low energy configurations then are compact aggregates of chains entangled with each other and with perfectly condensed counterions. The latter play the role of intermediate ions that lead to attractive interactions between the polymers.[20] Also the configurational properties of strongly charged polyelectrolytes accompanied by counterions and salt ions in dilute solutions are simulated. For the very high, middle and low temperatures in the systems with low molecular mass salt addition the behavior of polyelectroylte complexes is similar to the one mentioned before, without salt addition. Polyelectrolytes and ions morphology, depending on the temperature, ranges from uniformly distributed, throughout more outstretched to the

collapsed polymer systems. The amount of condensed ions also depends on the quantity of added salt and is larger for higher concentrations of the latter. Furthermore in the extremely low-temperature regime the recorded low energy configurations become compact aggregates of chains entangled with each other and with condensed ions of both signs.[21]

2. Aggregation of two linear polyelectrolytes

Coulomb interaction between oppositely charged polyelectrolytes leads to spontaneous formation of interpolymer complexes. Such complexes are of high practical relevance from industrial applications as flocculants, coatings and binders, that are discussed for biological and medical purposes, and represent objects of interest in fundamental research.

Mixing solutions of polyanions and polycations leads to spontaneous aggregation under release of counterions. The level of aggregation depends on the nature of the components, on the medium and external conditions. For free polyelectrolyte chains the low molecular mass counterions are more or less localized near the macroions in the case of high charge densities, particularly because of counterion condensation. The driving force of complex formation is mainly the gain in the entropy due to the liberation of the low molecular counterions. However, other interactions such as hydrogen bonding or hydrophobic ones may play an additional part. From the energetic point of view, PEC formation may even be an endothermic process, because of the elastic energy contribution of the polyelectrolyte chains, impeding the necessary conformational adaptations of the polymer chains during their transition to the much more compact PEC structures. The reaction of polyelectrolyte complex formation can be described by the equation *(6)*.[5]

$$(-A^-c^+-)_n + (-C^+a^--)_m \Leftrightarrow (-A^-C^+-)_x + (-A^-c^+-)_{n-x} + (-C^+a^--)_{m-x} + xa^- + xc^+ \quad (7)$$
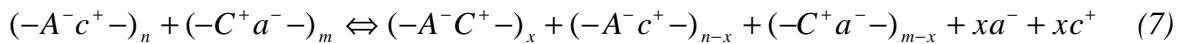
where A^-, C^+ -are the charged groups of the polyelectrolytes, a^-, c^+ -counterions, n,m- number of the anionic and cationic groups in solution. n/m or m/n = x –molar mixing ratio, θ=x/n, n<m or θ=x/m m<n, θ- degree of conversion. The degree of conversion determines whether the ionic sites of the components in efficiency are completely bound by the oppositely charged polyelectrolytes or whether low molecular counterions partly remain in the complex. Another characteristic quantity is the overall composition of the PEC structures at any mixing ratio. One of the components may be bound in excess, leading to an overcharging of the PEC particles. PEC formation leads to quite different structures, depending on the characteristics of the components used and the external conditions of the reaction.[5] As was mentioned in the "Motivation", two borderline cases for the resulting polyelectrolyte complexes (PEC) are discussed in the literature: *i)*Typically, PEC formation between polyions containing weak ionic groups and significant difference in molecular mass results in non-stoichiometric systems. Soluble complexes result. A model description may be the ladder like structure where complex formation takes place on a molecular level via conformational adaptation (zip mechanism). *ii)* PEC are described also by the "scrambled egg model", where a high number of chains becomes incorporated into a particle. [22] In case of highly aggregated scrambled-egg systems, polyions carry strong ionic groups and/or have comparable high molecular masses. Often macroscopic flocculation occurs. PEC formation takes place far from the thermodynamic equilibrium even in the presence of salt. In such complexes the presence of small molecular mass salt causes mainly secondary aggregation and flocculation. The influence of added salt also depends e.g. on the mixing ratio. In excess of one component a much lower level of aggregation accompanies slight increase of dimension. At low ionic strength, disintegration into subunits may take place.[23,24]

According to recent studies PEC particles consist of a neutralized, stoichiometric core and a shell of the excess component stabilizing the particle against further coagulation. [25,26] At a 1:1 mixing ratio macroscopic flocculation can be observed.[23] Many further investigations are

necessary to understand general tendencies, because superposition of multiple effects leads to a high individuality of the structure and behavior of the PEC particles.[24,26]

Comprehensive and systematic studies on soluble PECs started with the pioneering work of the groups of Kabanov[27-29] and Tsuchida[30-32]. They show that under appropriate salt condition, PEC formation between polyions with weak ionic groups and significantly different molecular weights in non-stoichiometric systems results in soluble complexes of ladder model morphology, consisting of hydrophilic single-stranded and hydrophobic double-stranded segments. Predominantly carboxylic group containing polyanions were used in combination with various polycations. The presence of a small amount of salt enables rearrangement and exchange process and shifts the reaction more to thermodynamic equilibrium, leading to a uniform distribution of the short chain component among all long chains of the counterpart. The further addition of salt leads at first to a shrinking of the PECs due to the shielding of their charges by the electrolyte. When a critical salt concentration is exceeded, a disproportionation of the short "guest" chains occurs, leading to completely complexed, precipitating species and pure "host" polyelectrolyte chains in solution[27,33,34]. At even higher salt concentration the precipitate dissolves again and both components exist as free polyelectrolyte chains in solution. Similar effects can be induced by changes of the pH value[28].

While at low ionic strength the PECs possess a high stability, they are able to take part in polyion exchange and substitution reaction at higher ionic strengths. Especially, the addition of a component of higher molecular mass or stronger ionic groups results in substitution reactions.[5,35,36] PEC formation in a concentration range of the component solutions below 10^{-3} g/ml resulted in stable dispersions of PEC particles when non-stoichiometric mixing ratios are used. In general PECs could be well described by the model of polydisperse systems of homogenous spheres. This sphere-like PEC particles as mentioned previously consist of a charge neutralized core, surrounded by an electrostatically stabilizing shell of the excess component. The structural parameters of PECs (mass, size, structure density) changes only slightly with the molar mixing ratio x up to about x=0.9. Mass and size of the complexes decreased somewhat in such a way that the structure density remained nearly constant. The decrease in PEC particle mass can be explained by the consumption of the excess component. Therefore, not a growth of the PEC particles, but the generation of new particles is the dominating process with increasing mixing ratio. Secondary aggregation and macroscopic flocculation occurred when the 1:1 mixing ratio was approached. Even in extremely diluted systems (less than 10^{-5} g/ml) the PEC particles consist of several hundred single polyelectrolyte chains.[5] The level of aggregation increases strongly with the rising concentration of the component solution up to several thousand chains per particle.[106] For strong polyelectrolytes and suitable charge densities of the components the structure density of the PECs is high and ranges normally from 0.3 to 0.7 g/ml, indicating very compact structures. Stronger mismatching of the charge distances of the components results in higher degrees of swelling.[5,38,39,40]

Because it weakens the electrostatic interaction and enables rearrangement processes salt should play a decisive part in the formation of highly aggregated PECs similar to the role of salt in the formation of soluble PECs mentioned before. The presence of small amount of NaCl led to a dramatic decrease of the level of aggregation for PECs between e.g. (sodium poly(styrene sulfonate)) NaPSS and poly(diallyldimethyl ammonium chloride) (PDADMAC) by nearly two orders of magnitude as compared to the systems without salt addition. Higher ionic strength caused secondary aggregation and again increase in PEC masses and sizes. Therefore, the level of aggregation can also be controlled by the amount of salt during complex formation. Comprehensive studies of various PEC systems[39,41-44] revealed that the response of polyelectrolyte complexes to the addition of NaCl is very different, strongly depending on the polyelectrolyte components used. The general tendencies may be

summarized as follows: After subsequent addition of salt to the system containing PECs between strong polyelectrolytes secondary aggregation up to macroscopic flocculation occurs. The complex salt stability decreases drastically with an increasing mixing ratio. This can be understood by the corresponding decrease in the thickness of the stabilizing shell of the excess component and in the degree of overcharging. Time dependent changes were detected after the addition of different amounts of NaCl to a complex between two polyelectrolytes. The complexation was competed after different times (20 hours to 30 minutes), depending on the amount of added salt.[5] Very slow long-term changes were also observed in the investigations of the exchange process of low molecular mass for high molecular mass i.e. NaPSS or NaPMA for NaPSS.[45] A complete exchange took place after 2 months in the presence of 0.1 N NaCl.[5]

Monte Carlo simulation studies have been performed for model systems representing aqueous solution of positively charged polyions and a varying number of negatively charged polyions.[44-55] Structural properties of the solution as well of individual chains have been investigated and formation of complexes has been observed. The interactions between the oppositely charged polyions cause increasing spatial correlation between beads on different positive polyions upon addition of negatively charged polyions. With the shorter bond length and well below the overlap concentration, distinct complexes possessing net charge are formed. The structure of solutions containing these complexes and/or free polyions of the same charge reflects the mutual long-range repulsion between the charged objects. With the longer bond length and closer to the overlap concentration (although still below it) larger and less well-defined clusters appear. The variation in the bond length leads to differences i) in electrostatic interactions due to the difference in charge density of the chains and ii) in the proximity to the overlap concentration as a result of the varying contour length. We do not know yet the relative importance of these effects behind the formation of the different structures.[46]

3. Colloids

Colloid and counterion -systems investigation forego the investigations of counterion condensation on the dendrimer surface. When dissolved in a polar solvent, mesoscopically sized colloidal particles and biological macromolecules typically become charged due to the dissociation of ionic groups at the particle surfaces into the solution. A second way to receive charge is by ion adsorption. In aqueous media surfaces usually posses a negative charge. Cations are usually more hydrated than anions and so have a greater tendency to reside in the bulk aqueous medium. Anions have the greater tendency to be specifically adsorbed. A third way to create charged particles in the aqueous medium is ion dissolution. This is defined as acquiring a surface charge by unequal dissolution of the oppositely charged ions of which the particles are composed. Dissolving in a polar solvent, colloidal particles lead to the highly charged objects which can be called a "macroion" or "polyion". Addition of salt ions to the solution tailors the degree of screening in the Coulomb system. Since the solvent approximately only enters via its dielectric constant, the interaction between the particles is mainly governed by Coulomb law, such that an ensemble of large highly charged particles together with the macroscopic counter- and salt ions represents a strongly coupled Coulomb system.[56] Classical theories of counterions binding are developed for hard-sphere colloids with a smooth surface. Because of the long-range nature of electrostatic forces, the colloid surface charge densities, or surface potentials (Ψ_0), play a major role in colloidal behavior. The other determinant of aqueous colloidal behavior is the distribution of counterions, which can be treated effectively by some form of the linearized Poisson-Boltzmann (PB) equation in the case of small Ψ_0. However, the behavior of highly charged particles with large Ψ_0 is complicated by specific and nonspecific "counterion binding" and hydration effects, as mentioned previously (chapter II.1).[23] The earliest theoretical studies of the behavior of an

electrified interface were made by Helmholtz over a century ago. His equations were interpreted by Perrin as implying a simple charge distribution in the solution, consisting of a plane layer of charge opposite to that on the solid. The equation for the electrical potential as a function of distance into the solution can readily be solved for this simple model of the double layer and they were able to explain some features of the behavior of double-layer systems. The success of the kinetic theory of molecular behavior made it clear, however, that the Helmholtz model was unrealistic- especially in the treatment of the electric charge in the solution. In the solutions ions of an opposite sign predominate over ions of the same sign but the latter are not completely excluded from the surface region. That surface region is also of significant thickness.[12]
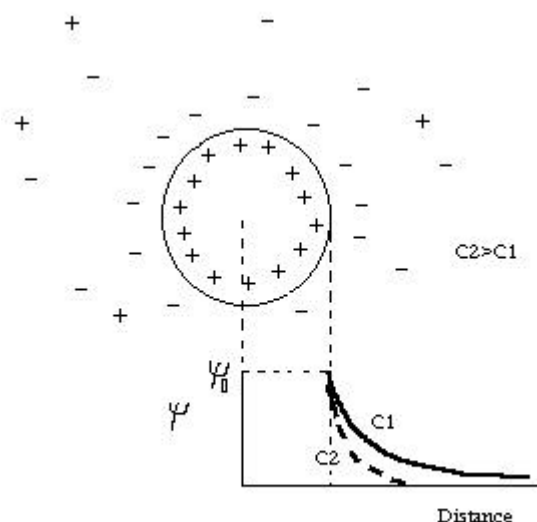
Fig.1: The electrostatic potential near an electrically

charged colloidal particle. The broken curve (C2) is

for a higher electrolyte concentration.

This region of varying charge density is referred to as the diffusive electrical double layer and stretches over distances of order 100 nm in dilute electrolyte solution and rather less at higher concentrations. The electrical charge and potential distribution must be determined via solving the relevant electrical and statistical thermodynamic equations to characterize the diffusive region. The problem was first tackled by Gouy (in 1910) and, independently, by Chapman (1913) and the result is referred to as the Gouy-Chapman model. Solution of that model depend of on the solution of what is called Poisson-Boltzmann equation and was mentioned in previous paragraph.[12] As well as counterions, linear polyelectrolytes may also aggregate with colloidal particles. Colloidal systems can be regarded as a model systems for counterions condensation on the dendrimer surface.

4. Self-assembly of dendrimers with small counterions

Poly(amidoamine) dendrimers (PAMAM) (in following work carrying COO^-Na^+ as surface groups) are densely branched molecules of well-defined covalent architecture. Lower generations are star-like, higher generations spherical. The radii of dendrimers can be varied synthetically. (generations) and the uniform surface charge densities can be modulated via pH. Titration studies reveal that the effective surface charge density of PAMAM G5 generation is lower than the geometric surface charge density, which is attributed to counterion binding.[57] Results obtained by Huang et al. suggest a critical condition for nonspecific counterion

binding to spheres, analogous but not identical to Manning condition for counterion condensation on polyelectrolytes.[57] Perfect adherence to the linearized PB equation has been found for small dendrimers under low ionic strength.[58] However, the general idea of counterion condensation around a spherical charged particle is still controversial. The effective charge (Q_{eff}) (as opposed to the geometric chemical charge Q_{geom}) is a powerful concept to illustrate the strong accumulation of counterions in the vicinity of the spherical particles. Q_{eff} is the relative surface charge limited by counterion condensation or pH of the environment. Q_{geom} is simply calculated number of charged groups on the dendrimer surface. Surface charge neutralisation due to the counterion condensation or pH modulation is in case of Q_{geom} disregarded. To investigate the surface charge of dendrimer particles, electrophoretic techniques can be used. Since the pioneer work of Smoluchowski [59] there have been many theoretical descriptions of electrophoresis of spherical particles. However, experimental data for the case of highly charged spherical particles are still very rare, especially data that demonstrate the relationship between the electrophoretic mobility and the surface charge density of the macroparticles. The sphericity, high monodispersity and relative uniform surface charge density of carboxyl-terminated dendrimers make them particularly suitable for fundamental electrokinetic studies.[59] Regarding the mobility of the dendrimers, one can observe the decrease of the mobility with increasing ionic strength. But for any fixed ionic strength, the mobility decreases with increase of dendrimer generation. Potentiometric titration results show that even though the geometric charge for G5 is much higher than that for G2, the effective surface charge density for G5 is actually lower, presumably due to counterion binding. Under conditions where G2 and G5 have the same effective charge density, their mobility's are similar. The nonlinear relationship between mobility and surface charge density is predicted by two theories: that of Wiersema, O'Brien and White (WOW) and that of Lozzada-Cassou et al., known as the "restricted primitive model" (RPM). Wiersema, O'Brien and White consider the deformation of the ionic cloud around the moving macroparticle (relaxation effect) assuming that the macroparticle is a hard sphere with a uniform charge density and that the surrounding counterions are point ions. According to WOW, three forces affect the mobility[60]: *i)*an electric force propelling the macroparticles that depends on the number of charges, *ii)*a force due to the hydrodynamic drag, that depends on radius and viscosity, and *iii)*relaxation force originating from the induced polarization within the diffuse layer of ions surrounding the macroparticles. WOW predicts maxima in the dependence of mobility on surface charge, but only for $\kappa a>3$, whereas maxima for G2 have been found at $\kappa a \approx 1.25$. "a" is a radius of the dendrimer. That means WOW is true when the radius of the dendrimer is approximately three times larger than the screening length. Huang, et. al. found maxima typical of WOW when the radius of the sphere was comparable with the Debye screening length.[58,60]

In contrast, the RPM model considers surrounding counterions as hard spheres of finite size and predicts that the mobility at a fixed surface potential ζ depends also on the size of the macroparticles. A larger mobility is observed for smaller particles. RPM is then in accordance with experimental observations for dendrimers.[60-62]

Generally, the electrokinetic properties, such as the potential at the surface of shear ("ζ potential"), are closely related to the Q_{eff} rather than Q_{geom}.[60] The ζ potential is moreover related to the electrophoretic mobility, defined as the particle velocity per unit electric field. One can calculate an "expected" ζ potential value for the dendrimer. According to the equation *(7)*.

$$V = \frac{Q_{geom}a}{\varepsilon_r \varepsilon_0 (1+\kappa a)} \qquad (8)$$

$$Q_{geom} = \frac{eN_t a}{4\pi u^2}$$, where N_t is the total number of ionizable group on the dendrimers. The value of ζ potential calculated in this way are unreasonably large as compared with the measured ones. The effective surface charge density can be calculated from potentiometric titration. [45]
The current state of knowledge about counterion binding to the dendrimers obeying calculations and experiment is following: *i)*the depression of the effective surface charge density of the higher generations of carboxyl terminated PAMAM dendrimers is observed as compared to lower generation due to the counterion binding *ii)*the mobility of lower generations is similar to the mobility of higher generation when their effective surface charge densities are similar *iii)*the formation of intramolecular hydrogen bonds (between undissociated carboxyl groups) is probable; such bonds would be favored by the increase in COOH surface density (growing dendrimer size; every increase of generation number increases the number of carboxylic groups by a factor of 2, whereas surface area increases less. Hydrogen bonds could weaken the acidity of dendrimer. Counterion condensation is controlled by the ratio of the energy of electrostatic interaction between counterions and the dendrimer surface to the thermal energy. [60]

5. Aggregation of linear polycations with colloids or dendrimers

The aggregation of particles carrying negative charges and linear cationic polyelectrolytes has been investigated. Polyelectrolyte condensation may be considered as a modification of the adsorption of neutral polymers, in which the entropy of adsorbed and free chains plays a major role. Theoretically, the problem was first treated by Wiegel[63] and, subsequently, Muthukumar[64]. Wiegel took into account the bio-model proposed in 1965 by Rubin. Rubin restricted the chain to the bonds of a lattice. According to Rubin's theory the attractive forces between the molecule and the surface have a range which is comparable to the size of a monomer unit. The most interesting aspects of the analytic solutions which this author found is the existence of a discontinuity in the adsorption behavior at some critical value of the adsorption energy in units of $k_B T$. Above these critical value, the macromolecule exist in an adsorbed state. Below critical adsorption energy- the heat motion is strong enough to tear it off the surface and shuttle it throughout the whole fluid. In view of the unknown character of the forces which act in the living cell between biopolymers and cell membranes it was of interest to study a model for adsorption which is the opposite of Rubin's model, in that the attractive force is long- ranged rather than short-ranged. Wiegel considered the case where the macromolecule carries a fixed charge on each repeating unit, and the membrane carries fixed charged on its surface with a constant surface charge density. The electrostatic forces between the repeating units of the macromolecule are neglected. For a weakly bound, very long macromolecule the adsorption problem has been solved mathematically. The adsorption behavior found by Wiegel is qualitatively similar to the behavior in Rubin's models with short-range forces. Adsorption occurs at a certain critical temperature which is influenced by e.g. composition of the cell fluid and the surface charge density of the membrane. [63]
Muthukumar observes that if the potential between the surface and the polymer is attractive, the chain prefers to be adsorbed on the surface. However such a chain configuration is of lower entropy and hence not a preferable state. These two opposing tendencies cancel out at a critical temperature. Below the critical temperature, the chain is adsorbed at the surface. Above the critical temperature, the chain is unbound from the surface due to the dominance of the chain entropy over the net attractive interaction with the surface. Muthukumar's theory is a generalization of Wiegel's theory to account for the proper chain configurations dictated by the conditions of the polyelectrolyte solution[64]. Evers et. al. modified the self-consistent mean-field theory developed for neutral polymer adsorption to the case of weak polyelectrolyte adsorption[65]. The theories of Odijk and Scheutjens et al. [65,66] predict a phase transition, corresponding to the appearance of a bound state at some critical surface charge

density. The critical surface charge density has been found to vary linearly with the Debye-Hückel parameter, κ[67,68] and inversely with δ, the charge per polymer repeat unit[69], i.e.:

$$s_c \, \delta \kappa^{-1} = const \qquad (9)$$

Odijk's theory as well approximates the surface as a plane and compares with some model micelles.[70] Micelle is an electrically charged particle built up from polymeric molecules or ions and occurring in certain colloidal electrolytic solutions like soaps and detergents. Surfactants i.e. form micelles when they reach the critical micelle concentration (CMC). Surfactants contain both hydrophobic and hydrophilic ends and will therefore be attracted to the surface of the polar phase. Surfactants first will line up along the surface of the polar phase, and when that is completely filled up, they will begin to form micelles of different shapes, dependent on their concentration. The micelles are a grouping of surfactant molecules where either the hydrophobic (in a polar continuous phase) or the hydrophilic (in a nonpolar continuous phase) ends cluster inward to escape the continuous phase.[71] Simulation of the binding of a flexible polyelectrolyte chain to an oppositely charged spherical micelle shows that increased chain stiffness results in decreased binding. Carboxyl terminated dendrimers may be treated as small, highly charged micelles. For the dendrimers the higher generation corresponds to the very large surface charge densities.. From the analysis of the titration curves of PAMAM dendrimers one can calculate the relationship between surface potential and surface charge density.[70] For the low generation dendrimers, this dependence is exactly congruent with the solution of the nonlinearized P-B equation. If the generations are higher, the deviations that occur can be understood in terms of ion (Na$^+$) incorporation. Theoretically if the length of a binding site on the polymer is comparable to a persistence length (relative sizes of polymer binding segment), considerable bending of the linear polymer must occur. The attractive electrostatic forces responsible for binding are opposed by the bending stress stored in the polymer as it deforms around the macroion in order to bring its charges into proximity with the charged sites on the macroion. A decreased electrostatic attractive energy would then be obtained only at the expense of an increased elastic energy of bending, and the competition between these two energy sources may constitute the principal factor determining binding. This model is able to explain an abrupt transition of nucleosome structure as a consequence of the elastic instability of the wrapped DNA which is a negatively charged stiff biopolymer. Regarding the interaction of a polyelectrolyte with small oppositely charged spheres one can find the essential reason for a binding threshold: binding can only occur when the charge density of the macroion is sufficient to overcome the elastic resistance to bending a polymer segment onto the curved macroion surface. However, the model described above contains severe simplifications and has to be regarded as highly tentative. The surface charge density is replaced by the linear circumferential density (rough approximation that charges are placed parallel-like on the surface of the sphere), the release of condensed counterions was not taken into account and finally the size of the polymer binding segment has been arbitrarily (within limitations) chosen. Also experimental results show that the simple model is not always sufficient for an explanation.[72] Complexation of DNA with histone proteins and the influence of varying salt concentration and sphere charge on the equilibrium complexation behavior were investigated by Kunze et al.[73] A numerical study has been performed to investigate a simplified model for the interaction between a charged sphere, characterized by its radius and charge, and an oppositely charged, semiflexilble PE, characterized by its bending stiffness and linear charge density. The DNA was described by a semiflexible polymer of a certain length L, (corresponding roughly to 146 base pairs of length 0.34 nm each) with a certain bare mechanical persistence length equal around 60% of L. The histone protein was approximated as a rigid sphere of a few-nanometer radius which exhibits no structural changes. Nature uses the binding of DNA to the positively charged histone proteins to compact and store the approximately 1 meter of human DNA in a nucleus of perhaps 10μm. The compact structure contains a repetitive structure whose basic elements are the

nucleosomal particles, consisting of DNA wrapped in about 2 turns around the histone protein. The stability of those nucleosomal particles is of importance for the biological activity of DNA.[73] Using a variety of different experimental techniques, the main characteristic of the complexation behavior are following. For a salt concentration close to the physiological value of about $100m$M, the DNA is tightly wrapped around the histone. For large salt concentration (of about $750m$M), the DNA is released from the complex. While for even larger salt concentrations the histone protein disintegrates. For very small salt concentrations (below $2m$M), the DNA takes an extended form, which is indicative of a partial dewrapping of the DNA from the histone. Good agreement between the numerical study and an experiment has been found.[73,74]

Recently experiments concerning effect of dendrimer size on electrostatic binding receive attention. Caminati et al. [75] studied the binding of surfactants to carboxyl starburst dendrimers, by varying the molecular weight and size systematically over a wide range. Lower generations of dendrimers (below generation 3.5) interact with surfactants (dodecyltrimethylammonium chloride) in a noncooperative way, whereas the higher generations bound polycations cooperatively. Thought to result from alkyl chain association induced by the closely packed charged groups on the dendrimer surface. The results of Caminati are consistent with a morphology change between generation 3.5 and 4.5, corresponding to a transformation from an open, branched structure to a closed, compact one. Recently Li and Dubin[76] studied the complexation between the same carboxyl starburst dendrimers and poly(diallydimethylammonium chloride) (PDADMAC). The work presented by Zhang et. al[70] constitutes a more systematic study comprising a broader range of generation number and ionic strengths. Potentiometric titration, turbidimetry and quasi-elastic light scattering measurements were used to investigate the interaction between carboxylated starburst dendrimers (generations 0.5, 3.5, 5.5 and 7.5) and PDADMAC over a wide range of ionic strength. The effect of generation number and ionic strength on the binding of the polycation to dendrimer surface has been described. Also an effect of binding on the dissociation of dendrimer generation 7.5 has been reported. The higher generation dendrimers readily form complexes with polycations since the head groups on the surface are relatively congested, leading to a higher surface charge density. The lower generation dendrimers only complex with polycations at higher degree of ionization or low ionic strength because of their lower surface charge density at any dissociation degree. At high ionic strength, complexes may not form.[70] Complex formation between a carboxyl-terminated cascade polymer (generation 3) and several cationic polyelectrolytes of varying linear charge density was studied as a function of ionic strength by turbidimetric titration and dynamic light scattering by Miura et al. [77] Tetramethylammonium chloride was used to adjust the ionic strength in order to avoid sodium counterion binding to dendrimer carboxyl groups. Complex formation occurs abruptly at a critical pH, as signed by a sudden change in either the turbidity or the apparent Stockes radius from dynamic light scattering. The critical pH value of incipient complex formation was converted to the critical surface charge density. Under condition of low or moderate ionic strength, it was confirmed that critical surface charge density is roughly proportional to κ/ξ, where ξ is the linear charge density of the polyelectrolyte. Electrostatic interactions between dendrimer of 3rd generation and polyelectrolytes of varying charge density confirm the occurrence of complex formation as a phase-transition-like phenomenon. When highly charged polyelectrolytes (such as PDADMAC) bind to the dendrimer 3rd generation at its small surface charge density, soluble complexes may appear because charge asymmetry precludes stoichiometric charge neutralization. [77]

There are no computer simulation data available which concern complex formation between dendrimers and linear polyelectrolytes. However, such a system has to be, to some extend, similar to micelle-linear polyelectrolyte complexes. The complexation between charged micelle and an oppositely charged polyelectrolyte was studied by Wallin and Linse.[78,79] They

used a simple model system with a particular emphasis on the electrostatic interaction and the polyelectrolyte rigidity. Structural data of the micelle-polyelectrolyte complex and thermodynamic quantities of the complexation as a function of the flexibility of the polyelectrolyte were obtained by using Monte Carlo simulation and thermodynamic integration. Moreover, the ratio of the critical aggregation concentration (CAC), and the critical micellization concentration was calculated. CAC is the lowest surfactant concentration at which the surfactants self-aggregate in the presence of polyelectrolyte. The results clearly show that the flexibility of the polyelectrolyte affects the structure of the complexes formed. Highly flexible polyelectrolytes form complexes without any significant increase in internal stress, whereas larger rigidity causes the internal stress to increase to maintain optimal electrostatic interaction with the micelle. When the persistence length of the polyelectrolyte becomes larger than about half of the effective circumference of the micelle, a much weaker electrostatic interaction with the micelle is obtained and the chain stress is released. Moreover the CAC was found to be up to two orders of magnitude lower than the CMC but it increases with chain rigidity. Both, the strong attractive electrostatic interaction between the micelle and the polyelectrolyte and the release of counterions were found to be important for the reduction of CMC. Preliminary comparison with experimental data shows that the obtained reduction of the CMC is reasonable and hence indicates that despite the simplicity of the model, it correctly describes the essential parts of the system.[78]

Wallin and Linse extended their previous study for the case of different linear charge densities of the polyelectrolyte.[79] The results show that the linear charge density of the polyelectrolyte affects the structure of the complexes formed. A high linear charge density leads to a strong accumulation of polyelectrolyte charges close to the micellar surface and a large reduction of the energy. At a lower linear charge density, the number of close polyelectrolyte charges is smaller and the reduction of the electrostatic energy is less. For nonflexible polyelectrolytes, the angular stress increases upon the complexation in order to maintain optimal electrostatic interaction with the micelle. The CAC was found to be up to 2 orders of magnitudes lower than the CMC, but increases with decreasing linear charge density and increasing chain rigidity. The cause of reduction of CMC is the strong attractive electrostatic interaction between the micelle and the polyelectrolyte. The interaction leads to a i)a strong complexation between the micelle and the polyelectrolyte and ii)a release of their counterions. This process is favored both energetically and enthropically. Since there is no hydrophobic interactions between the micelle and the polyelectrolyte in the model, the results show that electrostatic interactions only are sufficient to make CAC<<CMC. Of course if a hydrophobic component was present, it would enhance the stability of the complex and further reduce the CAC. Despite that the comparisons with experimental data with different linear charge densities and flexibility's are still only preliminary and that approximations have been used, the agreement between the prediction of Wallin and Linse and those data is encouraging.[79] Effects of linear charge density and chain length on polyelectrolyte-macroion complexation has been studied by Jonsson and Linse.[80] On the basis of Monte Carlo simulations of a model system representing an aqueous solution containing one polyelectrolyte and several charged macroions, the composition and the structure of the complexes formed have been investigated. Despite the strong electrostatic interactions, it has been demonstrated that the Monte Carlo simulation technique employed enables sufficient mobility in configurational space to make the simulations ergodic in practice. The strong attractive electrostatic interactions between the polyelectrolyte and a macroion make the polyelectrolyte-macroion complex well defined. A macroion is either complexed with a firm contact to the polyelectrolyte or clearly separated from it. The binding isotherms are Langmuir-like, and in excess of macroions the complex becomes overcharged by 50%-100% of the polyelectrolyte charges. After reaching the binding plateau, the structure of the complexes was not strongly affected by uncomplexed macroions for the cases studied. When complexed, macroions are located close to each other

despite their mutual electrostatic repulsion. A free polyelectrolyte is considerably extended by the repulsive electrostatic interaction between its segments. Upon complexation, the polyelectrolyte becomes locally less stretched and its overall shape sinks and it becomes more spherical. The smallest extension appeared for a neutral complex and it becomes expanded again in the overcharged state, although less expanded as compared to a free polyelectrolyte. A single macroion prefers to be complexed to the central part of the polyelectrolyte. No support of an asymmetric binding leading to tails of different length was detected. When the number of complexed macroions is increased, they still prefer to complex to the central part of the polyelectrolyte, but by necessity segments further away are engaged and the dangling tails become shorter. In the overcharged state, essentially no tails are left. A reduction of the linear charge density of the polyelectrolyte leads to i) reduced capacity to complex macroions and ii) a looser complex as inferred from smaller number of complexed segments and longer separation between macroions in the complex (at the same number of complexed macroions). A reduction of the polyelectrolyte length at conserved linear charge density leads to i) a reduced capacity to complex macroions, ii) a more compact complex, iii)a smaller contraction of the polyelectrolyte. Finally an increase of the macroion charge results in i) a reduced capacity to complex macroions (fewer macroions) but an increased overcharging limit, ii) a more compact complex, iii) a larger contraction of the polyelectrolyte. The study has been focused on rather short polyelectrolytes as compared to real ones to make a fairly detailed examination of several systems possible. Nevertheless, many aspects emerging from this study have to be also valid for longer polyelectrolytes.[80]

III. Compounds of the Investigated System
1. Dendrimers

Figure 2. presents the roots of dendrimer species.
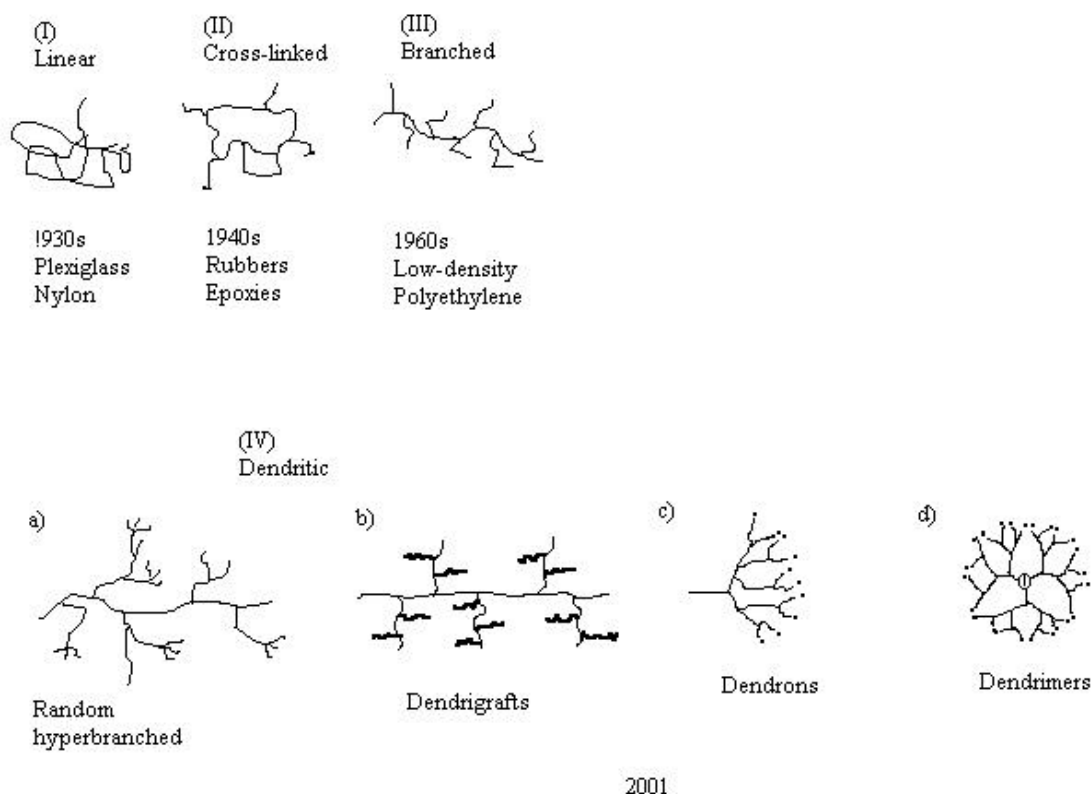
Figure 2. History of the dendrimer morphology.

1.1. Flexible dendrimers[81-87]

In addition to traditional synthetic polymers, linear, cross-linked (bridged) and branched polymers, the "dendritic" structure has recently come into focus in research and for potential applications. In contrast to other branched structures they have a regularly branched architecture. Dendrimers allow the precise control of size, shape and placement of functional groups. To our knowledge, there are two examples of molecular level (nm) dendritic structures in biological systems; in each case, they are derived from polysaccharides. These include glycogen, amylopectin and proteoglycans. The former is involved in energy storage in plants and animals, and the latter are important constituents that determine the viscoelastic properties of connective tissue. Poly(amidoamine) (PAMAM) dendrimers represent on of the first complete dendrimer family that has been synthesized, characterized and commercialized. Since 1979, two major strategies have been developed for dendrimer synthesis. The first was the divergent method in which growth of a dendron (molecular tree) originates from a core site (root) (Fig.2a). This approach involved assembling monomeric modules in a radial, branch-upon-branch motif according to certain dendritic rules and principles. This divergent approach is currently the preferred commercial route used by worldwide producers including Dendrimax (Ann Arbor, MI, USA), DSM Fine Chemicals (Geleen, The Netherlands) and The Perstorp Group (Perstorp, Sweden). A second method that was pioneered by Fréchet is the convergent growth process. It proceeds from what will become the dendron molecular surface (i.e. from the leaves of the molecular tree) inward to a reactive focal point at the root (Fig.3b). This leads to the formation of a single reactive dendron. To obtain a dendrimer structure, several dendrons are reacted with a multi-functional core. Using these two synthetic strategies, >100 compositionally different dendrimer families have been synthesized and these

are reviewed in other literature. Common characterization methods verify the chemical structure.
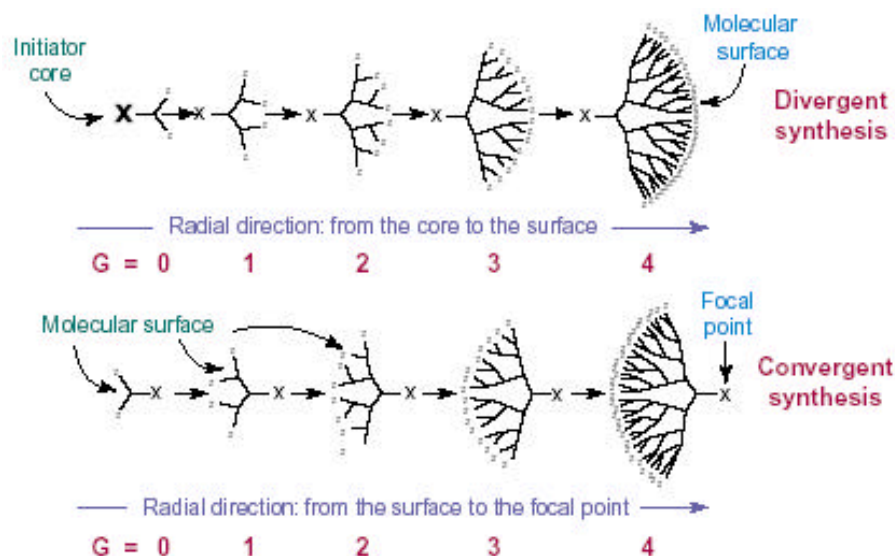
Figure 3: Two principle synthetic methods for constructing dendritic macromolecules: **(a)** the divergent method, **(b)** the convergent method.

Size and shape of such molecules is provided by AFM, TEM, SEC, viscometry and scattering methods. Computer simulations give an orientation about the geometry and dynamic in a dendritic system (mobility, shape persistence, end groups disposition).

1.2. Stiff Dendrimers

Poly(phenylene) dendrimers (PPd) represent a different, new class of dendrimers: stiff dendritic molecules. In particular, we investigate the dendrimers based on a tetrahedral core. Especially first generation of poly(phenylene) drimers with COOH –surface groups is of our interest. The working name of these compound is G1td(cys(glu)$_5$)$_8$ (see Fig.5). Cys(glu)$_5$ is peptide composed of cysteine and glutamic acid.
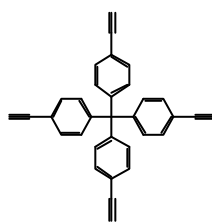
Figure 4. Tetraphenylmethane (tetrahedral) core

G1td(Cys(Glu)$_5$)$_8$

MW 9762

48 carboxylic groups
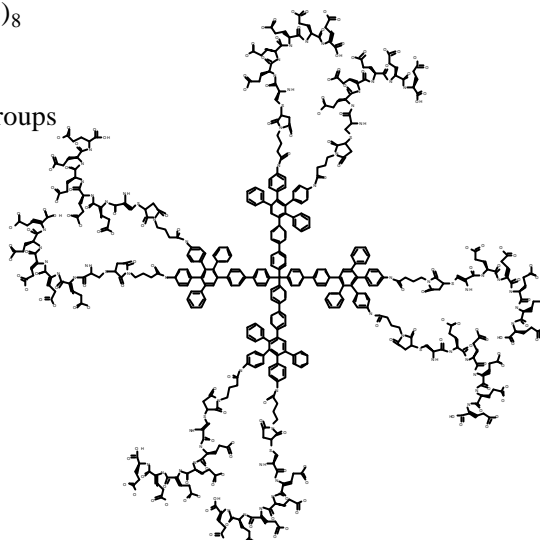
Figure 5. Poly(phenylene) dendrimers of first (G1) generation.

The dendrimers are provided by the research group of Prof. Müllen. Synthesis and characterization of these compounds is a part of the PhD thesis of George Mihov. For further usage we will call G1td(Cys(Glu)$_5$)$_8$ simply G1. Monodispersity of PPd polymers, as well bearing functional groups at the end of the "branches", is confirmed by m/z ratio, i.e. the molar mass determined by MALDI-TOF (matrix-assisted laser desorption/ionization time of flight mass spectrometry) as compared to the calculated molar mass. Molecular masses of the dendrimers calculated from SEC and based on poly(styrene) (PS) standard are lower than the nominal masses and the differences increase with increasing molecular mass. This phenomenon is due to more globular shape of the dendrimers as compared to the PS random coils. The dynamics of PPd (according to the solid-state NMR) shows the increase of mobility of dendrimers with each generation. This is supposed to be a reason why higher generations are better soluble. Slow dynamics (typical frequencies 10^{-1}-10^3 Hz) are limited within the poly(phenylene) dendrimers to the 10 Hz value which is due to the local flip motions of single phenyl rings. Dendrimers based on tetrahedral core are less mobile than those based on the biphenyl core (which shows mobility along the inner biphenyl bond of the core; 60° vibration of phenyl groups around their linking bond calculated). Generally the PPd can be regarded as a rigid molecules. Dendrimers based on the tetrahedral cores (for example: G1 and G2) show a *diabolo*-like molecular shape which resembles the shape of the core. Due to the large number of benzene rings around the central methane unit, the branches are hindered in their rotation, and the internal mobility of the molecule is lowered.[87]

2. Ionenes

Ionenes were first successfully synthesized by Rembaum.[88] Ionenes are polyelectrolytes with quaternary ammonium groups in defined distance. A broad spectrum of structures exists ranging from simple aliphatic chains to aromatic rings where ammonium groups may belong to the ring.

Below presented are the different morphology of aliphatic chain-like ionenes.
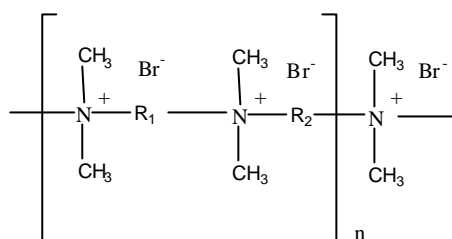
For so called symmetrical molecules:

$$R_1 = R_2 = \quad -(CH_2)_n-$$

or

$$R_1 = R_2 = \quad -CH_2-\langle\bigcirc\rangle-CH_2-$$
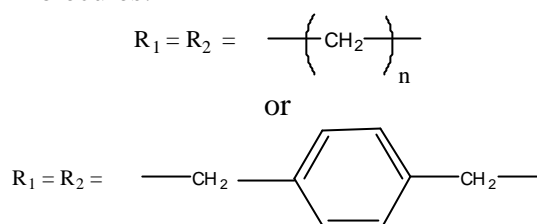
In case of unsymmetrical molecules $R_1 \neq R_2$.

Fig.6 The morphologies of aliphatic chain-like ionenes

The synthesis bases mostly on the Menschutkin reaction between $\alpha,\omega-$alkanediamines and $\alpha,\omega-$dibromoalkanes.

N,N,N´,N´-tetraalkyl-α,ω–diaminoalkanes α,ω–dihaloalkanes $1 = 2$ and $m > 3$ or $1 > 3$ and $m > 3$
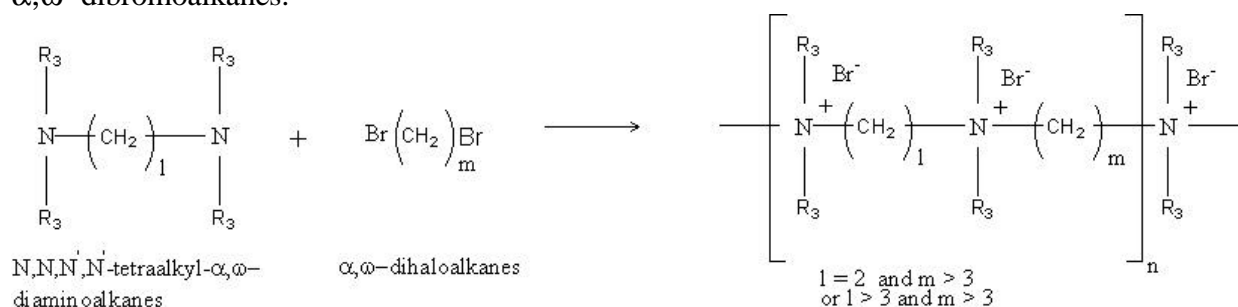
The Menschutkin reaction can give symmetrical and unsymmetrical ionenes.
To obtain symmetrical aliphatic ionenes one uses $\alpha-$halo-N,N-dialkylamino-alkanes:

$\omega-$halo-N,N-dialkylamino-alkanes $m = 3$ $m > 7$
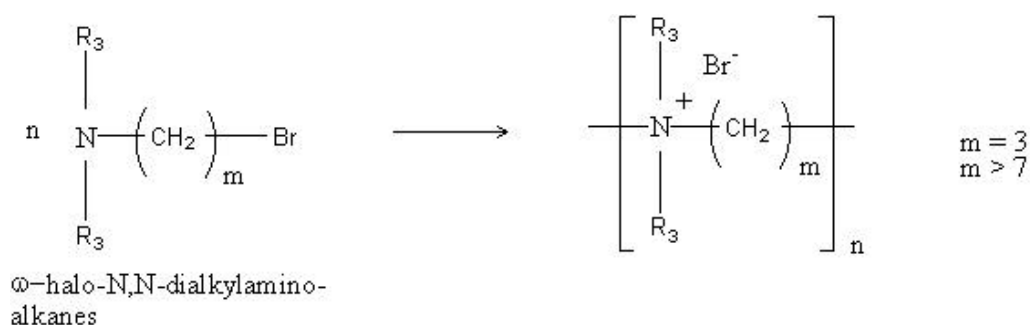
R1 is equal R2 for symmetrical ionenes, while R1 differs from R2 for unsymmetrical.

Aromatic ionenes result mostly from the reaction between aliphatic or aromatic diamines with p-xylenechloride [88-90]

$$ClCH_2 - \bigcirc - CH_2Cl$$

p-xylenedichloride
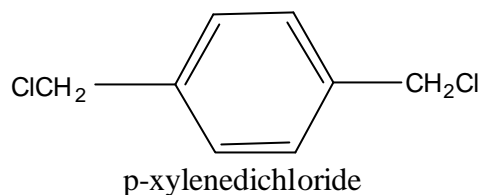
Compounds in this work are synthesized by the Menschutkin reaction which is known as a classical nucleophilic bimolecular substitution (S_N2). The kinetics of such reaction is influenced by several parameters i.e. polarity of the solvent, steric hindrance of substituents, nucleophilicity and mobility of the leaving groups and pressure.

Several publications regard the Menschutkin reaction as a normal, second order kinetics. However the detailed kinetic of such reaction was studied by *in-situ* ^{13}C NMR.[91] Two types of reactive groups represented by two types of monomers have to be distinguished: R_1-Br called M_1 and R_2-Br called M_2. besides there are in the system so called "reactive end-groups" where an ionic charge (amine group) is located next to the reactive group. Charge and reactive group are separated by the monomer segment e. g. R_1. R_n-$N^+(Me)_2$-R_1-Br designated as M^*_1 and R_m-$N^+(Me)_2$-R_2-$N^+(Me)_2$- designated as M^*_2. The polymerization was regarded as a step-growth reaction with four elementary steps:

1. (12) Reaction of M_1 and M_2 – reaction rate constant k_{12}

2. (12^*)Reaction of M_1 and M^*_2 – reaction rate constant k_{12}^*

3. (1^*2) Reaction of M^*_1 and M_2 – reaction rate constant k_{1^*2}

4. (1^*2^*) Reaction of M^*_1 and M^*_2 – reaction rate constant $k_{1^*2^*}$.

If reaction rate constants are equal the polycondensation can be regarded as an ideal case of step-growth polymerization reaction. The most probable distribution of products and their molecular mass distribution can be predicted. Investigations however show that the reaction is not ideal. Differences in kinetics are observed. Each reaction gives rise to a different product. Reactivities of "end groups" seem to be regulated by the specific chain sequence and the distance of ionic charge from the nucleophilic reaction center. At the reaction beginning the medium contains an equimolar mixture of diamine and dibromoalkanes in the solvent. At the end, the medium changes into a mixture containing polymer salt. Such a change must influence the kinetics of the reaction. The initial products (dimers, trimers) are reagents and solvents for the next reaction steps. Moreover the starting reaction mixture is concentrated and the activity coefficient may be of importance. It has been found that the reactions (12^*), (1^*2) and (12^*) take place at very early polymerization stages. The reaction rate constants are not all the same, and mixed kinetic behavior must be regarded. Additionally (1^*2^*) is assumed to be pure S_N2 reaction with well defined reaction rate constants. It can be assumed that the monomer concentration is close to zero at this stage and other reactions can be neglected in comparison with the (1^*2^*). The functional group concentrations are much lower than at the beginning of the polymerization. The reaction mixture of (1^*2^*) can be treated as an approximation of the ideal solution.

Additionally, the influence of solvent must be regarded. The Menschutkin reaction is sensible to the solvent polarity. The transition state solvation theory of Hughens and Ingold explains the influence of protic and aprotic solvents on the reactions. The quaternization

transition state can be stabilized in solvents with high dielectric constants. The ionene polymerization rate found in DMF/methanol mixture is 3-5 times larger than in methanol. The molecular weight of growing polymer as well as its molecular mass distribution might be affected by the solvent. Additionally if the reactivity of homologues is higher than the reactivity of their monomers high polydispersity results. Therefore the polydispersity of the ionene is expected to be broad, with a considerable amount of low molecular mass fractions as a result of the variable reactivity of functional groups. The so-called salt effect plays a role when charged particles are in the system. The reactions between charged species during ionene synthesis was accelerated via presence of the salt. The presence of salt according to the classical Debye-Hückel theory should reduce the reactivity of charged compounds because of screening and reducing the electrostatic forces between species in the system. On the other hand, in terms of the activated complex theory, the enhancement of rate constant is possible due to electrostatic interactions. The strong solvation of salts reduces the solvation of reagents. Additionally the polarity of the reaction medium improves after salt addition and stabilizes the transition state during polymer growth.

The side reactions play also significant role. Hoffmann degradation is not only a side reaction but also a termination reaction during the ionene formation:
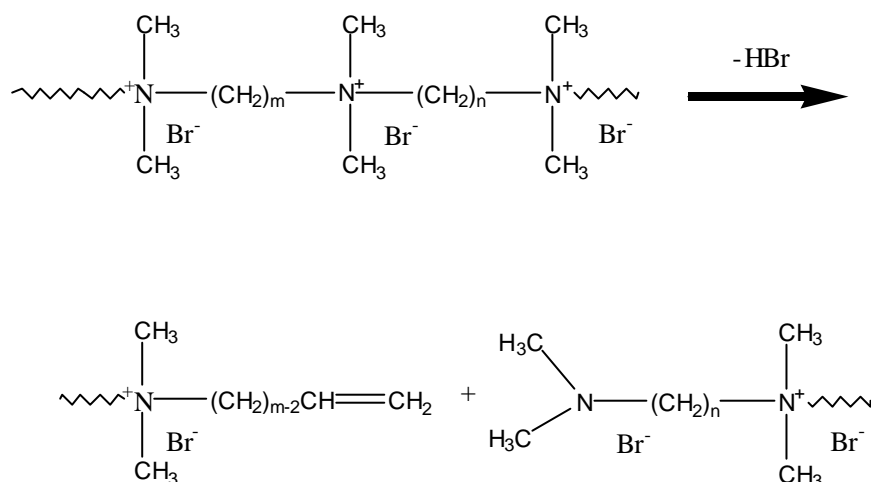
Figure 7. Hoffmann degradation on ionenes.

It produces "new" amine end-groups which can interfere with the polymerization by changing the soichiometry. The intramolecular cyclization leads to the stable small-ring products due to the reaction between alkanediamines with dihalogenoalkanes. Cyclization to rings larger than C_6 is negligible in the ionene synthesis because of the low probability of the ring closure reaction. NMR-spectra show 5mol-% of cyclic products in the reaction mixture after 46h of synthesis[91]

IV. Characterization Methods
1. Viscosity

To characterize the viscosity of macromolecules or colloidal systems, different interpretations of the viscosity parameters are used. The most obvious is viscosity of the solvent or continuous phase, η_s given in (Pa s). The ratio of the suspension viscosity (η) to the solvent viscosity is defined as a relative viscosity $\eta_r = \dfrac{\eta}{\eta_s}$ and is dimensionless.

One can also distinguish specific viscosity $\boldsymbol{h}_{sp} = \dfrac{\boldsymbol{h} - \boldsymbol{h}_s}{\boldsymbol{h}_s}$, which is dimensionless and reduced

viscosity $\boldsymbol{h}_{red} = \dfrac{\boldsymbol{h}_{sp}}{c}$ given in (Pa l/mol). c is the concentration of a dispersed phase. Intrinsic

viscosity, $[\boldsymbol{h}] = \lim\limits_{c \to 0} \boldsymbol{h}_{red}$ (m³kg⁻¹) will be discussed in details in the following section.

1.1. Viscosity of polymer solutions

The presence of macromolecules affects the viscosity of the medium and thus viscosity measurements can give information about size and shape of macromolecules. The effect is large even at low concentrations because the large molecules affect the flow of the surrounding fluid. At low concentrations of solute, the viscosity of the solution η is related to the viscosity of the pure solvent $η_s$ by:

$$\boldsymbol{h} = \boldsymbol{h}_s + \boldsymbol{h}_s [\boldsymbol{h}] C_p + \ldots\ldots\ldots = \boldsymbol{h}_s \left\{ 1 + [\boldsymbol{h}] C_p + \ldots\ldots \right\} \qquad (10)$$

The intrinsic viscosity [η] can be found experimentally by regarding the limes at infinite dilution:

$$[\boldsymbol{h}] = \lim\limits_{Cp \to 0} \left\{ [(\boldsymbol{h}/\boldsymbol{h}_s) - 1] C_p \right\} \qquad (11)$$

[η] is a measure of the hydrodynamic volume of a single polymer chain and has the dimension of inverse concentration (e.g. l/g)

A common method to measure viscosity is by the Ostwald viscometer, essentially a capillary connected to two reservoirs. The time that the solutions flows through the capillary is measured and compared with a standard sample. The method is particularly suitable for obtaining [η] because the ratio of the viscosity of the solution and the pure solvent is proportional to the drainage time t_{drain} , if a correction for different densities ρ and $ρ_s$ is made.

$$\frac{\boldsymbol{h}}{\boldsymbol{h}_s} = \left(\frac{t_{drain}}{t_{sdrain}} \right) \left(\frac{\boldsymbol{r}}{\boldsymbol{r}_s} \right) \qquad (12)$$

The value of this ratio can be used directly in equation (9). Measurement of the viscosity of solutions must be precluded by the measurement of calibrated samples, and can be used for assessing the molar mass M_v.[92] (see paragraph 1.2 and 3 in the experimental part). Viscosity thus represents a relative method for molecular mass determination. The dependency of the reduced viscosity ($η_{red} = η_{sp}/c$) on the concentration c for uncharged, flexible polymer chains is described by the Huggins equation:

$$\frac{\boldsymbol{h} - \boldsymbol{h}_s}{\boldsymbol{h}_s c} = \frac{\boldsymbol{h}_{sp}}{c} = [\boldsymbol{h}] + k_h [\boldsymbol{h}]^2 c \qquad (13)$$

k_h- Huggins constant
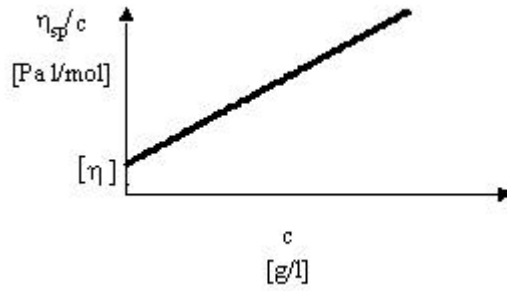
Figure 8. Extrapolation of the reduced viscosity
to the zero concentration. As a result- intrinsic
viscosity [η].

1.2. Viscosity measurement- relative method to calculate molecular mass

The viscosity of polymers changes with molecular mass. Based on the viscosity measurement it is possible to calculate the viscosity average molecular mass of polymers M_v.[93]

The intrinsic viscosity [η] is correlated with molecular mass via the Mark-Houwink equation *(12)*.

$$[\mathbf{h}] = KM_v^a \qquad (14)$$

Parameters "K" and "α" are constants specific for the solvent and temperature used in the measurement. For many polymer – solvent systems these constants are tabulated. Parameters K and α change with the morphology and chemistry of the polymer. K and α are also dependent on the temperature and solvent used. The constants K and α can be obtained by linear regression of Mark-Houwink plots where number average and weight average molecular weight are included. (e.g. Fig.9. Poly(trimethylene terephthalate, PTT in hexafluoroisopropanol, HFIPA).[94]
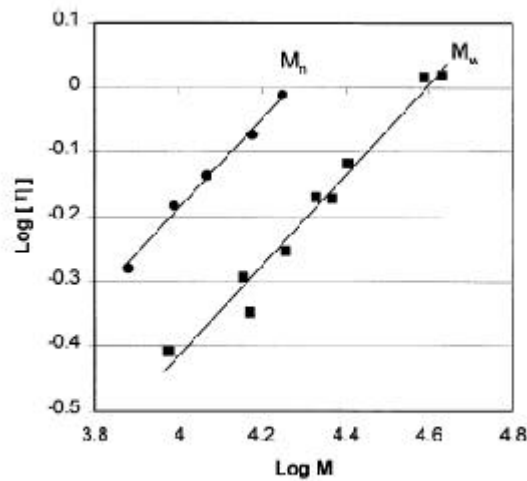
Figure 9. Linear regression of Mark-Houwink
plots for PTT in HFIPA.

Mark-Houwink parameters can be determined by both linear and non linear regression methods. If there are several molecular weight monodisperse samples of a polymer available, the Mark-Houwink parameters of the polymer (in certain kind of solvent at certain temperature) can be determined accurately by linear regression of the Mark-Houwink plot. The monodisperse samples of a few kind of polymers, such as polystyrene, can be obtained by well-controlled ionic polymerizations, while that of other polymers can only be obtained by fractionating polydisperse samples of the polymers. Due to the difficulty in fractionation, methods using polydisperse samples directly to determine the Mark-Houwink parameters have been developed, for example, calculation of the Mark-Houwink parameters from the GPC data.[95]

1.3. Viscosity of Polyelectrolytes

For polyelectrolytes in solution- the polyelectrolyte effect plays a significant role. In contrast to neutral polymers, it was found already by Staudinger that the reduced viscosity of polyelectrolyte solution increases upon dilution. In older text books this behavior is described by the Fuoss law[96]:

$$\frac{\boldsymbol{\eta}_{sp}}{c} = \frac{A}{(1 + Bc^{1/2})} \qquad (15)$$

and explained by a "coil-to-rod" transition.

According to this expression a straight line is observed when $\frac{c}{\boldsymbol{\eta}_{sp}}$ is plotted versus $c^{1/2}$, but

the values obtained as an intercept as c=0 is inverse of the intrinsic viscosity are anomaly large. The explanation of such phenomena based on the expansion of the polymer coil to rod. However at very low polymer concentrations, the reduced viscosity goes down again with decreasing concentration [93] A peak in reduced viscosity is not only observed for the random coil, but also for the globular particle which can not transfer into a rod.

Over the years a number of articles dealing with polyelectrolyte solutions have appeared which report the existence of a peak in reduced viscosity η_r vs the polymer concentration C_p. Such behavior has been demonstrated for a number of linear polyelectrolytes e.g., hyaluronate (HA)[94,97], carboxyl-methyl cellulose[98], thymonucleate[99], gum arabate[100], poly(4-vinylpyridine)[101], poly(2-vinylpyridine)[102] and poly(styrene sulfonate)[93,103] but also for globular polyelectrolytes of a fixed geometry i.e. proteins, micelles, microgels. The viscosity of solutions containing charged particles increases as ionic strength decreases, and that in solutions containing little or no excess of salt, the reduced viscosity increases with decreasing solute concentration.[104]

Witten and Pincus present an argument for how polyelectrolyte concentration affects persistence length, apart from ionic strength effects, and rationalized Fuoss law for polyelectrolyte reduced viscosity η_r.[105] The latter, however contains only the monotonic increase of η_r with decreasing c, and so the existence of a peak is not addressed.

Cohen, Priel and Rabin investigated the dependence of the viscosity for different molecular mass polyelectrolytes.[93] They also observed a peak when reduced viscosity has been regarded as a function of polymer concentration. The position and height of the maxima depend on the salt concentration. Increase in salt concentration moves the maxima towards higher polymer concentration and lowers the value of the reduced viscosity. The slope is independent on the molecular mass. The reduced viscosity at the maximum increases linearly with the molecular mass of the polyelectrolyte. The slopes and intercepts of these linear dependency decrease with increasing salt concentration.[93]
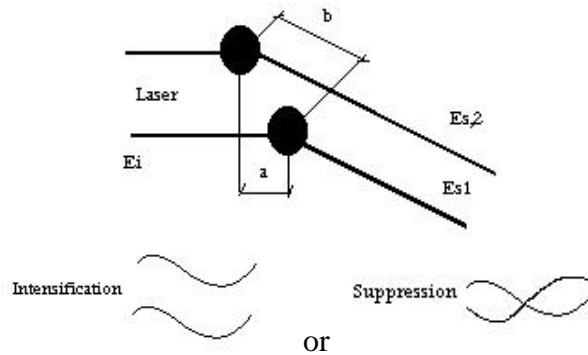
Reed proposed a conformationally based mechanism to explain the major features of the peak of reduced viscosity vs polyelectrolyte concentration for solutions of long-chain, semiflexible polyelectrolytes at very low ionic strength.[104] No fundamental theory was given, but demonstrations show plausibility and semiquantitative agreement with experiment. Because experimental data show how strongly the mean square radius of gyration of semi-flexible polyelectrolytes changes with ionic strength, it was demonstrated that these large dimensional changes lead to the observed viscosity behavior. According to Reed[104], when one dilutes a polyelectrolyte solution with an aqueous solution of fixed added salt concentration, the dilution process is not isoionic since the osmotically free counterions of the polyelectrolyte itself contribute to the solutions total ionic strength decreases as concentration of polyelectrolyte (c_p) decreases. The decrease in ionic strength (c_s) leads to a continuos expansion of the polyelectrolyte so that the square of the viscometric volume occupied by a given molecule increases more rapidly than the mass concentration c_p decreases, leading to a measurable increase in the reduced viscosity of the solution as c_p decreases. As c_p continues to decrease, the molecules begin to approach their maximum size, the viscometric volume of each polymer starts to become independent of c_p and c_s , and so the reduced viscosity decreases again as c_p decreases, and a peak in $\eta_{reduced}$ vs is obtained.

Theory, however, cannot explain why the same effects are found for a polyelectrolytes (PE) of fixed geometry. Approaches such as the Mode-Mode-coupling developed by Hess and Klein in contrast predict the specific polyelectrolyte viscosity behavior for charged spheres. However in this theory a postulate for the interaction potential of charged spheres needs to be made or derived from scattering results. While the Hess-Klein approach points towards the importance of intermolecular interactions in PE-behavior, a complete fundamental understanding is still missing so far. Still lacking is a general theory for $[\eta]$, which accounts for electrostatic, draining, and excluded volume effects, and hydrodynamics.[105-107]

2. Scattering techniques

Scattering techniques are methods used to investigate morphology and dynamic properties of matter e.g. polymers, colloids, micellar systems, aggregates, etc. Neutrons, X-ray or light radiation is used. The specific properties of the source and their characteristic interactions with the sample allow to explore a spatial scale from 1 to $2 \cdot 10^4$ nm and a dynamic range from seconds to picoseconds.[108] In Figure10 the typical scattering experiment is shown. Incident radiation meets the sample or scattering medium. A part of the radiation passes through the sample unaffected, a part is scattered. A detector is placed at the scattering angle θ, and the intensity $I(\theta,t)$ of the scattered radiation is measured. The hypothetical homogenous medium does not scatter radiation away from the incident direction. Scattering is caused by fluctuations in the medium, variation in density of scattering material within the medium. Interference of two different waves on the detector depends on the position of scattering particles (scattering centers). The scattering experiment bases on the assumption that the way of radiation/light (laser-particle-detector) is different for every particle (scattering centers). Intensification of signal on the detector is observed when the path difference is equal λ. λ is the wavelength. The intensification repeats for the way difference $(b-a) = \dfrac{2n\boldsymbol{l}}{2}$. Fig.10a and the scattering experiment setup Fig.10b.
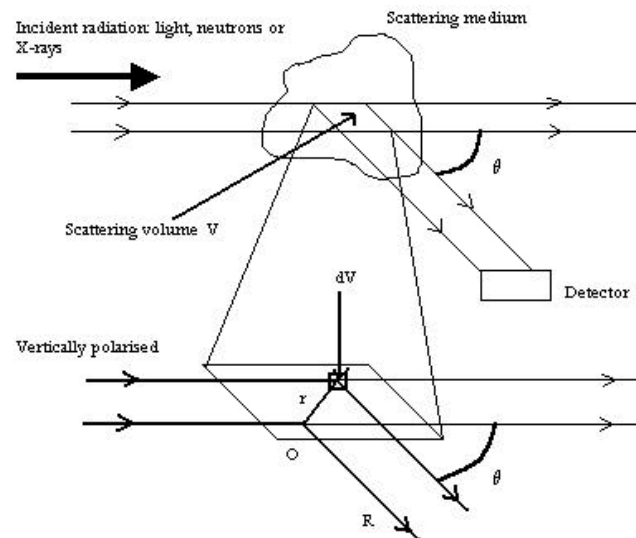
Figure10. The way of radiation for two
a)scattering centers and b)Scattering
experiment setup.[94]

Two basic types of scattering experiments can be performed. Static scattering measures the dependence on angle of the average scattered intensity. Static scattering provides structural information. In the diluted system the information concerns the shape of individual particles. In concentrated samples positional correlation of particles can be measured, however the data analysis becomes more difficult. If the scattering measurement is further done at the fully calibrated equipment, the absolute magnitude of scattered intensity (averaged over the time or frequency) gives information on the mass or molecular weight of the scattering objects. The second type of scattering is the analysis of time dependence of fluctuations in the scattered radiation (or analysis of frequency or energy changes) - so called dynamic or quasielestic scattering. The dynamic scattering provides information about the diffusion of the objects in the sample: about Brownian motion of particles.[108]

2.1. Static light scattering

The beam of plane-wave, monochromatic light is described by the oscillating electric field amplitude:

$$E_1(r,t) \equiv E_0 \exp[i(k_I r - \omega t)] \qquad (16)$$

E_0 is electric vector polarized perpendicular to the scattering plane (the "plane of the paper") is incident on a region of scattering medium; k_I is the propagation vector of the incident light, having magnitude $\quad k_I \equiv |k_I| = k = \dfrac{2\pi}{\lambda}$.

λ is the wavelength of light in the medium, ω is an angular frequency. We assume that the scattering is weak. Most photons pass through the sample undeviated, a few are scattered once, and the probability of double or higher-order scattering is negligible. The incident beam is not distorted significantly by the medium (in the context of general scattering it corresponds to the first Born approximation; in the context of light scattering- to the Raileigh-Gans-Debye approximation). It is assumed as well that the scattering is "elastic". Thus the magnitude of k_S of the propagation vector k_S of the scattered light is also $2\pi/\lambda$. Maxwell's equation can be applied to the plane electromagnetic propagating ware through a medium described by a local dielectric constant $\varepsilon(r,t)$. $\varepsilon(r,t)$ is the dielectric constant of the medium at position r, relative to an arbitrary origin O and at the time t. The amplitude $E_S(R,t)$ of the electric field of the radiation scattered to a point detector at position R in the far field is given by:[108]

$$E_S(R,t) = -\frac{k^2 E_0}{4\pi} \frac{\exp[i(kR - \omega t)]}{R} \int_V \left[\frac{\varepsilon(r,t) - \varepsilon_0}{\varepsilon_0} \right] \exp(-iqr) d^3r \qquad (17)$$

ε_0 is the average dielectric constant of the medium, V is the scattering volume, and the scattering vector q is defined as the difference between the propagation vectors of the scattered light k_S and incident light k_I:

$$q \equiv k_S - k_I \qquad (18)$$

$$q \equiv |q| = \frac{4\pi}{\lambda} \sin \frac{\theta}{2}. \qquad (19)$$

E_s can be written as a sum of the amplitudes of the fields $dE_S(R,t)$ scattered by the volume elements $\{dV \equiv d^3r\}$ at positions r:

$$E_S(R,t) = \int_V dE_S(R,t) \qquad (20)$$

where equation *(15)* covers the fundamental physics of light scattering. The scattered light field consist of a spherical wave emanating from the scattering volume with an angle- or q-dependent amplitude. The light scattering center is an oscillating point dipole. This elementary dipole reradiates light in all directions ("Hertz dipole"). The amplitude of scattered light is the spatial Fourier transform of instantaneous variations in the dielectric constant of the sample. Any variation in time of the local dielectric constant is directly reflected in temporal variations of the amplitude of the scattered field (and its intensity). Light scattering probes directly the structure and dynamics of the sample in reciprocal space (q-space). If now the solution contains number N discrete scattering particles (polymer molecules, colloidal particles or micelle) which are spatially distributed in the scattering volume V- the centers of mass at time t of such particles are described by position vectors $\{R_j(t)\}$. $r_j(t)$ is the position of volume element $dV(= d^3r_j)$ in particle relative to it's center of mass. Including foregoing assumptions, equation *(15)* can be written as:

$$E_S(R,t) = -\frac{k^2 E_0}{4\pmb{p}} \frac{\exp[i(kR - \pmb{v}t)]}{R} \sum_j \left\{ \iint_{V_j} \left[\frac{\pmb{e}_p(r_j,t) - \pmb{e}_L}{\pmb{e}_0} \right] \exp\left(-iqr_j\right) d^3r_j \right\} \exp\left[-iqR_j(t)\right]$$

or

$$E_S(R,t) = -E_0 \frac{\exp[i(kR - \pmb{v}t)]}{R} \sum_j \left[\int_{V_j} \Delta\pmb{r}(r_j,t)\exp(-iqr_j)d^3r_j \right] \exp\left[-iqR_j(t)\right] \qquad (21)$$

V_j is the volume of particle j and $\Delta\pmb{r}(r_j,t)$ can be regarded as a measure of the local density of scattering material and is defined as:

$$\Delta\pmb{r}(r_j,t) = \frac{k^2}{4\pmb{p}} \left[\frac{\pmb{e}_P(r_j,t) - \pmb{e}_L}{\pmb{e}_0} \right],$$

$\pmb{e}_P(r_j,t)$ is the local dielectric constant at position r_j in particle j. $\pmb{e}_L$ is the average dielectric constant of the solvent, and $\pmb{e}_0$ is the average dielectric constant of the whole system. The strength of the scattering depends on the difference between the dielectric properties of the particles and the solvent.

Equation *(19)* can be rewritten as:

$$E_S(R,t) = -E_0 \frac{\exp[i(kR - \pmb{v}t)]}{R} \sum_j b_j(q,t)\exp\left[-iqR_j(t)\right] \qquad (22)$$

$b_j(q,t) = \int_{V_j} \Delta\pmb{r}(r_j,t)\exp\left(-iqr_j\right)d^3r_j$ is the scattering length of the scattering center j.

From equation *(20)* the total scattered electric field is the sum of the fields scattered by the individual scattering centers. Each of these is the product of a scattering length, determined by the instantaneous distribution of material within the particle and a phase factor determined by the instantaneous position of the particle in the sample. Intensities and fields are related by $I(q,t) = |E(q,t)|^2$. From equation *(20)* the instantaneous scattered intensity averaged over all directions and all particles in solution is:

$$\left\langle I_S(q) \right\rangle = \frac{E_0^2}{R^2} \left\langle \sum_{j=1}^{N} \sum_{k=1}^{N} b_j(q)b_k^*(q)\exp\left[-iq(R_j - R_k)\right] \right\rangle \qquad (23)$$

Equation *(21)* is the general result for the average intensity scattered by an assembly of discrete particles.[108]

In the diluted systems the individual particles are , on average, widely separated spatially, so that their behaviors are uncorrelated. The average scattered intensity is a sum of the average intensities scattered by the individual particles. Thus, the measurement of $\left\langle I_S(q) \right\rangle$ as a function of q gives information on the size , structure and shape of the particles, averaged over orientation and over any distribution of size and shape. The average intensities scattered by identical particles are the same so that:

$$\left\langle I_S(q) \right\rangle = N\left\langle |b(q)|^2 \right\rangle \qquad (24)$$

which can be written as

$$\left\langle I_S(q) \right\rangle = N\left\langle |b(0)|^2 \right\rangle P(q) \quad \text{with } P(q) = \frac{\left\langle |b(q)|^2 \right\rangle}{\left\langle |b(0)|^2 \right\rangle} \qquad (25)$$

P(q) is called the *form factor* of the particle. It is defined so that $P(q) \to 1$ as $q \to 0$.

The form factor can be calculated for certain geometry of the particle i.e. a homogenous hard sphere or random-coil polymer molecule. In the concentrated system so called structure factor

$S(q)$ represents the modification of the intensity due to the spatial correlation of the particles.[109]

$$\langle I_S(q)\rangle = Nb^2(0)P(q)S(q) \tag{26}$$

However, in the following work we do not investigate concentrated systems and avoid the spatial correlation of the particles.

In case of small particles: R<<λ (R is now the radius of the particle) the scattering equation can be written as a virial equation *(25)*. Virial equation takes into account intra- and intermolecular interferences:

$$\frac{Kc}{I_S(q,c)} = \frac{1}{M_W I_n(q)} + 2A_2(q)c + ... \tag{27}$$

$I_n(q)$ is the single particle scattering function, normalized in such a way that $I_n(0) = 1$. $I_n(q)$ is then so-called structure factor *S(q)*. M_W [g/mol] is the average molecular weight, A_2 is second virial coefficient, c is the concentration of particles in the solution. K - the optical constant [mol cm^2/g^2] and depends on the source of radiation.

$$K = f_c \frac{4\pi^2 n_S^2}{\lambda_0^4 N_L}\left(\frac{\partial n}{\partial c}\right) \qquad f_c = \begin{cases} 1 \Rightarrow vertical, \;\; polarized \;\; light \\ \cos^2\theta \Rightarrow horizontal, \;\; polarized \;\; light \\ \dfrac{(1+\cos^2\theta)}{2} \Rightarrow unpolarised\,(I_0) \end{cases} \tag{28}$$

n_S is the refractive index of the solvent, λ_0 is the light wavelength, N_L is the Avogadro number, $\left(\dfrac{\partial n}{\partial c}\right)$ means the refractive index increment for the solvent and finally f_c is so called Cabanne coefficient, which can be neglected by isotropic scattering. When particles in the solution are of the order of magnitude R ≈ λ then the scattering follows the so called Raileigh-Debye-Gans (RDG) principles. Particles with maximal diameter 2a or particles with low contrast must implement

$$2a\frac{2\pi n_S}{\lambda_0}|m-1| << 1 \tag{29}$$

$m = \dfrac{n_P}{n_S}$ and n_P is the refractive index of the particles and a in case of spherical objects is the radius of sphere.[109]

Equation *(27)* allows interpretation of scattering phenomenon to extract average molecular weight, radius of gyration and the second virial coefficient from the scattering data. The scattering data interpretation will be explained later.

The principles of the scattering methods are the same for light, x-rays and neutrons. Only the scattering length which gives a quantitative representation of the strength of the interaction of the radiation and the elementary scatter differs for that three cases. In the light scattering the associated particle is a photon of energy about 10 eV. The radiation has electromagnetic interaction with the polarisable elementary scatter. In x-ray the particle is a photon of energy of about 10^4 eV. The magnitude of electromagnetic interaction here is characterized by the z electrons of the electromagnetic shell of atoms. The scattering length of an atom $\left(b_j^x\right)$ is given by $b_j^x = z b_0^x$ and $b_0^x = 2.8\cdot 10^{-15}$ m. The material can be described by

its local density of electrons. When the energy of the photons is lower (light scattering experiment), the photons are scattered only by the outer part of the electronic cloud of an atom. The scattering length density is therefore higher for x-ray than for light. In case of light scattering and x-ray scattering the scattering length has always positive values. In neutron scattering the neutrons normally used have an energy of about 10^{-3} eV. The interaction is nuclear and the value of local scattering density depends on the nature of the nuclei only. It differs from one isotope to another and is sensitive to the state of a nuclear spin. The problem of calculation of b for neutron scattering is yet unresolved. Thus b-values are experimentally determined and tabulated. A well known example is that of hydrogen. The b-value (-3.74 10^{-15} m) of which is very different from that of its first isotope, the deuterium (+6.67 10^{-15} m). The scattering length of an elementary scatter is the sum of the scattering lengths of its atoms for x-ray and for neutron. For the light, it is deduced from the refractive index, as is was shown before.[110]

For data evaluation and interpretation often helpful are four plots, so called Zimm-Plot, the Berry-Plot, the Gunier-Plot and the Kratky-Plot. The Zimm plot origins from equation *(27)* and results in a family of parallel lines. These lines can be extrapolated to the zero scattering angle for each concentration and to the zero concentration for each scattering angle. The Zimm equation:

$$\frac{Kc}{I_S(q,c)} = \frac{1}{M_W S(q)} + 2A_2(q)c \qquad (30)$$

allows to calculate the molecular mass, radius of gyration and second virial coefficient.

The Zimm-Plot finally results into the two limiting lines $\frac{Kc}{I_S(q,c)}\big|_{c=0}$ and $\frac{Kc}{I_S(q,c)}\big|_{q=0}$. The first yields the mean square radius of gyration $\langle R_G^2 \rangle$ (z-average). The ordinate intercept yields $1/M_W$. The initial slope of the $\frac{Kc}{I_S(q,c)}\big|_{c=0}$ yields the second virial coefficient. Obtained radius of gyration and second virial coefficient greatly depend on the range over which the extrapolation has been performed and on the extrapolation procedure itself. In many cases the Zimm-Plot is not applicable. E.g. the upturn due to the branching can start at rather low q-values and an extrapolation to zero angle can become very difficult in the common linear Zimm-Plot. In this cases, it is often useful to apply the so-called Berry-Plot, where the square root of $\frac{Kc}{I_S(q,c)}$ is plotted against $q^2 + kc$. This plot was suggested by Berry for polymers in good solvent, where the concentration dependence is no longer linear, but is also affected by the virial coefficient. However, neither Zimm, nor Berry-Plot are applicable in the case of high branching. At such high branching one can expect that the density profile of the segments has approached that of a sphere with the two essential differences i)the outer chains are dangling around and ii)the chains are flexible, not rigid. This model can be called "soft sphere". Guinier showed that the scattering intensity of the spherical (globular) structures can over a wide range of q^2 be approximated by the following equation $I(q,r) = \exp\left(1 - \langle R^2 \rangle \frac{q^2}{3}\right)$. Thus the Guinier plot should give a straight line for such globular structures. The Zimm plot shows straight line over a large q-range only for the scattering function of Gaussian coils or samples with a peculiar broad molecular distribution. The Zimm plot yields a higher values of the radius of gyration as compared to other models used e.g. Gunier plot.[111] The Guinier model is more suitable for extrapolation of the scattering

functions of collapsed coils or of globular particles. A combination of Zimm- and Gunier plot are used for better estimation of particle parameters. Both of the models are used for the data evaluation in following experimental part of this work. Finally, the Kratky plot. It may help to detect branching. Here $I(q,r)q^2$ is plotted against q. Linear randomly coiled chains result in an angular independent asymptote. A maximum appears for stars and other regularly branched chains. This maximum becomes more and more pronounced with increasing branching density.[111] Scattering techniques are direct methods to calculate parameters of a substance. Standard, comparative samples are not required.

2.2. Dynamic light scattering

The dynamic scattering provides information about the diffusion of the objects in the sample: about Brownian motions of particles, how their shape and configurations fluctuate in time.

Every movement of particles causes fluctuations in the scattering intensity. Random movement of smaller particles (Brownian motions) gives a rise to a stochastic signal. The velocity of fluctuations replies the velocity of particles. The waves must be coherent (monochromatic with parallel phases over larger areas). The scattering volume should be small due to fast loose of coherence. Depending on the setup two autocorrelation function (ACF) can be measured[109]:

1. Homodyne Autocorrelation Function ($=g_2$)- only light from the scattering volume enters the detector; the result is an Intensity-ACF:

$$g_2(t) = \lim_{T \to \infty} \frac{1}{T} \int_{t'=0}^{T} |E_S(t')| \, |E_S(t'+t)|^2 \, dt' = \left\langle |E_S(0)|^2 |E_S(t)|^2 \right\rangle \qquad (31)$$

2. Heterodyne Autocorrelation Function ($\sim g_1$)- the scattered light is mixed on the detector with reference light; the result is an amplitude of ACF:

$$g_1(t) = \left\langle E_S^*(0) E_S(t) \right\rangle \qquad (32)$$

The velocity and length scale of movement has to be approachable for the instrument resolution level. Depending on the kind of movement, the ACF follows different laws.

Then the amplitude of ACF is: $g_1(t) = \langle N \rangle \begin{cases} \exp(-D_T q^2 t) \Rightarrow \textit{diffusion} \\ \exp(\dfrac{kT}{2M_w} q^2 t^2) \Rightarrow \textit{directed\_motion} \end{cases} \qquad (33)$

D_T is the translational diffusion coefficient, k the Boltzmann constant. To calculate D_T a cumulant analysis can be performed. Based on the diffusion coefficient a hydrodynamic radius can be calculated by Stocks-Einstein relationship:

$$R_H = \frac{kT}{6 \pi \eta_S D_T} \qquad (34)$$

η_S - viscosity of the solvent

T - temperature.[109]

In the real systems however, the particles possess distribution of sizes which has to be reflected in the dynamic behavior of the sample. Instead of single diffusion coefficient value for the real system, the normalized intensity-weighted distribution of the diffusion coefficients is measured. The inverse Laplace transformation of the measured field correlation function (or intermediate scattering function ($f^M(q,t)$)) with respect to the time, yields P(D), and hence the information on the distribution of the particle sizes.[109]

3. Diffusion coefficient of polyelectrolyte solutions

The dynamic behavior of polyelectrolytes is much more complicated than the behavior of uncharged polymers. This is due to the multiplicity of interactions present in the solution of polyelectrolytes. Not only one type of diffusion as a result of Brownian motion is observed. In the solutions of polyelectrolytes two modes (so called fast- and slow mode) may be observed. The physical origin of the slow diffusive process is not understood yet. There are reports in the literature that the presence of the slow mode as well as the distribution of relaxation rates depends on the treatment of the solutions. One explanation of the slow mode as a result of the diffusion of large domains in the solution. Domains can be formed by a number of molecules "incompactly connected" i.e. by electrostatic interactions. The fast mode reflects the diffusive properties of single macroions or at least large segments of single macroions. [110] Double mode can be caused via so called polyelectrolyte effect. Polyelectrolyte effect is the increase of reduced viscosity with decreasing concentration. The nature of it is also not fully understood yet. Polyelectrolyte effect was supposed to appear due to the conformational changes of the molecules in the system. In the most dramatic cases from coil to the rod like molecules (historically: coil to rod transition) Nowadays polyelectrolyte effect is supposed to be an effect of electrostatic intermolecular interactions between molecules in the system. Polyelectrolyte effect may be caused by increase of the electrostatic screening length or interparticle coupling which occurs with decreasing concentration. However some conformational changes are also taken into account i. e. following dilution of the system coil expansion of a linear polyelectrolyte.[119] Sometimes a third, "intermediate" mode appears. The origin is like in case of slow mode not explained yet but may appear due to the hydrophobic domains.[110]

The polyelectrolyte solution can be investigated with low molecular weight salt addition. To screen interactions. If the samples with low molecular mass salt addition are investigated, three areas can be distinguished when looking at the dynamic behavior. A one process area for $\lambda \ll 1$, where λ is so called transition point and is defined as

$$\lambda = H \frac{C_p}{C_s}, \quad C_p \text{-polymer concentration,} \quad C_s \text{-salt concentration,} \quad H \text{- dimensionless parameter}$$

(e.g. quaternization degree).

The second area is the so called transition regime, where $\lambda \approx 1$, followed by a two diffusion modes regime with $\lambda \gg 1$. Under sufficient salt concentration only one diffusion mode is present. Approaching the transition regime, the diffusion coefficient value increases with increasing λ and the slow mode gradually appears. For higher polymer concentrations fast and slow mode are present.[113-117]
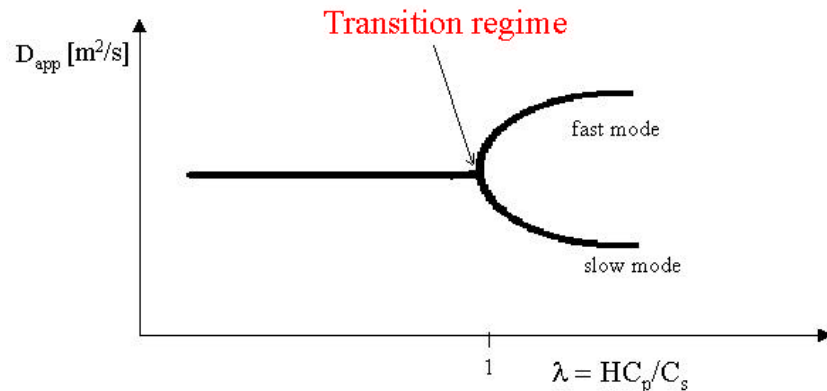
Figure 11. Diffusion behavior for polyelectrolytes.

The nature of the diffusion modes in polyelectrolyte solutions is still a matter of discussion. However, from the theory, the positive slope or lack of the slope of diffusion coefficient

versus scattering vector square indicates diffusive behavior. Negative slopes of the diffusion coefficient versus scattering vector square are known for the fast mode and postulated to be due to movement of polyelectrolyte segments coupled with counterions.[114]

B: RESULTS
I. Synthesis of ionenes

All ionenes used in the experimental part have been synthesized via the Menschutkin's reaction between α,ω−alkanediamines and α,ω−dibromoalkanes. The synthesis of I-2,5-MeBr (I25MeBr, I25) and I-6,5-Me-Br (I65MeBr, I65) has been performed in an organic solvent (DMF/methanol mixture). The yield of reaction was in both cases more than 90 per cent. See Appendix for the details. We synthesized the following ionenes: I65MeBr (M_w=39000 g/mol), I65MeBr$_{lower\ molecular\ mass}$ called here also I65MeBr$_{(1)}$ (M_w=29150 g/mol) and I25MeBr (M_w=23700 g/mol). Molecular masses were measured by static light scattering and viscosity, discussed in chapter 5.

II. System compounds characterization
II.I. Ionenes-polymer characterization
1.NMR

The NMR analysis is the first analysis which is done during the synthesis procedure. It allows to decide about the end point of the synthesis and about a purity of synthesized compounds.

The NMR spectra of the I65MeBr is presented in Fig.1 (for I65MeBr) and Fig.2 (for I25MeBr).
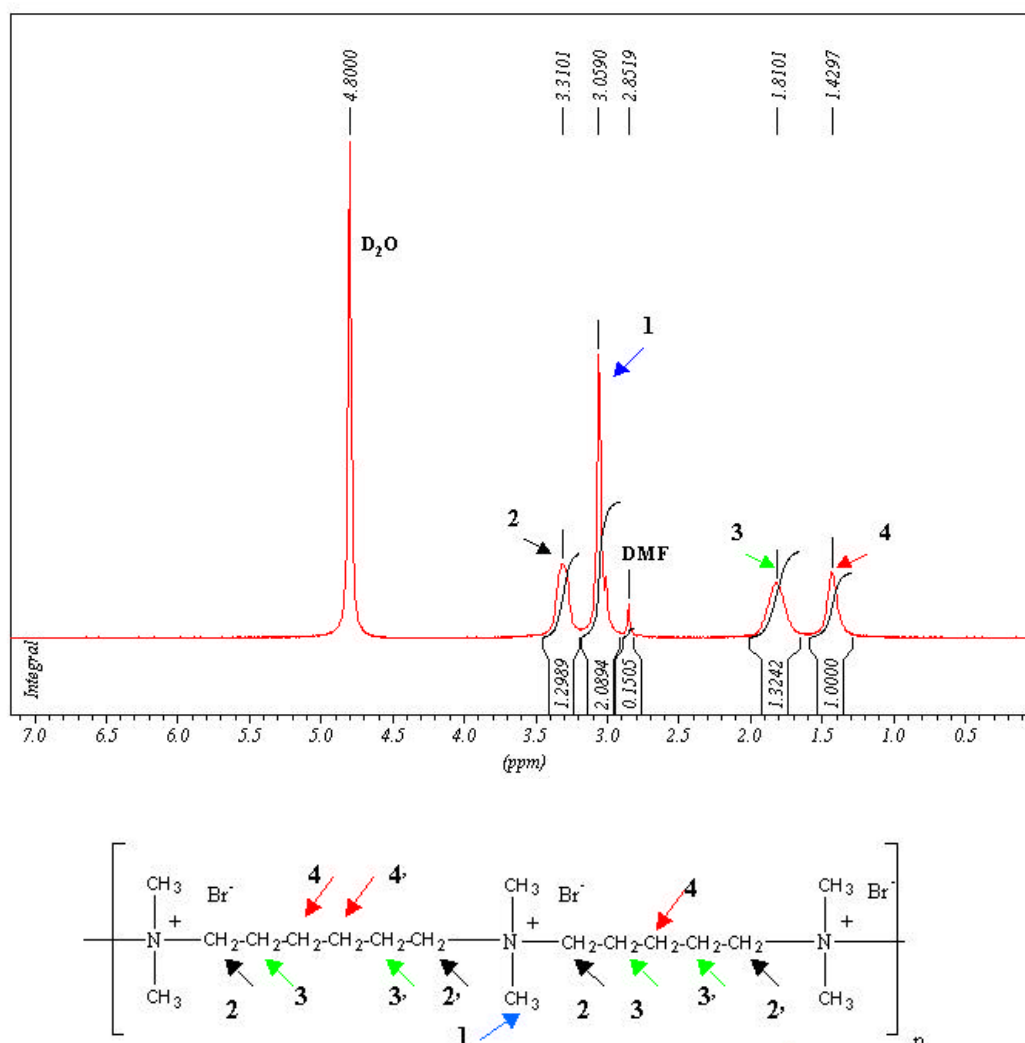
Fig.1: ^{1}H NMR spectra of I65MeBr in D$_2$O.
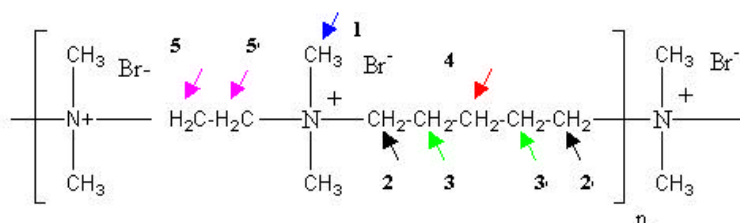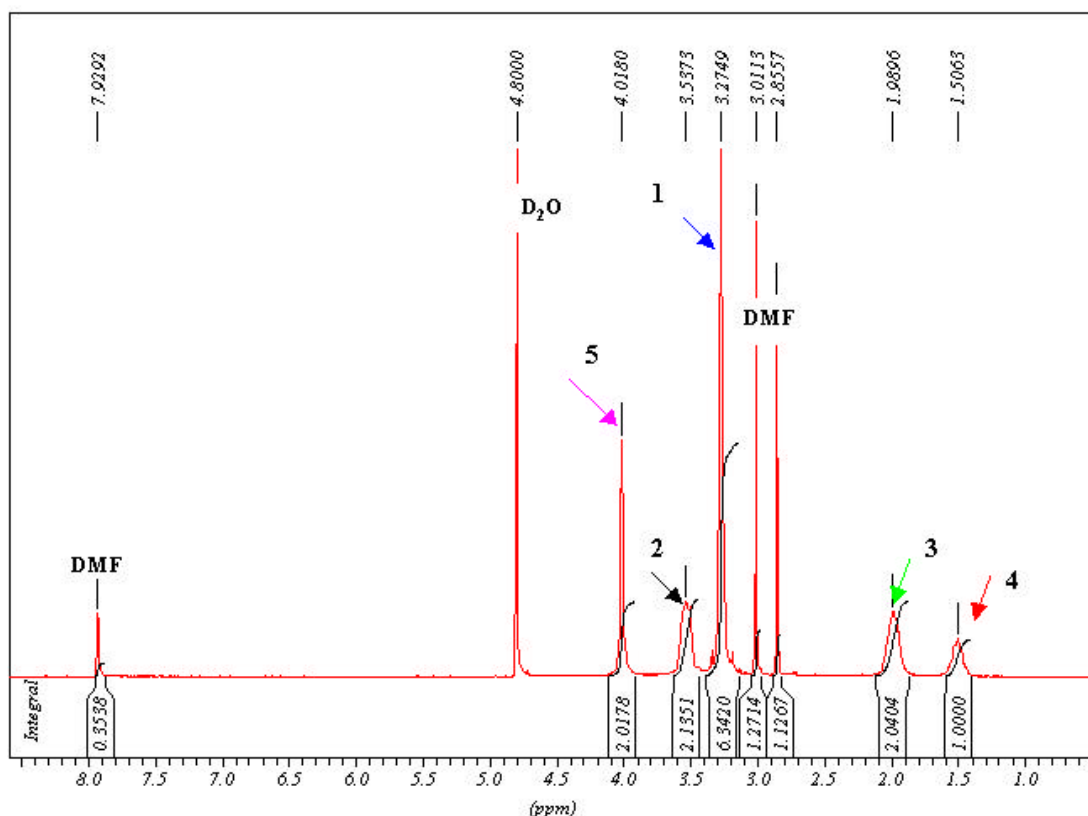
Fig.2: ^{1}H NMR spectra of I25MeBr in D$_2$O.

I25MeBr contains vestigial amounts of DMF.

2.pH- characteristics

pH measurement is one of the basic analysis which was performed to understand the nature of the compounds used later for self-assembly systems. The pH value as a function of concentration is shown in Fig.3 for I65MeBr, in Fig.4 for I65MeBr$_{(1)}$. Fig.5 shows the pH value dependency for the I25MeBr. The average pH value of I65MeBr is equal pH$_{aver}$ = 7.6 (based on the data in Fig. 3). The concentration of [H^{+}]$_{aver}$ = 10^{-pH} = 2.5 10^{-8} M in that case, i.e. [OH^{-}]$_{aver}$ = 4 10^{-7} M.
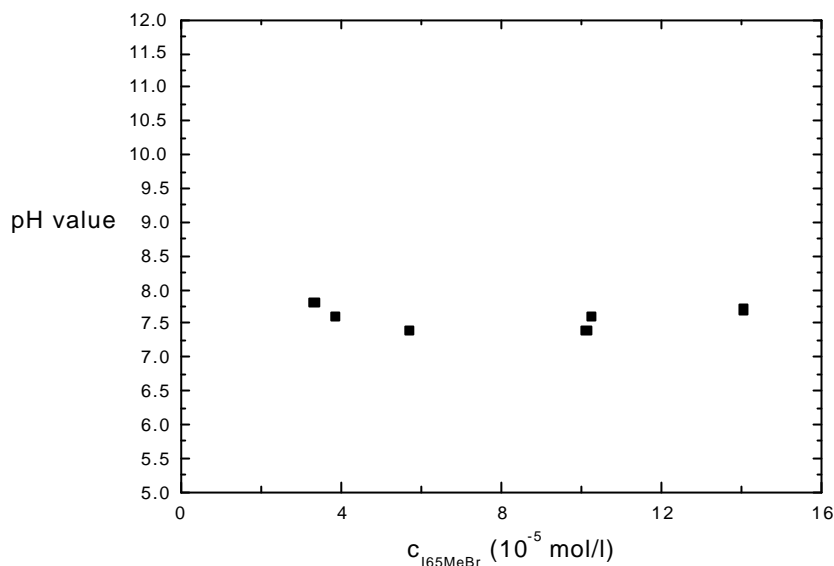
Fig.3. pH value for I65MeBr as a function of concentration

$pH_{aver(1)} = 7.8$ equals for the lower molecular mass I65MeBr, which gives $[H^+]_{aver(1)} =$ $= 1.6 \ 10^{-8}$ M. $[OH^-]_{aver(1)} = 6.1 \ 10^{-7}$ M. Values calculated for the data in Fig.4.
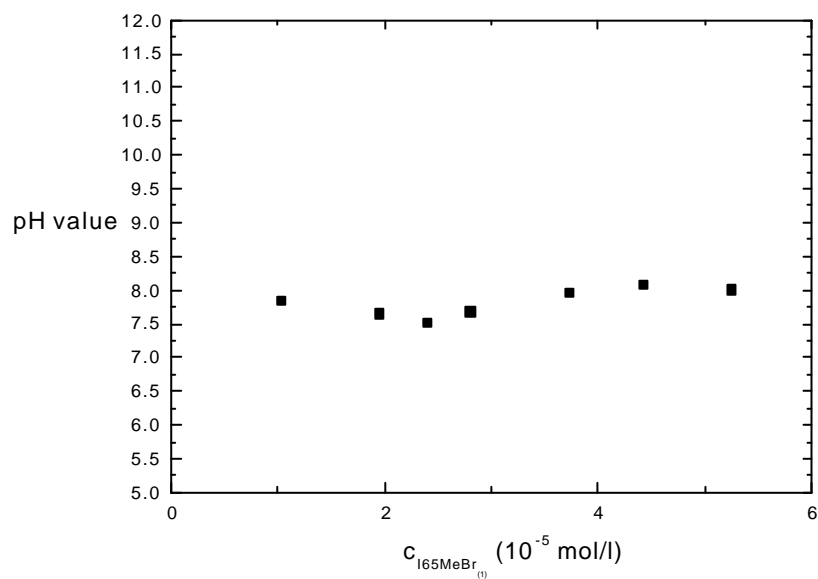
Fig.4. pH value for I65MeBr$_{(1)}$ (lower molecular mass
polymer) as a function of polymer concentration.

In case of I25MeBr, the average pH value is equal $pH_{aver} = 7$. Calculated for the data in Fig. 5 $[H^+]_{aver} = 10^{-7}$ M and $[OH^-]_{aver} = 10^{-7}$ M.
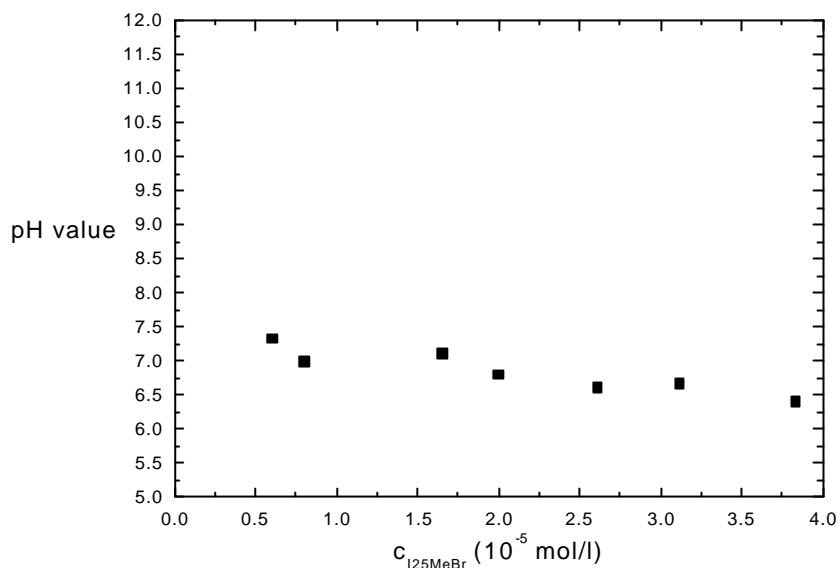
Fig.5: pH value for I25MeBr as a function of concentration

The pH of pure water used for the sample preparation was equal 7. Based i.e. on the pH measurements, we are able to investigate the complexation properties of molecules. (See chapter III). The sample concentration within an investigated concentrations range does not influence the dissociation of quaternary ammonium groups on the polymer chain. The ionene pH value almost does not change with the concentration. Also the molecular mass of the polymer does not influence the pH value significantly. I65 of the molecular mass of 39 000 g/mol possesses an average pH value of 7.6. $I65_{(1)}$ of the molecular mass equal 29 150 g/mol possesses the average pH value of 7.8. In the case of I65 and $I65_{(1)}$ mentioned already, the linear polymer charge density is equal 1 charge per nm. In the case of I25 (average pH value around 7), the charge density is higher, 1.5 charges per nm. The charge density influences the dissociation of ionene quaternary ammonium groups. The highest charge density, the lowest dissociation degree. That is why the pH value of strongly charged I25 is slightly lower than those of I65.

3.Viscosity

To characterize the polymer itself viscosity measurements have been performed. Casson and Rembaum for the first time investigated the viscosity for ionene samples. They found that the viscosity decreases with increasing concentration of added, low molecular weight salt.[74,75] The reduced viscosity reaches a plateau at 0.4M KBr or KNO_3. Upon further increase of salt concentration the reduced viscosity stays constant. Ionenes I-6,6-Me-Br and I-3,4-Me-Br were investigated in 0.4M KBr and 0.4M KCl. The reduced viscosity observed increases linearly with increasing polymer concentration, and the parameters "K" and "α" were calculated by Casson and Rembaum $K_{KCl} < K_{KBr}$. High value of K indicates bad solvent condition.
Casson and Rembaum calculated the reduced viscosity in salt free ionene solution according to the Fuoss equation:

$$\frac{\boldsymbol{h}_{sp}}{C_p} = \left(\frac{A}{1 + Bc_p^{1/2}} \right) + D$$

The experimental relationship between A and the molecular mass for I-3,4-Me-Br is given by the expression $A = 3.1 \ 10^{-7} \ M_v^2$ and for that case $B = 0.77 \ M_v^{-0.58}$, for I-6-Me-Br $A = 2.3 \ 10^{-7} \ M_v^2$ and
$B = 0.04 \ M_v^{-0.82}$. During the A-parameter estimation Casson and Rembaum expect about 20% error bar.[89-91]

3.2. Results

Before the measurement of each concentration 300 s waiting time is applied. The flow time measurement is repeated five times for every concentration.
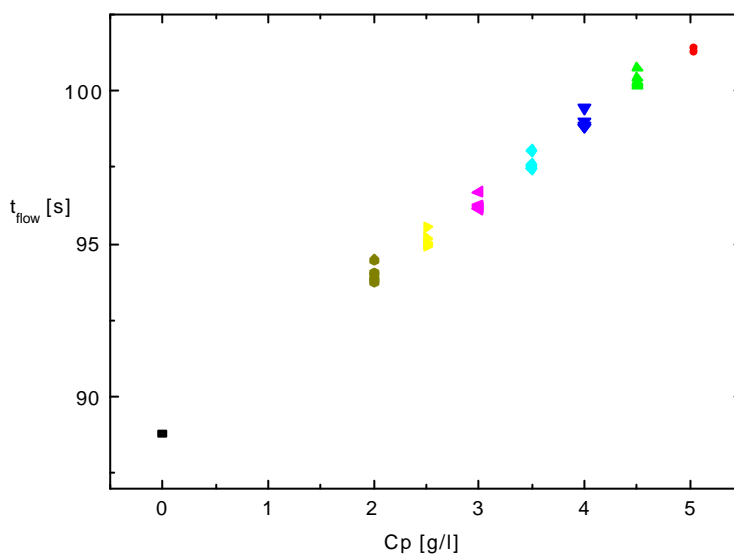
Fig.6: Time required to flow through the capillary as a

function of the I65MrBe sample concentration.

Symbols of one color belong to the same sample

(with non-constant flow time).

Solvent flow time: black symbol.

For every sample a variation of the flow time is observed (Fig.6). Although for the second sample series the waiting time foregoing next concentration is prolonged to 600 s, the results are not better. Still instability in the flow time is observed. To measure a third sample series we choose the waiting time of 7200 s foregoing every concentration change.
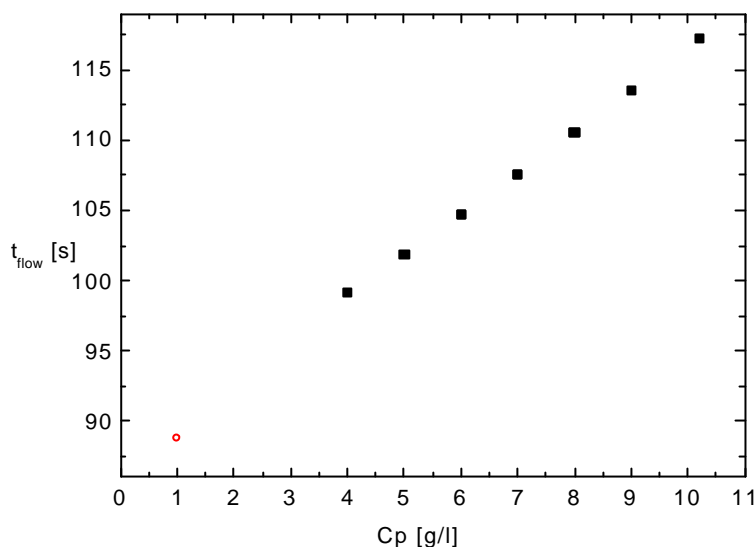
Fig.7. Time required to flow through the capillary
as a function of the I65MrBe sample concentration.
Waiting time prefacing each concentration: 2h.
Red symbol: solvent flow time, black symbols:
sample flow times.

The flow time was again measured five times for every sample. This time no variation has been observed (compare Fig.7). When waiting time of 300 s before every concentration change has been applied, the intrinsic viscosity could not be obtained. The statistic of these measurement is bad. Waiting time of 600 s gives better statistic of the measurements but still the fluctuation in the flow time are observed. Waiting time of 7200 s before each concentration is long enough to get the repeatable results. Intrinsic viscosity $[\eta] = 0.29$ is obtained (see Fig.8). Fig.8 shows reduced viscosity as a function of polymer concentration.
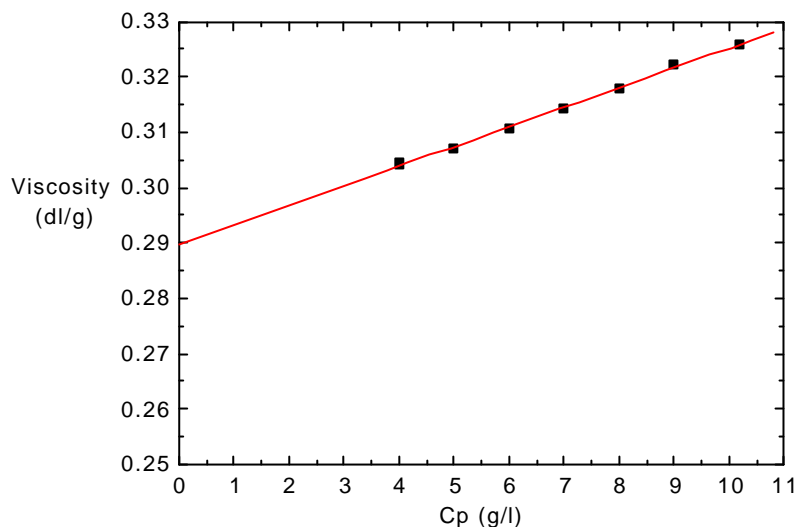
Fig.8. I65MeBr solution reduced viscosity as a function

of ionene concentration.

The viscosity average molecular mass M_v was calculated. Parameters K and a were taken from Casson and Rembaum for I-6-Me-Br. K= 6.22 10^{-4}, and α=0.58 Intrinsic viscosity $[\eta] = 0.28960$ dl/g.

If:

$$M_v = \left\{ \frac{[\eta]}{K} \right\}^{1/a}$$

The calculated viscosity average molecular mass is M_v = 39 000 g/mol.

Sample flow time may not enclose fluctuations and has to be repeatable for all runs measured for one concentration. This is the case of 2h waiting time before the next concentration is measured. The determined viscosity average molecular mass M_v stays for I65MeBr in good agreement with the M_w value obtained from SLS (see paragraph 5). Additionally it is known from the literature, that α values between 0.5 and 0.8 indicate random coil morphology of an investigated molecule.[118]

3.3. Comments on the viscosity measurements

The dilution of ionene solution requires long stabilization time before the new equilibrium is reached. With 300 s waiting time between two measured concentrations, no reproducible flow time was observed. 7200 s waiting time is sufficient and good reproducibility is obtained.

Strong electrostatic interaction is present in the system without salt addition. High ionic strength of the sample (0.4M KBr) is required to diminish the interaction and measure viscosity behavior analogous to neutral polymers.

Viscosity is a relative method to obtain the molecular mass but in case of I-6,5-Me-Br gives results which are in good agreement with results obtained from the absolute method (SLS).

The viscosity average molecular mass calculated for I-6,5-Me-Br may contain an error. The K and α value used for the calculation was obtained from I-6-Me-Br by Casson and Rembaum. I-6-Me-Br differs from I-6,5-Me-Br by one (-CH$_2$) for every polymer unit. To establish K and α

exactly for our system, the molecular mass from an absolute method has to be known for samples with different degree of polymerisation and of low polydispersity. However the polymerisation method for ionenes is a polycondensation reaction that typically gives broad molecular mass distribution of the product and fractionation is difficult due to strong polyelectrolyte nature of the product. However in case of I-6,5-Me-Br viscosity average molecular mass and molecular mass obtained from static light scattering were in good agreement. Determination of viscosity average molecular mass for I25MeBr is not possible. The parameters K and α included in I65MeBr molecular mass calculation can not be used for I25MeBr. I25MeBr is similar in morphology to I65MeBr, however constitutes of another chemical body.

4. Gel Permeation Chromatography (GPC)

The aim of GPC measurement is to find the molecular weight and polydispersity of ionene I65MeBr and I25MeBr. Results are collected in Table 1. GPC measurement is difficult for charged particles due to their interactions with the column material. The lack of an appropriate standard for the measurement of ionene complicated the measurement additionally. GPC is a relative method for the measurement of the molecular mass of substances and requires high morphological and chemical identity between standard and an investigated substance. It is difficult sometimes to find such a standard. For the ionene analysis common standards like PEO, PQVP, PSSNa or PMANa are not suitable. There are discrepancies between the morphology and chemistry of ionenes and these substances. During the polylelectrolyte measurements the interaction between polymer and column can be regulated via the solvent selection. In case of ionene measurement we tried different solvents, different standards and columns. The most successful standard was polysaccharide, "pullulan[*]" (-1,4'- ;-1,6'-Glucan), compare Fig.9 and as a solution ammonium formate (HCOONH$_4$) 9g/l aqueous solution. Pullulans have strictly linear chain structure, since they are synthesized by micro organisms.
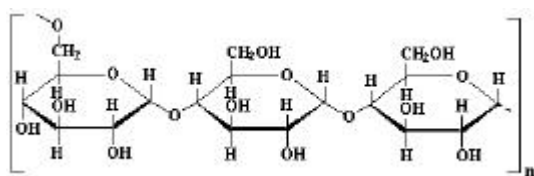
Fig.9: Pullulan

The calculation of molecular mass is presented in Fig.10 and Fig.10a.
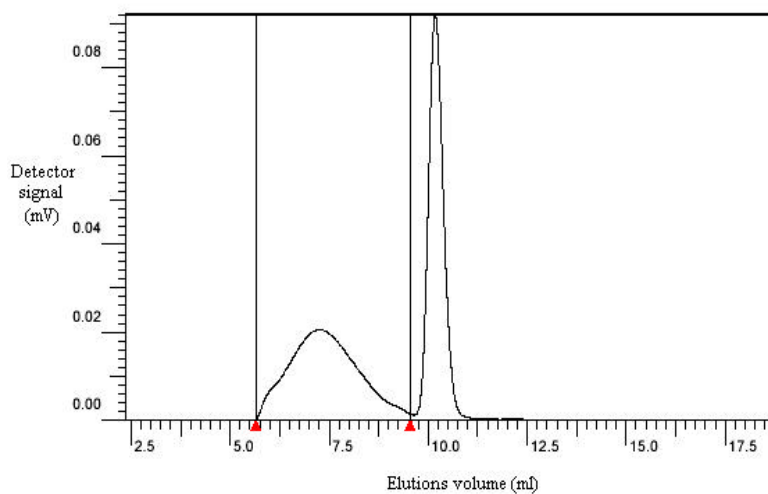
Fig.10. Detector signal as a function of the elution volume
for the sample I65MeBr.
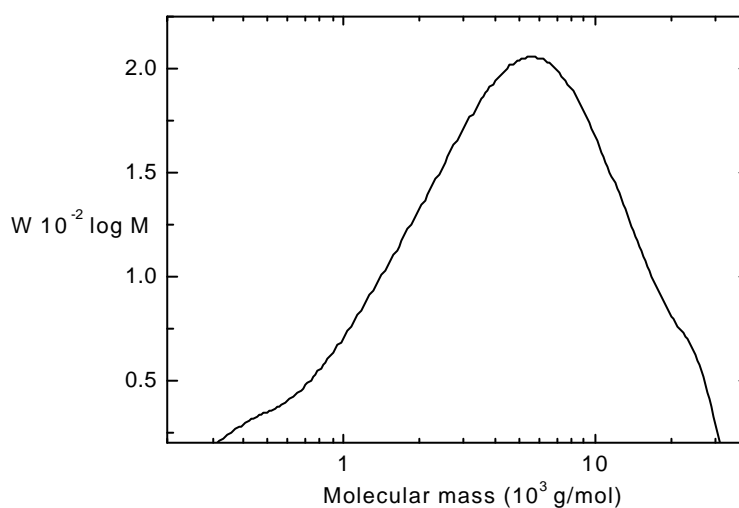
Fig.10a. An example of the molecular mass calculation for
the sample I65MeBr according to the GPC measurement.
Obtained M_w = 73756 g/mol.

For the details of measurement see Appendix. In the Table 1 molecular masses from GPC are compared with molecular masses from SLS. For the details of SLS analysis see subchapter 5.

Tab.1: Molecular weight comparison

Ionene	GPC			SLS	MwGPC/MwSLS
	Mw g/mol	Mn g/mol	Polydispersity	Mw g/mol	
I65MeBr	73756	34485	2.1	38650	1.9
I65MeBr	72729	33051	2.2	29150	2.5
I25MeBr	36965	22733	1.6	23700	1.5

Finally, molecular masses obtained are approximately two times higher than the molecular masses calculated from static light scattering. This can be due to the aggregation of ionene in the solution (dimers) or due to the interactions of ionene with the column. High ionic strength used eventually for screening interaction between ionene molecules may destroy the column, that is why we can not use i.e. 0.4 M KBr aqueous solution, which is suitable during light scattering analysis. Another problem arises if the column material is slightly positively charged. The repulsion between column fulfillment and ionene abbreviate an elution time. As a result ionenes are eluted from the column "earlier", what causes higher molecular mass values. For further calculations we will use the molecular masses obtained from the SLS analysis.

5.Scattering techniques

Scattering techniques as it was mentioned in the theoretical part of this work allow to find the molecular mass (SLS) of the compounds as well as the structural parameters (i.e. radii of gyrations from SLS, and hydrodynamic radii from DLS) can be calculated. Additionally second virial coefficient A_2 (from SLS) allows to predict the quality of the solvent in relationship with the investigated macromolecules.

5.1. Static Light Scattering (SLS)

Static scattering techniques take advantage of the Zimm analysis for an average molecular weight calculation (Fig.11-19). First calculation of the molecular mass of ionenes will be presented. For the calculation of molecular mass, samples with different concentration of ionene must be prepared. To avoid the interaction in the system samples in 0.4 M aqueous potassium bromide solution were chosen.
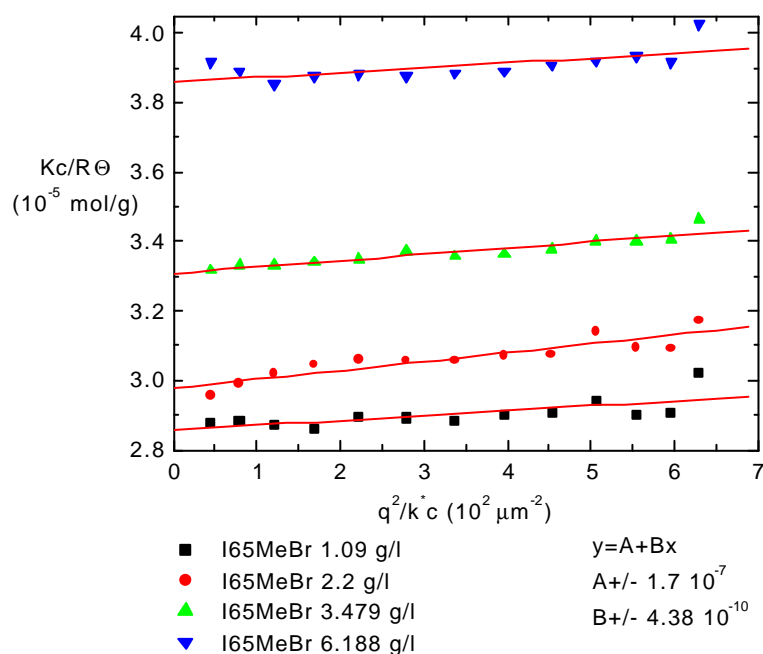
Fig.11. Zimm plot for I65MeBr.

For each measured concentration $\dfrac{Kc}{R\Theta}$ was extrapolated to zero scattering vector (Fig.11) and the intercepts were considered. From the slope of fitting line in Fig.12 second virial coefficient A_2 was calculated and from the intercept $1/M_w$.
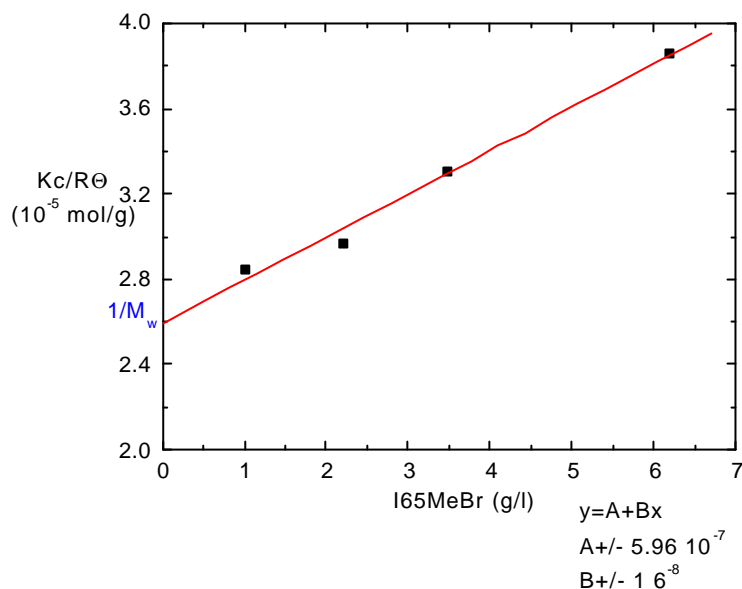
Fig.12: Zimm plot for the sample containing I65MeBr.

It is possible as well to calculate the radius of gyration (R_g) for each sample concentration (from the slope of fitting lines on Fig.11) and then to find an average radius of gyration (Fig.13). However the size of investigated molecules is close to the lower limit measurable by LS dimensions so the R_g calculation may contain a significant error (more than 20%).
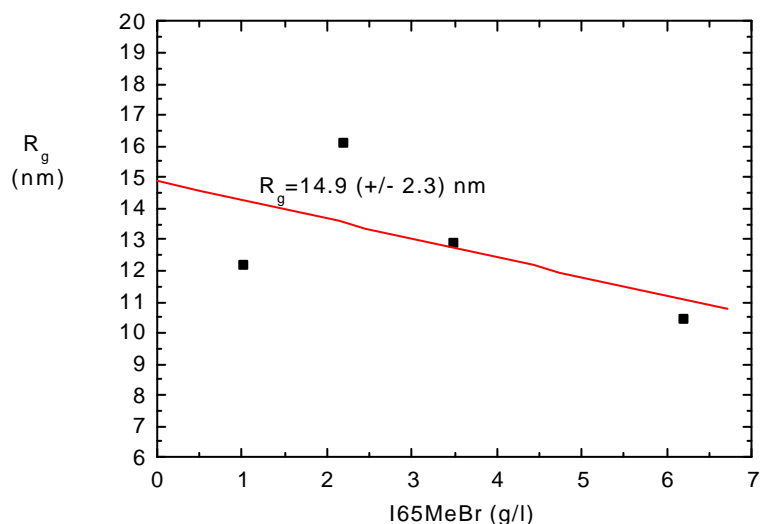
Fig.13 Radius of gyration for I65MeBr

Similar like for I65MeBr (Fig.11-13) the procedure to calculate the molecular mass is valid for the molecular mass calculation of I65MeBr$_{(1)}$ and for the I25MeBr (Fig.14-19).
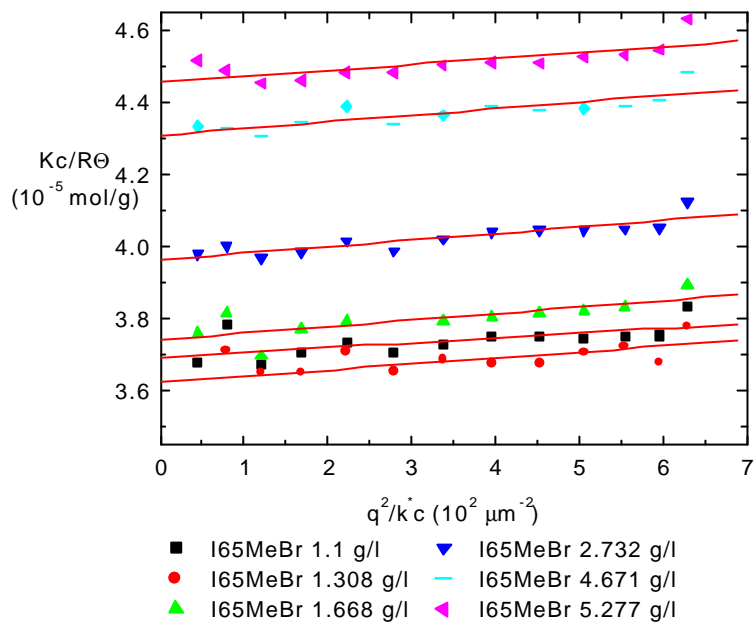
Fig.14: Zimm plot for the sample I65MeBr$_{(1)}$.
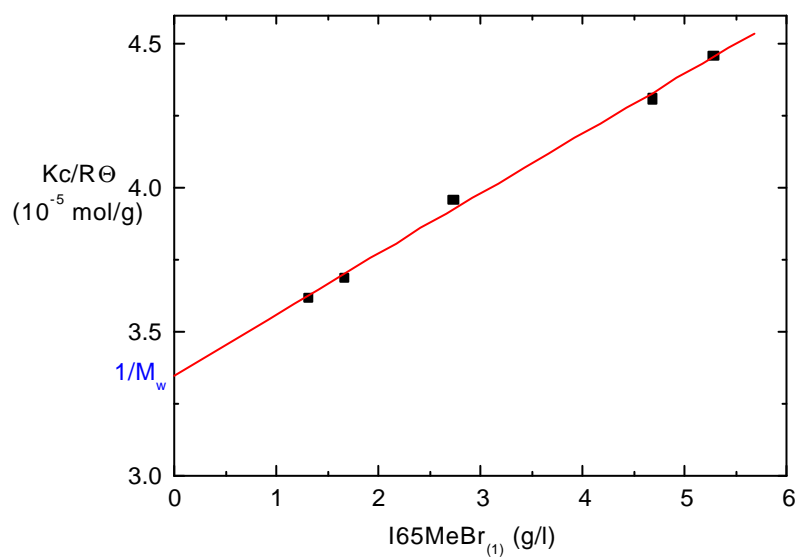
Fig.15: Zimm plot for the sample I65MeBr$_{(1)}$.
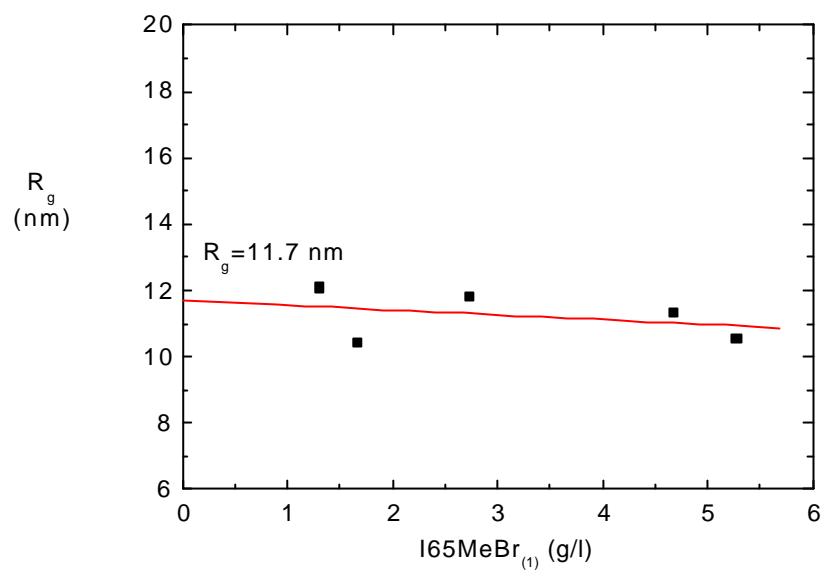
Fig.16: Radius of gyration for I65MeBr$_{(1)}$
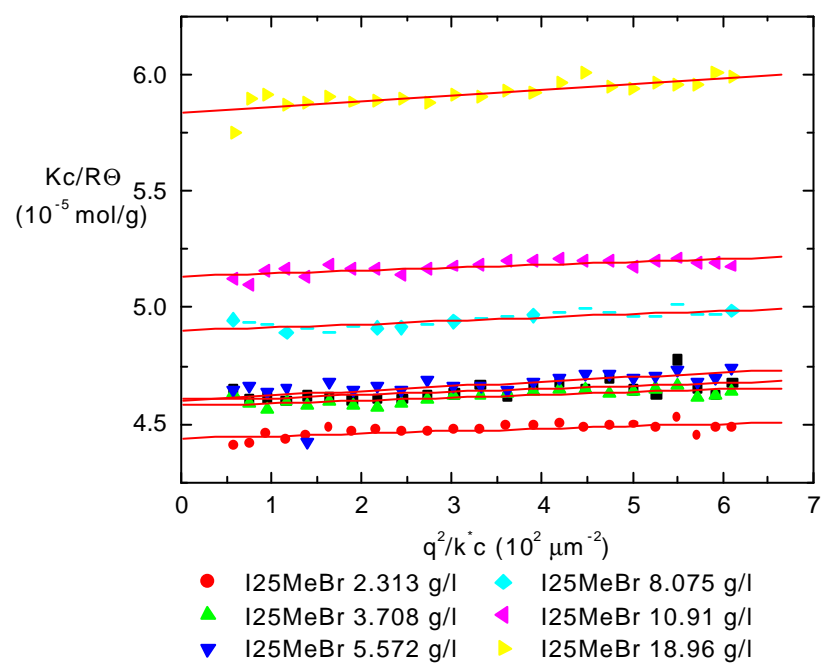
Fig.17: Zimm plot for I25MeBr
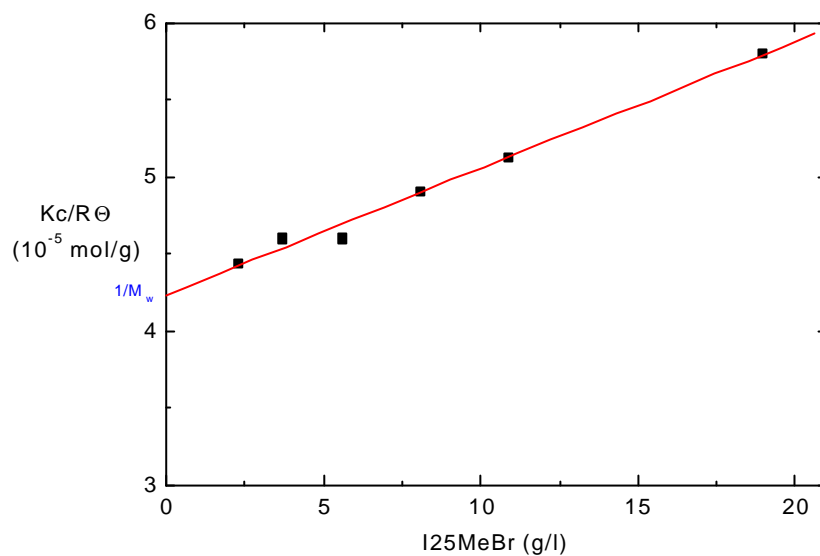
Fig.18: Zimm plot for I25MeBr
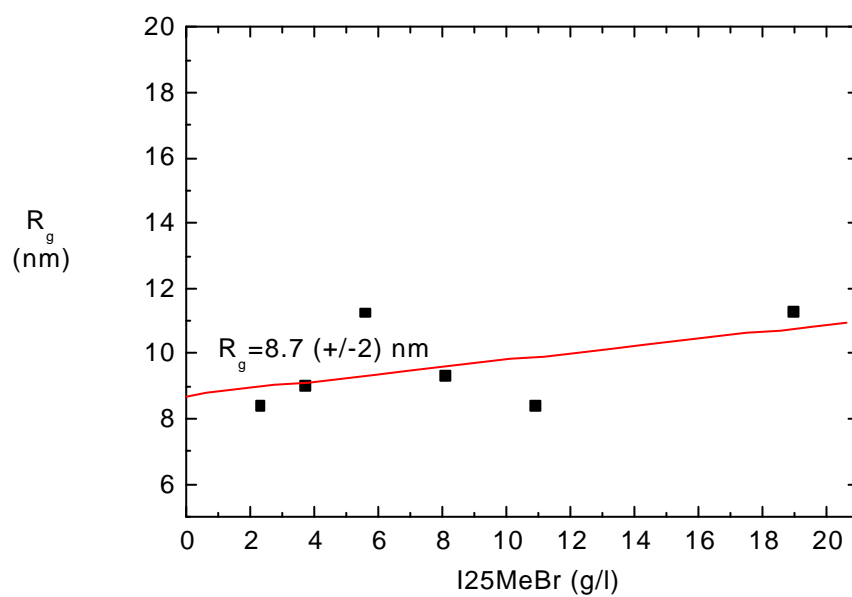
Fig.19: Radius of gyration for I25MeBr

5.2. SLS for ionene- comments

Values collected in Tab.2 have been obtained by the evaluation of static light scattering data.

Tab.2: Parameters calculated from SLS

IxyMeBr	Mw (mol/l)	A2 m3/mol	Rg (nm)
I65MeBr	38610	2.00E-06	14.9
I65MeBr (lower mass)	29150	2.10E-06	11.7
I25MeBr	23700	8.19E-07	8.7

The table contains average molecular weights calculated from the Zimm plot for I25MeBr and I65MeBr, second virial coefficient values and radius of gyration values. The radius of gyration values are suspected to contain a relatively large experimental error, due to the low intensity when ionene solutions are measured and due to the ionene dimension near to the lower detectable limit. Molecular weight of ionenes have been estimated. The accuracy of calculations equals M_w+/-2%, A_2+/-1% and R_g+/-15%. KBr containing water is a good solvent for ionenes, the second virial coefficient (A_2) has positive value.

5.3. Dynamic Light Scattering (DLS)

The ionene samples were investigated by the dynamic light scattering as well. As a solvent 0.4M aqueous KBr has been used. For all measured samples one diffusion mode was observed, as expected under screening by low molecular mass salt. The diffusion coefficient dependency found is almost independent on the concentration of the sample(Fig.20-21). The hydrodynamic radius has been calculated base on the Stoks-Einstein relationship, compare chapter IV in the theoretical part.
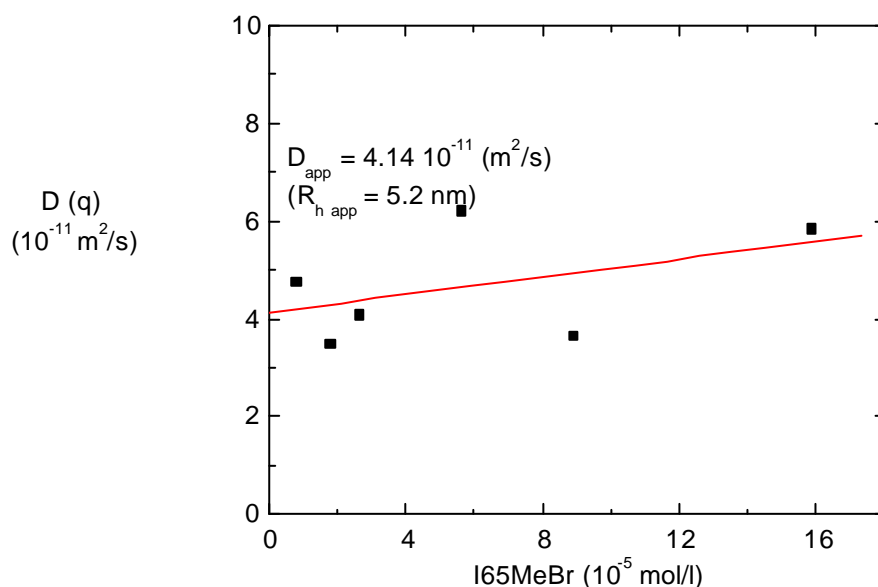
Fig.20: I65MeBr diffusion coefficient presented as

a function of ionene concentration. Concentration

of I65MeBr ranges from 0.302 to 6.188 g/l.

As a solvent 0.4 M KBr aqueous solution is used.

$D_{app} = 5.29 \ 10^{-11} \ (m^2/s)$
$(R_{h \ app} = 4.3 \ nm)$
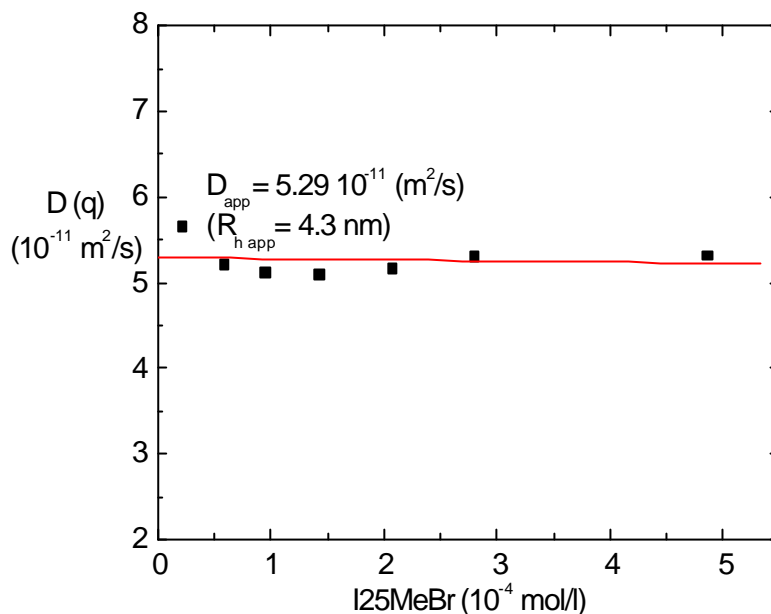
Fig.21: I25MeBr diffusion coefficient as a function of
ionene concentration.

5.4. SLS/DLS

In Table 3 parameters calculated for ionenes I65MeBr, I65MeBr of lower molecular weight and I25MeBr are collected. Calculation was performed based on the static and the dynamic light scattering experiment.

Tab.3. Parameters calculated for ionenes based on the LLS experiment.

IxyMeBr	Mw (mol/l)	A_2 m^3/mol	Rg (nm)	Rh (nm)	Rg/Rh	Monomers per chain	Charges per chain
I65MeBr	38610	$2 \ 10^{-6}$	14.9	5.24	2.84	322	+ 322
I65MeBr $_{(1)}$	29150	$2.1 \ 10^{-6}$	11.7	5.3	2.2	240	+ 240
I25MeBr	23700	$8.2 \ 10^{-7}$	8.7	4.3	2.2	254	+ 254

The R_g/R_h ratio indicates random coils in good solvent. The literature value of ρ parameter (R_g/R_h ratio) calculated for an ideal random coil case (linear, polydisperse chain) is 2.05. The deviation from such a value can be caused by the low resolution level as compared to the molecular weight of an investigated polymer. In addition, the scattering intensity of investigated samples was low.

6. Additional comments on the ionene analysis

When some simplifications are assumed and certain models taken into account (here "valence angle chain") it is possible to estimate the following parameters given in the Tab.4.

Tab.4: Parameters calculated for the ionenes base on the valence angle chain.

Substance	N	l (nm)	Ree (nm)	Rg (nm)	Rc (nm)	Number of charges per chain, n	Charge density, per unit length, d (1/nm)
I65MeBr	161	1.974	35.4	14.4	318	322	1
I65MeBr(1)	120	1.974	30.6	12.5	237	240	1
I25MeBr	127	1.358	21.6	8.8	172.5	254	1.5

N is the number of monomers, l- the length of monomer, R_{ee} is end to end distance, R_g is the radius of gyration. R_c means contour length. The parameters are taken/calculated as follow:
[-C-C-] bond length 154 pm
[-C-N-] bond length 147 pm

$$R_{ee} = \sqrt{2N}\,l$$

$$R_g = \sqrt{\frac{N}{3}}\,l$$

$$R_c = Nl$$

$$d = \frac{n}{R_c}$$

Good agreement is obtained between calculated values of R_g (Tab.4) and the values obtained from SLS (Tab.3). However, the calculated radius of gyration value depends on the model chosen, here valence angle chain.

II.II. Dendrimers - polymer characterization

To investigate the complexes, components of the system must be investigated in advance. In the chapter II.I the data analysis of ionenes has been presented. The dendrimer analysis bases on the pH measurement and dynamic light scattering.

1. Dependency of pH on dendrimer concentration
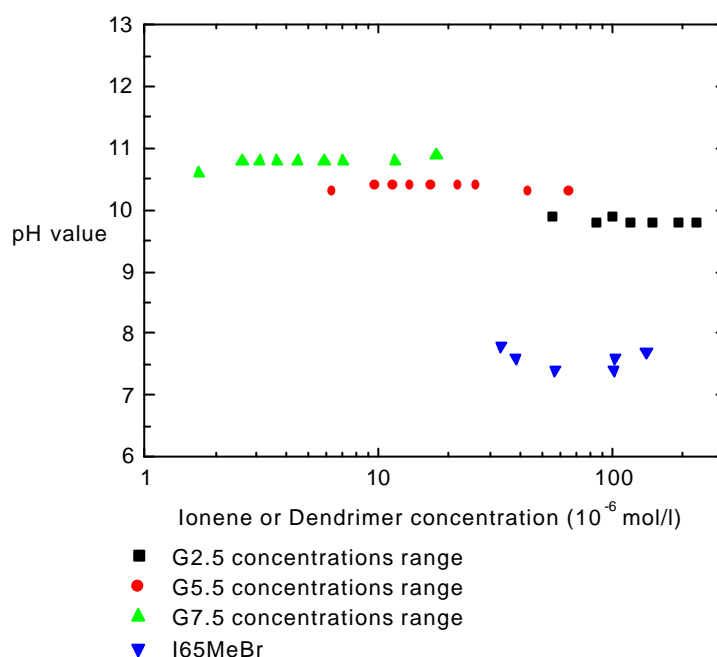
Fig.22: pH value as a function of charge ratio for different

PAMAM dendrimer generations

In the investigated range of concentration the pH changes for the dendrimer only slightly as compared to the changes of ionene pH over investigated concentration range, see Fig.22. The dendrimers are terminated with COONa groups after dissociation in aqueous medium giving alkaline pH. The pH of poly(phenylene) dendrimer generation G1 solution is acidic and equal 6.1. The samples containing G1 with ionenes were prepared only for fixed concentration of the dendrimer and ionene concentration range. Average pH values for the dendrimers are as follows: $pH_{averG2.5} = 9.8$, $pH_{averG5.5} = 10.4$, $pH_{averG7.5} = 10.8$.

Tab.5. Dissociation parameters of PAMAM dendrimers calculated based on the

concentration c, surface group numbers n and pH measurements. $[OH]_{max} = c \, n$,

$[H]_{max} = c \, n$, $[OH] = 10^{-pOH}$, $[H] = 10^{-pH}$, α is the dissociation degree.

Generation	c (mol/l)	Surf. group nr., n	$[OH]_{max}$	pH	pOH	[OH]	α
G2.5	$1.46 \, 10^{-4}$	32	$4.7 \, 10^{-3}$	9.8	4.2	$6.3 \, 10^{-5}$	0.99
G5.5	$1.36 \, 10^{-5}$	256	$3.48 \, 10^{-3}$	10.4	3.6	$2.5 \, 10^{-4}$	0.93
G7.5	$4.5 \, 10^{-6}$	1024	$4.6 \, 10^{-3}$	10.8	3.2	$6.31 \, 10^{-4}$	0.86
Generation	c (mol/l)	Surf. group nr., n	$[H]_{max}$	pH	pOH	[H]	α
G1	$1.056 \, 10^{-4}$	48	$5.1 \, 10^{-3}$	6.1	-	$7.94 \, 10^{-7}$	1

There are –COONa groups on the surface of the PAMAM dendrimer. Such groups are built from a weak acidic (COO$^-$) and a strong base (NaOH). To calculate the degree of dissociation of PAMAM dendrimers we have to include pOH instead pH. We compare the concentration of hydroxyl group $[OH]_{max}$ calculated based on the total dendrimer concentration and the number of surface groups on the dendrimer molecule with the concentration of hydroxyl groups $[OH]$ calculated based on the pOH. From that comparison the degree of dissociation α of the dendrimer molecule can be estimated (see Tab.5). The inner amine groups of PAMAM dendrimers are not taken into account, since they are not protonated significantly at alkaline pH. We found that small (G2.5) generation of PAMAM dendrimer are more dissociated than the larger ones (G7.5), which is in agreement with literature.[45] The dendrimer dissociation degree modulated additionally via ionic strength after linear polyelectrolyte addition gives rise to a complexation reaction between PAMAM dendrimer and ionene. For the details see chapter 7.

2. Dynamic light scattering of poly(phenylene) dendrimers

First we consider the interplay of interactions in the "pure" dendrimer G1, i. e only the dendrimer in aqueous solution without low molecular weight salt added. We have investigated the 1.056 10^{-4} M solution of G1 by dynamic light scattering. The data obtained show a positive slope of the diffusion coefficient versus square of the scattering vector. The apparent hydrodynamic radius is obtained by the extrapolation to zero scattering vector. The resulting hydrodynamic radius $R_{h\ app}$ is equal 21.7 nm. For comparison see Fig. 23. The dendrimer structures however must be smaller than 21.7 nm, which is confirmed by calculations based on bond length and the structural formula. From the simulations the dimension of one dendrimer molecule is equal 4.5 nm.
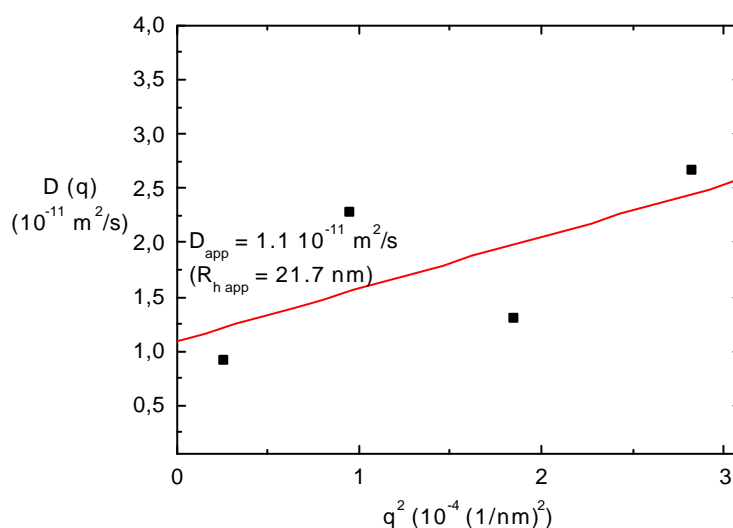
Fig.23: Diffusion coefficient as a function of scattering vector square for G1 water solution of the concentration 1.056 10^{-4} M

Normalized Intensity Correlation Function $g^2(\tau)$ and distribution of radii (here for 90° chosen as an example) are presented in Fig.24 and 25.
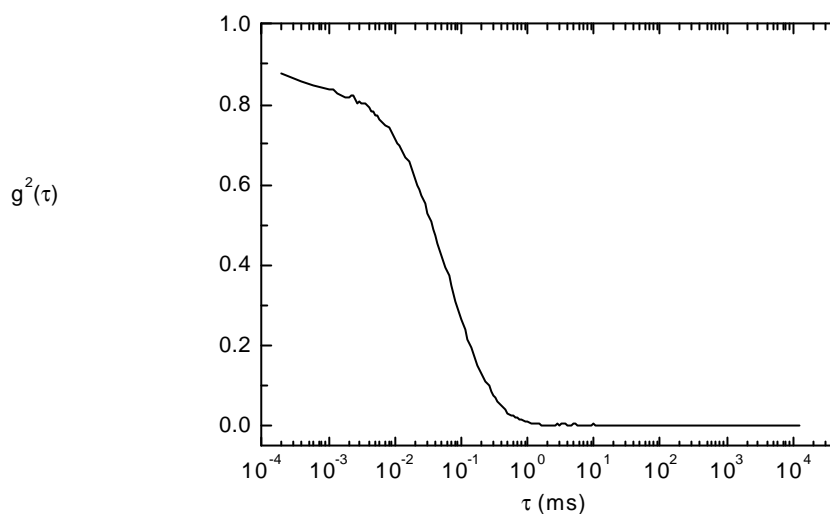
Fig.24: Normalized intensity correlation function for
G1 1.056 10^{-4} M (angle: 90°).
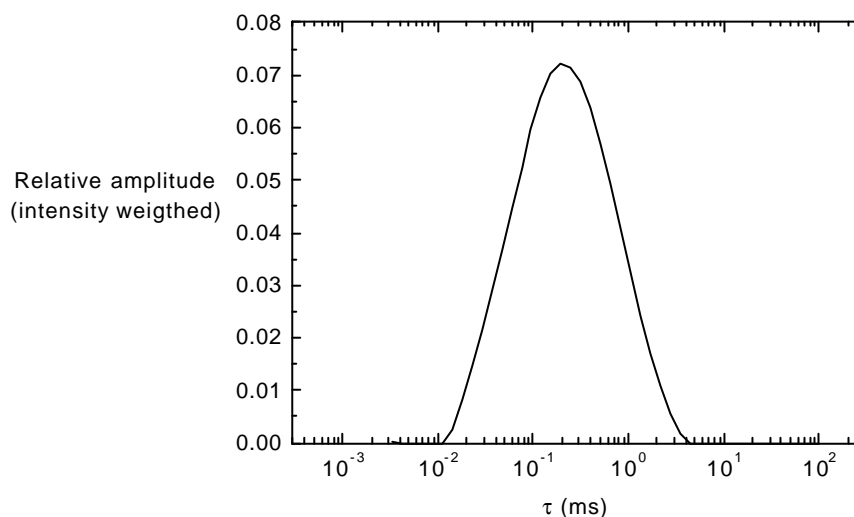
Fig.25: Distribution of the decay times for 90° measurement.
G1 sample concentration is equal 1.056 10^{-4} M

One diffusion mode is observed, however the distribution of the decay times is broad and translates into a broad hydrodynamic radii distribution. The diffusion behavior is more complicated. Such distribution of radii may be caused by a mixture of different particle sizes in the solution or by polyelectrolyte effect. This can be due to aggregations: small dendrimers can form bigger aggregates. Big particles can be also formed from smaller aggregates. Another explanation of such phenomena could be due to the polyelectrolyte effect. As discussed in theory chapter 3, the slow mode observed in polyelectrolytes diffusion, the origin of which is still under discussion, may be due to the formation of "domains" or a "plasma" of many polyelectrolyte molecules moving cooperatively. We investigate our samples with small

molecular weight salt addition to confirm or to exclude the presence of the particles of radii mentioned above as well as to confirm or to exclude polyelectrolyte type effect interactions.

For flexible PAMAM dendrimers of generation 2 (32 charged surface groups) we know that the 0.4M aq KBr is sufficient to screen the interactions between dendrimer molecules and to enable the measurement of the behavior of single dendritic molecule (see next subchapter). In case of stiff G1 (48 charged surface groups) it seems to be not sufficient. The sample is "by eye" clear (opalescence not observed) and in the laser beam one can always distinguish two modes corresponding to the R_h= 150 nm ($1.46 \cdot 10^{-12}$ m^2/s) and R_h= 4.65 nm ($3.87 \cdot 10^{-11}$ m^2/s). Slow and fast mode almost do not depend on q^2 value (Fig.26).
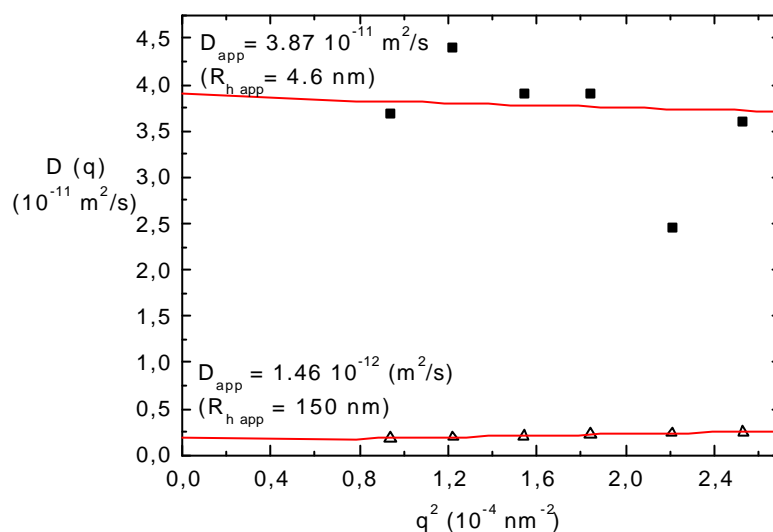
Fig.26: Diffusion coeficient as a function of scattering

vector square for $1.056 \cdot 10^{-4}$ mol/l G1 in 0.4M KBr.

Observations of fast and slow mode under addition of low molecular weight salt confirm presence of aggregates of dendrimer molecules in aqueous solution. The slow mode can be due to the movement of aggregates formed by several dendrimer molecules and the fast mode could be observed due to the movement of single dendrimer. The hydrodynamic radius calculated for the fast mode is additionally well comparable with the value mentioned before calculated from computer simulation (4.5 nm) (the simulations have been done as a part of another dissertation[138]). These observation supports the theory of two species present in the solutions with small molecular mass salt added. One of them is the pure dendrimer of the radius around 4.5 nm, the second one is the aggregated state of the radius around 150 nm (see Fig. 26). The observation of alone dendrimer molecule in aqueous solution is not possible due to this aggregation. The size of the aggregates is in the order of 22 (without low molecular weight salt addition) to 150 (with salt addition) nm.

3. Dynamic Light Scattering of the PAMAM dendrimers generation 2.5, 5.5 and 7.5

Experiments were performed under high ionic strength of the solution (KBr addition). 0.4M aqueous KBr solution is sufficient to screen the interaction between dendrimer molecules in the solution and to derive hydrodynamic radii of dendrimer molecules (Fig.27-29). We begin with G2.5. The hydrodynamic radius found for that generation is equal 2 nm (see Fig. 27).
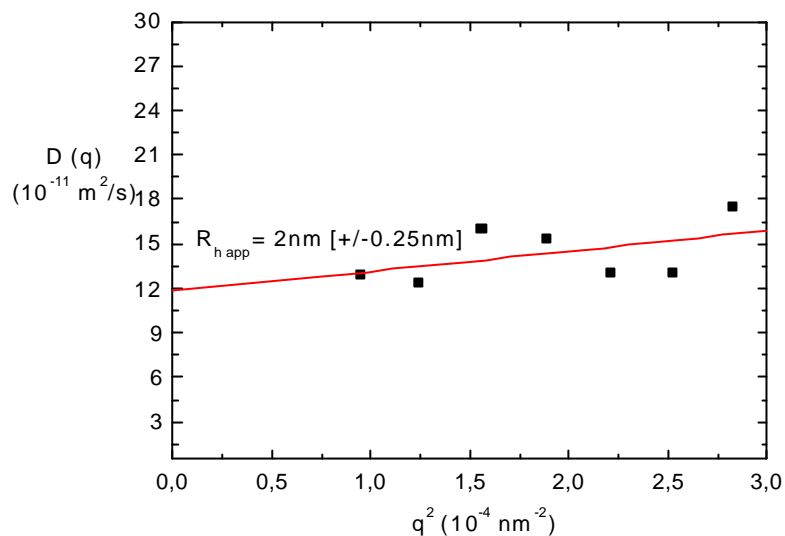
Fig.27: Diffusion coefficient as a function of the scattering vector square for G2.5 1.909 10^{-4} M in 0.4M aq KBr

D_{app} = 1.17 10^{-10} (m^2/s) [+/- 2.2 10^{-11}) (m^2/s)]

In case of fifth generation of carboxyl-terminated PAMAM dendrimer the hydrodynamic radius of 3.7 has been found, see for comparison Fig.28.
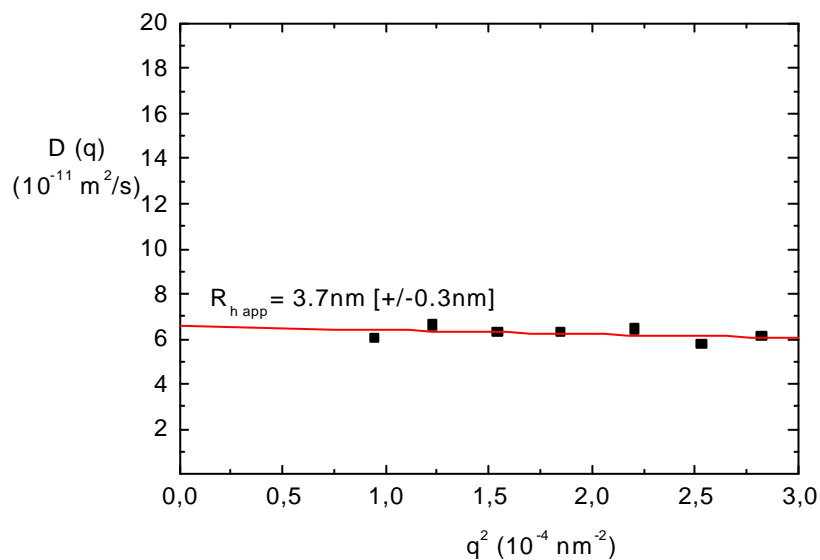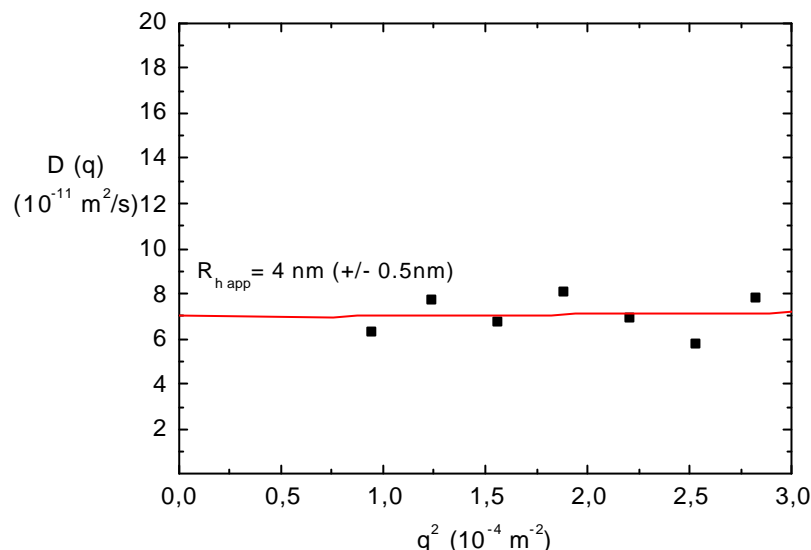

Fig.28: Diffusion coefficient as a function of the scattering vector square for G5.5 (2.187 10^{5} M) in 0.4M aq KBr.

D_{app} = 6.8 10^{-11} M (m^2/s)[+/-1.1 10^{-11} M (m^2/s)]

Surprisingly no big difference in hydrodynamic radii between fifth and seventh generation has been found. The hydrodynamic radius for G7.5 equals approximately 3.5 nm.

Fig.29: Diffusion coefficient as a function of the scattering vector square for G7.5 2.86 10^{-6} M in 0.4M aq KBr.

D_{app} =6.9 10^{-11}) (m^2/s) [+/- 1.1 10^{-11} (m^2/s)]

It was almost no slope observed in the dependency of the diffusion coefficient on the scattering vector square in all of three investigated cases (see Fig. 28-29). Thus, there is no influence of the intermolecular structure due to interactions on the diffusion behavior observed here in the solution under high ionic strength condition. It also indicates that there is no large polydispersity.

4. Comments on the dendrimers analysis

PAMAM G2.5 possesses lower hydrodynamic radius than G5.5 and G7.5. This result is expected because of the lower molecular mass for G5.5 than for G7.5 (given by the producer). Tab.6 sumarizes results of the dendrimer measurements done, the information provided by the producer and the information taken from the literature. In the systems containing poly(phenylene) dendrimers one can always expect aggregations additionally connected after further ionene addition. The calculated dimensions of PAMAM dendrimers -COOH surface terminated (e.g. G5.5) are comparable with the dimensions calculated for appropriate –NH$_2$ terminated generations e.g. G5. Thus the measured dimension of "full" and surface terminated generation must be comparable. Based on this assumption, we are able to construct Tab.6. R_g(lit) values given in the Tab.6 obey "full" PAMAM generations: G2, G5, G7 respectively.

Tab.6: Parameters of the dendrimers

Dendrimer	Mw g/mol	Number of surface groups	R_h nm (DLS)	R_g(lit.) nm for	R_g/R_h
G1	9418	48	aggregates	not applicable	not applicable
G2.5	6267	32	2	0.92 (MC)	0.46
G5.5	52901	256	3.7	2.43 (sans)	0.66
G7.5	212739	1024	4	3.44 (sans)	0.86

Taken from the literature, experimental value of R_g(lit) for G2 has been calculated according to Monte Carlo (MC) method by Maiti et. al.[126] The values of R_g(lit) for G5 and G7 have been measured (SANS, SAXS) by Topp, Tomalia and Amis.[128-129] No information about the R_g/R_h ratio of PAMAM dendrimers in the literature is found. The size and shape of the PAMAM dendrimers are mostly predicted based on the experimental methods. AFM (Atomic Force Microscopy) on PAMAM dendrimers have been studied by J. Li et. al.[130] AFM images of the dendrimers on mica surface indicate that lower generations (up to G4) are dome-shaped instead of being spherical. This was confirmed by the computer simulation made by Goddarad and coworkers.[131] They found highly asymmetric shapes for generations G1 to G3 and nearly spherical shapes for generations G5 to G7. The generation G4 is the transition form between highly asymmetric and spherical structures. The results of the computer simulation by Goddard et. al. have been experimentally confirmed by Turro, Tomalia and coworkers. [132]

The ratios of R_g/R_h we have calculated, indicate in case of G2.5 loose structure, without any special e.g. hard sphere-like or star-like shape. The values of R_g/R_h between 0.3 to 0.6 suggest loose, so called microgel structure.[125] In the case of G5.5 and G7.5 the value of R_g/R_h suggest a spherical form of the molecule. The theoretical value of R_g/R_h equal 0.778 indicates homogenous hard sphere.[125] The deviations of the R_g/R_h values calculated in the Tab.6 for G5.5 and G7.5 from the theoretical one are 15% and 3% respectively. This deviations can be caused by the different experimental conditions e.g. solvent, low molecular mass salt addition, temperature etc. used in our experiment as compared to the experiments of Topp, Tomalia and Amis.[128-129] The differences in R_g (for the same dendrimer generation) caused by the differences in e.g. solvent composition may range more than 10%.[128] Thus our calculations concerning dendrimer shapes within an error are in the agreement with the findings given in the literature.[126-130]

II.III. Dendrimers and ionene comparison

In the following Table 7, we summarize the data concerning ionenes and dendrimers. The molecular mass of the biggest dendrimer (G7.5) is 5.5 times higher than that for the largest ionene (I65MeBr). Whereas the radius of the biggest dendrimer is 1.5 times lower than the radius of I65MeBr. We expect that the dendrimer is a much more compact structure than the random coil of ionene in a good solvent. The R_g value of I65 according to SLS equals 14.9 nm, for lower molecular mass I65$_{(1)}$ R_g equals 11.7 nm, and finally for I25, 8.7 nm. The R_g/R_h ratio for I65 is 2.84, for I65$_{(1)}$ is 2.2, and for I25 equals 2. These values indicate random coil morphology (compare paragraph 5.1).[125]

Tab.7: Parameters of system compounds

IxyMeBr	Mw (mol/l)	Rh (nm)	Number of charges per chain, n	Charge density per unit length $\mathbf{d}$ (1/nm)
I65MeBr	38610	5.24	322	1
I65MeBr$_{(1)}$	29150	5.3	240	1
I25MeBr	23700	4.3	254	1.5
Dendrimer	**Mw g/mol**	**Rh (nm)**	**Number of surface groups**	
G1	9418	not possible	48	
G2.5	6267	2	32	
G5.5	52901	3.7	256	
G7.5	212739	4	1024	

Ionene hydrodynamic radii are generally larger than the hydrodynamic radii of dendrimers, however dendrimers posses 5 to 9 time higher molecular mass than respectively ionene I65 and I25 (Tab.7). In a rough approximation, the dendrimer molecules can be treated as a spheres and further the charges per area of the sphere can be calculated, compare Tab.8. For this we use a sphere of the radius R_h as basis, assuming this approximates best the "effective" size.

Tab.8: Parameters calculated for the dendrimers

Dendrimers	R_h (nm)	Number of charges per molecule	Area of sphere $[4\pi R_h^2]$ (nm^2)	Geometric charge per area (1/nm^2)
G1	aggregates	48	aggregates	aggregates
G2.5	2	32	50.2	0.64
G5.5	3.7	256	171.9	1.5
G7.5	4	1024	201	5.1

The calculated charge density for dendrimers differs dramatically one from each other. The density of G2.5 constitutes 10 per cent of the G7.5 surface charge density. At this point calculated number of charges per unit area (see Tab.7) must be compared to the percentage of really dissociated surface groups. Per analogy to the chapter 4 (in theoretical part) we call the calculated number of charges per unit area "geometric charge", and the number of really dissociated surface groups as concluded from pH, "effective charge". The pH measurement (data collected in Tab.5, paragraph 1) provides information of the percentage of really dissociated dendrimer surface groups equals around 99% for G2.5, 93% for G5.5 and around 86% for G7.5. For single G2.5 molecule the number of effective charges equals (99% 32) = 31.7, for G5.5 (93% 256) = 238, for G7.5 (86% 1024) = 881 under condition like in Tab.5. Now the effective surface charge density can be obtained. In case of G2.5 it is 31.7/50.2 = 0.63 charges per nm^2, in case of G5.5 238/171.9 = 1.38 charges per nm^2 and finally for G7.5 881/201 = 4.38 charges per nm^2. The effective charge density is slightly lower than the geometric one in case of G5.5 and G7.5. For the case of G2.5 almost all surface groups are dissociated, and the effective surface charge density is equal geometric one, compare Tab.8. Such difference between the geometric and an effective charge density can be a result of counterion condensation on the dendrimer surface. Additionally the dissociation degree of polyelectrolytes and so their surface charge density or relatively their linear density is influenced by several factors i.e. solvent, pH, temperature. We expect strong charge density influence on the ionene/dendrimer complex formation.

III. & IV. Complexation
III.I. Complexation between ionenes and flexible dendrimers

1. Introduction

Complexes built by the association of COO⁻ terminated PAMAM dendrimers and ionenes were investigated. We used three dendrimer generations: G2.5 (32 surface COO⁻ groups), G5.5 (256 surface COO⁻ groups), G7.5 (1024 surface COO⁻ groups) and two species of ionenes: I-6.5-Me-Br (322 positively charged groups per chain) and I-2.5-Me-Br (255 positively charged groups per chain).

In order to obtain a first indication and overview about complex formation we measured pH value and transmission (by means of UV-spectroscopy) as a function of concentration and charge ratio for all our systems, i.e. ionene/dendrimer-complex samples and the solutions of pure ionene and pure dendrimer in water. After that results of scattering techniques, ζ-potential measurements and potentiometric titration will be presented. The data for pH measurement, turbidity, and diffusion coefficient from the light scattering measurements are presented in most cases as a function of charge ratio.

The idea of sample preparation for the following work was to investigate different parameters influencing complex formation, e.g. ionene and dendrimer concentration, molecular masses of compounds, charge densities of used species, etc. During the measurements it turned out that *charge ratio* is important to describe it. The idea to use charge ratio was initiated in the literature on polyelectrolyte complexes.[133-135] In this paragraph we show that charge ratio is a reasonable parameter for data presentation based on pH experiment. Charge ratio means the ratio of molar concentration of ionene charges to the molar concentration of dendrimer charges $\frac{C_{IxyMeBr}}{C_{Gm.n}}$. The formation of self-assembly structures depends i.e. on the charge ratio of complexing species. The charge ratio range was kept constant for all sample sets. The charge ratio as a mutual (common for all sample series) parameter, allows to compare well these sample sets. Besides dealing with the charge ratio we are "independent" on the sample concentration and can compare samples of different concentration. When using charge ratio to describe pH, dependencies basically correspond to simple "titration curves". Thus is very obvious to use this parameter here. However, also when using charge ratio to present other experimental phenomena such as turbidity or diffusion coefficient, dependencies are also more obvious (see Fig.30, Fig.31).
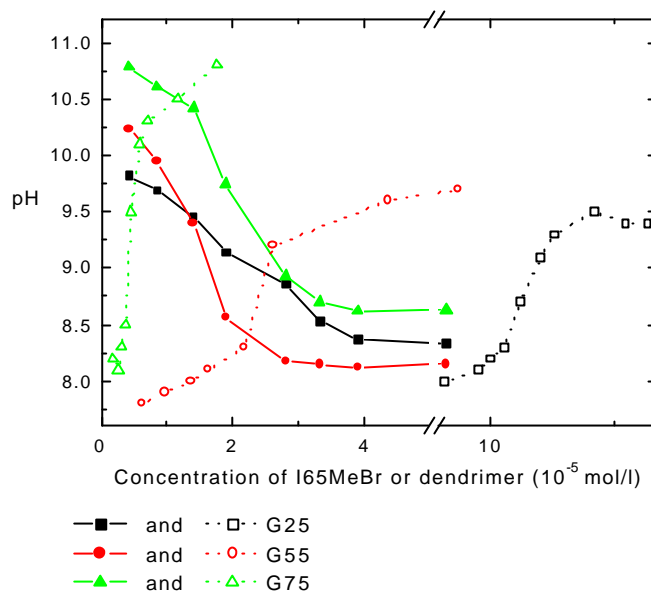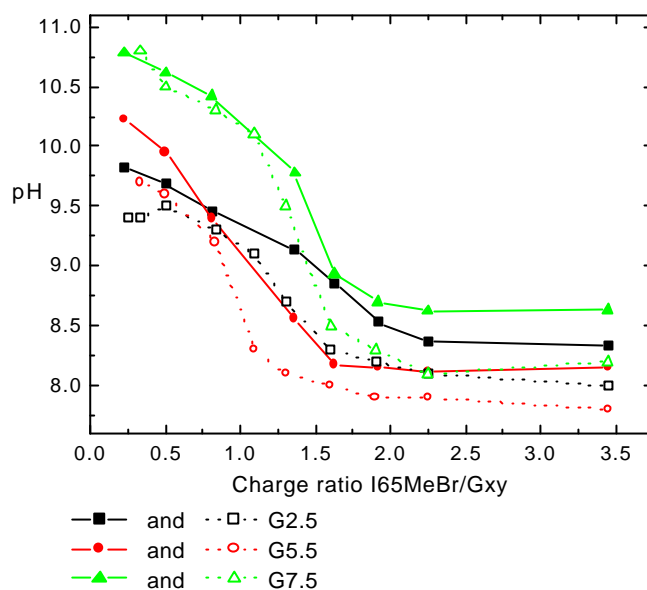
Fig.30: pH-value as a function of concentration

Full-filled symbols for constant Gxy concentration

G2.5 equal $1.909 \cdot 10^{-4}$ M; G5.5 equal $2.187 \cdot 10^{-5}$ M;

G7.5 equal $5.866 \cdot 10^{-6}$ M

Empty symbols for constant I65MeBr concentration

of $1.8 \cdot 10^{-5}$ M

For example, the dependence of pH on ionene concentration for a fixed dendrimer concentration and the pH in dependence of dendrimer concentration for a series of experiments with fixed ionene concentration is given in Fig. 30. Both data sets can be described by using the charge ratio rather than the concentration itself as parameter. Fig.31 presents the pH dependency on the charge ratio. The similarity of the pH profiles is observed. Additionally those similarity is better to identify in Fig.31 (pH as a function of the charge ratio) than in Fig.30 (pH as a function of concentration).

Fig.31: pH-value as a function of charge ratio

Full-filled symbols for constant Gx.y concentration

G2.5 equal 1.909 10^{-4} M; G5.5 equal 2.187 10^{-5} M;

G7.5 equal 5.866 10^{-6} M

Empty symbols for constant I65MeBr concentration

of 1.8 10^{-5} M

III.I.A. Complexes without low molecular weight salt addition.
1.UV-vis

The first observation after mixing two (or more) compounds is the behavior of transparence/turbidity, and whether precipitation occurs.

Tab.9. Investigated samples overview.

Charge ratio Ionene/ Dendrimer	I65MeBr/ G25	I65MeBr/ G55	I65MeBr/ G75	I65MeBr/ G25	I65MeBr/ G55	I65MeBr/ G75	I65MeBr/G25	I65MeBr/ G55	I65MeBr/ G75	I25MeBr/ G25	I25MeBr/ G55	I25MeBr/ G75
	Mw_{ionene}= 39000 (g/mol)			Higher for G2.5)/Lower (for G5.5, G7.5) concentrated samples; Mw_{ionene}= 39000 (g/mol)			Mw_{ionene}= 29150 (g/mol)			Mw_{ionene}= 23700 (g/mol)		
0.25	clear	clear	clear	clear	clear	clear	clear	clear	clear	clear	clear	clear
0.333	very slightly turbid	clear	clear	clear	clear	clear	very slightly turbid	clear	clear	clear	very slightly turbid	very slightly turbid
0.5	slightly turbid	very slightly turbid	clear	very slightly turbid	clear	clear	slightly turbid	clear	clear	very slightly turbid	clear	very slightly turbid
0.833	very slightly turbid	very slightly turbid	very slightly turbid	slightly turbid	very slightly turbid	clear	very sightely turbid	slightly turbid	clear	turbid	clear	very slightly turbid
1.09	clear	slightly turbid	slightly turbid	turbid	clear	clear	clear	clear	clear	turbid	slightly turbid	very slightly turbid
1.2	very slightly turbid	very slightly turbid	turbid	turbid	clear	very slightly turbid	clear	turbid	turbid	turbid	very slightly turbid	very slightly turbid

1.3	very slightly turbid	clear	slightly turbid	turbid; stratified	clear	very slightly turbid	clear	turbid	slightly turbid white flocks	turbid	very slightly turbid	slightly turbid
1.6	very slightly turbid	clear	very slightly turbid	turbid stratified	clear	clear	very slightly turbid	clear	turbid; white flocks	slightly turbid	slightly turbid	slightly turbid
1.9	clear	clear	slightly turbid	turbid; stratified	clear	clear	very slightly turbid	clear	turbid	very slightly turbid	turbid	clear
2.25	clear	clear	very slightly turbid	turbid; stratified	clear	clear	clear	clear	slightly turbid	slightly turbid	slightly turbid	turbid/ white precipitation
3.45	clear	clear	clear	turbid; stratified	clear	clear	clear	clear	clear	slightly turbid	clear	turbid/ white precipitation

Investigated samples and the sample condition are listed in the Table 9. These table contains sample prepared only by such a way that the concentration of ionene has been varied and the concentration of dendrimer is fixed. However to investigate the systems also samples with fixed ionene concentration have been prepared.

For more quantitative characterization of turbid samples and precipitation the sample transmission is analyzed. The following graphs (Fig.32 with 33, and Fig.34 with Fig.35) of transmission indicate qualitatively the turbidity of the samples.
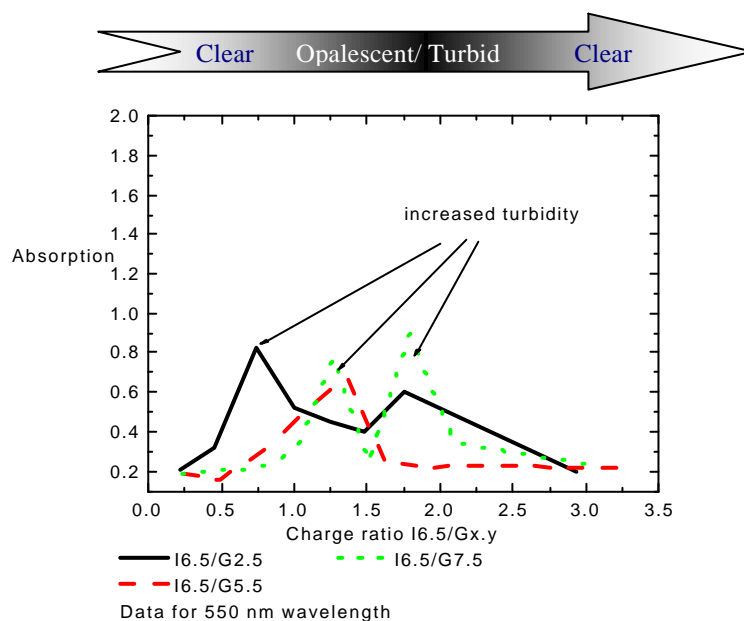
Fig.32. Samples prepared by fixed dendrimer

concentration and ionene concentration range

The maximum on the curve means absorption and therefore also turbidity is higher for certain sample as compared to the neighboring ones. This observation allows to distinguish samples where larger structures are expected that are "visible" even by eye. If macromolecular compounds are not detectable by eye, and as a result of mixing the sample becomes turbid, we expect larger assemblies of macromolecules in the solution, compare Fig.32-36.
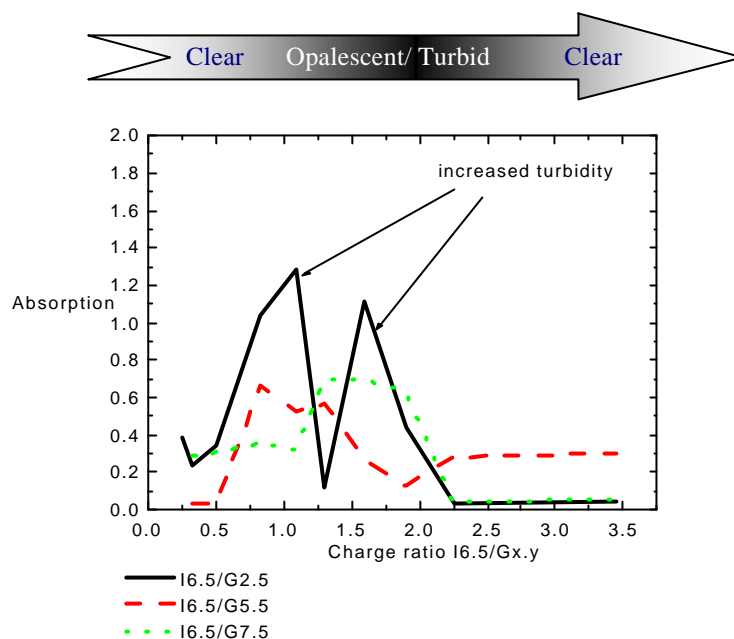
Fig.33. Samples prepared with fixed ionene concentration

and dendrimer concentration range

Higher or lower turbidity appears in case of every ionene - dendrimer sample series. It can by a consequence of aggregation. For certain samples by at least 1.5 times higher amount of ionene as compare to the dendrimer white precipitation appears, compare Fig.34, Fig.36.
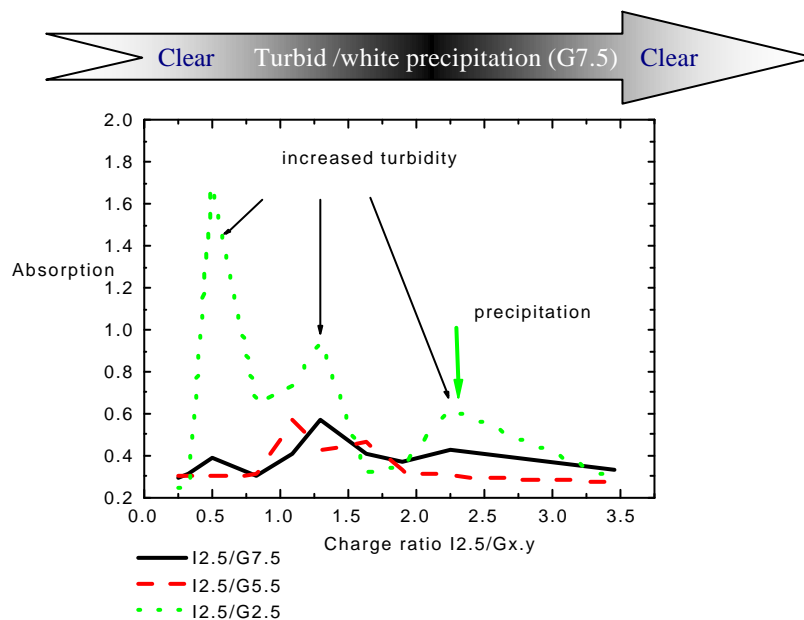
Fig.34. Samples prepared for the fixed ionene

concentration and dendrimer concentration range

The lowest turbidity level of the samples is observed for the case of ionene I25MeBr with PAMAM dendrimers. Such case is presented in Fig. 34 and 35. Only for I25/G2.5 samples the

turbidity is much higher (see Fig.34). In contrast, the intensity of the turbidity is similar for all samples I65/Gx.y. This may indicate more specific binding I25 and PAMAM dendrimers. In case of I25 and PAMAM complexes appear under certain charge ratios. The condition of I65 to the dendrimer binding seems to be less specific.
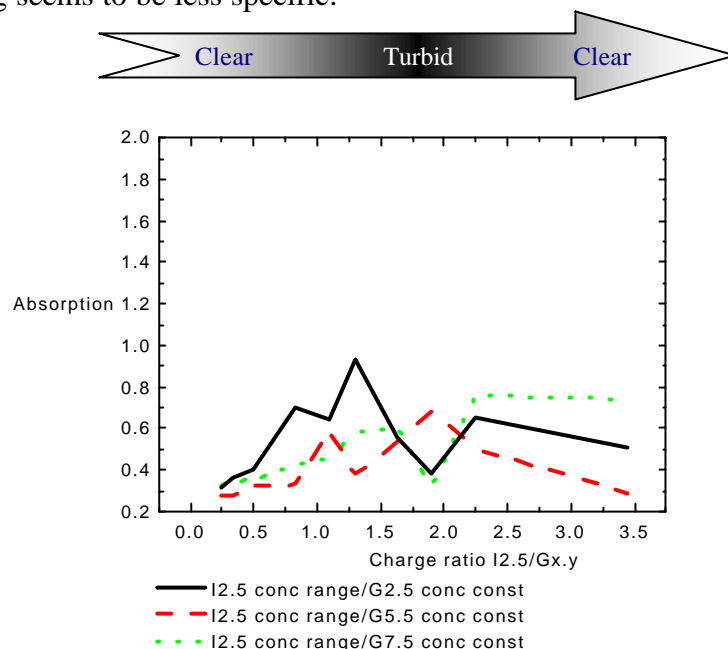
Fig.35. Samples prepared for the fixed dendrimer concentration and ionene concentration range
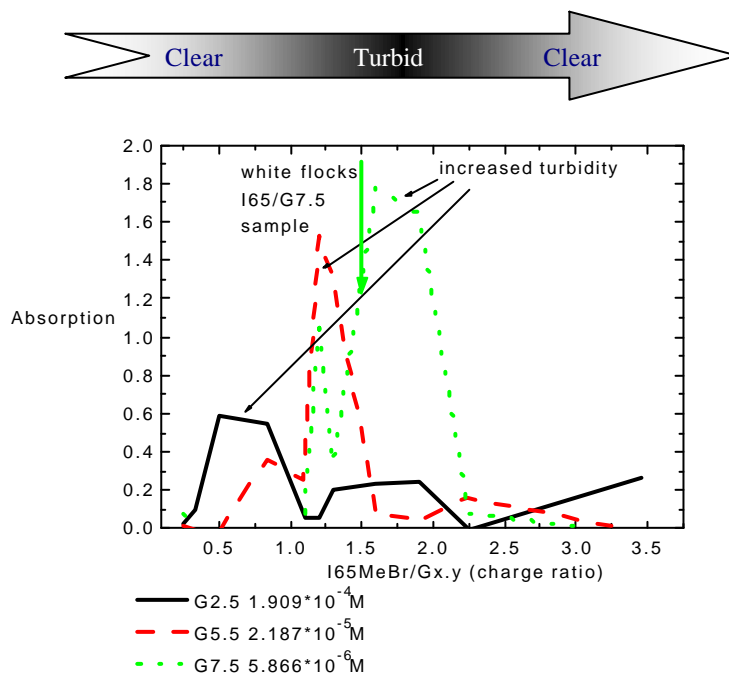
Fig.36: Conentration range of I65MeBr$_{(1)}$ with mentioned above fixed dendrimer concentration

Lower molecular mass I65MeBr used in complexes with PAMAM dendrimers gives, especially with higher dendrimer generations, strongly turbid samples, see Fig.36. These can now indicate

appearance of insoluble complexes. Such complexes may precipitate from the system and be seen as a white flocks (I65$_{(1)}$ / G7.5 system in Fig.36). The comparison of all sample series is possible when one mutual parameter is taken into account. As mentioned before, the charge ratio was chosen to compare all sample sets. The charge ratio as a parameter allows to compare samples with constant ionene and constant dendrimer concentration as well as different concentrated samples, see paragraph 1.

Summarizing, strongly absorbing, turbid samples are expected to contain larger aggregates that cause opalescence or turbidity. The pronounced change in transmission for all samples was observed between: 0.5 and 2 charge ratio of the I65MeBr to dendrimer (Gx.y). For ionene I25MeBr dendrimer the area of sample transmission changes is broader (charge ratio 0.25 to 3) than in case of I65MeBr. The change in transmission must be caused by processes happening in the sample. Transmission changes have to follow an appearance of larger aggregates in the system. We suppose not only the transmission changes are a consequence of assembly formation. I.e. pH value changes are also expected. Therefore pH-value have been measured the for the same sample series and discussed in the following chapter.

2.pH measurements

The differences in sample turbidity have to be connected with the change of other sample parameters e.g. pH. Fig.37-41 present such pH-changes observed in the systems. Both compounds of the system ionenes and dendrimers, posses alkaline pH (see Tab.5). The pH value of complexes lies always between the pH of pure dendrimer (strongly alkaline) and the pH of pure ionene (neutral to slightly alkaline). For different compound ratios the pH of the system changes strongly from basic (10< pH <11) to about 8.5> pH >7. It additionally supports the hypothesis, that the compounds of the system "neutralize" each other and build assemblies.
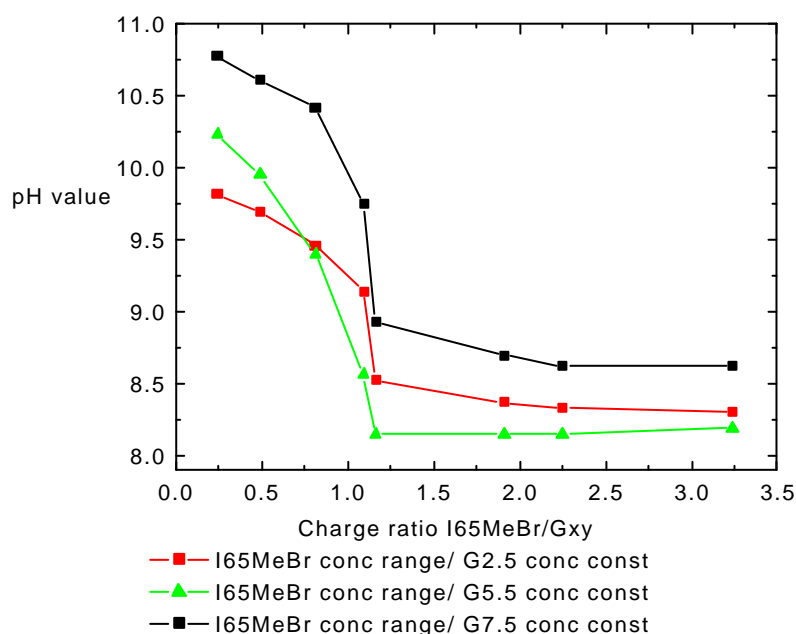
Fig.37: pH value as a function of charge ratio
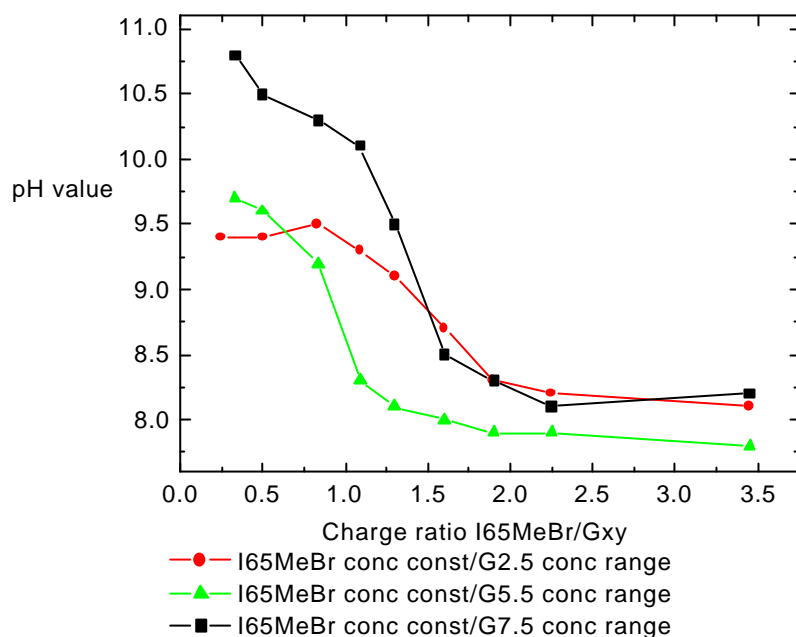
Fig.38: pH value as a function of charge ratio

Fig.37 and Fig.38 present pH values for the samples with I65MeBr and three dendrimers when the concentration of the dendrimer is constant (Fig.37) and when the ionene concentration is constant (Fig.38). The area where a pH decay is observed agrees with the "turbidity area" of the transmission data. Such observation is true for the larger as well as for the smaller ionene I25MeBr, the data for which are given in Fig.39-40.
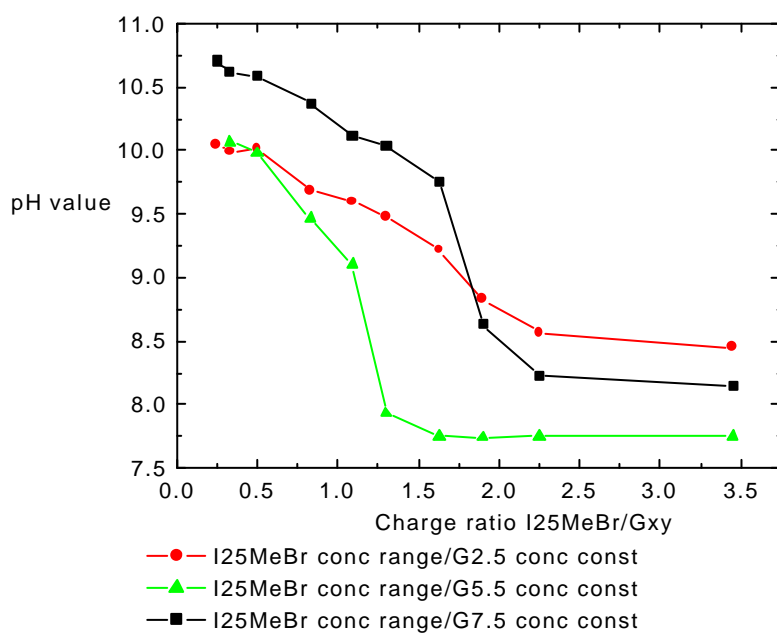
Fig.39: pH value as a function of charge ratio
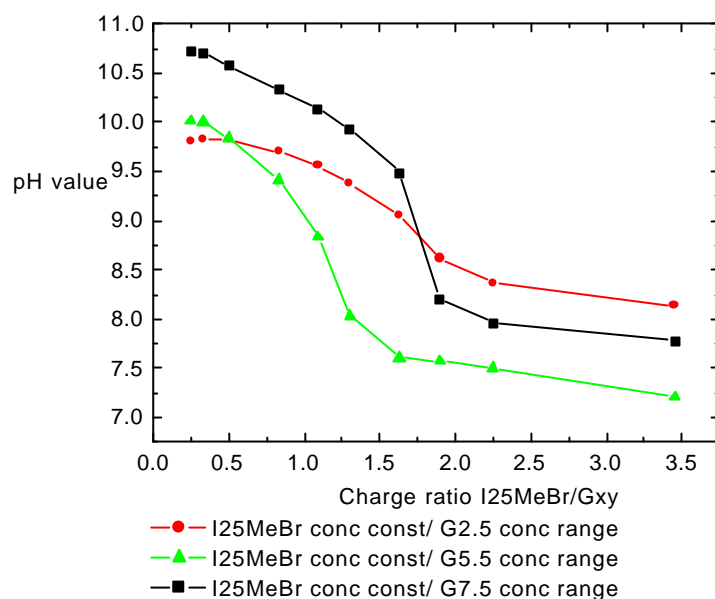
Fig.40: pH value as a function of charge ratio

In case of I25MeBr also the area where the pH curve decay is observed agrees with the "turbidity area" on the UV-spectroscopy data. pH value changes were investigated also for lower concentrated samples (Fig.41). Additionally, pH was measured for the complexes of lower molecular weight polymer (I65MeBr). All pH- data are compared in Fig.41.
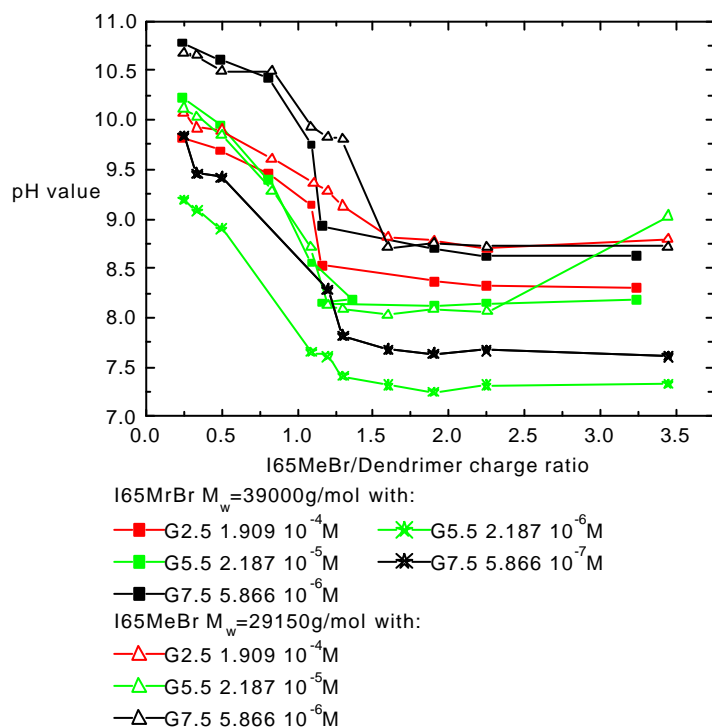
Fig.41: pH value as a function of charge ratio

From Fig.41 the pH value for different molecular masses (by constant solution concentration) stays the same. The charge ratio of ionene/dendrimer is the factor that determines the pH drop. The range of charge ratios when turbidity and pH value change agrees with the transition regime of diffusion modes in the light scattering experiment (subchapter 3). The highest pH values are observed for the systems containing the G7.5 (the highest number of COONa groups). The dendrimer G7.5 itself possesses the highest average pH value (10.8), compare with paragraph II.II). Intermediate pH values are observed for the G2.5 dendrimer systems due to the higher concentrations used, however the average pH value of G2.5 itself equals 9.8, and is the lowest within dendrimers investigated here. The average pH value of pure G5.5 equals 10.4. But since the concentration of the sample influences the pH values of the system, the complexes Imn/G5.5 possess lower pH values than those of Imn/G2.5. The pH value of the complexes lies always above the average pH value for pure ionene compound and below the average pH value of the pure dendrimer compound. It indicates the complexation ("neutralization") between ionenes and dendrimers. The complexation occurs especially in the Imn/Gx.y charge ratio range, where the pH value decreases significantly. Further information concerning complexes may be obtained from the scattering techniques and will be discussed in the following.

3.Scattering techniques

3.1. DLS

3.1.1. I65MeBr/Three Generations of Dendrimers

In order to characterize the size distribution of species present in the solution we use dynamic light scattering. Based on DLS we analyze the diffusion modes and in certain cases calculate the hydrodynamic radii from the diffusion modes. Several DLS experiments were performed. In one set the ionene concentration was varied for fixed dendrimer concentration while in a second set fixed concentration of the ionene was used and the dendrimer concentration varied in a concentrations range. Both were for I25MeBr and I65MeBr with three generations of PAMAM dendrimers. First data obtained for particular samples of ionenes and dendrimers will be presented in detail. Secondly, we will compare the other data. The concentrations of compounds were I65MeBr (4.2 10^{-6} M to 1.3 10^{-4} M), G2.5 from 5.5 10^{-5} M to 1.909 10^{-3} M, G5.5 from 2.187 10^{-6} M to 6.5 10^{-5} M, G7.5 from 5.866 10^{-7} M to 1.7 10^{-5} M. The sample transparency (sample can be clear solution-like, opalescent or turbid) has been described in the Tab.8. To provide dust free-condition of the light scattering experiment, every sample has been filtrated before the measurement. The turbid samples after filtration become opalescent, opalescent and clear samples do not change their transparency condition after filtration.

3.1.2 I65/G5.5 System

We begin with the analysis of I65MeBr with addition of PAMAM G5.5. For further usage such system is our relevant system to compare the behavior of all other systems measured. It seems useful to repeat the pH curve here for comparison (Fig.42).
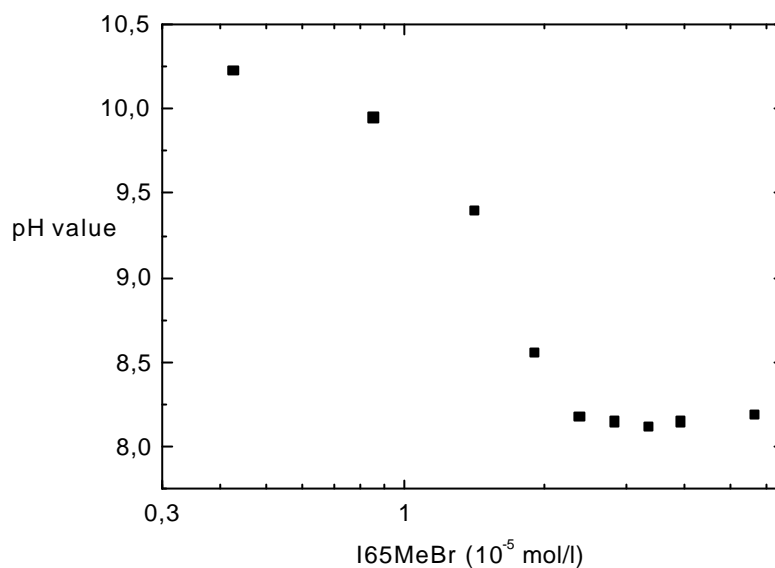
Fig.42: pH value as a function of charge ratio for I65MeBr

concentration range, G5.5 fixed concentration (2.187 10^{-5} M)

Fig.42 presents pH value dependency for the I65MeBr concentrations range, G5.5 PAMAM dendrimer concentration 2.187 10^{-5}M. The diffusion profile is presented in the Fig.43. In Fig.43 as well as in every further figure showing D_{app} as a function of concentration or molecular charge ratio, lines are drawn to guide the eye.
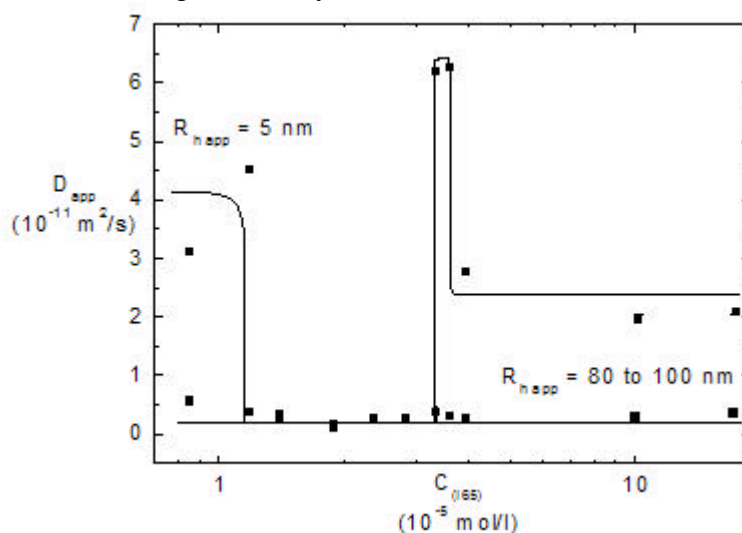

Fig.43. Apparent diffusion as a function of concentration of

I65MeBr. Semilogarytmic plot. I65MeBr concentration range

with G5.5 (2.187 10^{-5}M)

A transition from two to one diffusion process and again splitting into two processes is observed when analyzing the diffusion profile. An overlapping between the area where the pH value decays and the area where transition from two to one and again to two modes occurs in

DLS is found. Additionally one can estimate the apparent hydrodynamic radius ($R_{h\ app}$) from apparent diffusion coefficient D_{app}. Calculated for samples showing one diffusion mode, the apparent R_h value represents a "real" hydrodynamic radius of the particle in solution. The apparent hydrodynamic radius calculated for two diffusion modes samples may indicate the dimension of macromolecules or aggregates coexisting in the system if the presence of more than one species in the double mode system is confirmed. The two diffusion modes can not only be caused by the presence of two different species in the solution. So-called polyelectrolyte diffusion (PE-diffusion) could be an alternative reason for two modes. However PE-diffusion often is indicated also by a negative slope of the fast diffusion coefficient versus scattering vector square, which is not the case of our samples. In the two diffusion mode samples the fast mode has either no slope, or a positive slope. This observation supports our hypothesis of different sized aggregates as a reason of the two diffusion modes. Therefore we give values of apparent hydrodynamic radii for the processes in the two diffusion mode samples here. The presence of different sized species in the system will be discussed in details later. For the two modes samples where the double mode is caused by PE-diffusion, calculation of a hydrodynamic radii makes no sense. The hydrodynamic radius is calculated by Stokes-Einstein relationship, (compare paragraph IV in the theoretical part):

$$R_H = \frac{kT}{6\pi\eta_S D_T}$$

$\boldsymbol{\eta}_S$ - viscosity of the solvent

T - temperature.[109]

Looking at the diffusion coefficient versus scattering vector square in the one diffusion process area a slightly positive slope of it found (Fig.44).
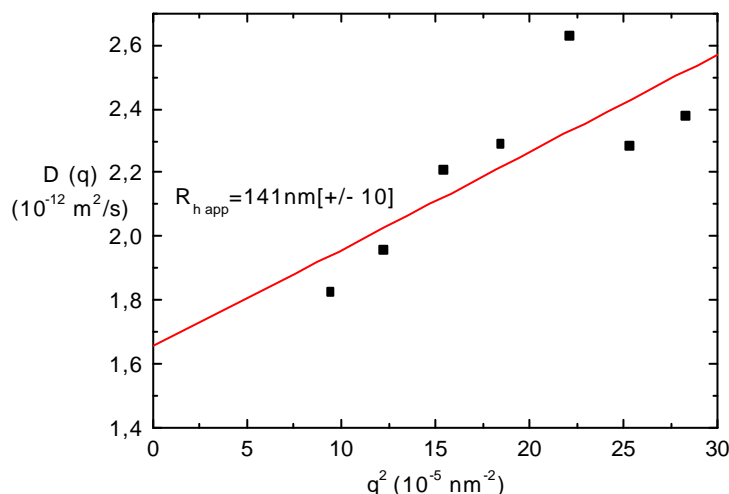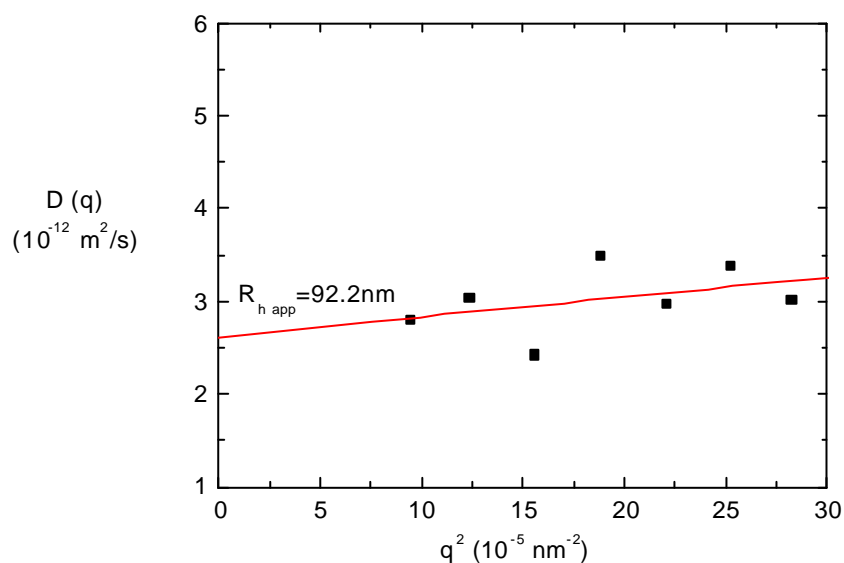

Fig.44: Diffusion coefficient as a function of scattering vector square for the sample I65MeBr 0.74 g/l(1.89 10^{-5} M) with G5.5 2.187 10^{-5} M G5.5. For that sample the charge ratio I65/G55 = 1.09/1. Sample is opalescent. D_{app} = 1.65 10^{-12} (m^2/s) [+/-1 10^{-12} (m^2/s)]
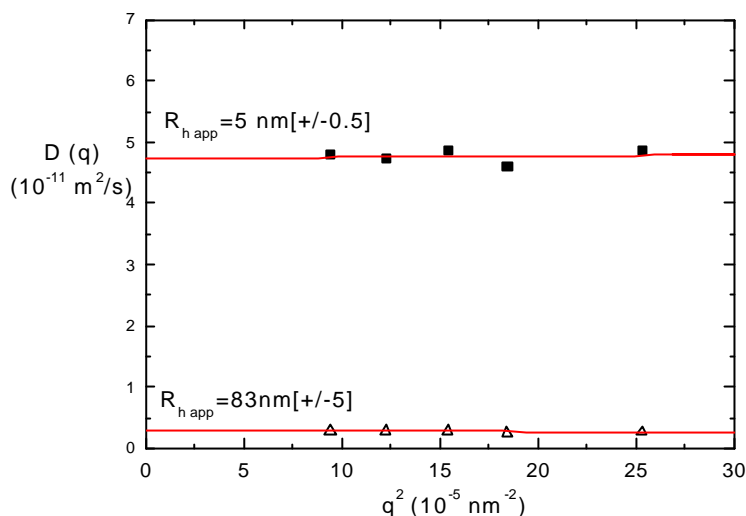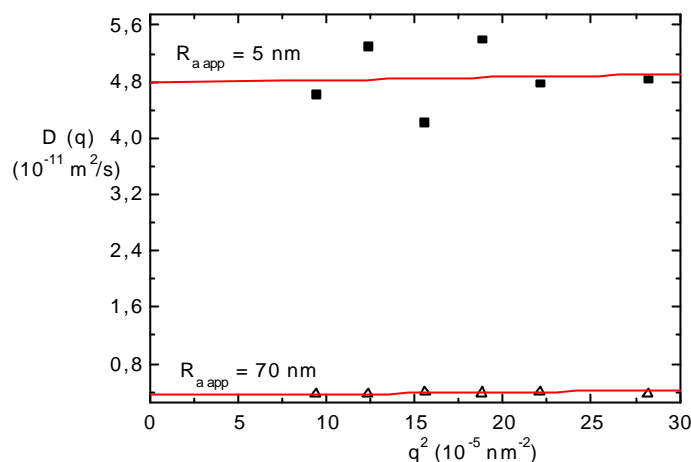
Fig.45: Diffusion coefficient as a function of scattering vector square for the sample I65MeBr 1.4 g/l (3.6 10^{-5} M) with G5.5 2.187 10^{-5} M G5.5. For that sample the charge ratio I65/G55 = 2.06/1. Sample is clear solution.

$D_{app\ slow}$ = 2.9 10^{-12} (m^2/s) [+/-1.7 10^{-13} (m^2/s)]

$D_{app\ fast}$ = 5.4 10^{-11} (m^2/s) [+/-57 10^{-12} (m^2/s)]

For two diffusion mode samples (Fig.45) the slow and the fast mode are almost independent on q square. As it was mentioned before, two diffusion modes can be caused via the presence of two species (two types of aggregates, dendrimers and aggregates etc.) or due to the special diffusion behavior of polyelectrolytes (fast and slow mode of one polyelectrolyte species). To recognize the reason of the two diffusion modes low molecular mass salt has been added to the system to screen the interactions and decrease possible polyelectrolyte effects. For two diffusion mode samples even for high (10^{-3}M) salt concentrations a change in diffusion coefficients is not observed. For the details see paragraph III.I.B. This supports the hypothesis of the species different in size causing two diffusion modes.

To investigate the influence of the concentration on the sample behavior, samples with 10 times lower concentrations of ionene and dendrimers were prepared. Those samples consequently were prepared without low molecular mass salt addition. Samples with 10 times lower concentrations of ionene and dendrimers were prepared in case of I65 (I25) with G5.5 (G7.5). Samples with G2.5 contain higher concentrations of the compounds. The reason is a low level of the scattering intensity measured, which suggests lack of the complex structures. For the measured samples I65/G25 in the concentration range of 10^{-5}M, always two diffusion modes have been present. Fig.46 shows the diffusion coefficient as a function of concentration for lower concentrated samples of I65 and G5.5. As mentioned before, the sample concentration is 10 times lower as compared to the presented in Fig.42-45.
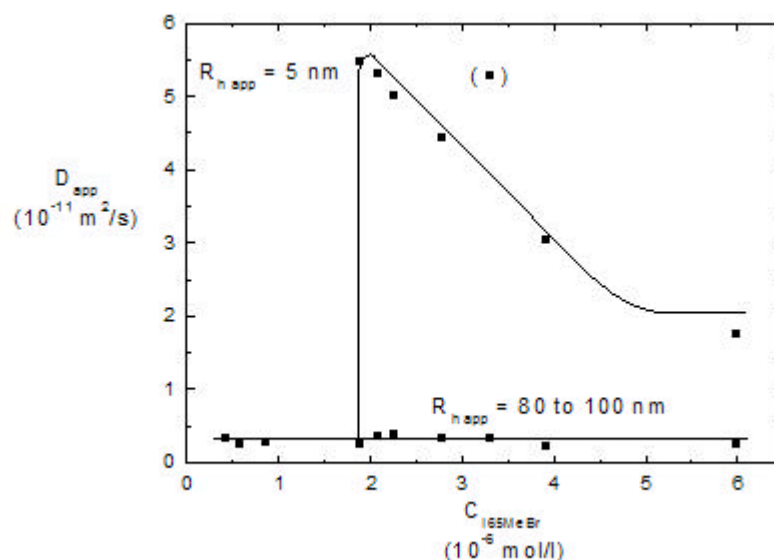
Fig.46. Diffusion coefficient as a function of I65 concentration

for the sample I65 concentration range with G5.5 2.187 10^{-6} M

In the one process area the diffusion coefficient is almost independent on the scattering vector square (Fig.47).

Fig.47: Diffusion coefficient as a function of scattering vector

square for the sample I65MeBr 0.0226 g/l (5.8 10^{7} M) with

G5.5 2.187 10^{-6} M. The charge ratio is I65/G5.5 = 1/3.

Sample is clear solution.

D_{app} = 2.62 10^{-12} (m^2/s)

Fig.48: Diffusion coefficient as a function of scattering

vector square for the sample I65MeBr 0.1288 g/l (3.3 10^{-6} M)

with G5.5 2.187 10^{-6} M G5.5. For that sample the charge ratio

I65/G55 = 1. 9/1. Sample is clear solution.

$D_{app\ fast}$ = 5.27 10^{-11} (m^2/s)

$D_{app\ slow}$ = 3.4 10^{-12} (m^2/s)

In the two diffusion processes area (Fig.48) the slow and the fast mode are almost independent on the scattering vector square.

As it was explained in the introduction to the complexation chapter, it is useful to compare our systems using charge ratio as a reference X-axis.
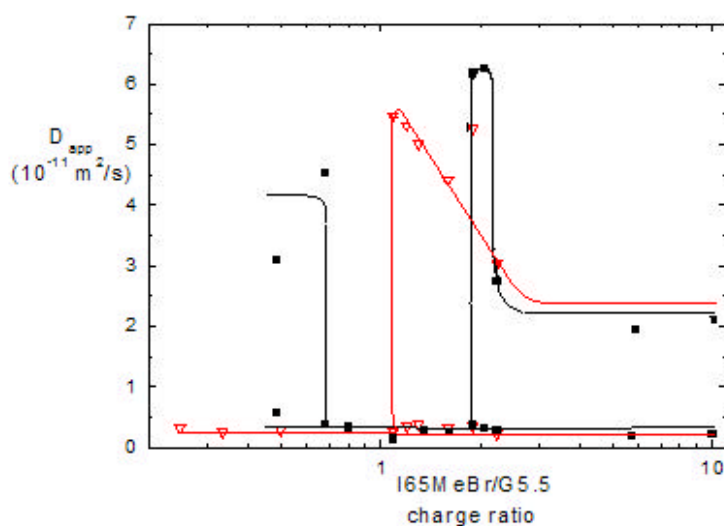
Fig.49. Diffusion coefficient as a function of the I65/G5.5

charge ratio. I65 concentration range have been used

and two fixed G5.5 concentration: 2.187 10^{-6} M (triangles)

and 2.187 10^{-5} M (squares).

Fig.49 represents two diffusion profiles for both cases mentioned above, lower (2.187 10^{-6}M) and higher (2.187 10^{-5}M) concentrations of dendrimer G5.5 with adequate ionene concentrations, as a function of the charge ratio. A general overlap of the two curves becomes obvious. The plot shows that the diffusion process in case of I65MeBr with dendrimer G5.5 is slightly dependent on the total concentration and in case of lower concentration splitting into two processes occurs at lower charge ratio of I65MeBr to the G5.5 than in case of higher concentrated solutions. Two processes at the low charge ratio regime of the diffusion profile are observed only for the more concentrated data set. This supports our hypothesis of two species causing the double mode at lower charge ratio. In the less concentrated samples all molecules may have aggregated. In higher concentrated samples, fast mode may be caused via an excess of building blocks (ionene or dendrimer macromolecules).

Further, the system with a concentration range of dendrimers at fixed ionene concentration was investigated. The sample series was prepared for higher concentration of compounds e.g. G5.5= 2.187 10^{-5}M and appropriate ionene concentrations. The charge ratios were similar like for experiments presented before. Results are shown in Fig.50-52.
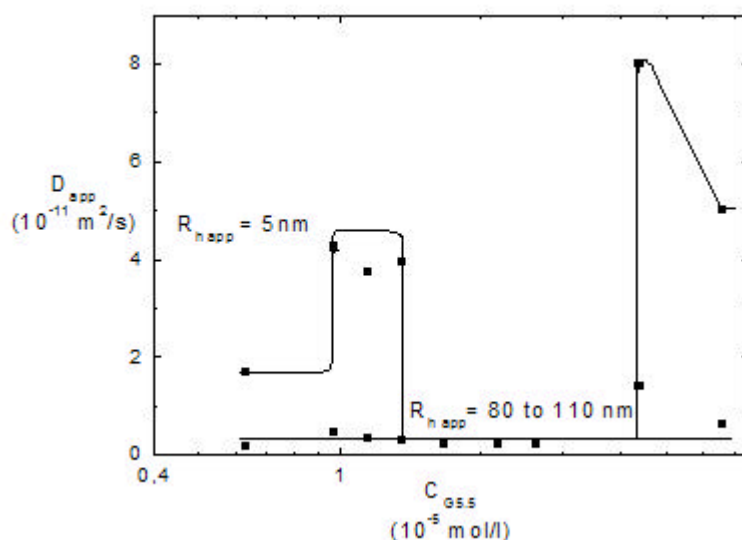
Fig.50: Diffusion coefficient as a function of G5.5

concentration for the sample 0.74g/l I65 and

G5.5 concentrations range.

Like in the case of samples with constant G5.5 concentration, also in this in case of samples with constant ionene concentration two diffusion modes samples as well as one diffusion mode samples are observed in certain concentration regimes. Two diffusion modes in the beginning of the concentration scale are observed, and one diffusion mode that splits again into two modes for higher concentrations of dendrimer added (Fig.50). The splitting occurs for $C_{G5.5}$= 1.68 10^{-5} mol/l and $C_{G5.5}$= 2.62 10^{-5} mol/l. Based on the I65/G55 diffusion profiles as a function of the charge ratio, one can postulate the stoichiometric binding during complex formation. Only between the charge ratio of 0.7 to 1.7 the complexes may be formed (one diffusion mode). Below λ of 0.7 and above λ of 1.8 an excess of one of the macromolecule species complete. It may be that the compound is present in addition to the complex and causes a second diffusion process.

Fig.51 and Fig.52 present the behavior of the diffusion coefficient versus scattering vector square.
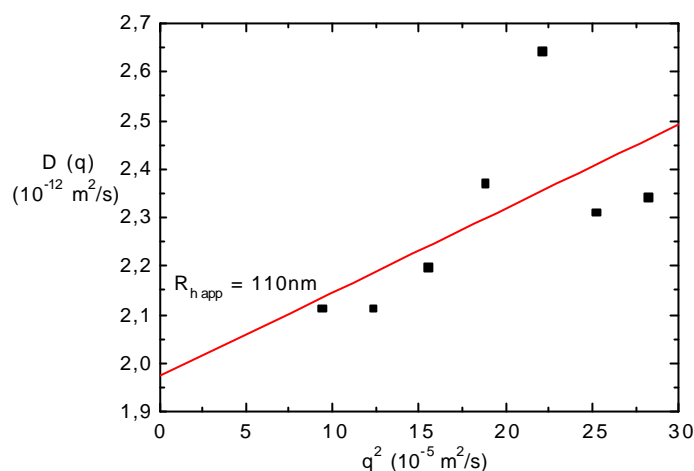
Fig.51: Diffusion coefficient as a function of the scattering vector square for the sample I65MeBr (0.74 g/l) with G5.5 2.624 10^{-5} M. Charge ratio equals I65MeBr/G5.5 = 1/1.2. Sample is opalescent.

$D_{app} = 1.97 \ 10^{-12} \ (m^2/s)$

In the range of concentrations where one diffusion mode is observed the diffusion coefficient is characterized by a positive slope of the q-dependence (Fig.52).
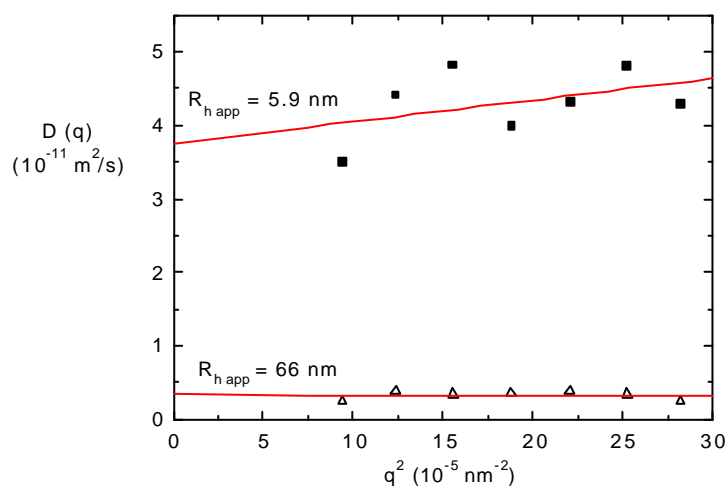

Fig.52: Diffusion coefficient as a function of scattering vector square for the sample I65MeBr 0.74 g/l (1.15 10^{-5} M) with G5.5 1.15 10^{-5} M. For that sample the charge ratio I65/G55 = 1. 9/1. Sample is clear solution.

$D_{app \ fast} = 3.75 \ 10^{-11} \ (m^2/s)$

$D_{app \ slow} = 3.39 \ 10^{-12} \ (m^2/s)$

Within the two diffusion modes area, the slow mode is almost independent on the scattering vector square, while the fast mode shows a slightly positive slope (Fig.52).

Trying to understand the nature of diffusion processes in our system the diffusion coefficient for constant G5.5 concentration (2.187 10^{-5}M) and the diffusion behavior for constant I65MeBr concentration (1.9 10^{-5}M) are combined in Fig.53, again using the charge ratio as a parameter.
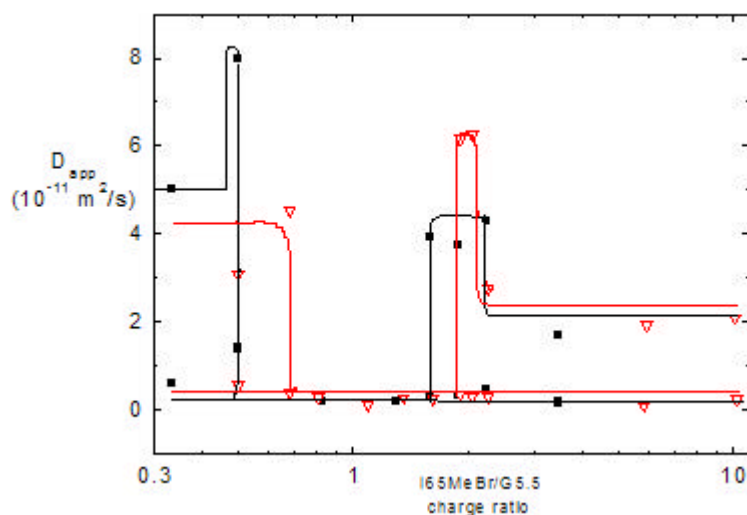
Fig.53. Apparent diffusion as a function of the charge ratio for the samples I65MeBr (0.74 g/l) with G5.5 concentration range (black line) and I65MeBr concentration range with G5.5 (2.187 10^{-5} M) (red line).

Good agreement between the two data series is observed when representing diffusion coefficient data as function of charge ratio. For typical polyelectrolytes with low molecular mass salt addition, a transition range from one to two processes, so called "ordinary-extraordinary" transition is observed when the charge ratio is around:

$$\boldsymbol{l} = \frac{C_p}{C_s} \approx 1$$

In the case here, shifting of the splitting point to the value of $\boldsymbol{l}_{spliting} \approx 1.74$ is observed. To get the value of 1 and the splitting point on the typical for polyelectrolytes place, we have to multiply as follows:

$$\frac{\text{Ccharges of ionene}}{\text{Ccharges of dendrimer}} \cdot 0.575 = 1.$$

Most importantly, not only the transition from one to two processes occurs in the systems investigated here. For lower charge ratios the system shows transition from two to one processes. This is not the typical polyelectrolyte behavior and is likely to be caused by the different sized species present in the system, what will be confirmed in the paragraph concerning samples with low molecular mass salt addition.

3.1.2.a I65/G5.5 System- summary

A comparison between the behavior of I65/G5.5 systems with normal polyelectrolyte behavior, "normal polyelectrolyte behavior schema" is presented in Fig.54.
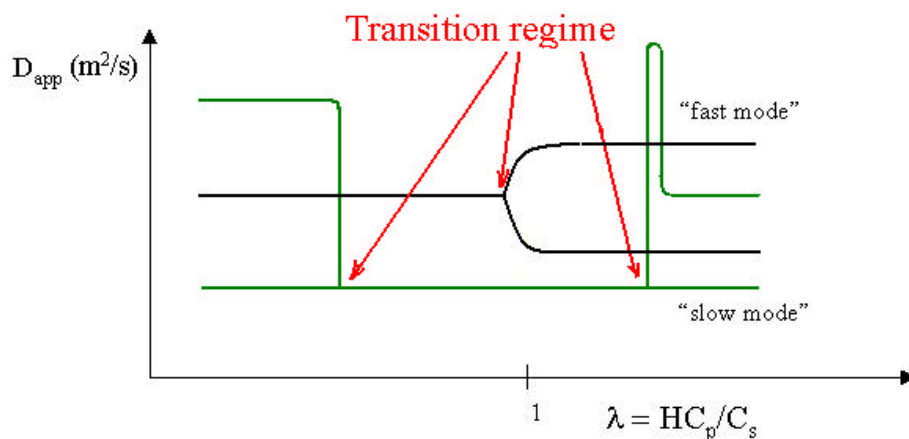

Fig.54. Normal polyelectrolyte behavior (black line) as compared

to the I65/G5.5 system. H is the parameter which can be attributed

to e.g. the degree of quaternization for certain polyelectrolytes.

For normal polyelectrolytes under low ionic strength the fast mode (D_{fast}) is independent of C_p/C_s and molecular weight. The slow mode (D_{slow}) decreases slightly with increasing C_p/C_s and also with increasing molecular weight. The fast mode is "faster" than the diffusion in the one mode range, slow mode is "slower" than the diffusion in the one mode range (black line in Fig.54). For the I65/G5.5 systems not only two transition regimes can be observed, but also the differences in the velocity of particles are significant. For the I65/G5.5 systems the one mode regime covers movement of the complex particles (R_h 80 to 150 nm) whereas for the normal polyelectrolytes in one mode range particles are of the single macromolecule order of magnitude (single polymer molecules). Besides the I65/G5.5 systems in the one mode regime are opalescent to turbid, what suggests the presence of complex structures. When G5.5 (2.187 10^{-5}M) with I65 concentration range samples are regarded, a peak occurs after the second transition regime in the fast mode. This behavior is also not typical for the normal polyelectrolytes and will be discussed in the general summary of I65/PAMAM complexes.

Two diffusion modes can be due to the special diffusion behavior of polyelectrolytes so called polyelectrolyte effect or due to the presence of two species in the solution (two types of aggregates). The second hypothesis seems to be much more probable in the case of I65/Gx.y systems. The pro-argument is the positive slope of the diffusion coefficients versus scattering vector square for the I65/G5.5 sample series. Samples in the two diffusion mode range are charged on the surface as can be shown by the ζ-potential measurements (compare chapter III.VII), thus are soluble in the medium (water). Samples are clear or slightly turbid like I65/G5.5 samples in the two modes range. However, to further recognize the roots of two modes, samples with low molecular mass salt addition will be investigated (see subchapter III.I.B).

3.1.3   I65MeBr/G7.5 and I65MeBr/G2.5 systems

Next step in the analysis of our systems is to compare the behavior of ionene I65MeBr samples containing middle size dendrimer G5.5 and samples with a bigger (G7.5) dendrimer as well as a smaller (G2.5) one. The transmission and pH characteristic was presented earlier in chapter number 1. and 2. In Fig.55 diffusion data of a sample series investigated at the fixed dendrimer concentration ($C_{G7.5} = 5.866 \cdot 10^{-6}$ M) and I65MeBr varying concentrations are presented.
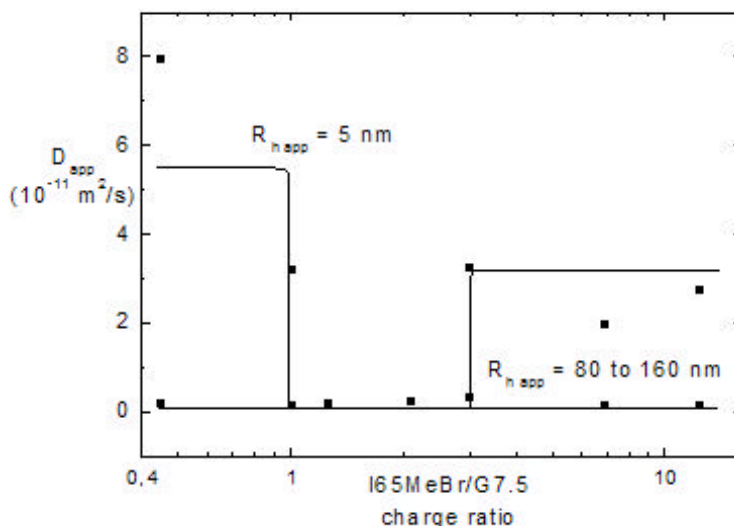
Fig.55: Diffusion behavior of the samples containing

I65/G7.5 at fixed dendrimer concentration,

$C_{G7.5} = 5.866 \cdot 10^{-6}$ M as a function of I65 concentration.

Like in case of complexes with G5.5, the sample series of G7.5 starts with two processes at low ionene concentrations, then a one diffusion coefficient area follows and at even higher concentration it again splits into two diffusion modes (Fig.55). One diffusion process samples show a slightly positive slope of the diffusion coefficient versus scattering vector square. For two diffusion mode samples, the fast mode has a slightly positive slope, while the slow mode is almost independent of the scattering vector. If we now compare the diffusion profile of the sample with samples of 10 times lower concentrations of compounds or the charge ratio, we find the same principle diffusion behavior as can be seen in Fig.56.
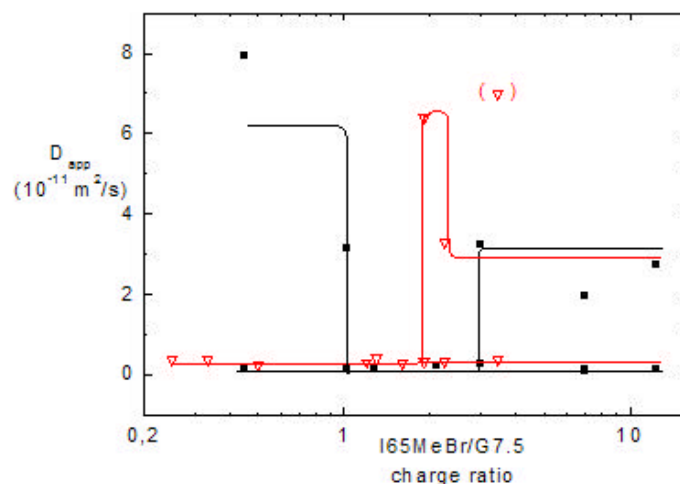
Fig.56. The diffusion coefficient as a function of I65/G7.5

charge ratio at varied I65 concentration. The dendrimer

concentration is fixed and equal 5.866 10^{-6} M (squares)

and 5.866 10^{-7} M (triangles).

As a function of charge ratio, the diffusion profiles overlap (Fig.56). However, the difference between them is that the transition area occurs for the lower concentrated samples at a lower charge ratio I65MeBr/G7.5 (Fig.56). Additionally for the lower concentrated samples firs transition regime is missing. This behavior is similar to the one presented for the "low concentrated" samples of I65MeBr and G5.5. Thus the total concentration does not play an important role for the fundamental diffusion behavior, while the charge ratio of ionene to dendrimer seems to be a crucial parameter.

It is noteworthy to investigate a sample series with fixed I65MeBr concentration and the dendrimer G7.5 concentration varied as given in Fig.57.
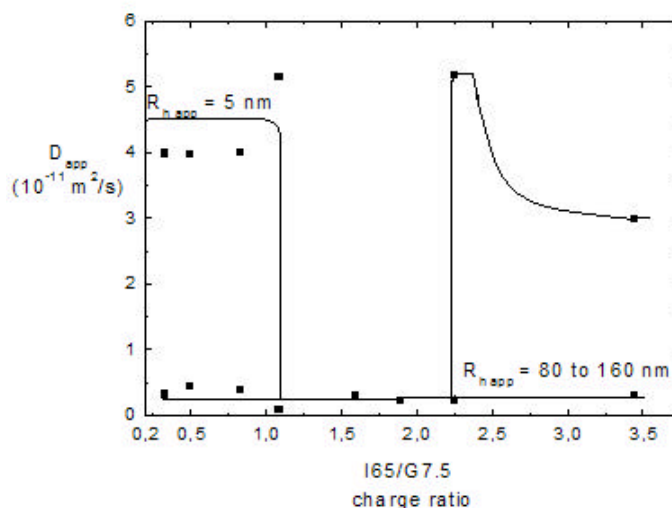
Fig.57. Diffusion coefficient as a function of charge ratio

for the I65/G7.5 system. I65 concentration is fixed and

equal 0.74 g/l ($1.9 10^{-5}$ M), G7.5 concentration range has

been used.

Splitting from two to one and again to two diffusion processes is observed (compare Fig.50 p.68 for I65/G5.5 system).
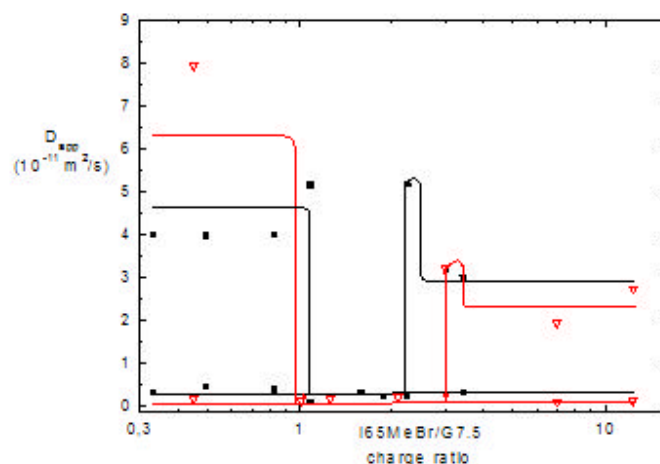
Fig.58. Apparent diffusion coefficient as a function of the molar charge ratio for the sample I65 (0.74 g/l) with G7.5 concentration range (squares) and I65 concentration range with G7.5 (5.866 10^{-6} M) (triangles).

Comparison of the two sample series (with constant dendrimer concentration (5.866 10^{-6}M) and with constant I65MeBr concentration (1.897 10^{-5}M)) shows a good agreement (Fig.58). The transition region from one to two diffusion process is however shifted to the higher ratio of molar charge concentration of the I65MeBr to the dendrimer in case of samples with I65 concentrations range. For typical polyelectrolytes with low molecular mass salt addition, the transition point from one to two processes is observed when their charge ratios λ are equal 1. In the case discussed here shifting of the splitting point to the value of $\lambda_{splitting} = 2.29$ is found. To get the value of 1 and the splitting point on the typical for polyelectrolytes place, we have to multiply as follows:

$$\frac{\text{Ccharges of ionene}}{\text{Ccharges of dendrimer}} \, 0.437 = 1$$

Besides like in case of the I65/G5.5 sample series, the first splitting point from two to one process is observed at lower charge ratio and is present for both cases: the I65 fixed concentration and G7.5 fixed concentration. Again like mentioned earlier for the I65/G5.5 systems, a peak in the progress of the fast mode as a function of charge ratio appears just after the second transition regime.

The 0.437 (+/-0.2) parameter found for the ionene/G7.5 system is comparable with the value of 0.575 (+/-0.2) found for ionene/G5.5 complexes. The difference between the splitting point observed for I65/G5.5 and I65/G7.5 is around 20 per cent and is larger than an error expected from the diffusion coefficient estimation (5 to10 per cent).

To further describe ionenes/dendrimers systems investigations of sample series with G2.5 have been performed. The morphology and dissociation ability of G5.5, G7.5 as compared to G2.5 differ significantly and may clarify our state of knowledge about all systems investigated. That is why the smaller dendrimer of generation G2.5 with I65MeBr sample series will be discussed.

Since the ionene/G2.5 samples scatter weakly, the DLS measurement was difficult especially for the samples with low ionene concentration. For the sample series with fixed I65MeBr (1.897 10^{-5}M) concentration as well as for the samples with fixed dendrimer G2.5 concentration (1.909 10^{-4}M), we observed two diffusion modes in whole range of concentration. The apparent hydrodynamic radius lies in the same order of magnitude for both series investigated. For comparison, the apparent diffusion coefficient versus charge ratio of I65MeBr/G2.5 is presented in Fig.59. The behavior observed is different from that for larger dendrimers with the same ionene I65MeBr and also different from the normal polyelectrolyte diffusion profile (compare e.g. Fig.54). To recognize the roots of this differences, discussion of the distribution of relaxation times will follow. In Fig.59a the distribution of relaxation times at 90° scattering angle is presented. The sample in Fig.59a contains I65 and G2.5 at the charge ratio of 0.83. Two diffusion modes are observed and the distribution of relaxation times is narrow. The distribution of relaxation times does not change with the scattering angle and when changing fitting parameters e.g. minimal/maximal decay time, number of grid points, which confirms the bimodal diffusion behavior. Narrowness of the decay time distribution and angular dependence suggest that the fast and slow mode are not caused by the common PE-diffusion, but they are observed due to the diffusion of different sized species. If the diffusion would be caused by PE-effect, the distribution of the relaxation times would be broad. PE-diffusion is caused by one species of macromolecules which may build fluctuating, domains having large dimensions in the solution. These domains are supposed to be a reason for the slow diffusion mode. The species present in samples in Fig.59 are charged on the surface (compare with the measurements of ζ potential in paragraph III.VI.) what gives a rise for the interaction between them. The hypothesis of two different sized species, charged on the surface, as a reason for two diffusion modes is additionally supported by the observation of the diffusion coefficient as a function of the scattering vector square. No expressed slope of the fast mode that is larger than the experimental error is observed. The slow mode also almost does not depend on the scattering vector square. The presence of interaction between charged assemblies and its possible consequences will be discussed later.
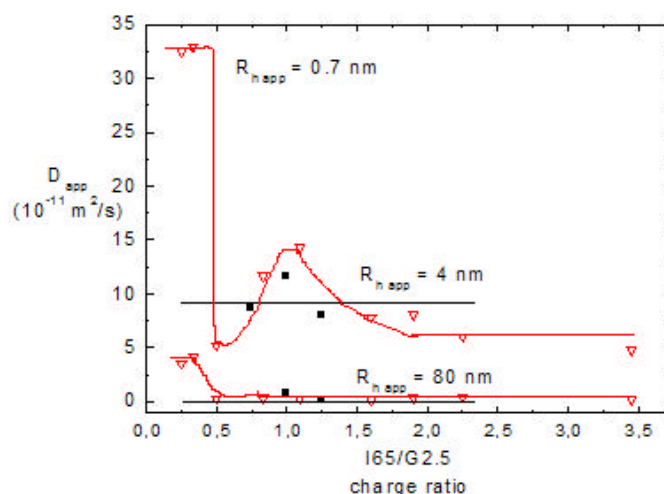

Fig.59: Apparent diffusion coefficient as a function of charge ratio for two I65/G2.5 systems: I65MeBr varied concentration with G25 1.909 10^{-4} M (squars) and I65MeBr 1.897 10^{-5} M with G25 concentration range (triangles).
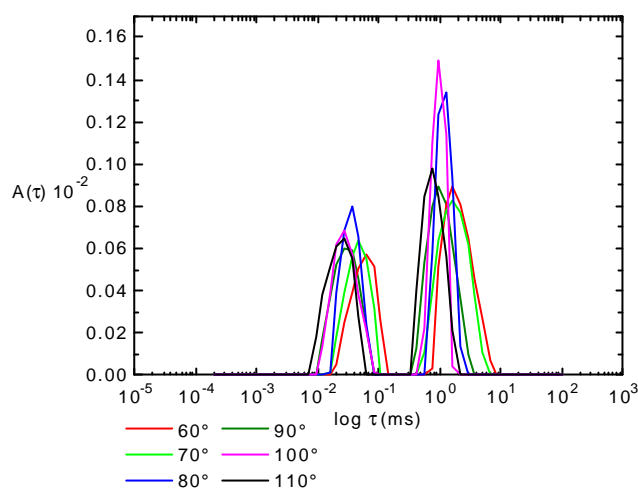
Fig.59a. Decay time distribution function for the

I65/G2.5 sample at the scattering angle 60°-110°.

The sample belongs to the series with fixed

(1.9 10^{-5} M) I65 concentration and G2.5

concentration range. The charge ratio of

I65/G2.5 = 0.83.

The sample of I65/G2.5 with 10 times lower concentration of compounds could not be measured due to the very low scattering intensity, so 10 times higher concentrated samples were investigated to monitor the influence of concentration. The behavior found is similar to the behavior of lower concentrated G2.5 samples. Two diffusion processes are always found (Fig.59). Additionally at a charge ratio I65MeBr /G2.5 between 0.5 and 2.25 honey like precipitation occurs. For comparison see Fig.60. This is in contrast to the I65/G5.5 and I65/G7.5 systems. Only for the I65/G7.5 white flocks observed at a charge ratio 1.3 and 1.6. But the results given in Fig.60 can only cautiously be taken into account.
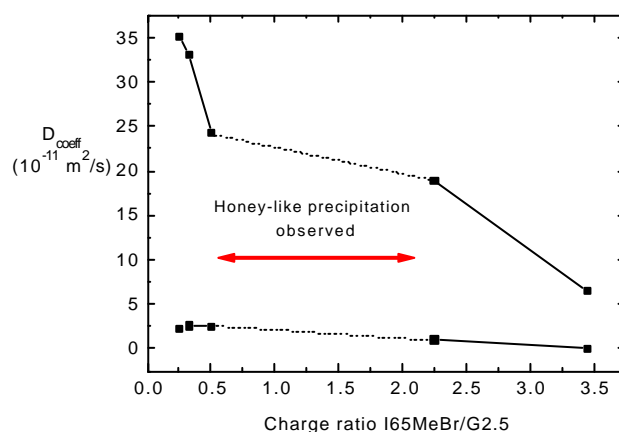
Fig.60: Apparent diffusion coefficient as a function

of charge ratio for the I65/G2.5 system I65MeBr

concentration range, G2.5 1.909 10^{-3} M

82

The value of hydrodynamic radii found (Fig.61) are smaller than for less concentrated samples.
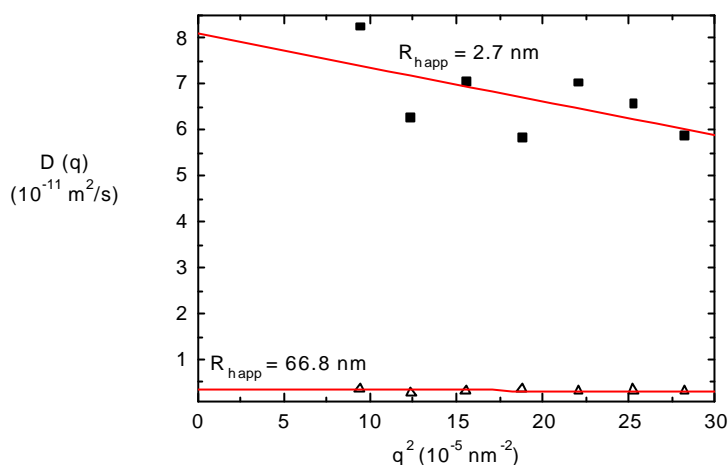
Fig.61: Diffusion coefficient as a function of the scattering vector square for the sample G2.5 (1.004 10^{-4} M) with I65MeBr (0.74 g/l). Charge ratio I65/G2.5 is equal 1.9/1. Sample is slightly opalescent. Diffusion coefficients are equal $D_{app\ slow}$ = 3.38 10^{-12} (m^2/s) and $D_{app\ fast}$ = 8 10^{-11} (m^2/s)

The general tendency dominating the behavior of diffusion coefficient versus scattering vector square for I65/G2.5 is that the slope of the fast mode is negative and the slope of slow mode is independent on the scattering vector square.

As a next step we would like to present our observations concerning I65$_{lower\ molecular\ mass}$ system and three generations of PAMAM dendrimers: G2.5, G5.5, G7.5 as well as the systems build of I25 with G2.5, G5.5, G7.5. We intend to support a hypothesis of behavior periodicity in the Imn/Gx.y systems, changing with the dendrimer generation or with the ionene species.

3.1.4. I65MeBr$_{lower\ molecular\ weight}$ /Three Generations of Dendrimers

The turbidity and pH analysis for these systems was mentioned in III.I.A. Below (Fig.62-64) the apparent diffusion coefficient dependency on the charge ratio is presented. The molecular mass of an investigated I65MeBr$_{lower\ molecular\ weight}$ (I65$_{(1)}$) constitute 75 per cent of the molecular mass of this sample. As in previous systems two transition regimes are observed in the case of I65 lower molecular mass/G5.5 and I65 lower molecular mass/G7.5. The samples containing I65$_{(1)}$ of lower molecular mass with G2.5 like in the systems previous analyzed do not possess one diffusion mode range, that means lack of the transition regimes (compare Fig.59 and Fig.59a). ξ-potential measurements for this system indicate strongly negatively charged surfaces (see subchapter III.VI). Similarly to for the case of I65/G2.5, strong interaction between charged objects can be a reason for two modes. In the two modes regime the fast diffusion coefficient as a function of the scattering vector square shows slightly negative slope again. The fast mode is mostly independent on the scattering vector square. A peak in the concentration dependence of the fast mode is observed in case of G2.5 (and presented later G7.5) samples with I65$_{(1)}$. The possible reasons for this peak will be discussed later. Again

samples with G2.5 (especially for lower charge ratios) show weak scattering intensity during the light scattering experiment.
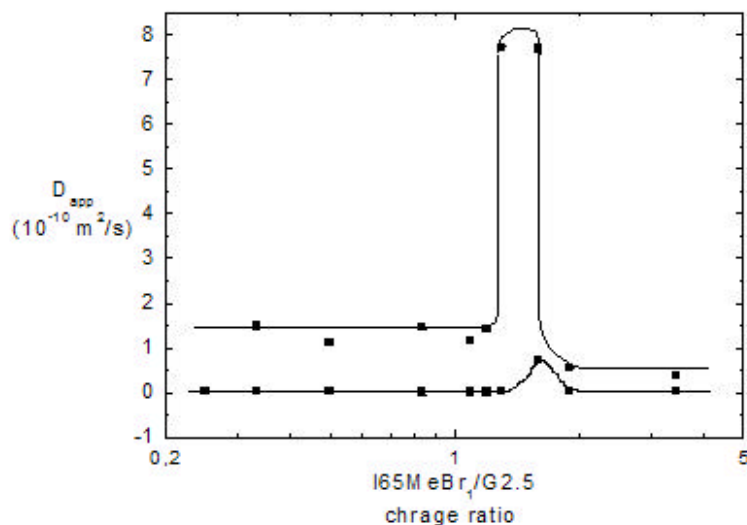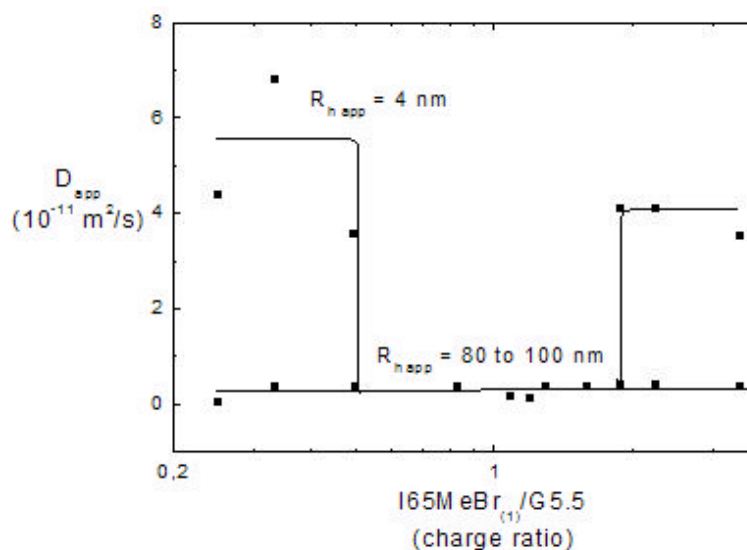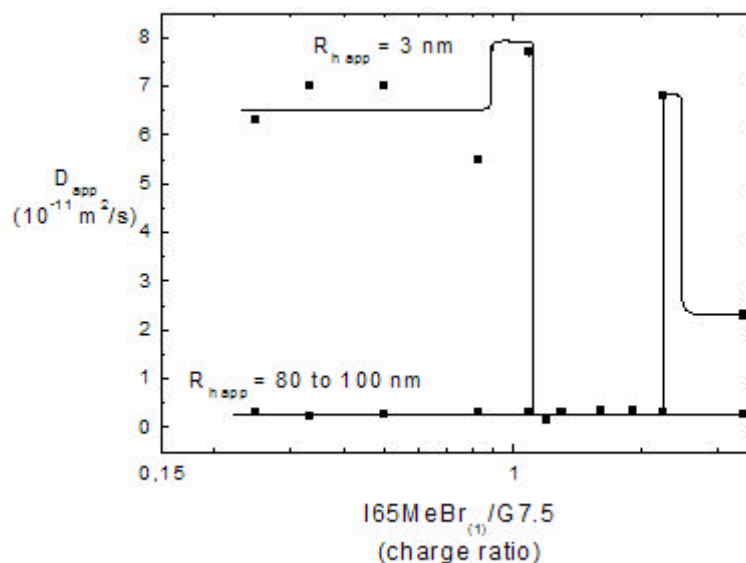

Fig.62: Apparent diffusion as a function of the charge ratio

for I65$_{(1)}$ of lower molecular mass with G2.5 sample series.

I65 varied concentration G2.5 fixed (1.909 10^{-4} M) concentration.

In the I65$_{(1)}$/G5.5 and I65$_{(1)}$/G7.5 sample series two transition points are observed. This is similar to the behavior of systems with "normal" molecular weight I65. The diffusion profiles for I65$_{(1)}$ /G5.5 and I65$_{(1)}$/G7.5 are presented in Figure 63-64.

Fig.63: Apparent diffusion as a function of the charge ratio

for I65$_{(1)}$ of lower molecular mass with G5.5 sample series.

I65$_{(1)}$ varied concentration G5.5 fixed (2.187 10^{-5} M) concentration.

Fig.64: Apparent diffusion as a function of the charge ratio

for $I65_{(1)}$ of lower molecular mass with G7.5 sample series.

I65 varied concentration G7.5 fixed (5.866 10^{-6} M) concentration

As in the case of I65/G5.5 or I65/G7.5 samples, there is almost no slope, eventually slight positive slope is observed in the diffusion coefficient versus the scattering vector square dependency for the one mode regime. The two mode regimes are characterized by either the lack of the slope or the slope becomes slightly negative. Table 10 presents the size of complexes in the one mode range and the value of splitting parameter for the diffusion profiles.

Tab.10: Size of $I65_{(1)}$ complexes

Complexes with fixed dendrimer concentration		Splitting parameter	
Compounds	*Size of objects within one mode area (nm)*	l_1	l_2
$I65_{(1)}$ /G5.5	60-80 (150, 200)	0.5	1.9
$I65_{(1)}$ /G7.5	80	1.09	2.25
$I65_{(1)}$ /G2.5	no single mode observed	no splitting point observed	

In the system $I65_{(1)}$/G5.5 and $I65_{(1)}$/G7.5 the presence of two modes after second transition point can be, like in previous cases, due to two aggregate species which interact with each other. In the lower concentration regime (before the first splitting point) two diffusion modes can be either due to the polyelectrolyte effect or again due to objects of different size, but again based on the observation of the samples containing higher molecular mass ionene, we suggest rather aggregates of different size then a normal polyelectrolyte effect. This postulate is due to the observation of slightly positive slope or the lack of the diffusion coefficient slope as a function of the scattering vector square. The solution may contain (like in the case of I65 complexes) different sized aggregates that are additionally charged on the surface. The charged aggregates, might act as huge macroparticles additionally giving rise to the kind of effect similar to the polyelectrolyte effect. About the origin of the two modes behavior at lower charge ratio we will be able to judge in detail after further analysis.

3.1.5   I65MeBr/Gx.y complexes- summary

In Tab.11 some important aspects of systems composed of I65 and flexible PAMAM dendrimers of generation G2.5, G5.5 and G7.5 are summarized. Generally samples investigated in this work represent a whole range of turbidity, starting from clear solutions up to the very turbid samples even with white flocks inside (for details see Tab.9). Samples of the highest opalescence or turbidity are observed in the range of one diffusion mode. In particular turbidity confirms the presence of bigger objects in the solution. The opalescence or turbidity range change coincides with a steep decrease of pH value.

Tab.11: Diffusion profiles for I65/PAMAM dendrimer systems- summary

Complexes with fixed dendrimer concentration		Splitting parameter	
Compounds	*Size of objects within one mode area (nm)*	l_1	l_2
I65/G5.5	80-90	0.68	1.92
I65/G7.5	80-100	1	3
I65/G2.5	no single mode observed	no splitting point observed	
Complexes with fixed ionene concentration		**Splitting parameter**	
Compounds	*Size of objects within one mode area (nm)*	l_1	l_2
I65/G5.5	80-110	0.5	1.6
I65/G7.5	80-110	1	2.25
I65/G2.5	no single mode observed	no spliting point observed	
Complexes with changed* concentration		**Splitting parameter**	
Compounds	*Size of objects within one mode area (nm)*	l_1	l_2
I65/G5.5	70-100	-	1.09
I65/G7.5	60-100	-	1.9
I65/G2.5	no single mode observed	no splitting point observed	

A general comparison of our systems with the normal polyelectrolyte behavior indicates the following differences: for normal polyelectrolytes under low ionic strength one transition regime from one to two diffusion modes is observed with increasing C_p/C_s. The fast mode (D_{fast}) is independent of C_p/C_s and molecular weight. The slow mode (D_{slow}) decreases slightly with increasing C_p/C_s, also with increasing molecular weight. The fast mode is "faster" than the diffusion in the one mode range, while the slow mode is "slower" than the diffusion in one mode range. For normal polyelectrolytes, the solution stays clear in the transition regime. In contrast, I65/Gx.y systems show two transition regimes and also the differences in the velocity of particles are significant. The slow mode for I65/Gx.y systems in all concentrations range corresponds to the movement of the complex particles ($R_{h\ app}$ 60 to 110 nm). I65/Gx.y systems in the one mode regime are opalescent to turbid and contain well defined aggregates of the R_h app around 100 nm. The fast diffusion mode in the low I65 concentration range corresponds to the movement of the particles of $R_{h\ app}$ between 5 and 10 nm. This means either pure ionene or dendrimer macromolecules, eventually oligoaggregates, build e.g. by one dendrimer and two ionene molecules. Whether we have at low ionene concentrations pure macroparticles in the system causing the fast diffusion mode or the fast diffusion is caused by the oligoaggregates, we can not distinguish. The size difference between pure macromolecules and oligoaggregates at low ionene concentration in our system is to small to be detected by DLS. The fast mode at higher ionene concentrations (above around $3\ 10^{-5}$ mol/l) is caused by the movement of oligoaggregates of $R_{h\ app}$ equal 15 to 30 nm. Here, the dimension difference between pure ionene or dendrimer macromolecule and the middle size complexes is sufficient to be detected. Thus the fast diffusion at higher I65 concentration must be caused by middle size aggregates only.

Often a "peak" in the fast mode (diffusion coefficient versus concentration) occurs after the second transition regime which also is not typical for the normal polyelectrolytes. In Fig.43*(R)* we regard again the sample series presented already in Fig.43 and try to explain the peak in the fast diffusion mode.
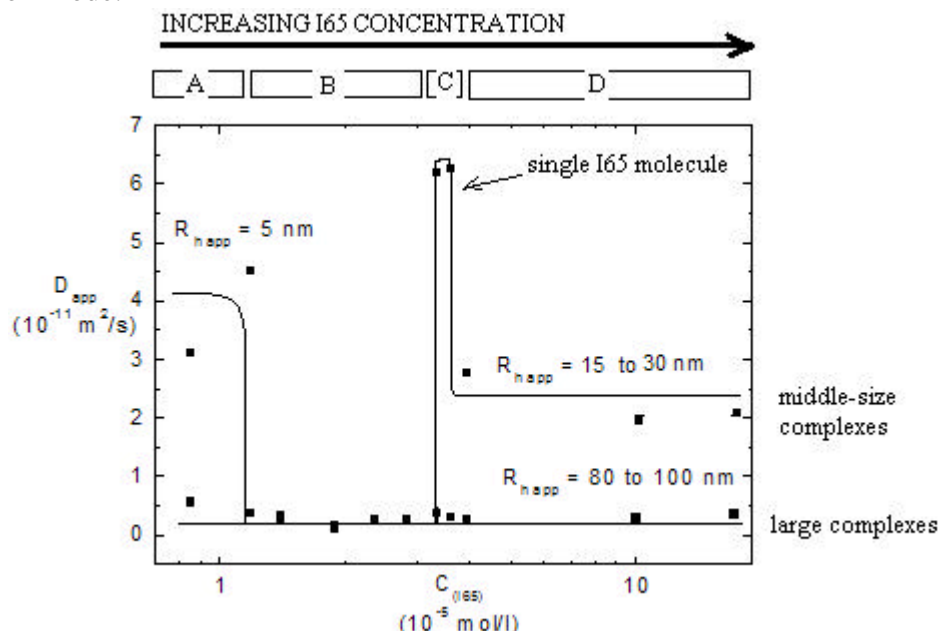

Fig.43 *(R)*. Apparent diffusion as a function of concentration of

I65MeBr. Semilogarytmic plot. I65MeBr concentration range

with fix G5.5 concentration (2.187 10^{-5}M)

The sample series in Fig.43*(R)* contains fixed dendrimer concentration and covers an I65 concentration range. The concentration of ionenes and then the ionic strength increases to the right (black arrow direction). At the beginning, at low I65 concentrations (section A) pure macromolecules and/or smaller aggregates are present in the system in addition to the larger aggregates. In the section B well defined, large aggregates exist after connection/recombination of those from section A. In the section C it may be an excess of ionene molecules that gives rise for the even faster diffusion ($R_{h\ app} \approx 5$ nm has been found). This "very fast" diffusion is not "slowed down" as in case of the fast mode at low I65 concentration, however the apparent hydrodynamic radii within an error are comparable for the fast mode in section A and C. As it was already mentioned, the fast mode at low I65 concentration (section A) can be caused by the mixture of macromolecules and oligoaggregates ($R_{h\ app}$ between 5 and 10 nm). and the diffusion coefficient represents an overlap (average) of the diffusion coefficient of single macromolecules and the diffusion coefficient of oligoaggregates. The very fast diffusion in section C disappears in the section D, where maybe only middle-size aggregates and the large aggregates are observed. The changes in the system may be caused by the changing, increasing ionic strength. Noteworthy is that for the excess of dendrimer molecules in the fast mode (direction "from the right to the left side" in mentioned figure) usually no peak can be observed. For comparison see also Fig.66 and Fig.67. This may be seen as a confirmation of the hypothesis that ionic strength plays a determining role here, which is increased only at the "right side" (increased concentration of ionene) of the one mode regime for the samples where ionene concentration is varied. It may be that due to the lower ionic strength no single macromolecules are present in this range but the fast mode in section A is caused by the

movement of oligoaggregates only. At low ionic strength the interaction between charged particles in solution are dominant, leading to the aggregation like in section A and B. With increasing ionic strength (again: black arrow direction), the interactions in the system becomes weaker.[136-137] This gives possibilities for single macromolecules to diffuse separately in the solution and not to be attached to an aggregate, compare section C. In section D, again two kind of species are present (not PE diffusion, see p.79). We are not able unequivocally judge about the nature of the species causing fast and slow mode on the "right side" of the one diffusion mode range. At even higher ionic strength (section D to the right), like it is known for usual polyelectrolytes, either secondary aggregation or the destruction of assemblies may take place due to decreased interaction because of screening.[136-137] The radii of structures causing the slow mode are comparable with the radii of structures in the one mode range. That is why we would suggest rather recombination of the assemblies existing in one mode range than destruction or secondary aggregation upon increasing ionic strength on the right side of the one mode regime. With growing ionic strength (black arrow direction in Fig.43(R)) the electrostatic interaction, keeping an assembly structure together, becomes weaker. A large assembly may be destroyed or at least looses building blocks from the surface. These building blocks, together with free ionene molecules in the solution may form again large and middle sized assembly structures.

The differences, when comparing the behavior of I65/Gx.y systems with the normal polyelectrolyte behavior can be due to the nature of "counetrions" used in both systems. When normal, linear polyelectrolyte systems are investigated low molecular mass salt is used. The radii of low molecular mass salt ions are around 0.2 nm. In case of our systems, dendrimer macromolecules accompany linear polyelectrolytes. The hydrodynamic radii of dendrimers used are around 2 to 6 nm. At least 10 to 30 times larger than the simply ions. Additionally, the "dendrimer counterion" carries many more charges than a small ion. The dissociation properties of low molecular mass salt are very simple as compared to the complicated mechanism governing dissociation of the dendrimer molecule. The radius of the dendrimer and the charge density apart from the environment properties like pH and ionic strength are in case of dendrimers of importance. Due to the multivalency of the dendrimer molecule, its properties can be described as much more "connecting-like" than "screening-like" as opposed to the monovalent ions of low molecular mass salt. That is why large aggregates in the dendrimer-ionene aqueous solution can be formed and give rise for turbidity or opalescence. In the system I65/G5.5 and I65/G7.5 due to the earlier discussed arguments we postulate rather different sized aggregates as a reason for the two diffusion modes. Figures 65-67 present the summary of the data for different I65/Gx.y cases.
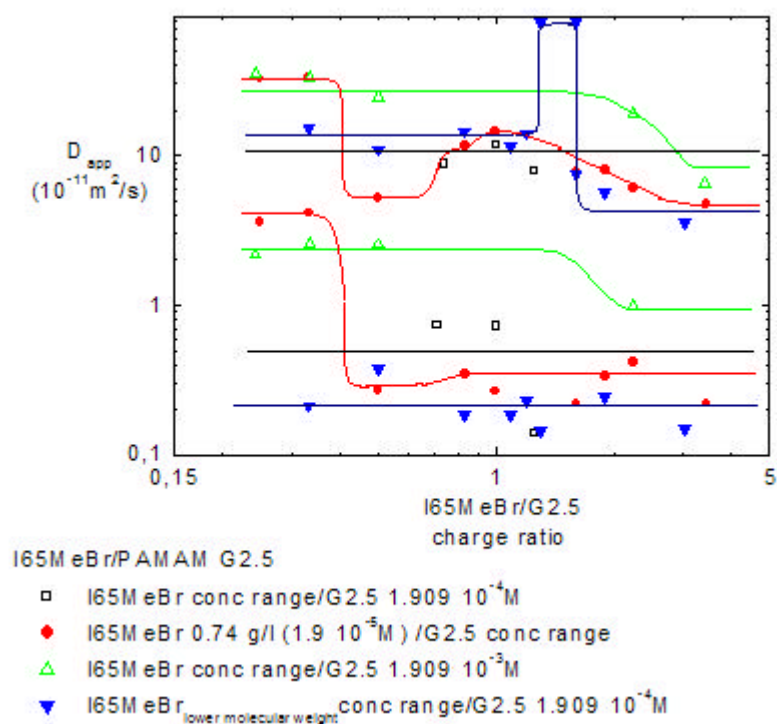
Fig.65: Apparent diffusion coefficient as a function of
charge ratio for I65/G2.5 systems.

The presence of different species in the solution is also confirmed when low molecular mass salt is added to the system. Before and after salt addition two diffusion modes are observed - even if the amount of added salt is high, more than one kind of objects exist in the system (see III.I.B). Thus it can be concluded that the two diffusion processes observed without salt do not represent polyelectrolyte diffusion (that would disappear upon salt addition).
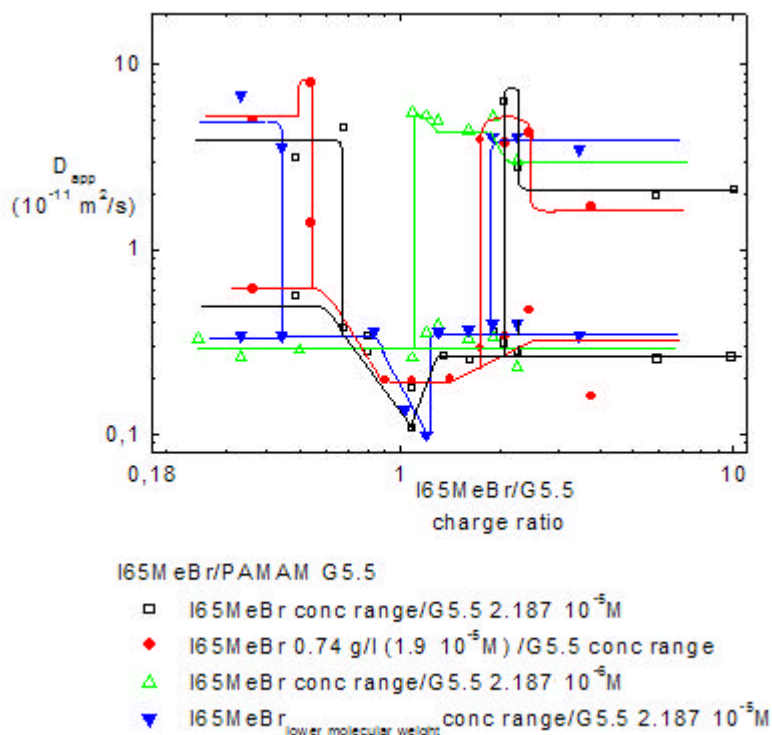
Fig.66: Apparent diffusion coefficient as a function of charge ratio for I65/G5.5 systems.

In Fig.66 we see an overlap of the diffusion profiles for the I65/G5.5 samples for fixed ionene as well as for fixed dendrimer concentration. One diffusion mode is present always around $\lambda = 1$. Even for lower molecular mass ionene the diffusion profile overlaps with the other I65/G5.5 (as for fixed ionene as fixed dendrimer concentration) diffusion profile. Only when the 10 times diluted system is regarded we see a shift in the diffusion profile and a lack of the "first" λ_1 i.e. no two-diffusion regime is observed for low charge ratios in this case. One can conclude that the molar charge ratio of the compounds of our systems influences formation of the complexes, but not only. A concentration effect is also observed.

Fig.67 shows an overlap of the diffusion profiles for the I65/G7.5 samples for fixed ionene as well as for fixed dendrimer concentration. It confirms our observation concerning the meaning of molar charge ratio and the concentration when I65/Gx.y complexes are formed. One diffusion mode is present again around $\lambda = 1$ to 2. Even for lower molecular mass ionene the diffusion profile overlaps with other I65/G7.5 (as for fixed ionene as fixed dendrimer concentration) diffusion profiles.
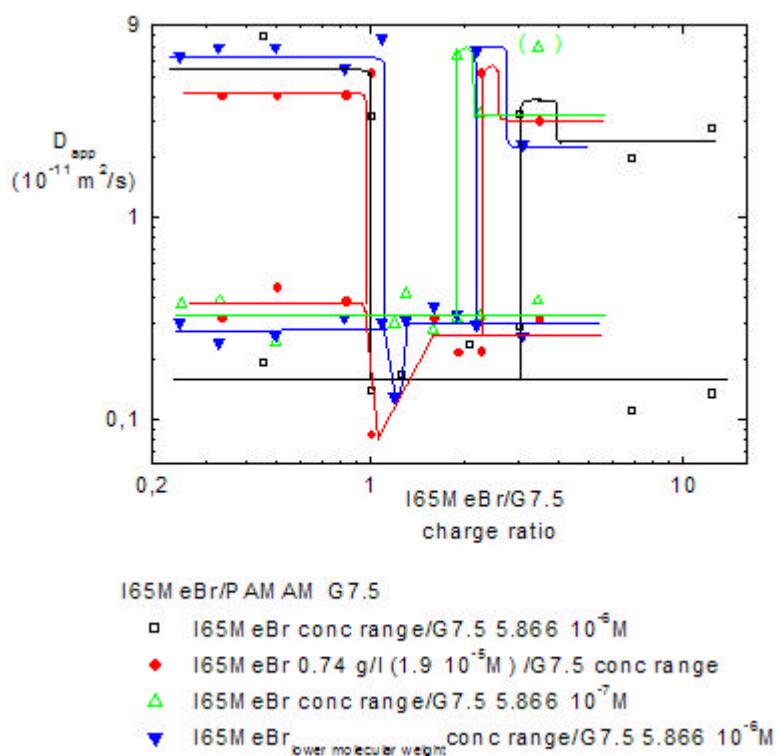
Fig.67: Apparent diffusion coefficient as a function
of charge ratio for I65/G7.5 systems

One further important aspect that needs to be considered is a kind of PE-effect which is caused in our systems not by usual polyelectrolyte molecules, but by the charged on the surface assemblies. According to the ζ potential measurements (see chapter III.VI) at certain ionene to the dendrimer charge ratio ranges, present in the solution assemblies are charged on the surface. This surface charge causes interactions in the system which can be a reason for the PE effect and double diffusion mode. On the other side, since the apparent hydrodynamic radii for the fast and slow mode in whole charge ratio range mostly do not change upon low molecular mass salt addition as presented in paragraph III.I.B, we exclude the charged assembly surface being the cause for diffusion behavior. Additionally positive slope (or no slope) of the diffusion coefficient versus scattering vector square in the two modes regime suggests presence of two kind of species. When PE-diffusion is observed rather the negative slope of the diffusion coefficient versus scattering vector square is expected. If then, the assembly particles are charged on the surface this charge is not of large importance on the diffusion behavior of the whole system.

3.2.1. I25MeBr/ Three Generations of Dendrimers

To understand the interplay of interactions governing the system built from ionenes and the dendrimers we measure the diffusion behavior of I25MeBr with dendrimers G5.5; G7.5; G2.5. For the turbidity and the pH data concerning such samples see III.I.A.1 and 2. According to the earlier analysis of I65MeBr we begin with I25MeBr and the G5.5 dendrimer. Since the charge ratio turned out be a useful parameter for further discussion of the results, all data are directly represented as a function of charge ratio. With growing charge ratio, i.e. with growing ionene I25MeBr concentration or with decreasing concentration of dendrimer the diffusion changes

from two modes into one and again splits to two modes (as it was observed in typical case of I65/G5.5), see Fig.68.
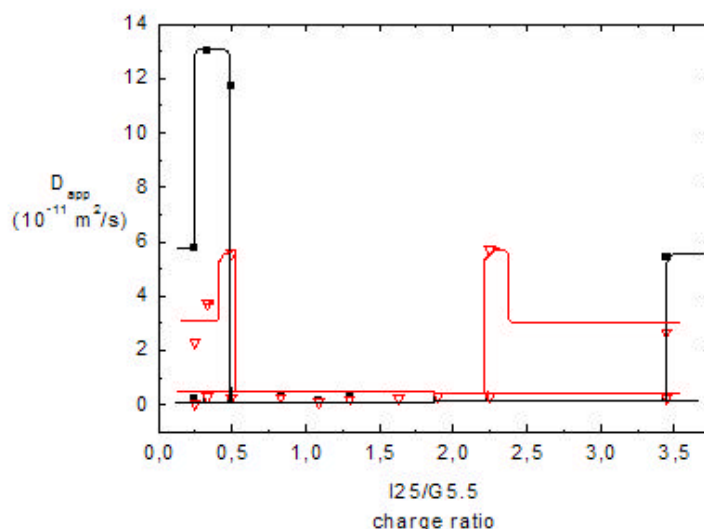

Fig.68. Diffusion coefficient as a function of charge ratio for

ionene I25 with G5.5 dendrimer. I25 concentration range and

G5.5 fixed (2.187 10^{-5} M) concentration is square marked.

I25 fixed (0.6 g/l, 2.53 10^{-5} M) concentration with G5.5 concentration

range is triangle marked.

Overlap of the diffusion profiles of I25/G5.5 (I25 fixed concentration) and I25/G5.5 (G5.5 fixed concentration) is observed. As is presented in Fig.69 and Fig.70, the diffusion coefficient versus scattering vector square shows a slightly positive slope for the area of one diffusion mode. When two diffusion modes are observed, fast diffusion is of the positive slope and slow diffusion is almost independent on the scattering vector square. This is the general tendency typical for the systems containing I25MeBr and the dendrimers.
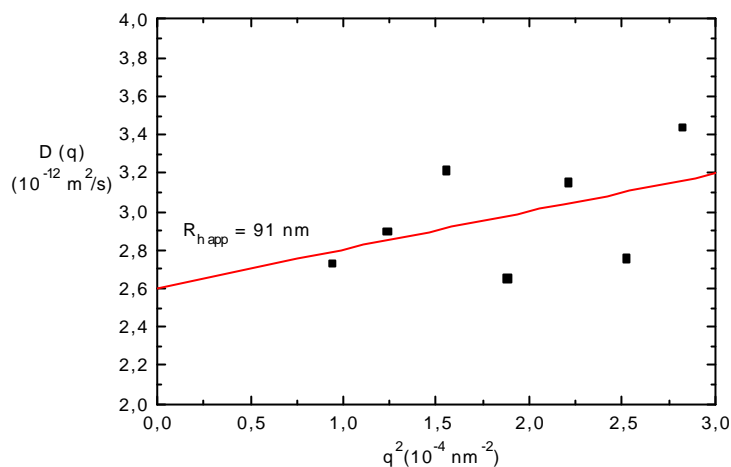
Fig.69: Diffusion coefficient as a function of the scattering vector square for the sample I25MeBr (0.6 g/l) and G55 ($1.57\ 10^{-5}$ M). Charge ratio I25/G5.5 = 1.63/1. The apparent diffusion coefficient is equal $D_{app} = 2.6\ 10^{-12}$ (m^2/s)
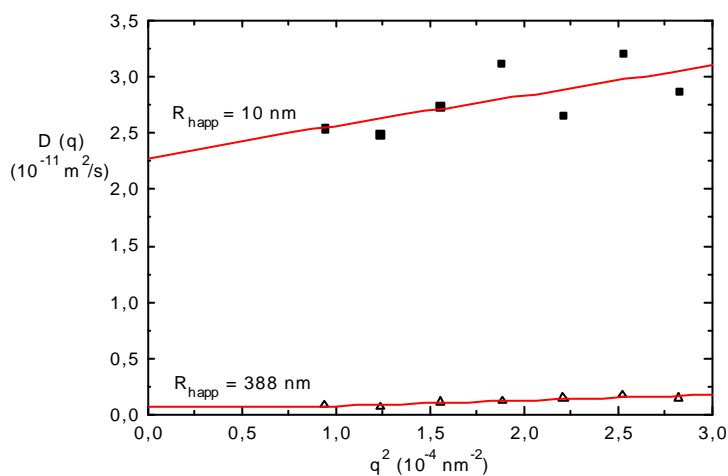
Fig.70: Diffusion coefficient as a function of the scattering vector square for the sample I25MeBr (0.6 g/l) with G5.5 ($1\ 10^{-4}$ M), where chrage ratio I25/g55 = 1/4. The apparent diffusion coefficients are equal $D_{app\ fast} = 2.3\ 10^{-11}$ (m^2/s)
$D_{app\ slow} = 2.7\ 10^{-13}$ (m^2/s)

For comparison the diffusion behavior of I25MeBr with G7.5 samples was investigated in Fig.71.
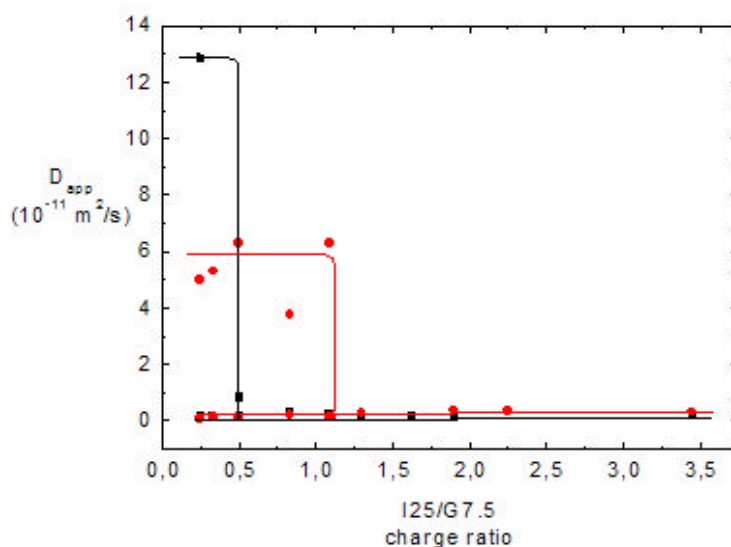
Fig.71. Apparent diffusion coefficient versus charge ratio
of I25 with G7.5 sample series. I25 concentration range at
fixed G7.5 (5.866 10^{-6} M) concentration is square marked.
I25 fixed (0.6 g/l (2.51 10^{-5} M)) concentration with G7.5
concentration range is circle marked.

The diffusion processes start with two modes for low concentrations of I25MeBr and connect in one diffusion mode for higher ionene concentrations. For comparison see Fig.71. This diffusion profile is different than the diffusion profile I65/G7.5: the second transition regime is missing. In Fig.71 a splitting point (transition from two to one processes) has been found at the ratio $C_{\text{charges I25MeBr}}/C_{\text{charges G7.5}} = 0.5$ or by the ratio $C_{\text{charges I25MeBr}}/C_{\text{charges G7.5}} = 1.09$ for fixed ionene concentration respectively. The observed phenomenon is opposite to the normal polyelectrolyte behavior, where around a splitting point value λ of 1, one diffusion mode changes into two diffusion modes.

Investigations of G2.5 with I25MeBr gives single diffusion modes in contrast to I65MeBr where always two diffusion mode samples were observed in the investigated range of concentrations (Fig.72).
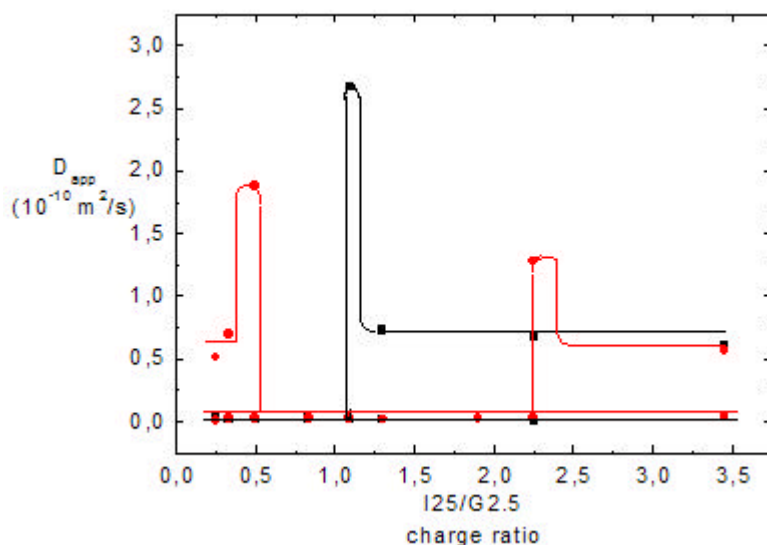
Fig.72. Apparent diffusion coefficient as afunction of
the charge ratio for I25 with G2.5 dendrimer systems.
Squares mean sample series with fixed (1.909 10^{-4} M)
G2.5 concentration and I25 concentration range. Circles
mean G2.5 concentration range with I25 fixed
(0.6 g/l (2.53 10^{-5} M)) concentration.

At low concentrations of the ionene one diffusion mode is observed for the samples with fixed dendrimer concentration. Furthermore, with growing concentration of the I25MeBr, the second mode appears, $\lambda = 1.09$. In opposite, for the samples at fixed I25 concentration, two transition points appear. At higher amount of the dendrimer added but also with very low dendrimer addition double mode diffusion is observed. "An intermediate region" is in that case limited by the splitting points $\lambda = 0.5$ and $\lambda = 2.25$ and is characterized by a single diffusion mode.

For both sample sets presented, charge ratio ranges are equal, however there are slight differences in the sample concentration between samples with fixed ionene and fixed dendrimer concentration. The differences in diffusion profiles observed in Fig.72 confirm concentration to be an additional factor during complex formation appart from the molar charge ratio and linear charge density of ionene compound.

3.2.1.a   I25MeBr/Gx.y complexes- summary

In Tab.12 we summarize some important aspects of systems composed of I25 and flexible PAMAM dendrimers generation G2.5, G5.5 and G7.5. The samples cover whole range of turbidity, starting from clear solutions to the very turbid samples even with white flocks inside (for details see Tab.9). Samples of the highest opalescence or turbidity are observed in the one diffusion mode range. Especially turbidity indicates the presence of large objects in the solution. Opalescence or turbidity ranges coincide with a rapid decrease of the pH value.

Tab.12: Diffusion properties of I25/PAMAM dendrimer complexes -summary

Complexes with fixed dendrimer concentration		Splitting parameter	
Compounds	*Size of objects within one mode area (nm)*	l_1	l_2
I25/G5.5	80-140	0.5	3.5
I25/G7.5	80-120 (200)	0.5	-
I25/G2.5	100	1	-
Complexes with fixed ionene concentration		Splitting parameter	
Compounds	*Size of objects within one mode area (nm)*	l_1	l_2
I25/G5.5	80-100	0.5	2.25
I25/G7.5	80-120	1	-
I25/G2.5	120-140	0.5	2.25

Again the expected differences between a normal polyelectrolyte behavior and our system are present. In particular, the fast mode is "faster" than the diffusion in the one mode range while the slow mode is "slower". The solution stays clear in the transition regime. For the I25/Gx.y systems not only two transition regimes can be observed, but also the differences in the velocity of particles are significant. Like for the I65/Gx.y complexes two transition regimes can be observed. The differences in the velocity of particles are significant as well. For the I25/Gx.y systems, like in the case of I65/Gx.y, the one mode regime shows diffusion of complex particles of the size of multiple building blocks (polyelectrolyte chains plus dendrimers) (R_h 60 to 200 nm), whereas for the normal polyelectrolyte particles in the one mode range particles are in the order of magnitude of the single macromolecule (single polymer molecules). Besides the I25/Gx.y solutions in the one mode regime are opalescent to turbid, whereas for the normal polyelectrolytes solution in one mode range is clear. Often a peak in the fast mode occurs either before or just after transition regime for the I25/Gx.y diffusion profile which is also not typical for the normal polyelectrolytes. The explanation of this phenomena must be similar like for the I65/PAMAM systems (see I65/PAMAM complexes summary). This very diffusion must be caused by the movement of free I25 macromolecules, which appear at higher ionic strength (screening of the electrostatic interactions in the system as in the case of I65/PAMAM complexes). Also a decrease of pH value is observed when analyzing pH dependency as a function of molar charge ratio (see subchapter 1 and 2 in III.I.A), which means the particles are "neutralized", so they have to be connected in the aggregates. However like in the case of I65/PAMAM complexes this aggregates are different in size in the two diffusion mode range and charged on the surface for certain I25/Gx.y charge ratio ranges.

III.I.B. Complexes with low molecular mass salt addition

To judge about the reason for two modes present in the systems of ionene and flexible PAMAM dendrimers, we investigate selected samples with low molecular mass salt addition (KBr). The concentration of salt in the samples ranges from 10^{-6} mol/l to 10^{-3} mol/l. For higher salt concentration in the sample, a salting out effect is observed, i.e. the sample precipitates. Investigated were samples of I65 and I25 with G2.5 and G7.5. We assume, based on the similarity in the diffusion profiles between samples containing G5.5 and G7.5 measured earlier, that their diffusion behavior under salt addition is also similar. If we observed after addition of a certain amount of salt only one diffusion mode (in the sample with originally two modes), this means interactions in the investigated system are screened via low molecular mass salt and initially two modes were caused via polyelectrolyte effect. If after some amount of salt added (in the originally two-modes-sample) still two modes are measured, that means the two modes

are caused by two species different in size that exist also under addition of salt. Although the behavior of the system investigated here may be even more complex since assembled structures themselves (not only intermolecular interaction) may change upon salt addition, the experiment with varying amounts of added salt are expected to facilitate further understanding of the system.

Fig.73-75 show the presence of two diffusion modes after salt addition. This confirms our expectation that in the system Imn with Gx.y two diffusion modes are caused by the different in size aggregates or single macromolecules and aggregates. The radius of particles corresponding to the fast diffusion is of the order of magnitude of single ionene or dendrimer macromolecule. Figures 73, 74, 75 show the distribution of decay times for different I25/PAMAM samples at different salt concentration. In Fig.73 the distribution function of the decay times is given for the sample I25/G7.5 at a charge ratio 0.833. The relaxation rate distribution is observed upon different amounts of low molecular mass salt addition. Changes in the size or in the ratio of system compounds can be observed. The sample in Fig.73 originally is a clear solution and shows two modes before low molecular mass salt addition. We assume that in the system investigated two modes are caused via two different species in the solution. Peak I in Fig.73 reflects the behavior of small objects, peak II reflects the behavior of larger objects. Upon salt addition, even at 10^{-6} M the solution becomes opalescent. It can be caused either via an increase of the number of aggregates or via increase of the radii of already aggregated structures i.e. by secondary aggregation. When the amount of aggregates in the solution increases, the intensity of the peak II (red line) increases. During secondary aggregation the maximum of the peak II should move to higher τ-values because of an enhancement in radii of secondary aggregated structures. This seems to be not the case, so in our system upon 10^{-6} M salt addition, the number of aggregates increases. The increase of amount of the aggregated structures should coincide with a decrease of the single molecules (building blocks) number, i.e. a decrease of the peak I intensity. Further salt addition may cause destruction of the aggregates. The intensity of the peak II decreases. The intensity of the peak I increases. There is larger number of free building blocks in the system. This hypothesis presented above about the aggregation and disaggregation of the building blocks upon salt addition seems to be a model which may fit the observed sample behavior. However, it is not sure that the sample really undergoes changes described via our hypothesis.

The increase in the relative peak height observed (sometimes even above 30%) was over the experimental error, and does not change with the fitting parameters during data evaluation. The peak height, broadness and its location changes are very narrow when comparing two measurements for the same sample. The distribution of relaxation times profiles are the same. A second measurements has been done 2h after the first one under the same condition. In addition, relaxation time distribution for the original sample and for its control probe are almost identical. The control sample set has been measured under the same condition like the original one. The stability of the decay times distribution upon salt addition is also confirmed by the measurements at different scattering angle.
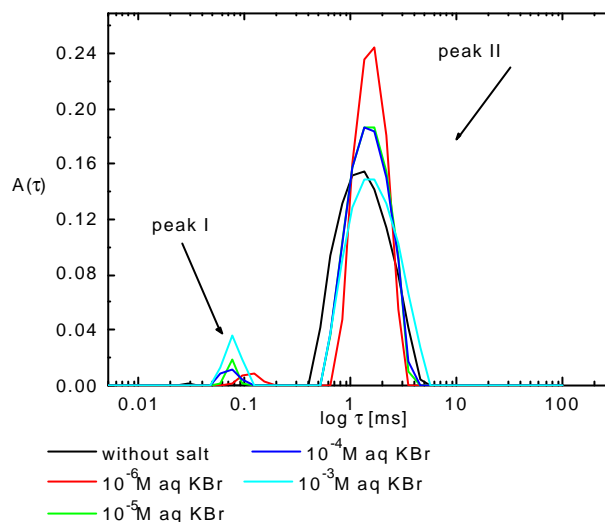
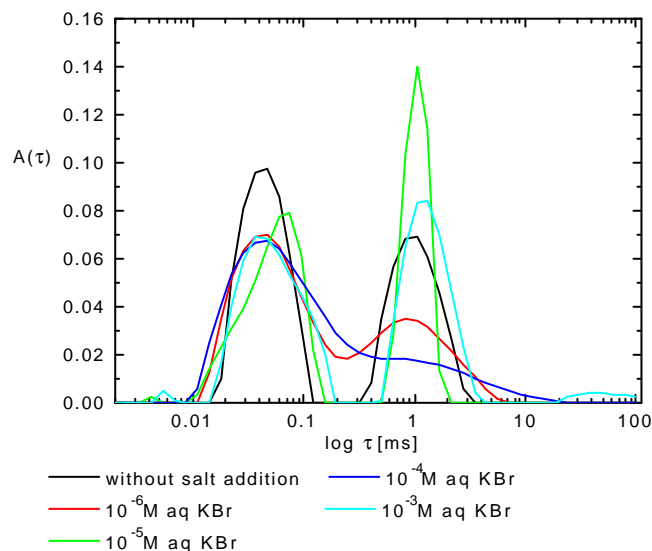Fig.73: Decay time distribution function at different

ionic strength for the sample I25MeBr/G7.5 at a charge

ratio 0.833. Scattering angle equals 90°

A similar experiment is presented in Fig.74 for the sample containing I25 and G2.5, and in Fig.75 for the sample containing I65 with G7.5. In both cases two peaks are observed. Peak I caused by small objects, peak II caused by the larger objects. The peaks do not disappear upon low molecular mass salt addition. Again two species, aggregates and macromolecules are expected to be a reason for two diffusion modes. Observed changes in relative peak height are not so systematic here (Fig.74-75) in comparison with the case of samples in Fig.73.

Fig.74: Decy time distribution function at differnt

ionic strength for the sample I25MeBr/G2.5 at

a charge ratio 3.45/1, at the 90° scattering angle
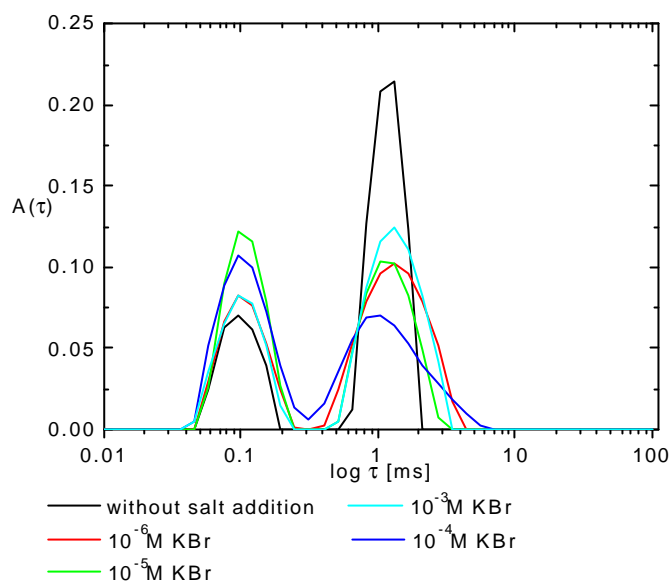
Fig.75: Decay time distribution at different ionic strength for the sample I65MeBr/G7.5 at a charge ratio 3/1 at the scattering angle 90°.

From Figures 73 to 75 we conclude that the salt addition does not fundamentally change the diffusion behavior of the sample. After salt addition still two modes are present in Fig.73-75. This observation suggests the presence of two species in the solution.

The originally one mode samples have been investigated as well with low molecular mass salt. In Fig.76 I25/G2.5 the sample at the charge ratio around 1 is presented as an example. Before salt addition the sample is opalescent and it stays opalescent at high ionic strength. A shift of the maximum to higher values of the decay time is observed. These can be caused by a recombination of the aggregated structures followed by slight increase of the radii of aggregates.
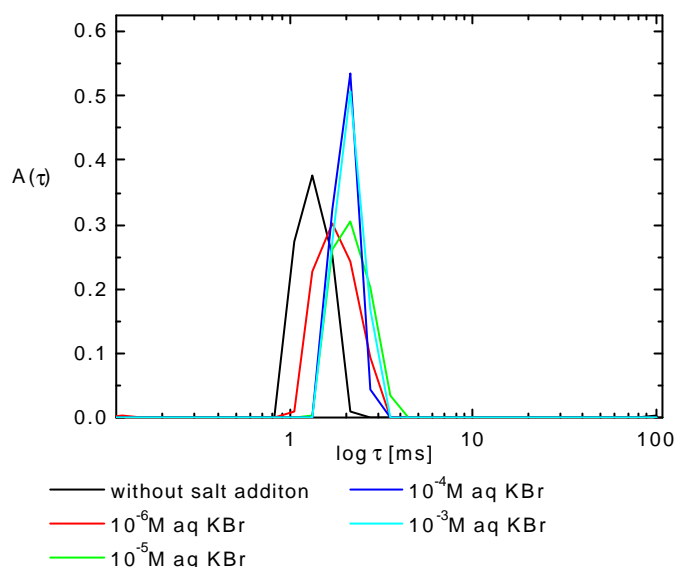
Fig.76: Distribution of decay times for "one mode"

sample and at different ionic strength. The sample

contains I25/G2.5 at a charge ratio of I25/G2.5 = 1.09/1.

The scattering angle equals 90°

Fig.76 contains data for the case of salt addition to the one mode sample. The structures observed in that case are stable under different ionic strength (different salt concentration in the sample). Almost no deviation from previous behavior (without salt addition) has been found. Fig.73-76 contain examples of the data obtained at 90° scattering angle. The reproducibility of this results has been proven with good agreement by comparing the original sample measurement with a control sample, the measurements of the same sample twice and the lack of angular dependency of the relaxation times, it can be seen in Fig.76.

III.I.C. I65MeBr/Gx.y and I25MeBr/Gx.y complexes- DLS results summary

Scattering techniques enable investigations of dynamic behavior of the solutions (see DLS) as well as investigations of the size of structures (SLS/DLS/SANS). The general diffusion profile for the ionene- PAMAM-dendrimer complexes (green curve) has been compared with the "normal polyelectrolyte" diffusion behavior (black curve) in Fig.54. Two transition regimes can be observed and besides differences in the velocity of particles as compared to the normal polyelectrolytes (see III.I.A.3) are significant. The transition regimes are observed before and after the one-mode regime around $\lambda \approx 1$. The fast mode is "faster" than the diffusion in one mode range. The slow mode does not change. It would be expected to be "slower" as the one diffusion mode if it would be due to a slow mode of PE-diffusion, which gives evidence for aggregates being the cause for the slow mode here. A peak in the fast mode appears around splitting points and might be caused by the excess of the ionene macromolecules. The one mode regime is characterized by turbid or at least opalescent samples what suggests the presence of larger objects. The transition regimes have been found from two to one and from one to two diffusion processes for the lowest dendrimer generation (G2.5) in its combination with I25 as opposed to the I65/G2.5 behavior. It indicates the influence of charge density on the

100

structure formation. Also the concentration of the sample is important for complex formation. For lower concentrated samples only one transition point around $\lambda_{splitting}$ of 1 occurs. Finally the molar charge ratio is an important parameter during the complex formation. In each case complexes appear in the solution around $\lambda = 1$. Increasing concentration "shifts" the diffusion coefficient dependency to higher charge ratios. The splitting points for all systems investigated are given in the Table 13. Two modes are caused by two different sized species present in the solution as becomes obvious since no interaction screening effect after low molecular weight salt addition is observed in both double-mode areas.

Tab.13. Diffusion profile parameters for ionene/dendrimer systems

λ parameter for different ionene/dendrimer samples			I65MeBr		I25MeBr	
			Mw (g/mol)	Surf group	Mw (g/mol)	Surf group
			39000	322	23700	255
G2.5	Mw (g/mol)	6267	no transition point observed; double mode samples		$\lambda_1=0.5$; $\lambda_2=1.09$	
	Surf group	32				
G5.5	Mw (g/mol)	52901	$\lambda_1=0.681$; $\lambda_2=1.74$		$\lambda_1=0.5$; $\lambda_2=2.25$	
	Surf group	256				
G7.5	Mw (g/mol)	212739	$\lambda_1=1$; $\lambda_2=2.29$		$\lambda_1=1.09$	
	Surf group	1024				

The case of I25MeBr with G7.5 and G2.5 looks like the "ideal case", as for normal polyelectrolytes $\lambda_{splitting}$ is close to 1. However the apparent hydrodynamic radii calculated from the one diffusion mode indicate complex structures as opposed to the normal PE-diffusion, where one diffusion mode is caused by single macromolecules. General tendency is that the $\lambda_{splitting}$ value (for the first and for the second transition point) in case of ionene/PAMAM sample series increases with increasing dendrimer generation. The splitting points appear for higher dendrimer generations (higher molecular mass and higher surface charge number) at higher λ which in case of ionene concentration variation also means higher ionic strength.

One of the participating molecules (of pronounced lower molecular weight) acts as a counterion while the other molecules (of higher molecular weight) play the polymer "role". The cases of I25MeBr with G5.5 and I65MeBr with G5.5 (and G7.5) are the cases where molecular weights are comparable and high. It may also influence the complex formation. However at this point we are not able to judge in details about this influence. When I65MeBr mixed with G2.5 always two modes are observed. Besides, honey like precipitation appears in the concentrated samples.

III.II. SLS of ionene/PAMAM dendrimer complexes

Static light scattering was involved to investigate the structure of chosen complexes. Data presented below are for the I65/G5.5 sample. The sample comes from the series where I65 concentration range and G5.5 fixed concentration was applied and belongs to the range with one diffusion mode. The sample is slightly opalescent. The scattering curve is given Fig.77.
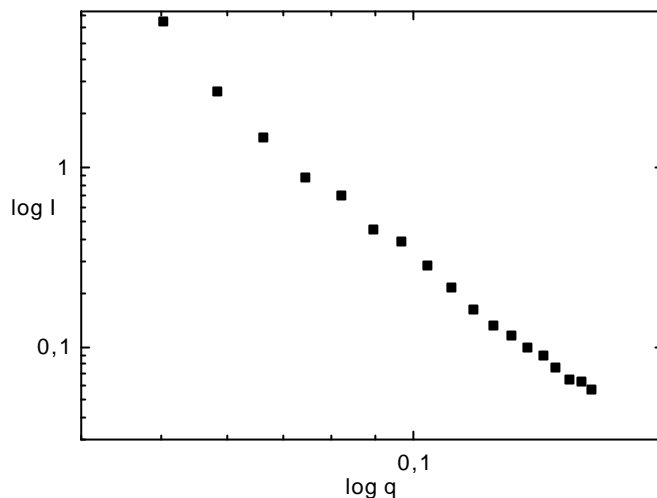
Fig.77: Scattering intensity as function of the scattering

vector q for the sample I65 (0.74 g/l) with G5.5

(2.187 10^{-5} M). The charge ratio I65/G5.5 = 1/1

According to the procedure discussed earlier we are able to calculate the radius of gyration R_g of such sample (from the Zimm plot (Fig.78)) and compare it with the hydrodynamic radius R_h.
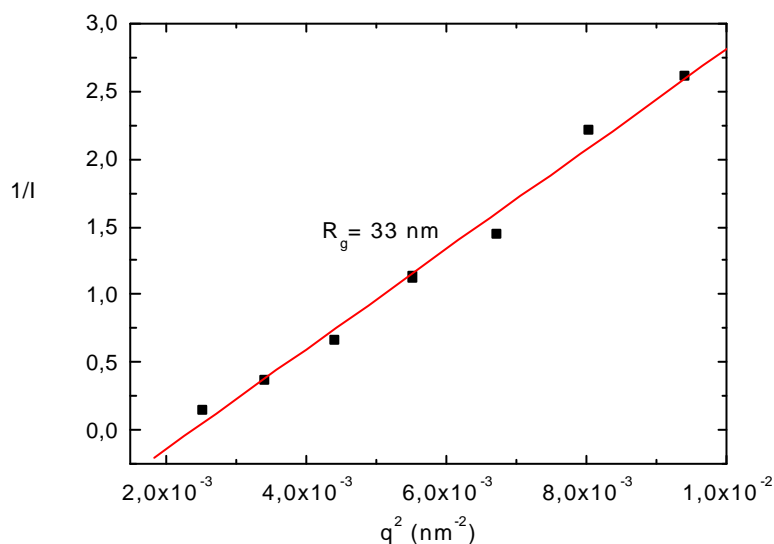

Fig.78: Zimm plot for the sample I65 (0.74 g/l) with G5.5

(2.187 10^{-5} M). The charge ratio I65/G5.5 = 1/1

The investigated sample was opalescent what may confirm the presence of bigger aggregates. The Zimm plot has been used to estimate the R_g of 33 nm. The hydrodynamic radius measured by DLS for this sample is R_h = 121 nm. The ratio $\rho = R_g/R_h$ = 0.3. From the literature it is the value for entangled structures or microgels.[125] However in some cases is difficult to judge

102

about the area of linearity of Gunier or Zimm plot. This phenomenon will be discussed in details for SANS data analysis. The reason of usage of the Zimm or Gunier plot is the shape of the investigated aggregates. From the slope of the linear relationship one can calculate the radius of gyration of the aggregate. If the assemblies present in the solution do not posses spherical shape, the Zimm plot should be much more appropriate. In practice, both plots, the Zimm and the Gunier plot are drawn and compared. We measured the SLS for the I65/G7.5 samples as well (Fig.79, Fig.80).

Fig.79: Scattering intensity I vs scattering vector q for the
sample I65 (1.528 g/l) with G7.5 (5.866 10^{-6} M).
The charge ratio is I65/G7.5 = 2.1

Form the Gunier plot the radius of gyration has been calculated (Fig.81): R_g = 34 nm
The hydrodynamic radius measured by DLS for this sample R_h = 94.4 nm.
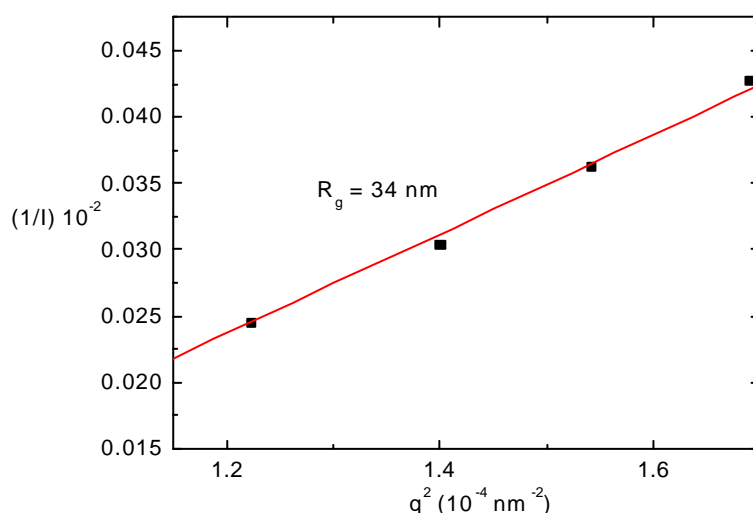
Fig.80: Zimm plot for the sample I65 (1.528 g/l) with
G7.5 (5.866 10^{-6} M). The charge ratio
is I65/G7.5 = 2.1

The ratio $\rho = R_g/R_h = 0.36$. Again the value of ρ for entangled structures has been found. An additional experiment (i.e. SANS) allowing to measure the R_g is required. For the SANS data analysis refer to paragraph III.IV.

III.III Light Scattering- supplement

Substantial differences in the diffusion behaviour of ionene/PAMAM dendrimer systems have been found as compared to the usual polyelectrolyte behaviour. For the details see subchapter 4a.5. The distribution of the hydrodynamic radii suggest well defined structures of I65/G5.5 and I65/G75 samples in the one diffusion mode range. The comparison of radii of gyration (calculated from the SLS) show that these structures possess star-like morphology and have a hydrodynamic radii of about R_h 100 to180 nm.

To judge about the radii of particles giving two modes notion we may compare the diffusion coefficients of pure ionene (pure dendrimer) with diffusion coefficients of expected complexes, compare Fig.82. From that comparison we will know where the fast mode comes from, whether it is due to the single ionene (dendrimer) macromolecule diffusion or is "faster" ("slower") as compare to the mode coming from single ionene (dendrimer) macromolecule diffusion.
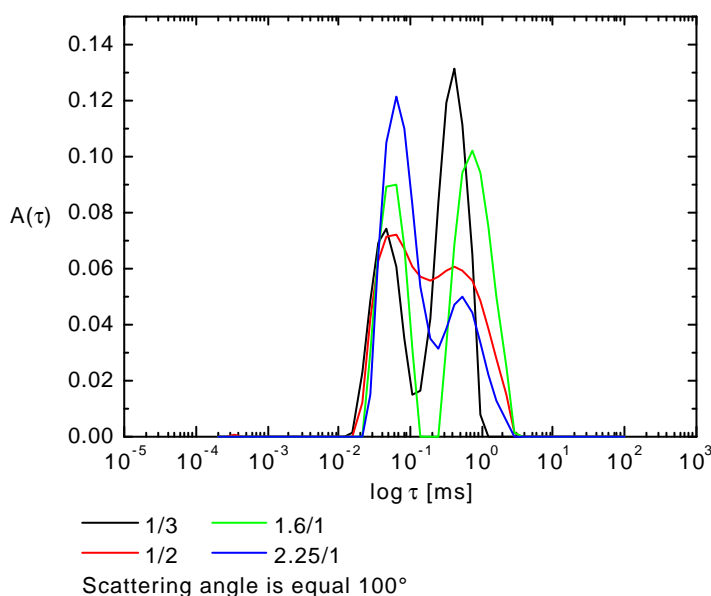
Fig.81. The distribution of the decay times for the sample

I65 (constant concentration) with G5.5 (concentration range)

for the charge ratios mentioned above

In Fig.81 the distribution of the decay times for the sample I65/G5.5 at different charge ratios is presented. The samples have been chosen from the two diffusion modes range. At the beginning the number of dendrimer charges is three times higher then the number of charges of ionene. It means, in case of the I65/G5.5 complexes, where a single I65 molecule contains 322 positive and a single G5.5 molecule 256 negative charges, the molecular ratio of I65/G5.5 equals 1.25 ionene molecules per 3.75 dendrimer molecules. Then the number of ionene charges in the solution gradually increases up to I65/G5.5 = 2.25/1, which means 3 ionene molecules per 1 dendrimer molecule. The observed modes in Fig.86 are partially not well

separated, however the peak maximum can be well seen in every case. The position of the maximum and the peak width does not significantly change in dependence on the degree of regularization during the normal data evaluation procedure in the inverse Laplace Transformation. The position of the first maximum corresponds to the hydrodynamic radius of 4 to 5 nm, the position of the second maximum corresponds to the hydrodynamic radius of 25 to 60 nm. The fast diffusion may be caused by the movement of small, single macromolecules, whereas the slow diffusion may be caused by larger, aggregated species. Thus the observed diffusion does not dramatically change from sample to sample. Two diffusion modes have to be caused by the movement of two species of the particles.

The strongest assembly properties occur around 1/1 ionene to the dendrimer molar charge ratio (around this ratio one diffusion mode is observed, compare chapter 4). In Fig.82 the diffusion profile of the sample series of I65/G5.5 at constant ionene concentration is present.
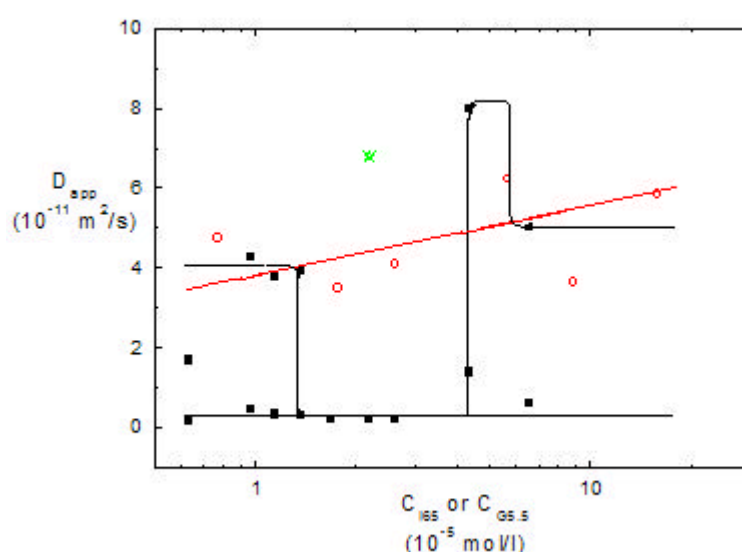
Fig.82. Apparent diffusion as a function of the concentration for the samples I65 (1.8 10^{-5} M) with G5.5 concentration range (full squares), I65 concnetration range in aqueous 0.4 M KBr solution (empty circles) and G5.5 2.187 10^{-5} M in aqueous 0.4 M KBr (star).

The fast diffusion mode of the complex samples lies in the range of diffusion of pure ionene and (within experimental error) in the pure dendrimer diffusion range. The fast mode observed for the complex samples has to be caused by the diffusion of pure ionene or/and pure dendrimer molecules plus the diffusion of middle-size aggregates. The radii of the middle-size aggregates are found to range from 10 to 30 nm ("dimers","trimers","tetramers" of macromolecular compounds). The radii of pure macromolecular compounds are between 2 nm (for G2.5) and 6 nm (for I65). The slow mode of the complex samples is caused by larger aggregates. This hypothesis is supported by the experiment with low molecular mass salt addition (paragraph III.I.B) and by the observation of the decay time distribution stability (Fig.81).

III.IV. SANS data analysis

To analyse the structure further, for some samples Small Angle Neutron Scattering (SANS) was performed. The scattering curve presented in Fig.83 shows data after solvent and incoherent background (Porod slope of (-4)) correction. The lack of the upturn in the low-q part of the scattering curve indicates the lack of the strong influence of interparticle interactions on the scattering curve. Presence of interparticle interactions makes the analysis of the scattering curve complicated. That is why based on the information from DLS, we have chosen for the SANS measurements one diffusion mode samples. One two diffusion modes sample has been also measured by SANS for comparison. Additionally the upturn in the initial part of the scattering curve may be due to the well defined geometry of the large objects so called "structure peak".

Well-expressed minima on the scattering curve for higher q-values indicate a defined aggregation. From the scattering curve the radius of gyration (R_g) was calculated. Two models were considered for R_g calculation. The Zimm model is appropriate for coils and systems with broad molecular mass distribution and yields a higher value of R_g ; the Guinier plot enables a better estimation of radii for collapsed coils and globular particles, the value of R_g obtained is lower than in case of Zimm plot. For the explanations of way of data treatment see chapter IV in the theoretical part.

1. I65MeBr/Dendrimers

The data analysis presented here for I65MeBr with G5.5 samples is based on four examples which are listened in Table.14.

Table.14: I65/G5.5 sample characteristic.

I65MeBr concentration (mol/l)	G5.5 concentration (mol/l)	Charge ratio ionene/dendrimer	Sample condition	Sample name
$8.717 \ 10^{-6}$	$5.64 \ 10^{-6}$	1.94	clear	M020
$2.35 \ 10^{-5}$	$2.187 \ 10^{-5}$	1.35	opalescent	M021
$1.92 \ 10^{-5}$	$2.187 \ 10^{-5}$	1.1	opalescent	M027
$1.37 \ 10^{-5}$	$2.187 \ 10^{-5}$	0.79	clear	M031

In the following we will first extract values for the radius of gyration for the different samples and afterwards consider possibilities for a more detailed analysis. The scattering intensity versus scattering vector for the M020 sample is presented in Fig.83-85.
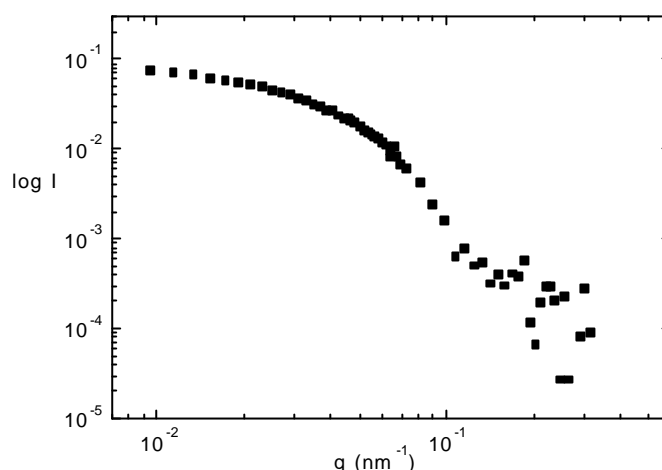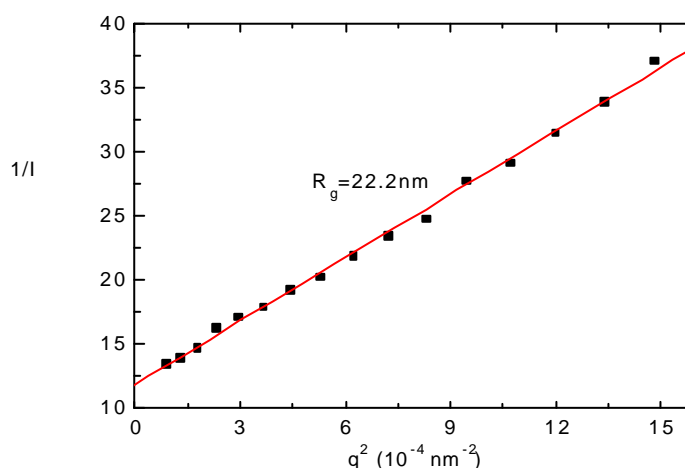
Fig.83: Scattering intensity I vs scattering vector q for the
sample I65MeBr 0.34g/l (8.717 10^{-6} M) in G5.5 5.64 10^{-6} M
The charge ratio I65M/G5.5 = 1.94/1. Sample is
a clear solution. Sample name is M020

The log I vs log q -plot does not show an upturn for the low q values. This indicates a lack of
the interactions between particles in the investigated solution. For the low scattering vector
values no structure peak is observed (Fig.83). Thus it is reasonable to further consider the
scattering curve as particle form factor, i.e. to extract information about particle size and shape
assuming that intermolecular interactions can be neglected. This is also in agreement with the
DLS-results of this samples where a single mode and no polyelectrolyte-effect was observed.
Zimm and Guinier plot seem to be useful for the R_g estimation (Fig.84, Fig.85).

Fig.84: Zimm plot for the sample I65MeBr 0.34g/l
(8.717 10^{-6} M) in G5.5 5.64 10^{-6} M. The charge ratio
I65M/G5.5 = 1.94/1. Sample is a clear solution.
Sample name is M020
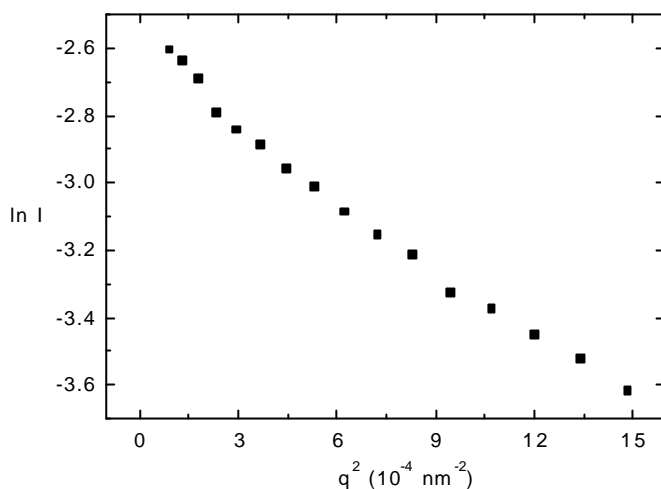
Fig.85: Gunier plot for the sample I65MeBr 0.34g/l
(8.717 10^{-6} M) in G5.5 5.64 10^{-6} M. The charge ratio
I65M/G5.5 = 1.94/1. Sample is a clear solution.
Sample name is M020

However when looking at the details, the initial part of the Zimm plot shows much better linearity than for Guinier plot. The resulting value for the radius of gyration from Zimm plot is R_g =22.2. For the sample M021 in Fig.86 higher concentrations of the compounds have been used and the charge ratio I65/G5.5 = 1.35. Corresponding plots are shown in Fig.86-88. As in the first case, there is no upturn of the intensity for low q values (Fig.86).
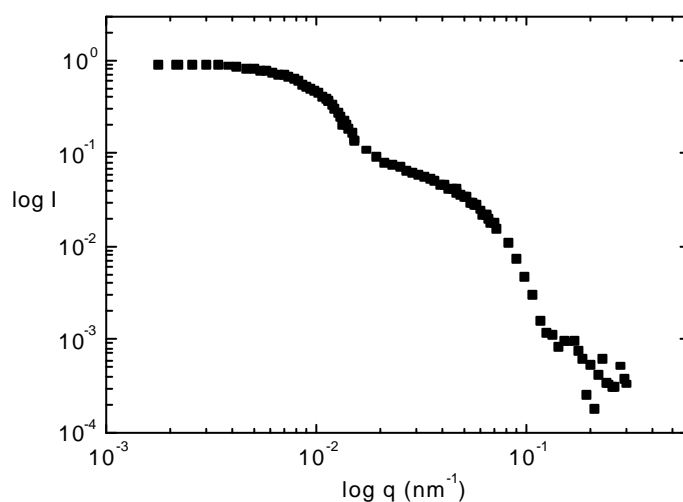
Fig.86: Scattering intensity I vs scattering vector q for
the sample M021 I65MeBr (0.915 g/l) in G5.5 (2.187 10^{-5} M)
Charge ratio is I65/G5.5 = 1.35/1. Sample is opalescent

In this case comparable linearity and good agreement is observed between Zimm and Gunier plot. R_{gZimm}= 16.5 nm whereas $R_{gGunier}$= 16.5 nm, as in Fig.87, Fig.88.
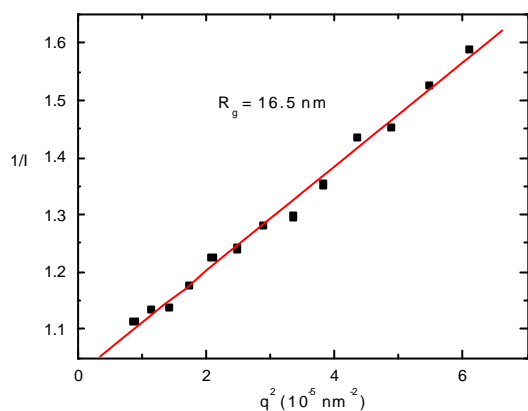
Fig.87: Zimm plot for the sample M021 I65MeBr (0.915 g/l) in G5.5 (2.187 10^{-5} M). Charge ratio is I65/G5.5 = 1.35/1. Sample is opalescent
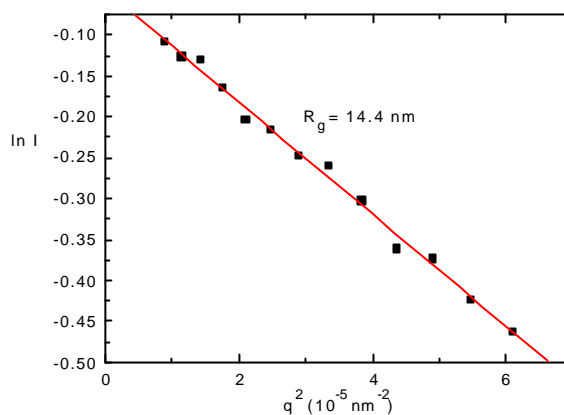
Fig.88: Gunier plot for the sample M021 I65MeBr (0.915 g/l) in G5.5 (2.187 10^{-5} M). Charge ratio is I65/G5.5 = 1.35/1. Sample is opalescent

Results for the sample M027 with a concentration comparable to M021, but a charge ratio I65/G5.5 = 1.1/1 as intensity versus scattering vector, Zimm and Gunier plot are presented in Figures 89-91. For this sample, expressed form factor minima in the scattering curve (Fig.89) are particularly obvious and indicate well-defined aggregates of narrow size distribution.
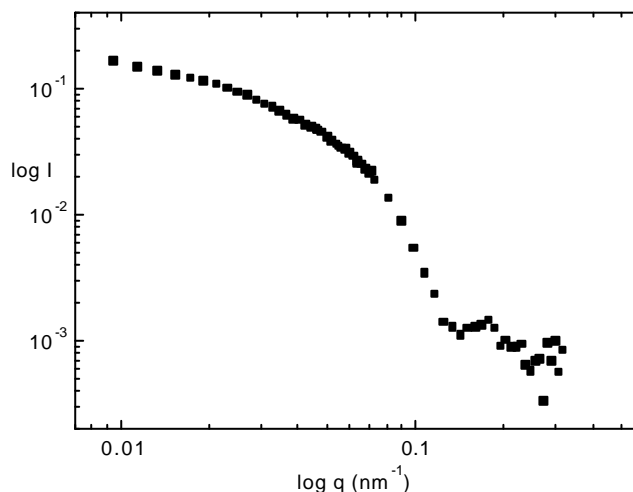
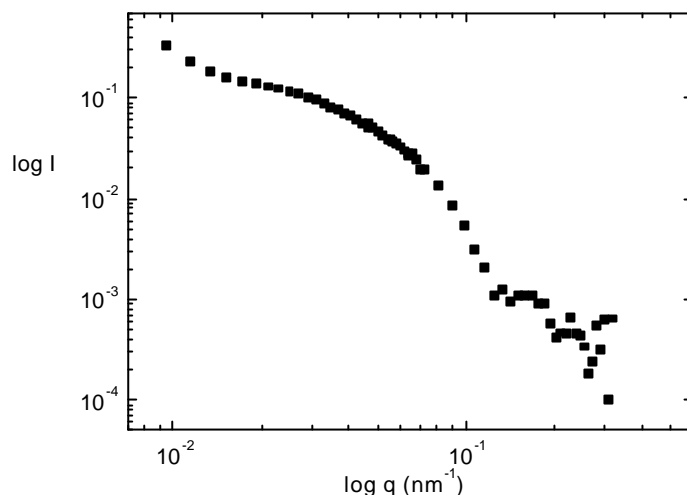

Fig.89: Scattering intensity I vs scattering vector q for the sample M027: I65MeBr (0.915g/l (2.346 10^{-5} M)) with G5.5 (2.187 10^{-5} M) at the charge ratio I65/G5.5=1.1/1. Sample is opalescent
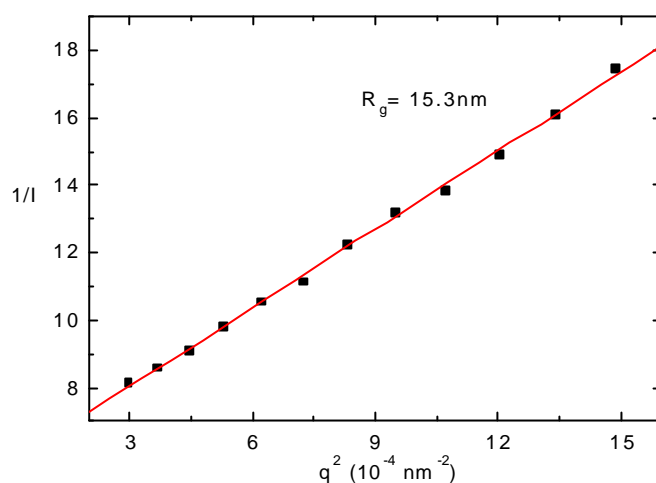
Fig.90: Zimm plot for the sample M027: I65MeBr
(0.915g/l (2.346 10^{-5} M)) with G5.5 (2.187 10^{-5} M)
at the charge ratio I65/G5.5=1.1/1.
Sample is opalescent

In this case Gunier plot is less appropriate (Figure 91).
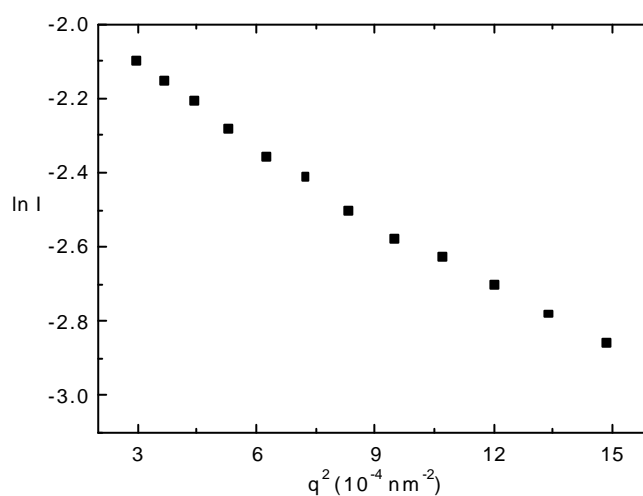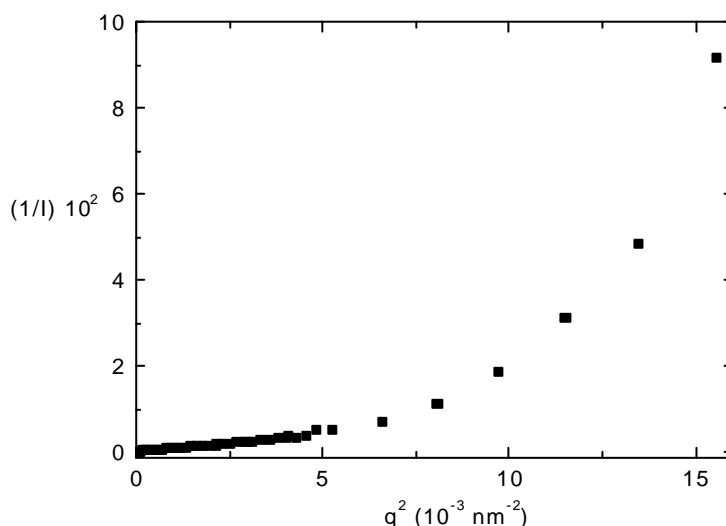

Fig.91: Gunier plot for the sample M027: I65MeBr
(0.915g/l (2.346 10^{-5} M)) with G5.5 (2.187 10^{-5} M)
at the charge ratio I65/G5.5=1.1/1.
Sample is opalescent

Here the Zimm plot shows a somewhat better linearity and is thus more suitable to determine R_g . Thereby R_g is found to be equal 15.3 nm (Figure 90).
Sample M031 similar in concentration of compounds to M027 and M021, but with a charge ratio I65/G5.5 = 1/1.26. It shows two modes in DLS and thus it is difficult to analyse also by static

scattering techniques. Domain formation and interaction effects are expected to complicate the data analysis, in particular at low q. The SANS data are shown in Figure 92-96.

Fig.92: Scattering intensity vs scattering vector q

for the sample M031 I65MeBr (0.535g/l (1.37 10^{-5} M))

with G5.5 (2.187 10^{-5} M) at the charge ratio
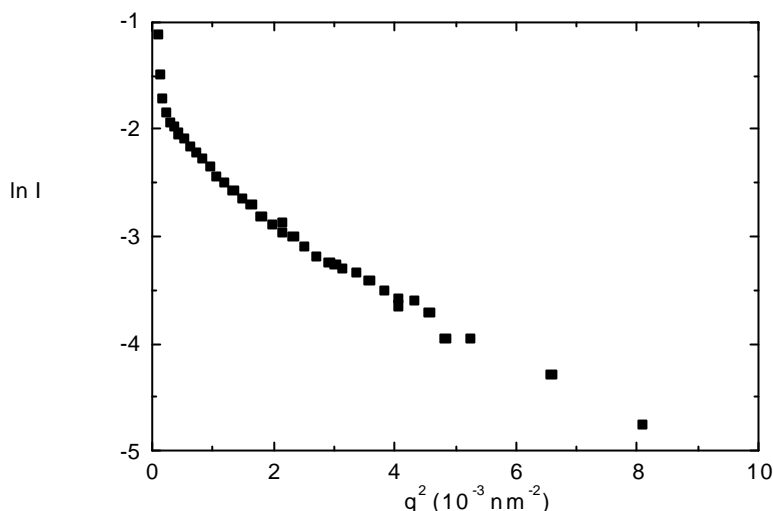
I65/G5.5 = 1/1.26. The sample is clear solution

As expected, an upturn in the scattering curve is visible at low q (Fig.92) and low q data show a deviation from linearity in both the Zimm and the Gunier plot. However at intermediate q a linear region can be detected, from which we determine an "apparent radius of gyration". Figure 93-96.

Fig.93: Zimm plot for the sample M031 I65MeBr

(0.535g/l (1.37 10^{-5} M)) with G5.5 (2.187 10^{-5} M)

at the charge ratio I65/G5.5 = 1/1.26.

The sample is clear solution

Fig.94: Gunier plot for the sample M031 I65MeBr
(0.535g/l (1.37 10^{-5} M)) with G5.5 (2.187 10^{-5} M)
at the charge ratio I65/G5.5 = 1/1.26.
The sample is clear solution

Even when looking at a smaller q-range, neither Zimm nor Gunier plot show complete linearity
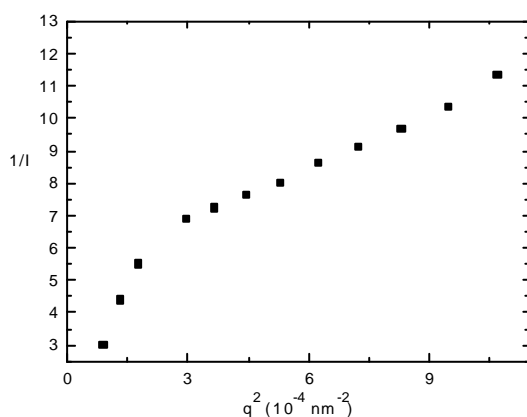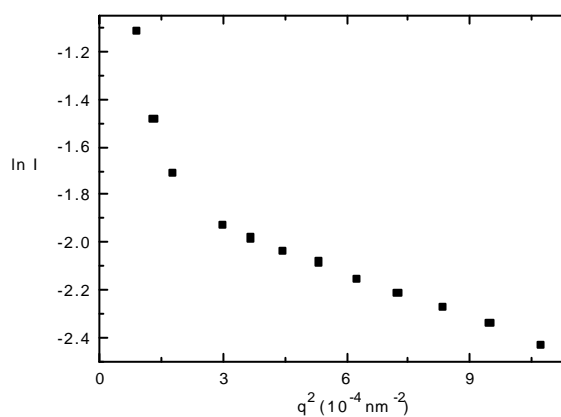(Fig.95, 96).

Fig.95: Zimm plot for the very low q^2 values for
the sample M031 I65MeBr (0.535g/l ,1.37 10^{-5} M)
with G5.5 (2.187 10^{-5} M) at the charge ratio
I65/G5.5 = 1/1.26. The sample is clear solution

Fig.96: Gunier plot for the very low q^2 values for
the sample M031 I65MeBr (0.535g/l ,1.37 10^{-5} M)
with G5.5 (2.187 10^{-5} M) at the charge ratio
I65/G5.5 = 1/1.26. The sample is clear solution

In the range where linearity has been found at intermediate q (higher q-range in Fig.95-96) the
objects shows a radius of gyration of a single macromolecule (of around 5 nm) in the Gunier plot
in Fig.96. The R_g (of about 13 nm) in Fig.95 indicates some aggregations, although small.

Additionally from the light scattering experiment (paragraph 4) we deduced that the two diffusion modes are caused by two species different in size. However, due to the complicated double mode behavior it is difficult to estimate further details of the morphology of species present in the solution. The double mode can be influenced also via electrostatic interactions between the species which has to be charged on the surface. It is known from the literature, that an appearance of the insoluble, neutral on the surface complexes ("seen" as i.e. opalescence, turbidity in the sample), is prefaced by the appearance of soluble, charged on the surface complexes.[120,121] If charged polyelectrolytes cause the polyelectrolyte effect, may be charged assembly also cause a kind of polyelectrolyte-assembly effect. The nature of polyelectrolyte effect is not fully understood yet and the nature of polyelectrolyte-assembly effect is expected to be more complicated, refer paragraph 3 in the theoretical part.

Further an example of SANS on a solution containing the I65MeBr and the G7.5 PAMAM dendrimers will be considered. Sample M040 contains I65MeBr 1.528g/l ($3.918 \cdot 10^{-5}$ M) and $5.866 \cdot 10^{-6}$ M G7.5 where the charge ratio I65/G7.5 is 2.1/1. This sample is turbid and after filtration opalescent. SANS and DLS were performed on the filtered solution. As discussed previously DLS shows one diffusion mode. SANS data are shown in Figure 97-99.
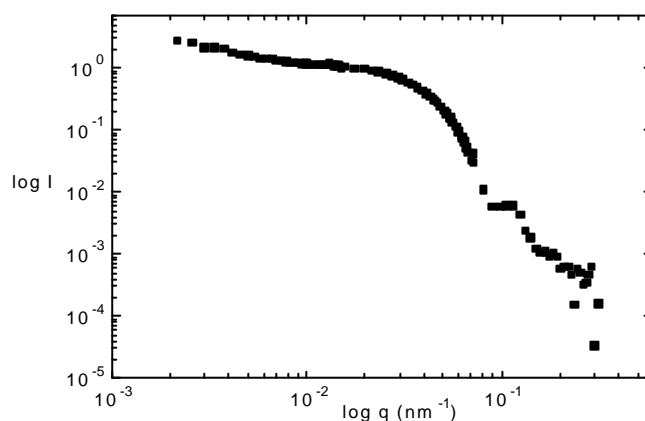

Fig.97: Scattering intensity I vs scattering vector q

for the sample M040 I65MeBr (1.528g/l ($3.918 \cdot 10^{-5}$ M))

with G7.5 ($5.866 \cdot 10^{-6}$ M) at the charge ratio I65/G7.5 = 2.1/1.

Sample is opalescent/turbid.

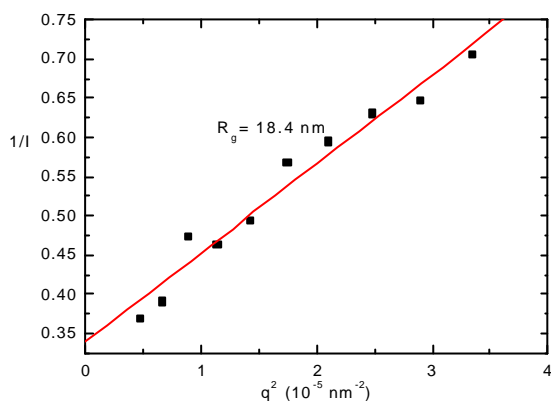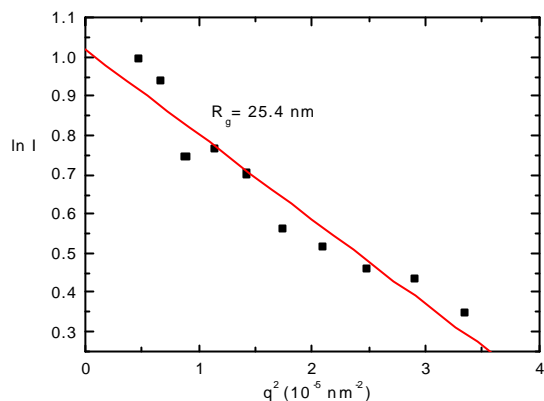Again Zimm and Gunier plot are involved in the calculation of the radius of gyration (see Figure 98, 99).

Fig.98: Zimm plot for the sample M040 I65MeBr (1.528g/l, 3.918 10^{-5} M) with G7.5 (5.866 10^{-6} M) at the charge ratio I65/G7.5 = 2.1/1. Sample is opalescent/turbid.

Fig.99: Gunier plot for the sample M040 I65MeBr (1.528g/l, 3.918 10^{-5} M) with G7.5 (5.866 10^{-6} M) at the charge ratio I65/G7.5 = 2.1/1. Sample is opalescent/turbid.

There is no large difference in linearity and values of R_g calculated for the sample M040 from Zimm (Fig.98) and from Gunier plot (Fig.99). R_g=18.4 nm and R_g=25.4 nm, respectively. Calculated size (R_g) and predicted shape of investigated objects will be discussed later in the subchapter 4.c -general summary of SANS measurements.

2. I25MeBr/Dendrimers

The following five graphs (Fig.100-104) consider samples with G5.5 PAMAM dendrimers. I25MeBr 0.567g/l (2.39 10^{-5} M) with G5.5 2.187 10^{-5} M, where charge ratio I25/G5.5=1.09/1. The M042 sample is turbid and after filtration opalescent.
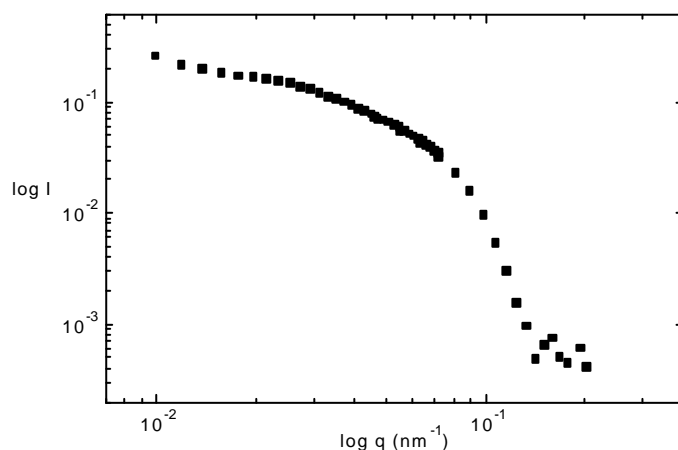

Fig.100: Scattering intensity I as a function of scattering vector q for the sample (M042) I25MeBr (0.567g/l (2.39 10^{-5} M)) with G5.5 (2.187 10^{-5} M) at the charge ratio I25/G5.5=1.09/1.The sample is opalescent/turbid.
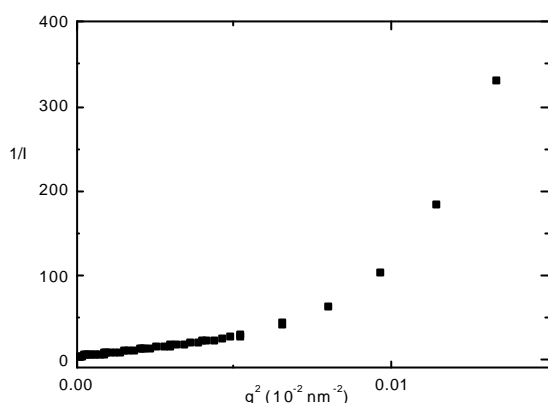
Fig.101: Zimm plot for the sample (M042) I25MeBr (0.567g/l (2.39 10^{-5} M)) with G5.5 (2.187 10^{-5} M) at the charge ratio I25/G5.5=1.09/1. The sample is opalescent or turbid.
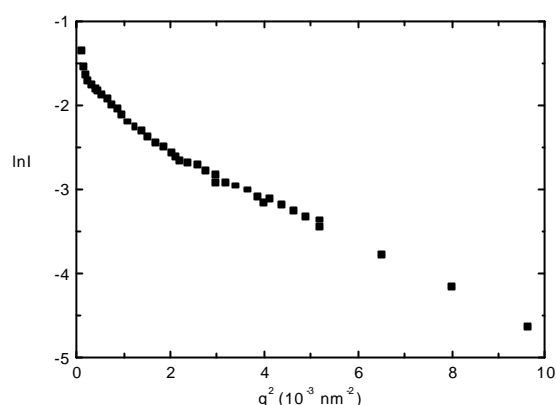

Fig.102: Gunier plot for the sample (M042) I25MeBr (0.567g/l (2.39 10^{-5} M)) with G5.5 (2.187 10^{-5} M) at the charge ratio I25/G5.5=1.09/1.The sample is opalescent or turbid.
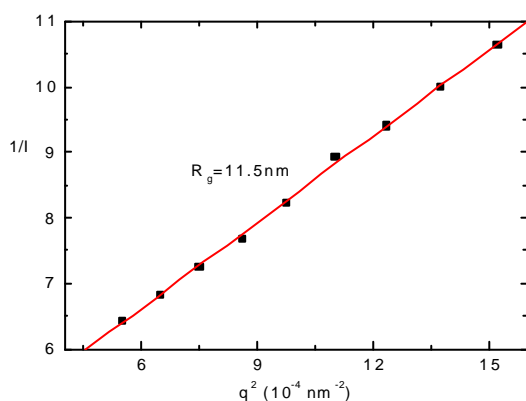

Fig.103: Zimm plot for the sample (M042) I25MeBr (0.567g/l (2.39 10^{-5} M)) with G5.5 (2.187 10^{-5} M) at the charge ratio I25/G5.5=1.09/1.The sample is opalescent or turbid.
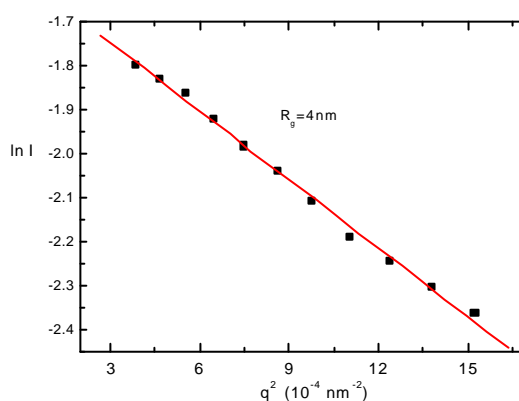

Fig.104: Gunier plot for the sample (M042) I25MeBr (0.567g/l (2.39 10^{-5} M)) with G5.5 (2.187 10^{-5} M) at the charge ratio I25/G5.5=1.09/1.The sample is opalescent or turbid.

In this case the deviation from linearity in the Zimm plot i.e. an upwards curvature (Figure 103 and 104) indicates a spherical structure. This is confirmed by the linearity of the Gunier plot. In the Gunier plot R_g is found to be 4 nm. Figure 105-106 show scattering curve and Zimm and Gunier plot for the sample M043 i.e. I25MeBr 0.893g/l (3.77 10^{-5} M) with G7.5 5.866 10^{-6} M where the charge ratio I25/G7.5 is 1.63/1. The sample was turbid and after filtration opalescent. Well expressed minima in higher q range indicate a defined aggregation.
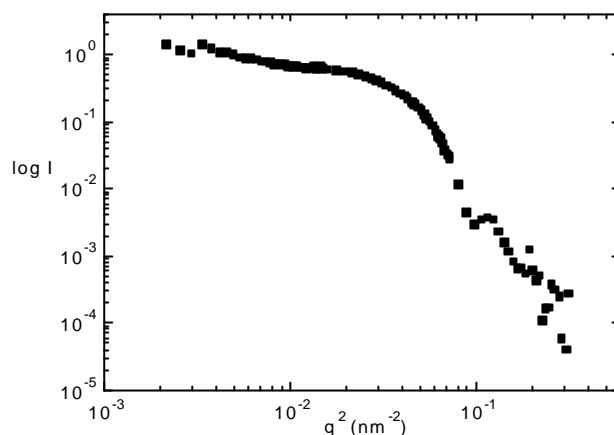
Fig.105: Scattering curve for the sample (M043) I25MeBr
(0.893g/l (3.77 10^{-5} M)) with G7.5 (5.866 10^{-6} M)
at a charge ratio I25/G7.5 = 1.63/1.
The sample is turbid/opalescent

Good agreement between the radius of gyration obtained from Zimm and Gunier plot is observed, R_g=23.6 nm and R_g=23.4 nm, respectively. See Fig.106, Fig.107.
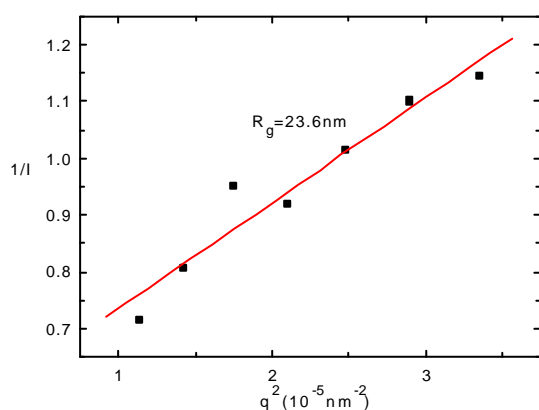

Fig.106: Zimm plot for the sample (M043) I25MeBr (0.893g/l (3.77 10^{-5} M)) with G7.5 (5.866 10^{-6} M) at a charge ratio I25/G7.5 = 1.63/1.The sample is turbid/opalescent
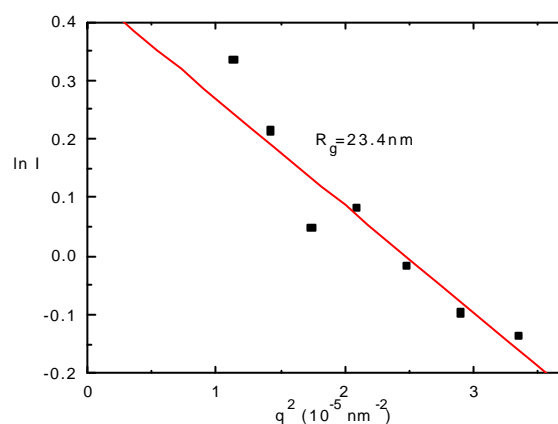
Fig.107: Gunier plot for the sample (M043) I25MeBr (0.893g/l (3.77 10^{-5} M)) with G7.5 (5.866 10^{-6} M) at a charge ratio I25/G7.5 = 1.63/1.The sample is turbid/opalescent

For the dendrimer G2.5 with I25 as opposed to the G2.5 with I65, one diffusion mode samples exist. Due to this behavior in DLS, SANS analysis is possible. For the neutron scattering the sample (M041) I25 0.392g/l (1.65 10^{-5} M) with G2.5 1.909 10^{-4} M was chosen. The sample before filtration was turbid, after filtration becomes opalescent. Charge ratio in this case I25/G25 equals 1/2. Figure 108-111 present the data
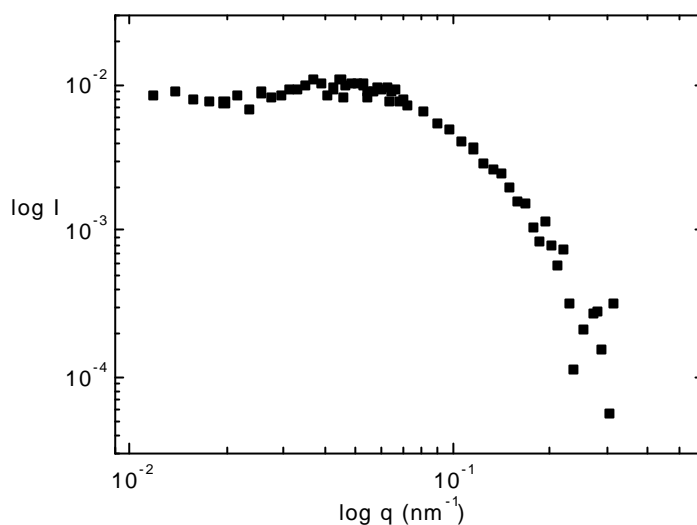
Fig.108: Intensity vs scattering vector for the sample
(M041) I25MeBe (0.392g/l (1.65 10^{-5} M))
with G2.5 (1.909 10^{-4} M) at the charge ratio
I25/G25 = 1/2. The sample is opalescent/turbid

Fig.109: Zimm plot for the sample
(M041) I25MeBe (0.392g/l (1.65 10^{-5} M))
with G2.5 (1.909 10^{-4} M) at the charge ratio
I25/G25 = 1/2. The sample is opalescent/turbid

Fig.110: Zimm plot for the sample
(M041) I25MeBe (0.392g/l (1.65 10^{-5} M))
with G2.5 (1.909 10^{-4} M) at the charge ratio
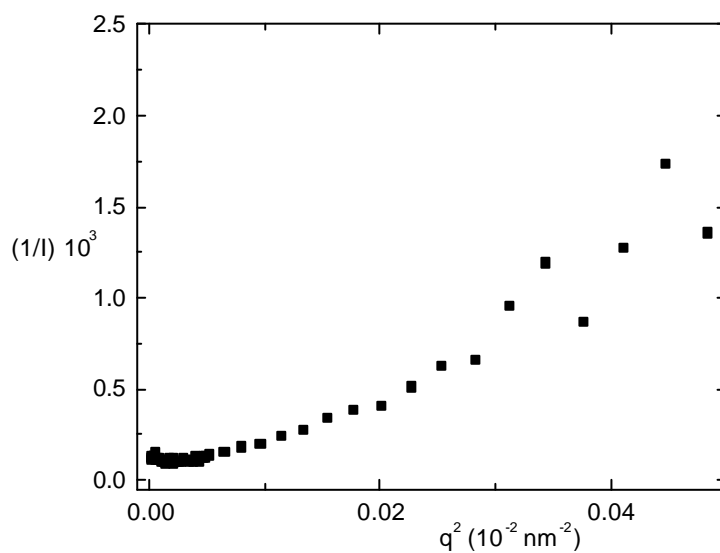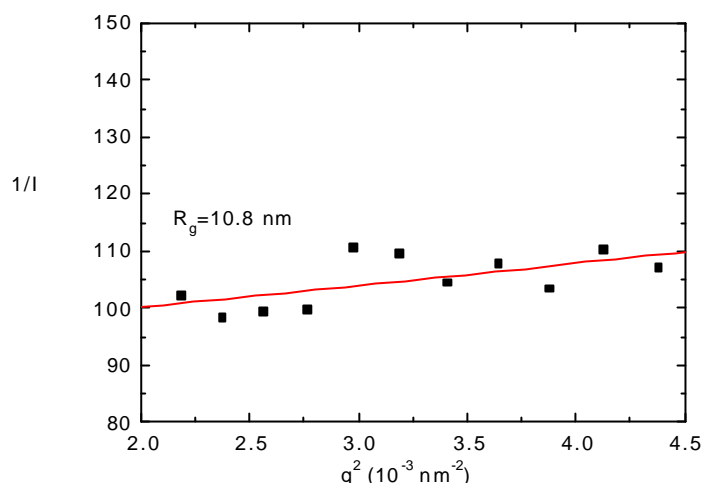I25/G25 = 1/2. The sample is opalescent/turbid

R_g estimation from Guinier plot is difficult. There is no clear linearity for the beginning of q-scala in case of Gunier plot.

3. SANS data analysis via Pair Distance Distribution Function P(r)

Pair distance distribution functions were calculated for the samples listed in the following Table 15. They result from a Fourier-Transformation of the scattering curve I(q).

$$P(r) = \frac{1}{2\boldsymbol{p}^2} \int_0^\infty I(q)qr \sin qr dq$$

i.e. without any assumptions about particle shape. This is possible for finite particles of random orientation. The Fourier –Transformation is done indirectly and under regularization. P(r) often gives further information about size and shape. P(r) data are only presented here if the Fourier-Transformation under regularization clearly gives a stable solution.

Table.15: Condition of the samples used during P(r) calculation

concentration (mol/l)	concentration (mol/l)	Charge ratio	Sample condition	Sample name
I65MeBr	Gx.y	ionene/dendrimer		
8.717 10^{-6}	5.64 10^{-6}	1.94/1 G5.5	clear	M020
2.35 10^{-5}	2.187 10^{-5}	1.35/1 G5.5	opalescent	M021
1.92 10^{-5}	2.187 10^{-5}	1.1/1 G5.5	opalescent	M027
1.37 10^{-5}	2.187 10^{-5}	1/1.26 G5.5	clear	M031
3.918 10^{-5}	5.866 10^{-6}	2.1/1 **G7.5**	opalescent	M040
I25MeBr	Gx.y			
2.39 10^{-5}	2.187 10^{-5}	1.09/1 G5.5	opalescent	M042
3.77 10^{-5}	5.866 10^{-6}	1.63/1 **G7.5**	opalescent	M043
1.65 10^{-5}	1.909 10^{-4}	1.0/2 G2.5	opalescent	M041

The scattering intensity versus scattering vector as well as its fit and pair distance distribution functions are shown in Fig.111-119.

For the sample M021 the assembly diameter is equal about 40 nm. For this sample an inhomogeneous inner structure with moieties of about 10 nm diameter has been found, for comparison see Fig.111 and Fig.112.
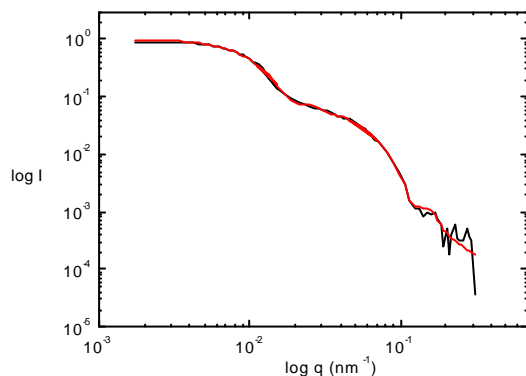

Fig.111. Scattering intensity for the sample (M021): I65 (2.34 10^{-5} M) with G5.5 (2.187 10^{-5} M) at the charge ratio I65/G5.5 = 1.35. The black line means an experimental scattering intensity as a function of the scattering vector q. The red line means the scattering intensity calculated via indirect Fourier-Transformation

Fig.112. Pair distance distribution function for the sample (M021):I65 (2.34 10^{-5} M) with G5.5 (2.187 10^{-5} M) at the charge ratio I65/G5.5 = 1.35

.

The sample in Fig.111 and 112 can represent a system with a well defined core-shell structure. For this particular sample from the DLS $R_{h\ app}$ = 73.3 nm has been calculated. From the SANS data analysis according to the Zimm plot R_g = 16.5 nm has been found. R_g / $R_{h\ app}$ ratio is equal 0.225. According to the P(r) analysis the radius R found is equal about 20 nm. The radii are related as follow: $R_{h\ app} > R \approx R_g$. Such order corresponds to the core-shell structure dimensions as indicated in Fig.113.
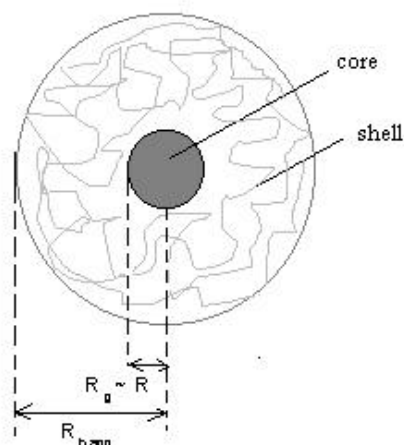
Fig.113. Sketch of the core-shell structure.

Particle dimensions comparison.

For such a core-shell structures the radius of gyration will be comparable with the inner radius calculated from the P(r) analysis. The radius of gyration, R_g is solely geometrically defined and describes the mean square distance between centre of mass of the particle and the scattering centres. The hydrodynamic radius result from the interaction of the macromolecule with the solvent.[125] The situation becomes more complicated when the assembly object is charged on the surface. At the certain ionene to dendrimer charge ratios arising particles are charged on the surface, compare paragraph III.VI.

Based on the further presented analysis, the calculation of R for other samples (even if the sample shows one diffusion mode when DLS is performed) becomes difficult. For comparison see Fig.114-117.

Fig.114. Scattering intensity for the sample(M020): I65 (8.817 10^{-6} M) with G5.5 (5.64 10^{-6} M) at the charge ratio I65/G5.5 = 1.94.The black line means an experimental scattering intensity as a function of the scattering vector q. The red line means the scattering intensity calculated via indirect Fourier-Transformation.
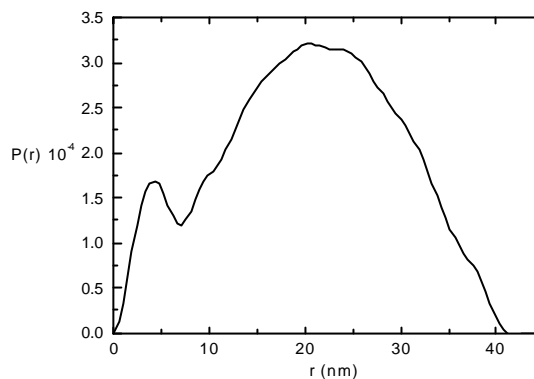

Fig.115. Pair distance distribution function for the sample (M020): I65 (8.817 10^{-6} M) with G5.5 (5.64 10^{-6} M) at the charge ratio I65/G5.5 = 1.94.

Fig.116 and Fig.117 present the pair distance distribution function for the sample close to the transition point, when diffusion properties are investigated. However the sample belongs to the one diffusion mode samples. The shape of the pair distance distribution function indicates one part of about 8 nm diameter. The maximum diameter of the whole structure is equal about 18 nm.
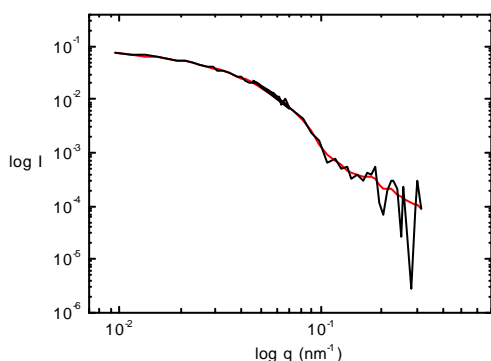

Fig.116. Scattering intensity for the sample(M027): I65 (1.92 10^{-5} M) with G5.5 (2.187 10^{-5})M) at the charge ratio I65/G5.5 = 1.1 The black line means an experimental scattering intensity as a function of the scattering vector q. The red line means the scattering intensity calculated via indirect Fourier-Transformation.
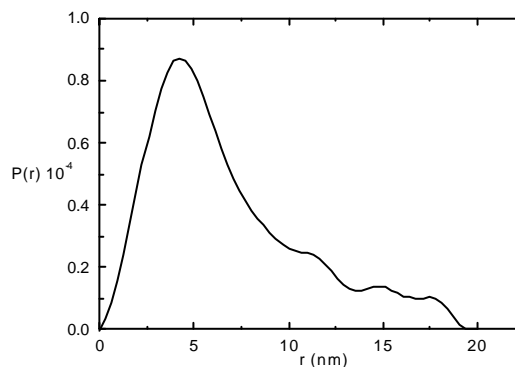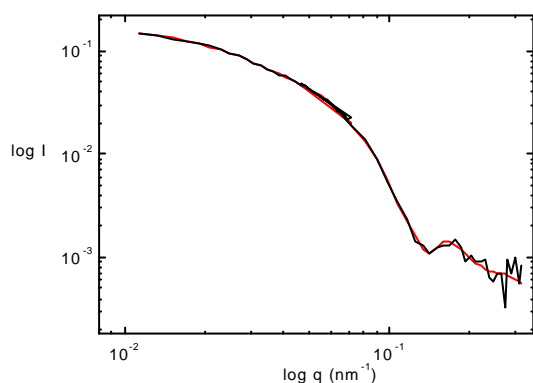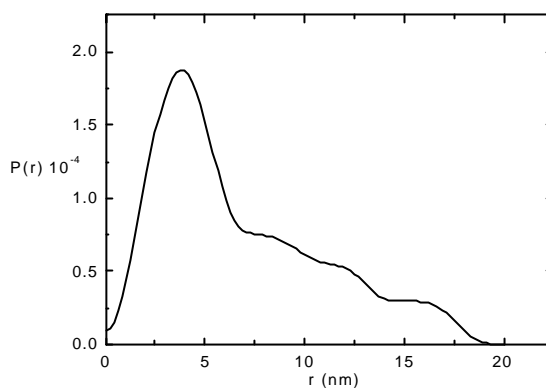
Fig.117. Pair distance distribution function for the sample (M027): I65 (1.92 10^{-5} M) with G5.5 (2.187 10^{-5} M) at the charge ratio I65/G5.5 = 1.1.

P(r) shapes found in Fig.115 and 117 may indicate a mixture of different sized particles or one species of anisotropic particles. Since samples selected for SANS are one diffusion mode samples, the presence of different sized objects in the system might be excluded. However, it may also be that species of two sizes (8 and 18 nm) are not different enough to be separated in light scattering. Possible anisotropic structures will be discussed in chapter III.V.

Fig.118 and 119 present the data for the I65/G7.5 sample. The shape of P(r) function in Fig.120 indicates a spherical object with a radius R of about 6 nm. It could mean the P(r) for pure G7.5 or for pure ionene. On the other hand, pure ionene sample with comparable to the M040 concentration does not have enough contrast to be measured by SANS. The scattering length calculated for the ionene is equal $b_{I65} = 71.4 \ 10^{-12}$ cm, the scattering length for the dendrimer G7.5 equals $b_{G7.5} = 177.5 \ 10^{-12}$ cm and for the solvent (D_2O) $b_{D2O} = 22.4 \ 10^{-12}$ cm. The dendrimer molecules have three times higher scattering length difference as compared to the ionene molecules. Additionally the dendrimer is much more compact structure as compared to the ionene random coil. The generation G7.5 is spherical and "homogenous" (for comparison see chapter 4 concerning dendrimers characterization). Spherical shape and homogeneity have been found also for the objects in Fig.119. Therefore Fig.119 could present pair distance distribution function of pure dendrimer G7.5 molecule. However, since the assembly structures for the case of sample M020, M021, M027 show enough contrast, the sample M040 in Fig.119 should behave similar. From the sample M040 we should be able to determine the dimensions of the assembly objects which we detect for this sample as one, well defined mode in DLS. However it is not the case. The pair distance distribution function in Fig.119 could be also valid for oligomers, middle

size aggregates of ionene with dendrimers but the radius R found for the object in Fig.119 is to small, to belong to an aggregate. Additionally we have found one species of well defined, aggregated structures of hydrodynamic radii about 100 nm. For the moment we cannot explain the reason why in case of e.g. M040, we do not see pair distance distribution function for whole assembly structures.
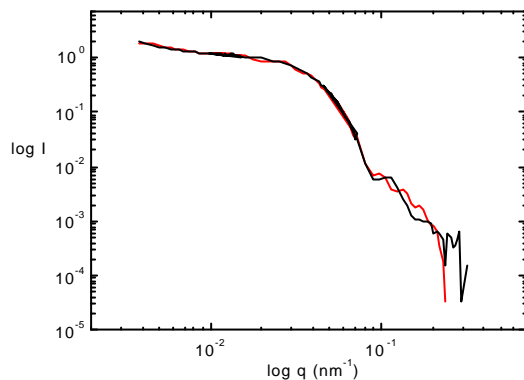
Fig.118. Scattering intensity for the sample(M040): I65 (3.918 10^{-5} M) with G7.5 (5.866 10^{-6} M) at the charge ratio I65/G7.5 = 2.1/1. The black line means an experimental scattering intensity as a function of the scattering vector q. The red line means the scattering intensity calculated via indirect Fourier-Transformation.
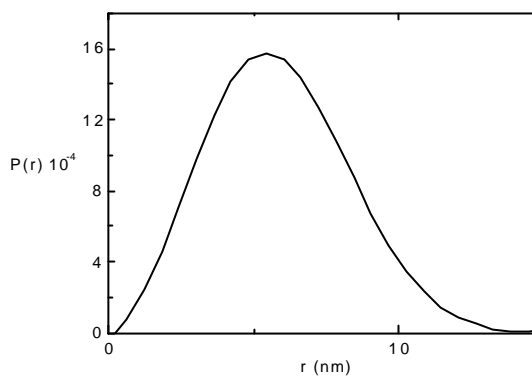
Fig.119. Pair distance distribution function for the sample (M040): I65 (3.918 10^{-5} M) with G7.5 (5.866 10^{-6} M) at the charge ratio I65/G7.5 = 2.1/1

The comparison of the pair distance distribution functions for the I65/G5.5 systems and for the systems of I25/G5.5 is present in Fig.120.
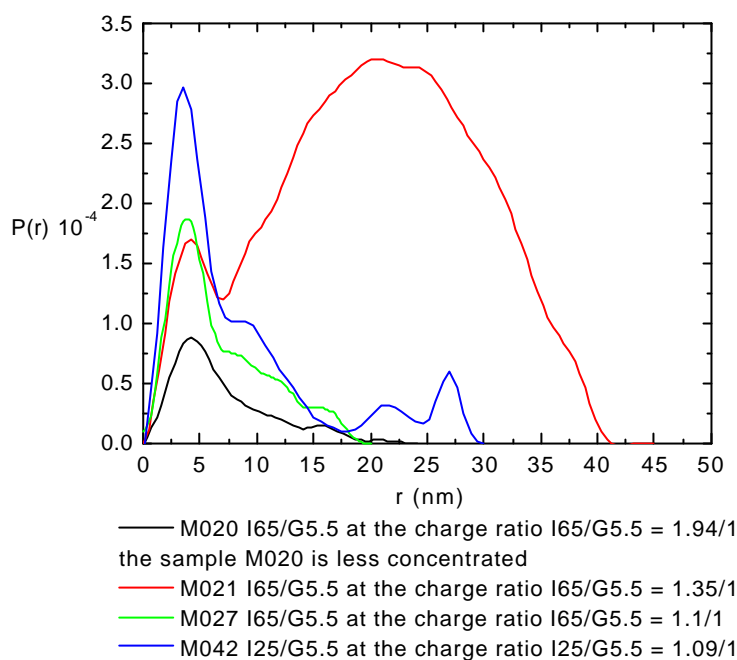
Fig.120. Pair distance distribution function comparison

A "characteristic inner part diameter " of 8-10 nm for the has been found in all investigated in Fig.120 cases. This inner part dimension is larger than those of pure G5.5. It could be that we find the pair distance distribution function for the building block of assembly structure, i.e. dendrimer G5.5 with I65 or I25.

The pair distance distribution functions for the I65/G7.5 and I25/G7.5 systems is presented in Fig.121 the radii R calculated from this functions are comparable with the radius of pure G7.5.
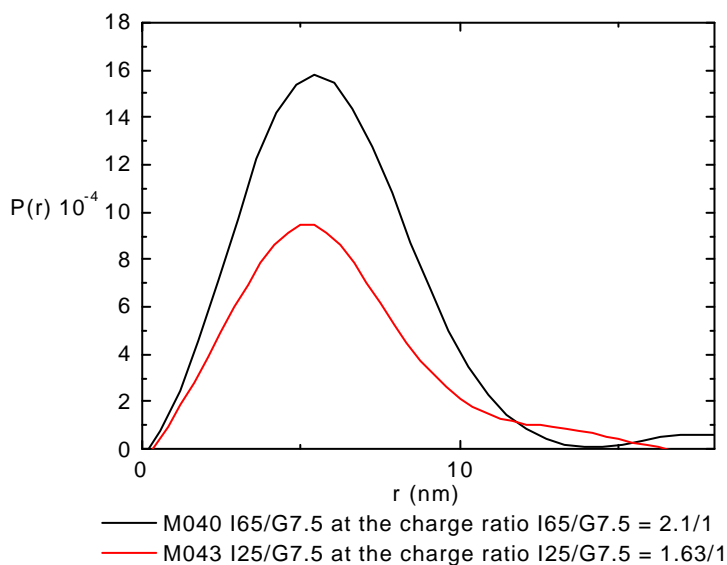
Fig.121. Pair distance distribution function comparison

The dimensions of the investigated assemblies which are found are in every case lower than the maximal dimension D_{max} covered by the scattering experiment.. D_{max} is characteristic for the certain configuration of the scattering setup. It can be calculated according to the

$$D_{max} = \frac{2\boldsymbol{p}}{q_{min}}.$$

The dimension of the smallest structure which can be measured is equal

$$D_{min} = \frac{2\boldsymbol{p}}{q_{max}}.$$

In practice the scattering vector q range, which determines D_{max} and D_{min} is regulated via the sample-detector distance. For most cases, during our experiments, the maximal sample-detector distance of 5.4 m was kept which allows to calculate the D_{max} of 63 nm. However for the sample M021, M040 and M043, the maximal sample-detector distance was 26 m. Then the D_{max} is equal 314 nm. The lowest measurable size limit is defined by the D_{min} of 2.1 nm.

III.V. Scattering techniques for the ionene PAMAM dendrimer complexes, summary

The values of R_g result from SANS data analysis presented in the paragraph 5a and 5b. R_h values are calculated from the diffusion coefficients. For regimes with one diffusion process, apparent hydrodynamic radii were calculated according to the Stokes-Einstein equation. The following Table16 gives an overview about resulting radii values. Further, we consider the ratio R_g/R_h that can give indications about particle shape and density.

Tab.16: Complex parameters

Sample name	I65MeBr concentration		Gx.y concentration mol/l	Charge ratio I65/G5.5	$R_{h\,app}$ DLS nm	R_g SLS nm	R_g SANS nm	$R_{gSANS}/R_{h\,app}$ and $R_{gSLS}/R_{h\,app}$	R SANS nm
	g/l	mol/l							
M020	0.34	$8.717\,10^{-6}$	$5.64\,10^{-6}$ G5.5	1.94/1	72.6	17	22.2	0.3 and *0.23*	10
M021	0.915	$2.35\,10^{-5}$	$2.187\,10^{-5}$ G5.5	1.35/1	73.3		16.5	0.225	20
M027	0.75	$1.92\,10^{-5}$	$2.187\,10^{-5}$ G5.5	1.1/1	121	33	19	0.16 and *0.3*	9
M031 double mode	0.535	$1.37\,10^{-5}$	$2.187\,10^{-5}$ G5.5	1/1.26	60.8		13.5	0.222	-
M040	1.528	$3.918\,10^{-5}$	$5.866\,10^{-6}$ **G7.5**	2.1/1	94.4	34	25.4	0.27 and *0.36*	18
		I25MeBr							
M042	0.567	$2.39\,10^{-5}$	$2.187\,10^{-5}$ G5.5	1.09/1	142		11.5	0.081	15
M043	0.893	$3.77\,10^{-5}$	$5.866\,10^{-6}$ **G7.5**	1.63/1	123		26.6	0.215	20
M041	0.392	$1.65\,10^{-5}$	$1.909\,10^{-4}$ G2.5	1/2	100	100	10.8	0.108	-

An R-value in the last column in Tab.16 corresponds to the radii found when pair distance distribution has been analysed. For comparison see paragraph 5c. The R_g value from the SLS and SANS as well as those R-values calculated from the pair distance distribution function in good agreement, see Tab.16. The hydrodynamic radii for ionene/PAMAM dendrimers always lot larger than the radii of gyration. Comparison of an experimental R_g/R_h ratios and calculated, presented in the literature values indicate the particle structure. For the very low R_g/R_h ratio so called "microgel nature" is indicated. The existence of an inhomogenous (e.g. core-shell) microgel systems was described by W. Burchard.[112,124,125] The values of R_g/R_h are significantly lower than that for compact sphere and appear to be out of the range of an experimental error.

The very low values of R_g/R_h must indicate the special spatial density distribution in the "microgel". The apparently larger Stoeks radius in comparison to the mean square radius of gyration of a hard sphere may for instance result from a crosslinked surface layer which has a much lower density than the microgel center but which may suffice to define a hydrodynamically effective large sphere radius while the mean square radius of gyration remains fairly small. [79] How the complexes might look like is presented in Fig.122.
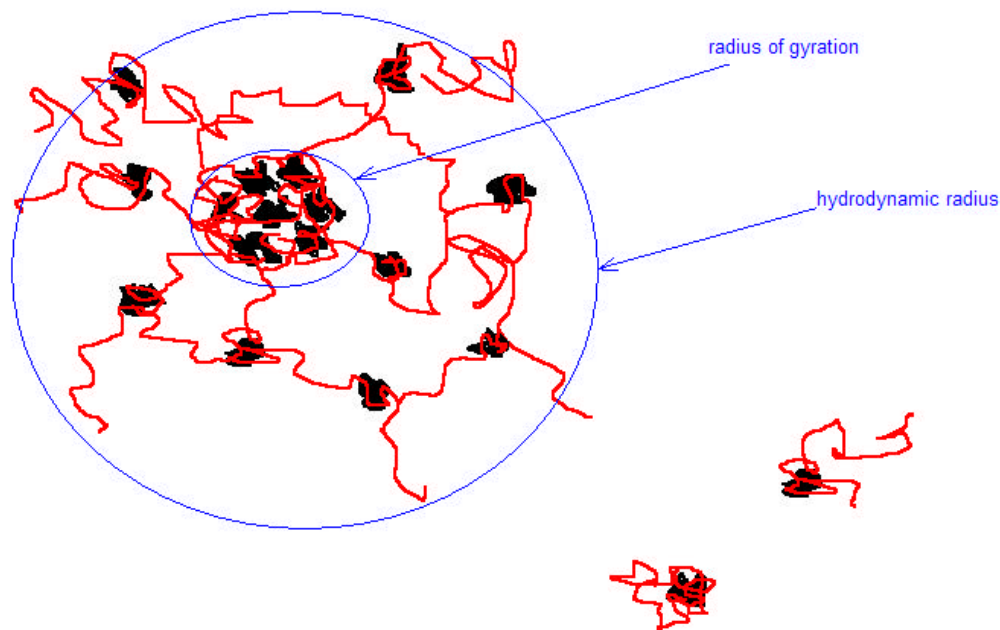
Fig.122: Cartoon of "microgel-like" structure that can cause

R_g/ R_h values much lower than 1. Isotropic and anisotropic

structures might be observed. Here anisotropic structure

is sketched.

The structure presented in Fig.122 is anisotropic ("not symmetrical") since also this kind of objects may appear in the ionene/PAMAM dendrimer system. This is confirmed by the pair distance distribution function P(r) analysis (compare paragraph 3).

It is noteworthy to regard, with respect to the LS and SANS investigations, the case of 1 to 1 ionene to the dendrimer molar charge ratio. The 1 to 1 molar charge ratio translates to the molecular ratio as follows (see Tab.17):

Tab.17. Molecular ratio of Imn/Gx.y at the molar charge ratio of 1.

Imn/Gx.y	G2.5	G5.5	G7.5
I65	1/10	1/1.25	3.2/1
I65(1)	1 /7.5	1/1	4.3/1
I25	1/8	1/1	4/1

The 1 to 1 molar charge ratio means only in case of ionene (Imn) with G5.5 systems 1 ionene molecule per 1 dendrimer molecule. In case of ionene with G7.5, 1 to 1 in charges means a three to four time excess of the ionene. This is opposite to the ionene with G2.5 complexes. In case of

Imn with G2.5 1 to 1 in charges means almost 10 dendrimer molecules per one ionene molecule. These observation would explain the lack of complexes in case of I65 and G2.5. There is not enough centrer where the building of a self-assembly structure may begin. However for the I25 with G2.5 systems, the formation of an assembly structures takes place, so the charge density (which is higher for I25 as compared to I65) must play a role. The ionene complexes with G5.5 and G7.5 formation is defined and takes place in the one diffusion mode range. These observation can be explained via "better" molecular ratio ("balance") of the compounds. Complex formation takes place around the charge ratio of 1 in case of Imn/G5.5. For the Imn/G7.5 complexes is slightly shifted to the higher charge ratio. Besides, as it was already proven (compare chapter III.I.B and III.III), the two diffusion modes are not caused by the polyelectrolyte effect. The two diffusion modes are caused by the particles diffusion, single macromolecules and middle-size aggregates. This argument additionally supports our hypothesis of the special assembly condition. If the charge ratio is optimised (around 1/1 for normal polyelectrolytes), but the number of particles is not in optimal condition (large excess of one species) the full assembly process does not take place. Several molecules are able to form aggregates, but the rest stays free. It seems that the charge balance and the molecular number balance must be fulfilled. The charge density of the compounds must be comparable. However in the case of our systems the comparison of the charge density is not direct. We do have a linear (ionenes) and three dimensional molecules (dendrimers) in the system.

III.VI. ζ potential

The ζ potential has been measured to receive information about the effective (apparent) surface charge of objects in the solution. For such measurements one diffusion mode samples were selected. Only in the case of I65/G2.5 the lack of one mode samples forced us to use two diffusion mode sample. Surprisingly even in the case of two mode sample only one narrow distribution of ζ potential values is seen. Figure 123 presents an example of ζ potential data for the sample I65 1.528 g/l with G7.5 5.866 10^{-6} M where charge ratio of I65/G7.5 = 2.1/1. The value of ζ potential for that case equals 30.8 mV.
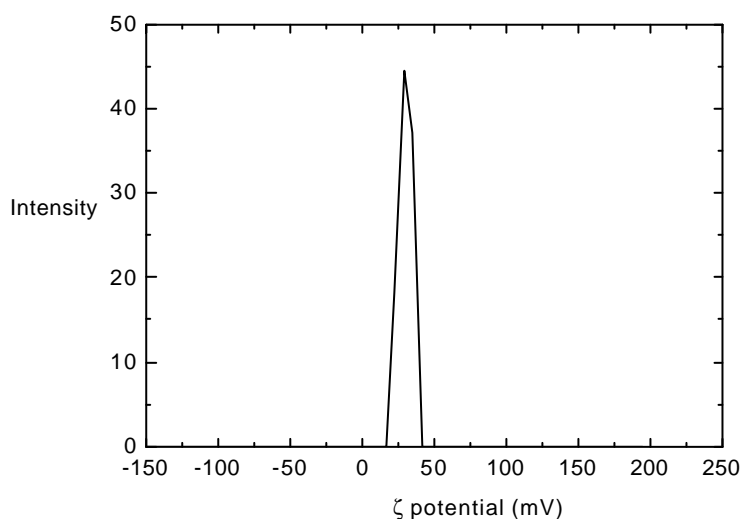

Fig.123: ζ potential value for the sample I65 1.528 g/l

G7.5 5.866 10^{-6} M. Charge ratio I65/G7.5=2.1/1

ζ potential = 30.8 mV

For the investigation samples with fixed dendrimer concentration have been used. We intended to measure the ζ potential for pure dendrimers at the concentrations used for complex preparation. However, under those condition any differences between the sample containing only mq water and the sample containing water solution of the pure dendrimer have been observed. In both cases obtained values of ζ potential within an experimental error were neutral. The detection level of diluted dendrimer solution lies under the detection boarder of the machine used. Table 18 contains the values of ζ potential (in mV) measured.

Tab.18: ζ potential values (mV) for selected sample

Complex parameters			Zeta potential (mV)	
I65MeBr/Gx,y molar charge ratio	**I65MeBr/G7.5 molecular ratio**	**I65MeBr/G2.5 molecular ratio**	**I65/G7.5**	**I65/G2.5**
0.45	1.5/1	1/22	-2.5 *clear*	-32.9 *slightly turbid*
1	3.2/1	1/10	1.6 *slightly turbid*	-15.6 *clear*
2.1	6.7/1	1/4.5	30.8 *slightly turbid*	2.16 *clear*
I25MeBr/Gx,y molar charge ratio	**I25MeBr/G7.5 molecular ratio**	**I25MeBr/G2.5 molecular ratio**	**I25/G7.5**	**I25/G2.5**
0.33	1.33/1	1/24	-38.6 *slightly turbid*	-45.16 *clear*
1	4/1	1/8	-34.8 *slightly turbid*	-19.8 *turbid*
2.25	7/1	1/3.5	25.7 *turbid*	30.9 *slightly turbid*

For the ionene I65 and G7.5 at a charge ratio lower or equal 1, aggregates formed are almost neutral. The molecular ratios indicate in all that cases an excess of the ionene molecules. The ζ potential values for the assemblies are $\zeta_{[I65/G7.5=0.45]}$ = -2.5 mV and $\zeta_{[I65/G7.5=1]}$ = 1.6 mV. For I25 and G7.5 at a charge ratio lower or equal 1 structures are negatively charged. In particular in solution of samples that are not so strongly turbid, negatively charged structures are observed. These may indicate the soluble negatively charged assemblies. In the case of I25/G7.5 complexes, the molecular ratios are comparable to the I65/G7.5 and the investigated samples contain always an excess of ionene molecules. As opposite, the samples I65/G25 and I25/G25 contain, independent on the molar charge ratio, an excess of the dendrimer molecules. The ζ potential values for such systems are strongly negative. One could expect the dendrimer molecules as an outer layer of the assemblies formed. At around twice excess of ionene charges, investigated objects are positively charged on the surface, even through slight molecular excess of the dendrimers in ionene/G2.5 complexes, compare Tab.18. Values of ζ potential measured are not equal though the molecular charge ratio which are comparable for all ionene/dendrimer samples. The tendency is however the same for every sample series: The more ionene the system contains, the more positively charged it is. This observation stays in agreement with the hypothesis of the positively charged ionene chains adsorbed on the dendrimer surface. Noteworthy is that for the system I65/G2.5 only one ζ potential value is observed however we expect at least two ζ potential values because of two modes during DLS measurement, but the slow mode is caused by the middle- size assemblies, which are seen by the zeta-sizer the fast mode may be caused by the single molecules. It may be that the machine can not detect low (as compare to the complexes present) molecular mass dendrimer or ionene which however can play a role in the diffusion processes measured by DLS.

III.VII. Potentiometric titration of I65/G7.5 complexes.

Titration experiments were performed to analyze the complex formation phenomena quantitatively. Based on the calculation procedure and cyclic diagram proposed by Dubin et. al., complexation energy for selected systems has been calculated according to equation *1-6*.[122] Dubin et. al. investigated the interaction between poly(diallyldimethylammonium chloride) (PDADMAC) and carboxylated starburst dendrimers of the 0.5, 3.5, 5.5 and 7.5 generation. The influence of ionic strength on the complex formation was investigated using potentiometric titration, turbidimetry and DLS. An effect of the dendrimer generation number and ionic strength on the binding of the polycation to dendrimer and the effect of the binding on the dissociation of the dendrimer G7.5 have been discussed. According to Dubin et. al. the higher generation dendrimers readily form complexes with PDADMAC since the head groups on the surface of the dendrimer are relatively congested, leading to a higher surface charge density. The lower generation dendrimers only complex with PDADMAC at higher degree of ionization or low ionic strength because of their lower surface charge density at any dissociation degree α. Potentiometric titration reveals the stoichiometric aspects of the complexation. In addition, the effect of the binding of PDADMAC on the pK_a of the dendrimer carboxylates can be used to calculate the free energy of binding. The cyclic diagram shown in Fig.124 presents the binding process of PDADMAC to the dendrimer. There are different binding steps presented and the energetic relationships between them. The diagram involves the different dissociation degrees of the dendrimer which are influenced by the linear polyelectrolyte complexation. The dendrimer molecule, in Fig.125 sketched as a circle, contains n^- to ($n^- + dn$) negative charges on the surface. The approaching of the linear polyelectrolyte molecule to the surface of the dendrimer influences the dissociation of the dendrimer molecule.[122]
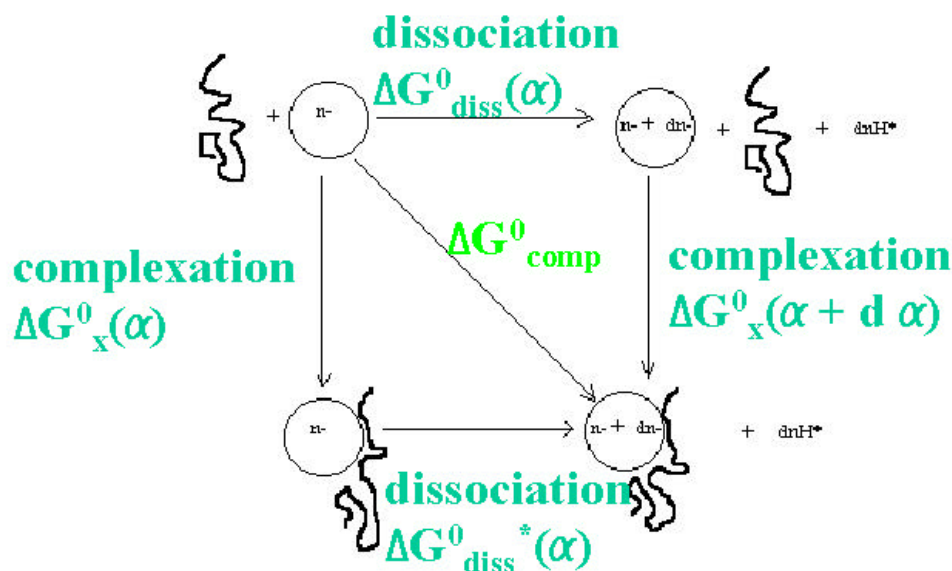

Fig.124. Cyclic diagram for the complexation process.[122]

Calculation details see p.120-123.

The calculation of the free energy of the complexation (ΔG^0_{comp}) bases on the assumption that the complexation energy consists of: *i)*the free energy change accompanying the transfer of one mole of carboxylate groups at α from the free dendrimer state to the complex state, *ii)*the free energy change for molecules at $(\alpha + d\alpha)$ *iii)*free energy changes accompanying the dissociation of pure dendrimer molecule and complex. Dubin's basis of such a cyclic diagram (Fig.124) is energy conservation law. The total inflow of energy into a system must equal the total outflow of energy from the system, plus the change in the energy contained within the system. The "system" here means the growing complex. The dissociation and complexation energies of building blocks are the elements of the assemblies complexation energy.[122] Our system consists also of a linear polyelectrolyte and PAMAM dendrimers of 2.5, 5.5 and 7.5 generation, however we did not investigate an ionic strength influences on the ionene/dendrimers complex formation.
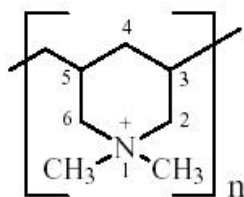

Fig.125. PDADMAC structure.

Also the molecular structure of PDADMAC here in Fig.125, is different as compared to the ionene structure. In case of PDADMAC the "+"charge is placed on the side group and every monomer carries the charge. The charge density of ionene chain is lower and the charge is placed on the main chain. In particular, the ionenes provide a system where linear polyelectrolytes of different charge densities can be investigated. However for the ionene/dendrimer systems the idea of the cyclic diagram can be used as well, and the complexation free energy can be calculated according to Dubin's procedure. We selected the sample 0.74 g/l I65MeBr in 5.866 10^{-6}M G7.5 with a molar charge ratio of the compounds equal to I65/G7.5= 1. For one dendrimer molecule there are 3.2 ionene molecules in the solution. The sample shows a single diffusion mode in DLS. The titration curve for the complex system was compared with titration curve of pure dendrimer G7.5. The pH value of G7.5 and I65/G7.5 was adjusted to pH = 10.5. At this pH all surface groups (COONa) for the pure dendrimer are expected to be ionized. Similar condition (pH = 10.5) has been applied for the I65/G7.5 complex titration. To adjust pH to 10.5, 0.5575 M NaOH was used. To titrate the systems 0.5 M HCl was added. Following figure presents the voltage changes as a function of volume of acid added during the titration experiment.
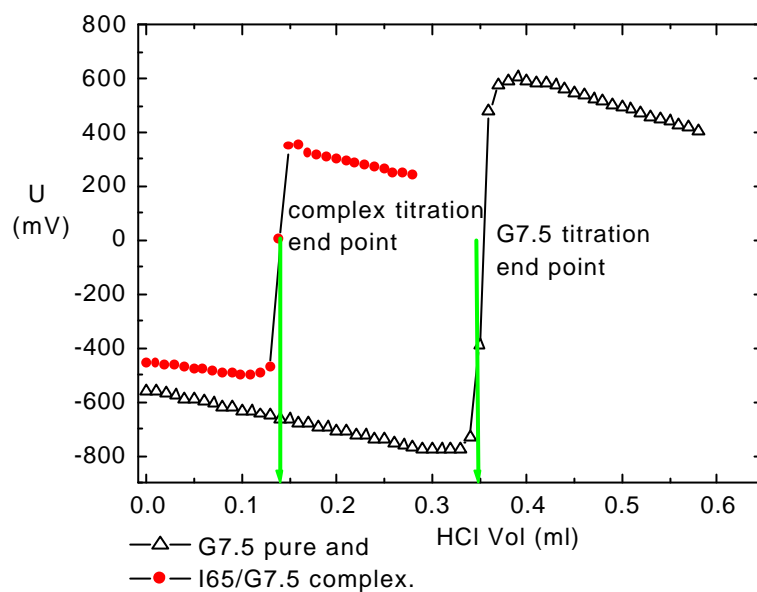
Fig.126: System voltage change as a function of
the amount of acid added

The pH dependency of pure G7.5 and I65/G7.5 as a function of added HCl volume is presented in Fig.127
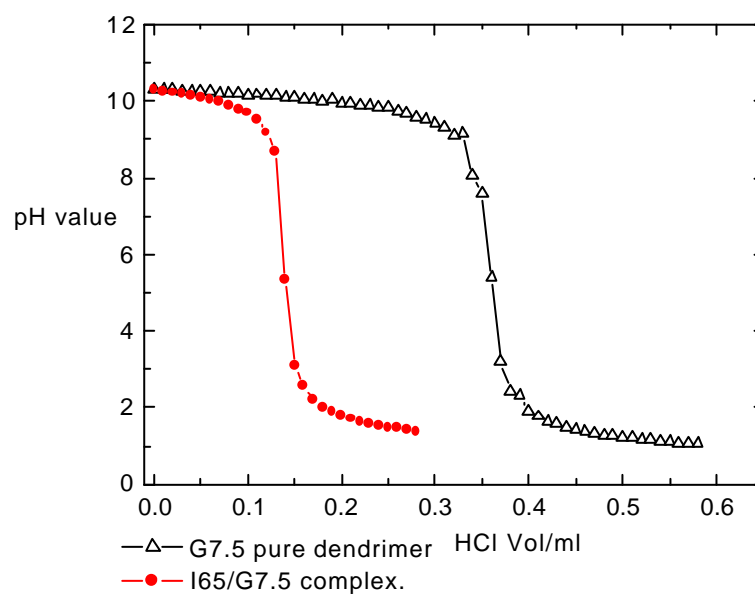

Fig.127: Titration curve for pure G7.5 and I65/G7.5 system

Based on the pH value the degree of dissociation of pure dendrimer and complex have been calculated. [122]

$$\boldsymbol{a}_i = \frac{[\text{amount of acid added at pH}_i]}{[\text{amount of acid needed to protonate the dendrimer completely }]} \tag{1}$$

Knowing the dissociation degree allows to calculate the dissociation constant pK$_a$.

$$pK_a = pH + \log\frac{(1-\boldsymbol{a})}{\boldsymbol{a}} \tag{2}$$

The pK$_a$ is related to the standard free energy change (ΔG_{diss}^0) for the dissociation of one mole of protons from the dendrimer surface at α_i via

$$pK_a = pH + \log\frac{(1-\boldsymbol{a})}{\boldsymbol{a}} = pK^0 + \frac{0.434\Delta G_{diss}^0(\boldsymbol{a})}{RT} \tag{3}$$

To calculate the free energy of complexation(ΔG_{comp}^0), is possible when complexation is regarded as a cyclic process according to the scheme present in Fig.124. Based on the cyclic process presented above changes in dissociation energy of dendrimer and complexes and changes in complexation energy can be related as follows:

$$\Delta G_{comp}^0 = \Delta G_{diss}^0(\boldsymbol{a}) + \Delta G_x^0(\boldsymbol{a}+d\boldsymbol{a}) = \Delta G_x^0(\boldsymbol{a}) + \Delta G_{diss}^{0~*}(\boldsymbol{a})$$

and further

$$\Delta G_{diss}^{0~*}(\boldsymbol{a}) - \Delta G_{diss}^0(\boldsymbol{a}) = \Delta G_x^0(\boldsymbol{a}+d\boldsymbol{a}) - \Delta G_x^0(\boldsymbol{a}) = \frac{\partial\Delta G_x^0(\boldsymbol{a})}{\partial\boldsymbol{a}} \tag{4}$$

The total free energy change accompanying dissociation of dendrimer from α_1 to α_2 in the absence of polymer is:

$$\Delta G_{diss}^0 = \int_{\boldsymbol{a}_1}^{\boldsymbol{a}_2} pK_a(\boldsymbol{a})\left(\frac{RT}{0.434}\right)d\boldsymbol{a} \tag{5}$$

Similarly the total free energy change accompanying dissociation of complexed dendrimer from α_1 to α_2 is given.

The total free energy of complexation is equal $\int_{\boldsymbol{a}_1}^{\boldsymbol{a}_2}\left(\frac{\partial\Delta G_x^0}{\partial\boldsymbol{a}}\right)d\boldsymbol{a} = \Delta G_x^0(\boldsymbol{a}_2) - \Delta G_x^0(\boldsymbol{a}_1)$ (6)

and is proportional to the area between pK$_a$ versus α curve for the complex and for the pure dendrimer. According to Dubin's procedure, selection of the α_1 lower than the α_c (dissociation degree when complexation begins) reduces the second term on the right hand site of the equation (6) to zero. The line-marked area in Fig.128 yields then the desired quantity $\Delta G_x^0(\boldsymbol{a})$. Dubin et. al. approximated the titration curves by a second order polynominal (Y$_1$ for the dendrimer alone titration and Y$_2$ for the titration of the complex) and assumed that the free energy of binding at every α lower than the α_c is equal zero. Then, the free energy of binding at any α can be calculated by integrating:[122]

$$\int_{\boldsymbol{a}_1}^{\boldsymbol{a}_2}(Y_2 - Y_1)\frac{RT}{0.43} = \Delta G_x^0(\boldsymbol{a}) \tag{7}$$

According to Dubin's procedure, the complexation energy per mol complex for the I65/G7.5 system has been calculated following equation (7). $Y_1 = 10.9 + 7.1X - 21.5X^2$ and $Y_2 = 13.6 - 15.6X + 0.17X^2$. The complexation energy of the system I65/G7.5 with charge ratio

I65/G7.5 = 1.09 is equal to (-9.1) kJ per mol complex. The minimal and maximal degree of dissociation of the dendrimer at which complexation occurs have been estimated from the Fig.137: $\alpha_1 = 0.2$ and $\alpha_2 = 0.85$.
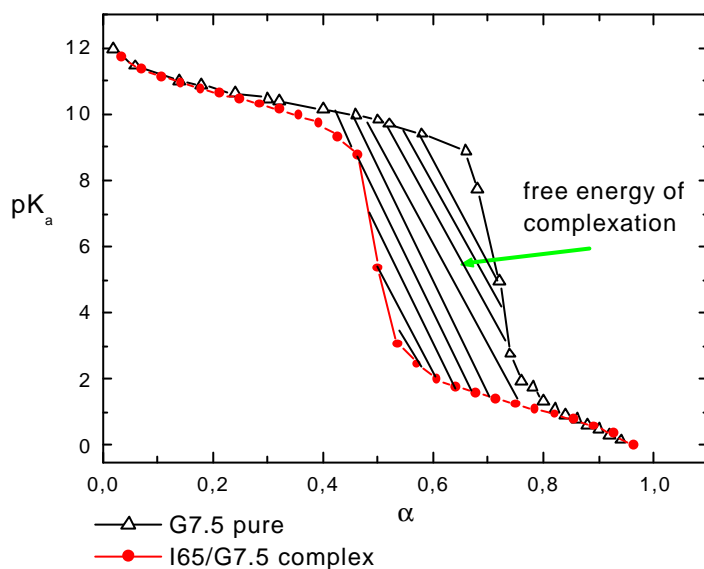

Fig.128: Dissociation constant as a function of the dissociation degree for pure G7.5 PAMAM dendrimer and its complex with I65. Molar charge ratio of I65/G7.5 = 1.09. Free energy of complexation equals 9.1 kJ/mol complexes.

The (-9.1) kJ/mol value calculated for I65/G7.5 system is higher than that of around (-2) kJ per mol complex for Dubin's systems. The negative value of the complexation energy indicates an exergonic process and suggests that the aggregated state is energetically preferred. Like in Dubin's system also in case of the I65/G7.5 complexation the energy decreases with an increase of the dissociation degree, for comparison see Fig.129. The more groups on the dendrimer surface are dissociated, the better complexation properties the dendrimer has. The difference between the complexation energy value calculated by Dubin et. al. and the complexation energy of the I65/G7.5 system is caused by the salt addition to the Dubin's system. Not only the nature of the linear compound (PDADMAC) is different as compared to the ionene. 0.1M NaCl addition to the Dubin's systems causes an appearance of the broad diffusive layer around the macroions in the solution. This makes the complexation much worse. In the case of I65/G7.5 without low molecular mass salt addition the complexation condition is better. The diffusive layer surrounding the macroions in the solution is thinner. The negative value of the complexation energy is lower.
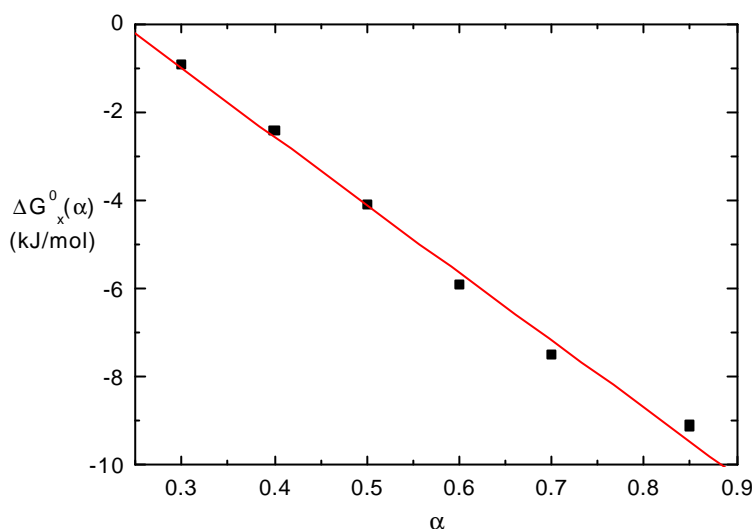
Fig.129. The complexation energy change as a function

of the dendrimer dissociation degree.

From the pK_a and pK_0 of pure dendrimer it is possible to calculate the surface charge potential for the single dendrimer molecule. Miura et. al. investigated the complex formation between a coarboxyl-terminated cascade polymer of 3rd generation and several cationic polyelectrolytes of varying linear charge density as a function of the ionic strength. [77] Miura, Dubin et. al. calculated pK_a using an equation:

$$pK_a = pH + \log \frac{(1-\alpha)}{\alpha} = pK^0 + \frac{0.434 \Delta G_{el}(\alpha)}{RT} \qquad (8)$$

Assuming $\Delta G_{el}(\alpha)$ to be the work of transferring a proton from the bulk solution to the dendrimer surface one can recalculate:

$$eN\psi_0 = \Delta G_{el}(\alpha) \qquad (9)$$

$$\psi_0 = 2.303(pK_a - pK_0)\frac{kT}{e} \qquad (10)$$

ψ_0 surface charge potential
e elementary charge ($1.6 \ 10^{-19}$ J)
N Avogadro's number ($6.022 \ 10^{23}$ mol^{-1})
k Boltzmann constant ($1.38 \ 10^{23}$ JK^{-1})
T absolute temperature (298 K)
The surface charge density σ_{GC} for a sphere can be written as a Gouy-Chapman relationship[77].

$$\sigma_{GC} = (\frac{e\psi_0}{4\pi})(\kappa + \frac{1}{a}) \qquad (11)$$

a radius of the sphere
ε dielectric constant of the solvent (taken as 80 for water)

κ Debye-Hückel parameter $\kappa^2 = 4\pi l_B I$, where $l_B = \dfrac{e^2}{\epsilon kT}$ is so called Bjerrum length. At 20°C

in pure water $l_B = 0.712$ nm.

ϵ the dielectric permittivity.

I ionic strength (compare with paragraph II. in the theoretical part)

For I65/G7.5 we calculate κ^{-1} [m] as follow:[127]

$$\kappa^{-1} = 3.04 10^{-8} |z|^{-1} c^{-1/2}$$

From this calculation κ^{-1} is equal 12 nm in our system. The ionic strength of our system is about 4 mol/l.

The surface charge density σ_{GC} can be compared with so called geometric surface charge density[77]

$$\sigma_g = (\frac{ne\alpha}{4\pi u^2}) \tag{12}$$

n is the number of surface groups, e.g. 1024 for G7.5. Miura's investigations show that the beginning of complexation between the cascade polymer of 3rd generation and polycation occurs at σ_{GC} and depends on the linear charge density of the polycation and the Debye-Hückle screening length. A quantitative behavior of $\sigma_{GC}\xi \approx \kappa^{1.1}$ has been found, where ξ is the linear charge density. These quantitative behavior reflects the complexation between the linear polycation and the cascade polymer of 3rd generation in tetramethylammonium chloride (TMACl). The investigated ionic strength range is between 0.025 and 0.25.[77]

Based on the titration of pure G7.5 and equations *8-12* we calculate a sphere geometric surface charge density and charge density of the sphere according to the Gouy-Chapman relationship, Fig.130 and Fig.131. The definition and the meaning of the real surface charge density and the geometric charge density have been already discussed in the paragraph 4 and 5 in the theoretical part. The value of the surface charge density which has an influence on the assembly formation is not the geometric one. The surface charge density is influenced not only by the number of surface groups and the dissociation degree. Also the dielectric constant of the solvent and the screening length play a role. We calculate the geometric closer to the real one, the Guy-Chapman surface charge for the case I65/G7.5 sample at the charge ratio I65/G7.5 of 1. The Guy-Chapman surface charge for the beginning of the complex formation is in that case equal 0.34. I65MeBr 0.74 g/l and 5.866 10^{-6}M G7.5 have been used. For one dendrimer molecule there are 3.2 ionene molecules in the solution. We are able to compare the behavior of the geometric and the Guy-Chapman surface charge as a function of the dendrimer dissociation degree. It was not our intention to estimate the σ_{GC} dependency on the linear polyelectrolyte charge density and the Debye-Hückl screening length. To do so, an additional experiment concerning different ionic strengths would have to be performed. In Fig.130 a change in potential of the system versus dissociation degree is presented. The end point of the titration of pure dendrimer is marked. The end point does not cover the $\alpha = 1$, because α in our system is defined as a ratio between the amount of acid added at the pH$_i$ to the amount of acid needed to protonate the dendrimer completely (see equation I).
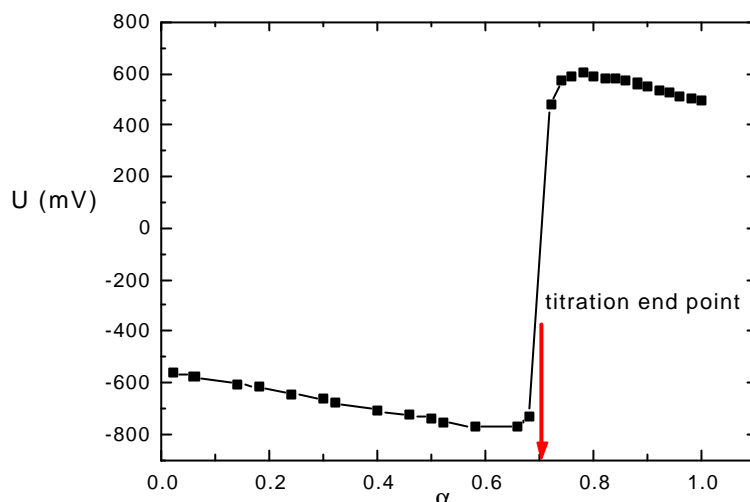
Fig.130: Changes in potential of the system pure ionene

G7.5 in mq H_2O adjusted to the pH of 10.5

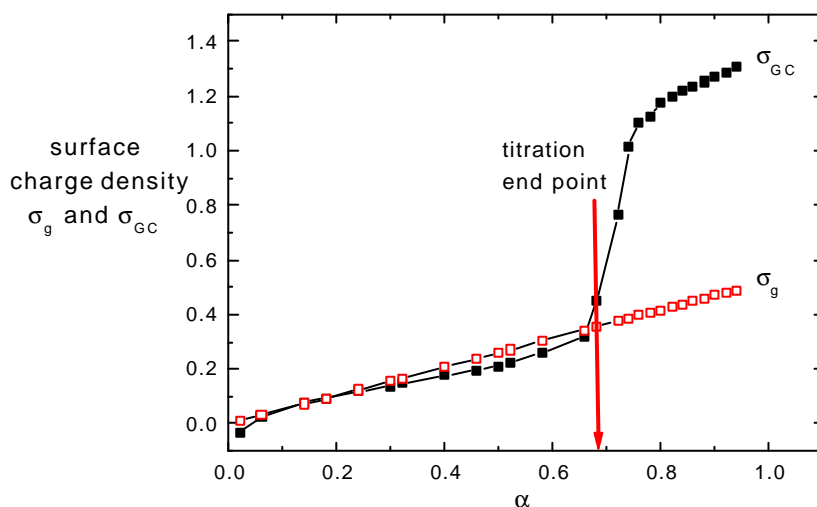(0.5575 M NaOH) and titrated 0.5 M HCl.

Fig.131: Surface charge density calculated from the

Gouy-Chapman relationship and geometric surface charge

density as a function of the dissociation degree -comparison.

In Fig.131 geometric surface charge density and surface charge density calculated according to the Gouy-Chapman equation are presented. For low α value $\boldsymbol{s}_{GC}$ is slightly lower than $\boldsymbol{s}_g$. This confirms the theory of not fully dissociated dendrimer surface groups in the solution. The geometric charge density concerns all charged surface groups and depends on the number of charges on the surface and on the dissociation degree. The surface charge density calculated from the Gouy-Chapman relationship concerns the surface potential (which depends on the relative

dissociation constant), Debye-Hückle screening length, and dielectric solvent properties. Above α around 0.7 the differences between two curves are observed however above α = 0.7 the titration end point is exceeded.

III.VIII. Flexible PAMAM dendrimers complexes-data recapitulation

Systems of ionene and flexible PAMAM dendrimers behave different as compared to usual polyelectrolytes. One and two diffusion modes samples are observed. In the one mode range samples are opalescent or turbid what already suggests the presence of larger complex structures in the system. This complexes of I65 and I25 with PAMAM dendrimers are formed around molecular charge ratio ionene/dendrimer 0.5 to 2. The complex structures posses hydrodynamic radii of $R_h = 60$ to 150 nm. For many cases two transition regimes have been found in the diffusion profile. The first transition point lies the in lower ionene concentration range, before the one mode range, the second transition regime occurs "after" the single diffusion mode range, at higher ionene concetration. Ionene to the dendrimer charge ratio and the sample concentration influence complex formation. The complex formation seems to be influenced also by the linear charge density of ionene and surface charge density of the dendrimer. Splitting point values increase with increasing dendrimer generation. Qualitatively, the dependency of complex formation may be expressed as:

$$\boldsymbol{\lambda}_{splitting} = \frac{c_{\text{Im},nMeBr} \cdot N_{\text{Im},nMeBr}}{c_{Gx.y} \cdot N_{Gx.y} u}$$

c is the molar concentration of ionene and dendrimer respectively, N means number of charges per molecule for ionene and the dendrimer respectively. U is a shifting factor which standardizes the diffusion behavior of all generations. We suppose u to be related to the surface charge density $\boldsymbol{\sigma}_{GC}$ of the dendrimer molecule.

As presented by different authors, for normal polyelectrolytes only one transition regime is observed.[111-117] These transition regime corresponds to the second transition regime in our system, $\lambda_{2\ splitting}$. The $\lambda_{1\ splitting}$ does not appear for the normal polyelectrolytes.

With low molecular mass salt addition experiment has confirmed that the double mode is caused by the different in size objects present in the solution. Core-shell nature of complexes has been predicted based on R_g/R_h ratio and pair distance distribution function analysis.

IV. Complexation between ionenes and stiff poly(phenylene) dendrimers
IV.I.A. Complexes of Ionenes and Stiff Dendrimers in salt free solution
1.pH

The analysis of the complexes formed by ionenes and stiff dendrimers of first generation (G1) was prepared using pH-metric techniques, DLS, SLS and SANS. The pH value of the stock solution of G1 (concentration $5.1178 \cdot 10^{-3}$M) is 6.1
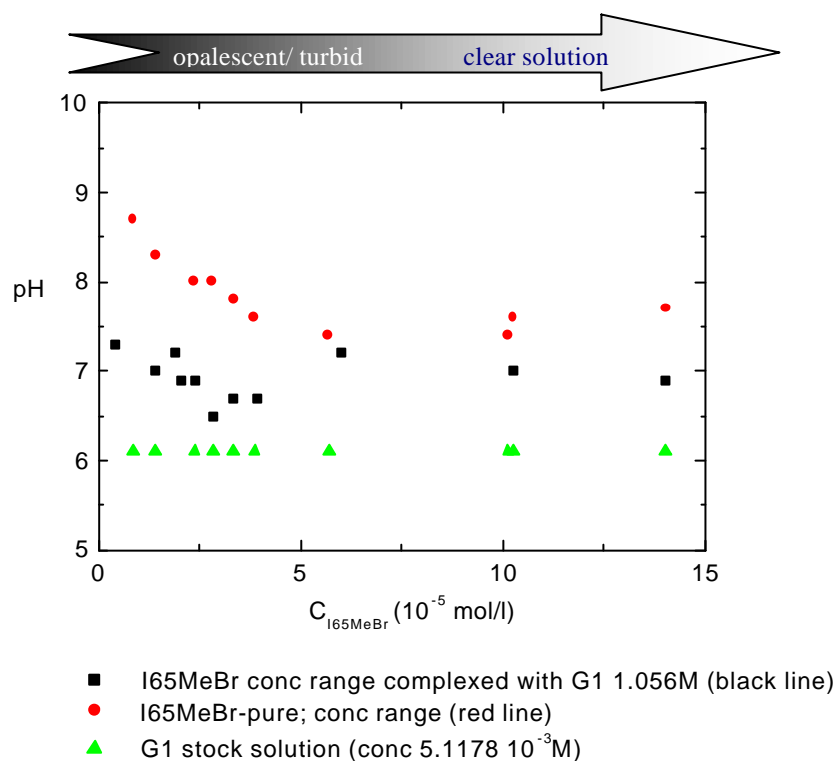

Fig.132: pH as a function of concentration for the complexes

for the ionene as compared to the dendrimer stock solution.

The pH value for the complex solutions lies in-between the pH value for pure ionene (higher) and pH value for stock solution of the dendrimer (lower) (Fig.132). There is no decay in pH value when samples become turbid. The dissociation of stiff first generation poly(phenylene) dendrimers (G1) seems to be independent of the concentration of ionene added. A calculated radius of gyration for G1 (computer simulation study for the PhD thesis of George Mikhov at MPI-P Mainz) is comparable with the dimensions of PAMAM G5.5 or G7.5. G1 carries 48 surface COOH groups, which is a low number as compared to the 254 or 1024 for G5.5 and G7.5 respectively. The surface charge density of G1 has to be significantly lower than the surface charge density for G5.5 or G7.5. The dissociation of charged polymer groups is related to the charge density (compare Manning's theory). On the other hand PAMAM dendrimer G2.5 (number of surface groups 32, R_h(DLS) = 2 nm) behaves like the other PAMAM dendrimers and a decay of pH value for ionene/G2.5 is observed. Summarizing, not only the density of charges influence the dissociation of surface groups in dendrimers. However in the pH curve for I65/G1 complexes a minimum of pH (pH~6.5) can be observed as well. The difference between this minimal value and the average pH for the rest of samples is larger than the error involved. The

minimal value of pH accompanies the largest measured hydrodynamic radii of particles R_h(DLS) = 100 nm. A detailed discussion will be presented in context with the scattering data below.

2. Scattering techniques

2.1. DLS of I65MeBr/G1 system

Fig.133 presents the diffusion profile of the I65/G1 system.
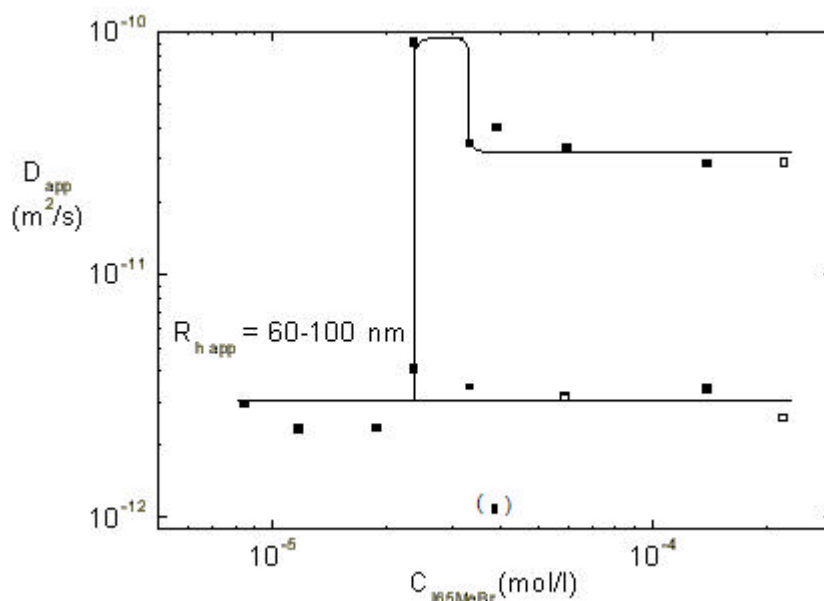

Fig.133. Diffusion coefficient as a function of the

concentration for the system I65 concentration range

with G1 1.165 10^{-4} M.

Like in the case of ionene/PAMAM dendrimer samples, one and two diffusion process ranges exist for the I65/G1 system. The presence of complexes in the one mode range is confirmed via the turbidity of the samples. Turbid samples as in case of complexes with PAMAM dendrimers show the existence of aggregates, detectable "by eye" giving the opalescence or turbidity. "Empty" squares at the diffusion profile (Fig.133) indicate samples where distinguishing between one and two diffusion modes was difficult. For small angle (30°- 90°) only one, broad, for larger angles (120°-150°) two diffusion processes were observed in the DLS experiment. In case of complexes, two modes behavior may be due to overlapping of aggregation and interaction effects or a very broad size distribution of particles in the investigated system. Addition of low molecular mass salt may help to indicate the nature of interaction in the system (see part about I65/G1 with low molecular weight mass salt addition"). Well defined self assembly structures here with R_h between 60 and 100 nm may cause the appearance of a one mode regime in the dynamic profile of the investigated samples. The samples in this area are either slightly opalescent or turbid, which proves the hypothesis of self assembly into particle sizes in this regime. Interaction between self assembly structures in the one diffusion process area seems not to disturb the light scattering analysis, nearly no slope in the D (q), q^2 -dependency presented in Figure 143 is observed. Diffusion coefficient does not depend on the scattering vector presented here for the sample I65 (1.18 10^{-5}M) G1 (1.165 10^{-4}M) where molar charge ratio of the

compounds is I65/G1 = 0.76. Narrow distribution of the intensity weighted relative amplitude and q-independence on the scattering vector square (compare Fig.134, 135) show that well-defined aggregates of a certain size are formed.
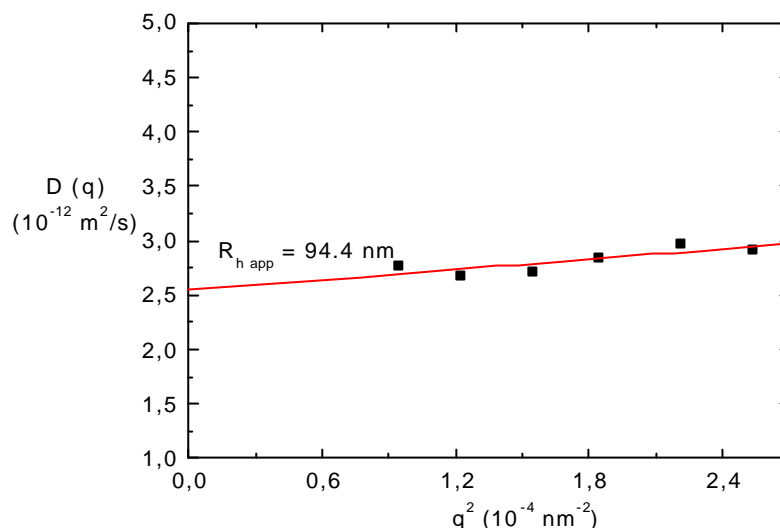

Fig.134: Diffusion coefficient as a function of the scattering
vector square for the sample 0.462g/l (1.18 10^{-5} M) I65MeBr
with 1.165 10^{-4} M G1 in aq solution at the charge ratio
I65/G1 = 1/1.32 (0.76). The diffusion coefficient is
equal D_{app}= 2.5 10^{-12} (m^2/s).

Aggregates found have a size of R_h around 80 to 100 nm. They have to be formed by the connection-*complexation*- of smaller structures. Complexation of ionene and dendrimer thus must occur. The radii found are larger than the radii of investigated "pure" ionene or "pure" dendrimer molecules in aqueous solutions. Even if pure dendrimers stay in the aqueous solution as oligo-aggregates (see analysis of pure compounds chapter IV.I.B) the radii of such oligoaggregates are smaller than the radii found for I65/G1 complexes in one diffusion mode regime. The diffusion coefficients in the area of two modes (above the concentration of I65MeBr equal 2.3 10^{-5}M) are only slightly dependent on the scattering vector square (Fig.135).
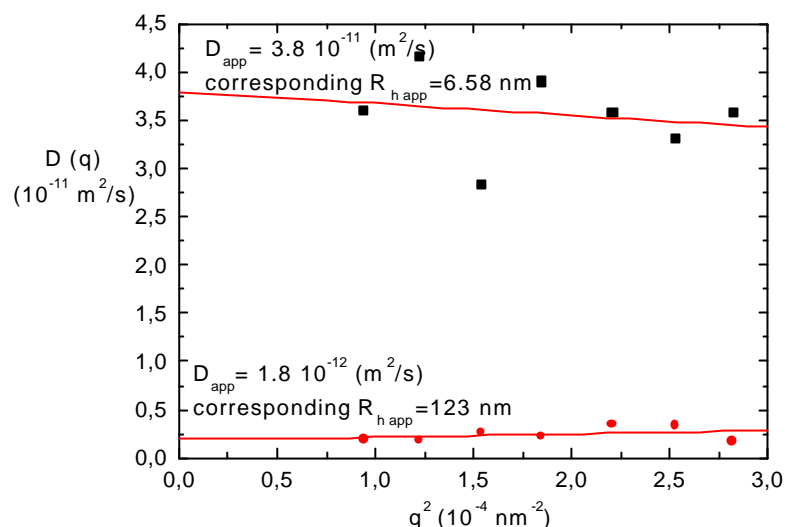
Fig.135: Diffusion coefficient as a function of the scattering vector square for the sample I65MeBr 1.528g/l (3.92 10^{-5} M) with G1 1.165 10^{-4} M at the charge ratio of I65/G1 = 2.49/1.

The slope of fast mode in Fig.135 (apparent diffusion coefficient equal 3.8 10^{-11} m^2/s) is slightly negative and the slow mode (apparent diffusion coefficient equal 1.8 10^{-12} m^2/s) slope is independent on the q^2 value. Such behavior suggests interactions between polymer structures presented in the solution, and can explain the appearance of a slow mode. Smaller structures, dendrimer molecules, ionene chains or small individuals formed by them can be a reason for the fast mode. The radius of the particles "moving" according to the fast mode corresponds to the value of 6.5 nm (near the radius of random coil of ionene or dendrimer molecule surrounded by the ionene). Such small structures may form bigger aggregates in the solution which cause the slow mode. Two diffusion modes may alternatively be caused via polyelectrolyte effect. This appearance of a second mode is observed when the charge ratio of ionene to dendrimer deviates from one (is higher than 1.2). To investigate the origin of double mode, samples with low molecular mass salt addition must be investigated (see IV.I.B).
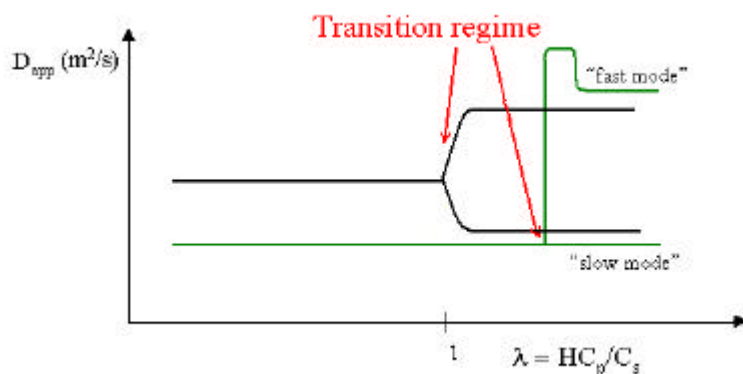
2.1.1 DLS of I65MeBr/G1 system- summary

Fig.136: Green curve- I65/G1 diffusion profile schema. Black

curve- normal polyelectrolyte behavior (compare sumary for

ionene/PAMAM dendrimer systems).

As compared to the normal polyelectrolytes (Fig.136), in the I65/G1 system turbid and opalescent samples are observed. The turbidity of samples coincides with the one diffusion mode regime of sample concentration. Transition regime is observed around $\lambda_{splitting} = 1$, so it is comparable with normal polyelectrolyte behaviour. Only one transition regime corresponds to the normal polyelectrolyte behaviour and to the less concentrated samples I65/PAMAM dendrimers. Anyhow in general I65/G1 systems stay in contrast to the typical ionene/PAMAM dendrimer systems which characterise two transition points. The fast mode is "faster" than the diffusion in one mode range, the slow mode does not change for the I65/G1 systems what corresponds to the ionene/flexible dendrimer complexes. A peak in the fast mode appears around the splitting point. The nature of this peak seem to be similar to the ionene with PAMAM dendrimers complexes. The two modes phenomena requires further investigation i.e. with low molecular mass salt added to the system.

The single dendrimer molecule has 48 charges, the ionene molecule 322 charges per chain. 1/1 in charges means around 7 times more dendrimer molecules. The stiff dendrimer molecules are nearly spherical. The dendrimer can be attached to ionene chains which may wrap around the dendrimer molecule (Figure.137 A) or form compact random coils on the surface of the dendrimer (Fig.137 B). In this case, the number of ionenes in the nearest neighborhood of dendrimer would be limited according to ionene random coil diameter. Another possibility is that the spherical dendrimer is attached to slightly stretched chains of ionene (Fig.137 C).

Fig.137: (A) ionene wraped around the dendrimer molecule.

(B) ionene compact random coils on the surface of the dendrimer.

(C) spherical dendrimer attached by slightly stretched chains of ionene.

The objects presented in Figure.137 can act as a buildings blocks for more complex structures which we detect in the solution by scattering techniques. Fig.137 is only a schematic picture of the kind of structures. The number of ionene and dendrimer molecules building structures A,B,C varies over the range of investigated charge ratio. Objects in Fig.137 may cause the fast diffusion mode in case of two diffusion modes samples. The static scattering techniques give a possibility to recognize the details of complexes morphology that is why next SANS data will be presented, discussed and finally compared with the light scattering measurements. Even in an aqueous solution of 0.4M KBr the G1-dendrimer system stays in an aggregated state (II.II).

2.2. SANS for the system of I65MeBr with G1

We have chosen some representative samples for neutron scattering measurements as indicated in Fig.138.
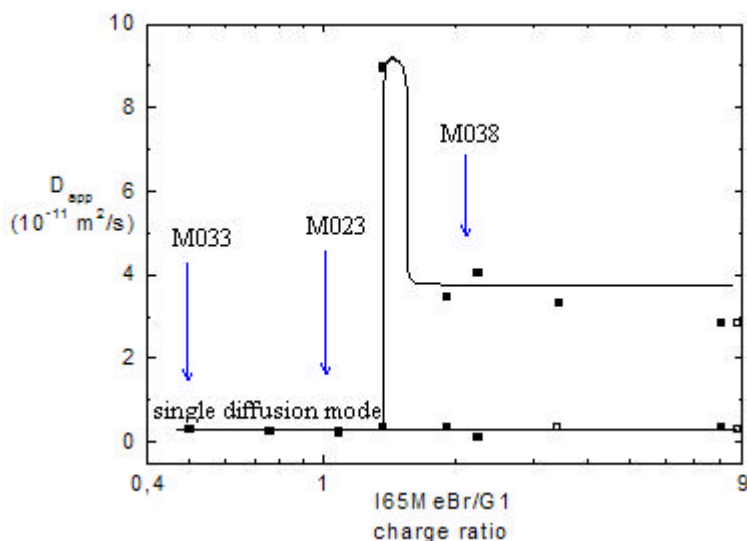

Fig.138. Apparent diffusion coefficient as a function of the

charge ratio for the ionene I65 with G1 polyphenylene

dendrimer systems. I65 concentration range have been used with

G1 1.165 10^{-4} M. M021, M033, M038- samples chosen for SANS.

The first one is 0.34g/l (8.717 10^{-6} M) I65MeBr in 1.165 10^{-4} M G1 aqueous solution. The charge ratio for such sample is equal to I65MeBr/G1= ½. The sample name is M033. M033 is opalescent and contains 1 ionene molecule per 14 dendrimer molecules.

The second sample chosen is 0.75g/l (1.897 10^{-5} M) I65MeBr with 1.165 10^{-4} M G1 with a charge ratio I65MeBr/G1 = 1.09/1. Sample name M023. This sample is opalescent and contains 1 ionene molecule per 7 dendrimer molecules. Finally, a 1.535g/l (3.93 10^{-5} M) I65MeBr with 1.165 10^{-4} M G1 sample was investigated. The charge ratio I65MeBr/G1 equals 2.26/1 and the sample name is M038. Sample is clear and contains 1 ionene molecule per 3 dendrimer molecules. The scattering curve of the sample M033 after corrections is presented in Fig.139.
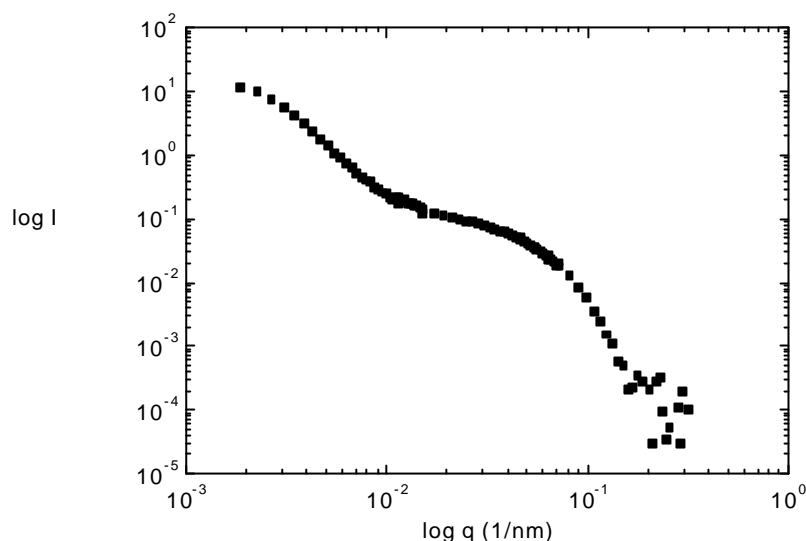
Fig.139: Scattering curve for the system 0.34g/l (8.717$10^{-6}$ M) I65MeBr in 1.165 10^{-4} M G1 aq, at the charge ratio I65MeBr/G1=1/2 the sample name is M033 and the sample is opalescent.

From the scattering curve the radius of gyration (R_g) was calculated. As for ionene/PAMAM dendrimers complexes, two models were considered for R_g calculation.

The Zimm model is appropriate for coils and systems with broad molecular mass distribution and yields a higher value of R_g. The Guinier plot enables a better estimation of radii for collapsed coils and globular particles. Here the value of R_g obtained is lower than in case of Zimm plot. For explanations of data calculation see chapter IV in the theoretical part concerning characterization methods.
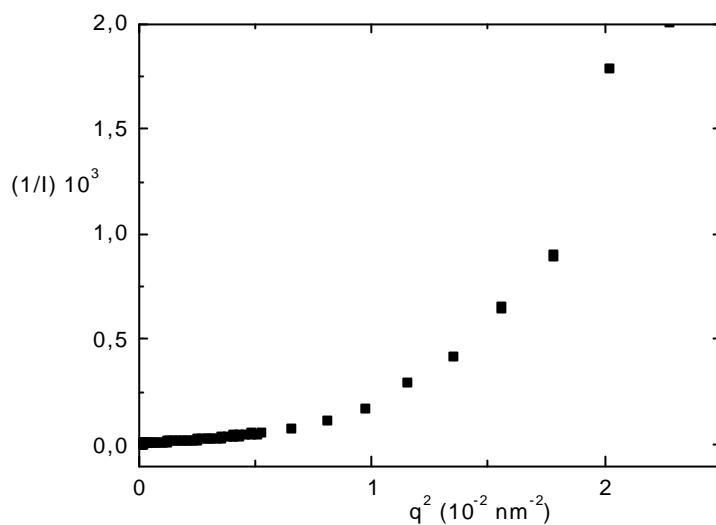
Fig.140: Zimm plot for the sample 0.34g/l (8.71710^{-6} M)
I65MeBr in 1.165 10^{-4} M G1 aq, at a charge ratio
I65MeBr/G1= 1/2. Sample name is M033 and
the sample is opalescent.
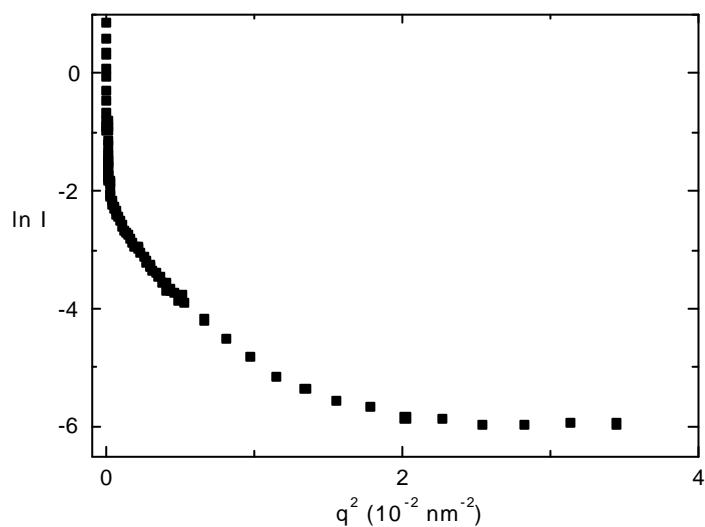
Fig.141: Guinier plot for the sample 0.34g/l (8.71710^{-6} M)
I65MeBr in 1.165 10^{-4} M G1 aq, at the charge ratio
I65MeBr/G1= 1/2. The sample name is M033 and
the sample is opalescent.

According to the Zimm plot the investigated structure is rather more spherical than coil-like and use of a Guinier plot is suitable (Fig.140,141).

The initial linearity of the Guinier plot confirms a spherical shape of the structures. From the slope one can receive the value of R_g. In case of the sample mentioned above: R_g= 57.2 nm (Fig.142).

Fig.142: Gunier plot, R_g determination for the sample 0.34g/l ($8.717 \cdot 10^{-6}$ M) I65MeBr in 1.165 10^{-4} M G1 aq, at the charge ratio I65MeBr/G1= 1/2. The sample name is M033 and the sample is opalescent.

According to a similar procedure R_g= 69.9 nm was found for the sample M023 with ionene I65 concentration 0.74g/l (1.897 10^{-5} M) and 1.165 10^{-4} M G1 (Fig.145). Charge ratio in that case is equal I65MeBr/G1= 1.09/1. Sample was opalescent. Below, in Fig.143, scattering curve as a function of scattering vector for mentioned above sample M023 is presented.
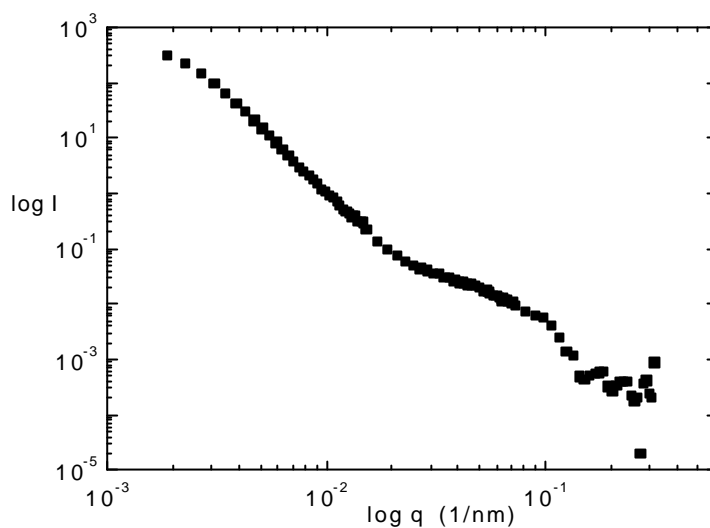
Fig.143: Scattering curve for the system 0.75g/l (1.897 10^{-5} M)
I65MeBr in 1.165 10^{-4} M G1 aq, at the charge ratio I65MeBr/G1=1.09/1.
The sample name is M023 and the sample is opalescent.

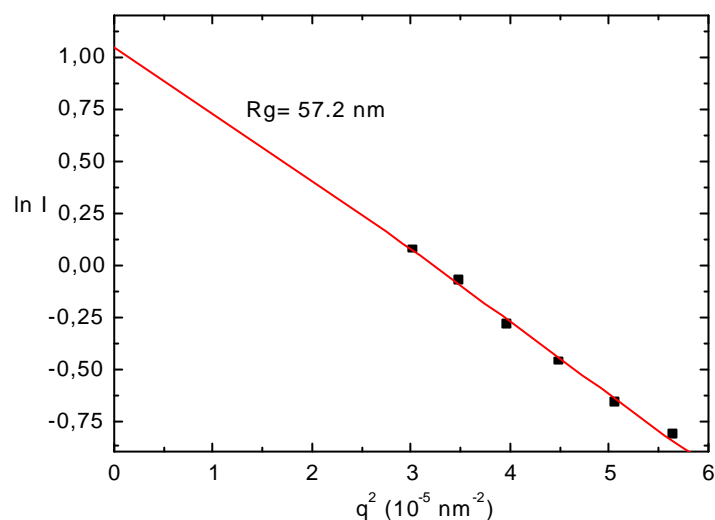Fig.144: Guinier plot, R_g determination for the sample
0.75g/l (1.897 10^{-5} M) I65MeBr in 1.165 10^{-4} M G1 aq
at the charge ratio I65MeBr/G1= 1.09/1. The sample name is
M023 and the sample is opalescent.

In case of the third sample selected for SANS (M038) containing 1.535g/l (3.93 10^{-5} M) I65MeBr in 1.165 10^{-4} M G1 and the charge ratio I65MeBr/G1= 2.26/1, representing a clear solution (Fig.145) the data analysis is not easy due to the complicated polyelectrolyte behavior of the

sample. The charge ratio of M038 I65MeBr/G1 = 2.26/1 corresponds to three times excess of the dendrimer molecules.
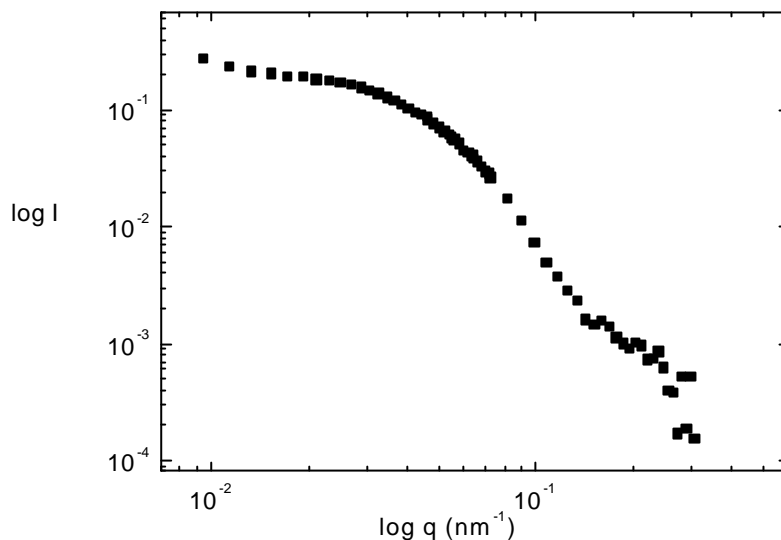
Fig.145: Scattering intensity as a function of the scattering

vector for the sample 1.535g/l (3.93 10^{-5} M) I65MeBr in

1.165 10^{-4} M G1 aq at the charge ratio I65MeBr/G1= 2.26/1.

The sample name is M038 and the sample is clear solution.

The sample in Figure145 was chosen from the area where two diffusion modes are observed in the DLS experiment. An upturn at the low-q range indicates either interactions in the system or different sized particles present in the solution. Further experiments, e.g. low molecular mass salt addition to the samples are required to judge unequivocally about the nature of the upturn of the scattering curve at law q-range. The sample contains 1.535g/l (3.93 10^{-5} M) I65MeBr in 1.165 10^{-4} M G1 and is a clear solution. The charge ratio I65MeBr/G1 is equal 2.26/1. The sample name is M038. The Zimm plot indicates spherical structures but neither from Zimm nor from the Gunier plot it is straight forward to extract the shape and expected size of particles or aggregates. In case of the Zimm plot R_g = 10 nm, in case of the Gunier plot R_g = 3.8 nm result. Compare plots in Fig.146-149.
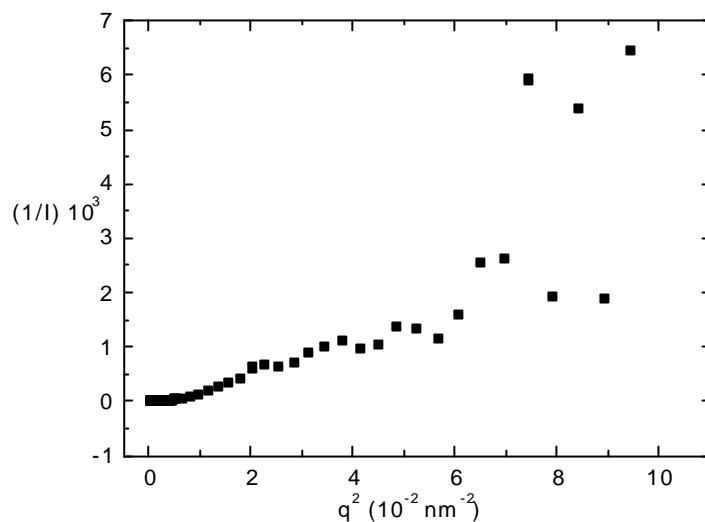
Fig.146: Zimm plot for the sample 1.535g/l (3.93 10^{-5} M) I65MeBr in 1.165 10^{-4} M G1 aq at the charge ratio I65MeBr/G1= 2.26/1. The sample name is M038 and their condition is clear solution.
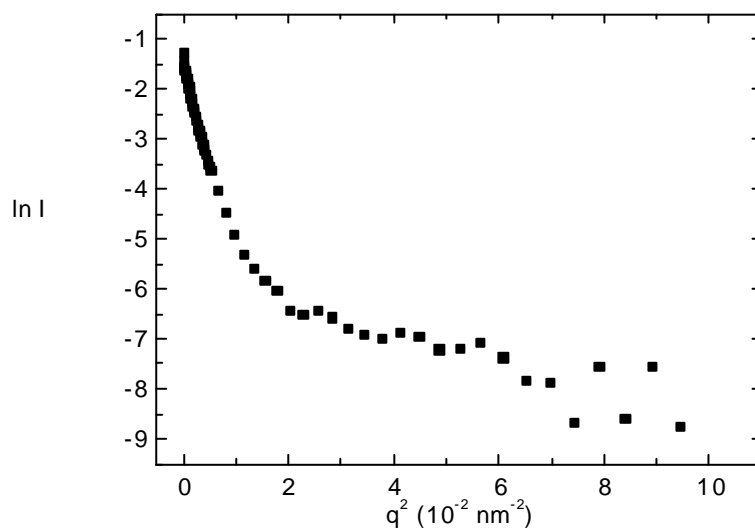
Fig.147: Gunier plot for the sample 1.535g/l (3.93 10^{-5} M) I65MeBr in 1.165 10^{-4} M G1 aq at the charge ratio I65MeBr/G1= 2.26/1. The sample name is M038 and the sample condition is clear solution.
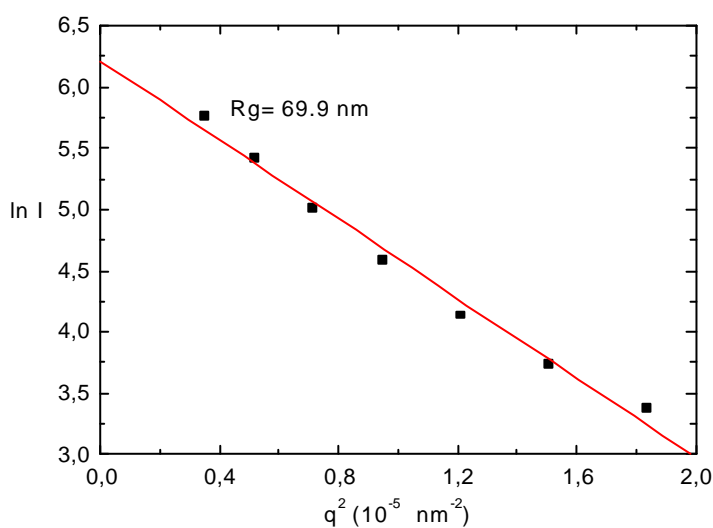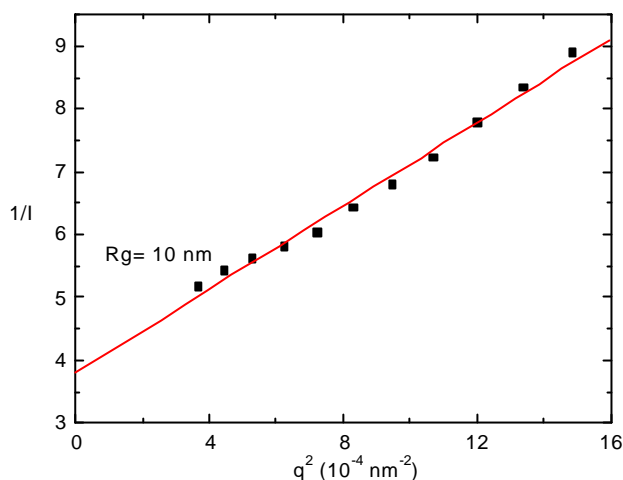
Fig.148: Zimm plot, R_g determination for the sample1.535g/l

$(3.93 \ 10^{-5} \ M)$ I65MeBr in $1.165 \ 10^{-4} \ M$ G1 aq, at

the charge ratio I65MeBr/G1= 2.26/1. The sample name is

M038 and the sample condition is clear solution.
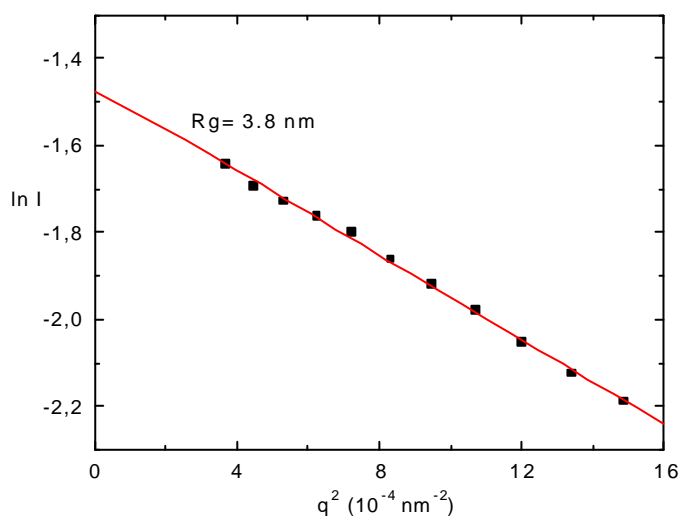
Fig.149: Gunier plot, R_g determination for the sample 1.535g/l

$(3.93 \ 10^{-5} \ M)$ I65MeBr in $1.165 \ 10^{-4} \ M$ G1 aq at the charge

ratio I65MeBr/G1= 2.26/1. The sample name is M038 and

the sample is clear solution.

Although radii found are in the same order of magnitude (10 nm and around 4 nm) one cannot easily determine size of the particles/aggregates because of the double diffusion mode in the DLS. The nature of the double diffusion mode in this sample is not sure: it can be caused by

different sized particles, but it can be also because of the polyelectrolyte effect. Polyelectrolyte effect is reflected in the strong upturn in the initial part of the scattering curve. Such upturn is observed in Fig.145. An influence of S(q) may cause also large difference between calculated from Zimm and Gunier plot radii of gyration. Similarly to the ionene/PAMAM systems, with salt experiment is required to judge unequivocally about the nature of mentioned above phenomenon. In the case of sample M033 which is I65MeBr/G1 with a charge ratio equal 0.5 and 1 ionene molecule per 14 dendrimer molecules, the excess of dendrimers is high enough to connect flexible ionene chains and shape persistent dendrimers into bigger aggregates.

The same situation is in the case of charge ratio I65MeBr/G1= 1.09 (M023), where 1 ionene molecule per 7 dendrimer molecules is present in the system. The sample is opalescent.

2.2.1 SANS for I65/G1 -summary

As in the case of ionene/PAMAM dendrimers some information about the shape of the objects investigated is obtained from the ratio of the radius of gyration to the hydrodynamic radius. For the sample with charge ratio of the I65MeBr/G1= ½ (M033) R_g = 57.2 nm and R_h = 75.3 nm which gives R_g/R_h = 0.759. This suggest that an investigated structure is homogenous and hard sphere-like, (from the theory R_g/R_h= 0.778 for homogenous hard sphere). Such structure is presented in Fig.150 A. For the sample M023 with I65MeBr/G1 charge ratio of 1.09/1, it is R_g = 69.9 nm R_h = 60.2 nm, which gives σ ratio of 1.16. This may indicate stars with polydispers arms (from the theory R_g/R_h for the regular stars with polydispers arms equals 1.225) as indicated in Fig.150 B. In case of the third sample (M038) with the charge ratio of I65MeBr/G1 = 2.26/1 and 1 ionene molecule per 3 dendrimer molecules, the calculation of the R_g/R_h ratio is not possible because there are, as explained before, two diffusion modes and indications of interactions in the scattering curves. At a large excess of the dendritic molecules, smaller, dense-packed structures can appear (Fig.150 A). When the excess of dendritic molecules becomes lower, larger structures appear (Fig.150 B).
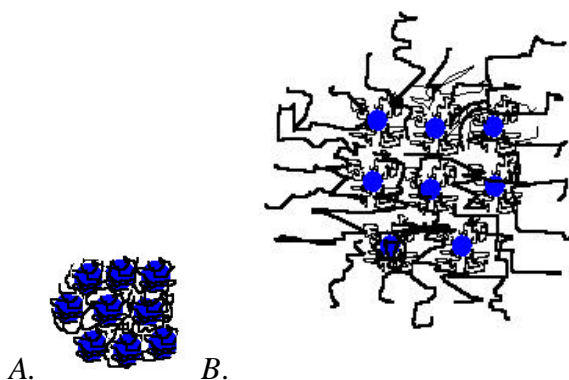

Fig.150: Assembly structures which could be formed by ionene and dendrimers in solution.

A: dense-packed, hard sphere-like structure and B: ionene molecules on the dendrimer.

IV.I.B. Complexes of Ionene with Stiff Dendrimers in the presence of low molecular mass salt

1. DLS experiment

To understand the influence of low molecular mass salt on the balance between dendrimer G1 and ionene in aqueous solution as well as the influence on the structures formed, KBr addition was employed. As stated previously, added salt is expected to screen electrostatic interactions, i.e. decrease interaction effects and thus allow a better analysis of particle size and shape in particular in the regime of two diffusion modes. On the other hand, the salt itself may influence the association behavior. However, a detailed analysis of salt-containing samples may provide important further information.

In the samples, a KBr concentration of $6.8 \cdot 10^{-4}$ M was applied. At higher concentration of added salt in the sample salting out effect was observed. The samples were first measured by DLS and SANS for selected samples was done. To present the behavior of the I65MeBr/G1 system three samples were selected:

- 0.462 g/l ($1.18 \cdot 10^{-5}$ M) I65MeBr in $1.056 \cdot 10^{-4}$ M G1 aq; $6.8 \cdot 10^{-4}$ M KBr

charge ratio I65MeBr/G1= 1/1.3

condition: slightly opalescent; 1 ionene molecule per 9 dendrimer molecules

one diffusion mode according to DLS

- 0.74 g/l ($1.89 \cdot 10^{-5}$ M) I65MeBr in $1.056 \cdot 10^{-4}$ M G1 aq; $6.8 \cdot 10^{-4}$ M KBr

charge ratio I65MeBr/G1= 1.2/1

condition: opalescent; 1 ionene molecule per 6 dendrimer molecules

one diffusion mode according to DLS

- 1.528 g/l ($3.92 \cdot 10^{-5}$ M) I65MeBr in $1.056 \cdot 10^{-4}$ M G1 aq; $6.8 \cdot 10^{-4}$ M KBr

charge ratio I65MeBr/G1= 2.5/1

condition: slightly opalescent; 1 ionene molecule per 3 dendrimer molecules

two diffusion modes according to DLS

As presented in Tab.19 charge ratio of I65MeBe/G1 and molecules ratio of I65MeBr to G1 are comparable between solutions investigated with and without salt addition.

Tab.19: The charge and molecular ratios of the I65/G1 systems with and without low molecular mass salt addition.

I65MeBr/G1		I65MeBr/G1	
Ratios with salt addition		Ratios without salt addition	
Charge ratio	Molecular ratio	Charge ratio	Molecular ratio
0.769	0.111	0.5	0.071
1.2	0.166	1.09	0.143
2.25	0.333	2.5	0.333

In the following results will be discussed. Similarly as in the case of ionene/PAMAM dendrimers the ratio of compounds must be around 1/1 in charges (of I65MeBr to G1 charge number) to obtain samples containing aggregates and single diffusion modes. As a first sample containing 0.462 g/l ($1.18 \cdot 10^{-5}$ M) I65MeBr and $1.056 \cdot 10^{-4}$ M G1 was investigated (Fig.151). The charge ratio I65MeBr/G1 is 0.769 and sample is slightly opalescent. The solution contains 1 ionene molecule per 9 dendrimer molecules. The concentration of KBr in the sample is equal $6.8 \cdot 10^{-4}$ M. Before low molecular mass salt has been added to the system only single diffusion mode was observed in the DLS. After salt addition the diffusion coefficient versus scattering vector squared shows a single mode as well. Extrapolation yields $D_{app} = 1.84 \cdot 10^{-12}$ m^2/s which corresponds to a hydrodynamic radius of $R_{h\ app}= 132$ nm.

Fig.151: Diffusion profile for the sample 0.462g/l
(1.18 10^{-5} M) I65MeBr in 1.056 10^{-4} M G1 aq at
the charge ratio I65MeBr/G1= 0.769. The sample is
slightly opalescent. 1 ionene molecule per 9 dendrimer
molecules is present in the solution.
The diffusion coefficient is equal D_{app}= 1.84 10^{-12} (m^2/s)
the radius of gyration is ($R_{h\ app}$ = 132 nm)

The distribution of the decay time for this sample at the scattering angle of 90° is presented in Fig.152. This distribution is narrow and confirms the presence of one defined species in the system.
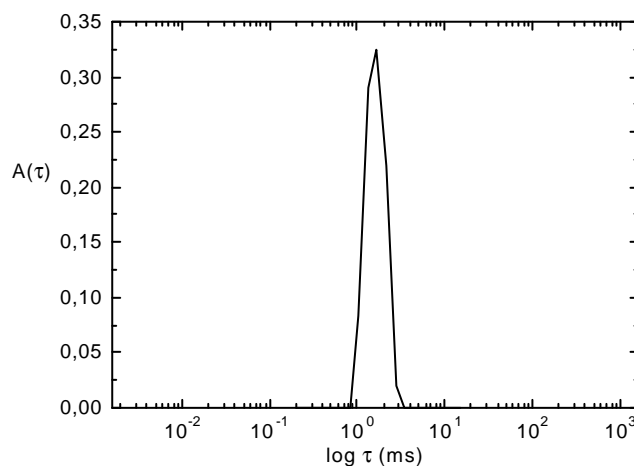
Fig.152. Distribution of decay times for "one mode sample"
of I65/G1 for the charge ratio I65/G1 = 0.769.
the concentration of I65 equals 0.462 g/l and the
concentration of G1 is 1.056 10^{-4} M.

The second case 0.74g/l (1.89 10^{-5} M) I65MeBr with 1.056 10^{-4} M G1 before salt addition was also single mode sample. The concentration of added further salt is 6.8 10^{-4} M KBr. Charge ratio I65MeBr/G1 is 1.2 and sample is opalescent. Per 1 ionene molecule 6 dendrimer molecules are in the solution. In that case two modes are observed: (1.7 10^{-12} m^2/s; $R_{h\,app}$= 167 nm and 4.35 10^{-13} m^2/s; $R_{h\,app}$= 734 nm) see Figure 153.
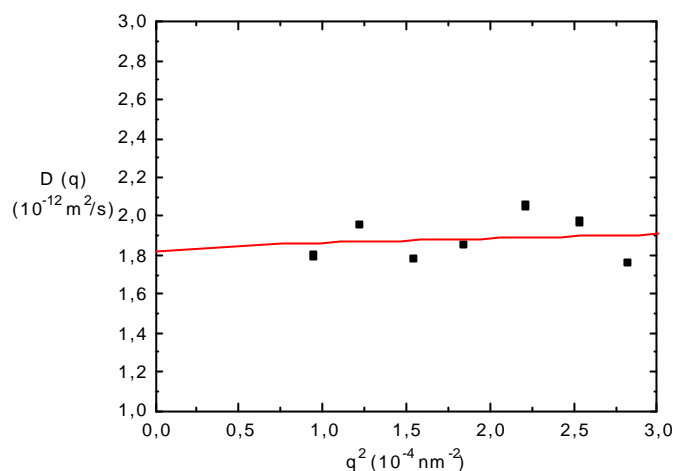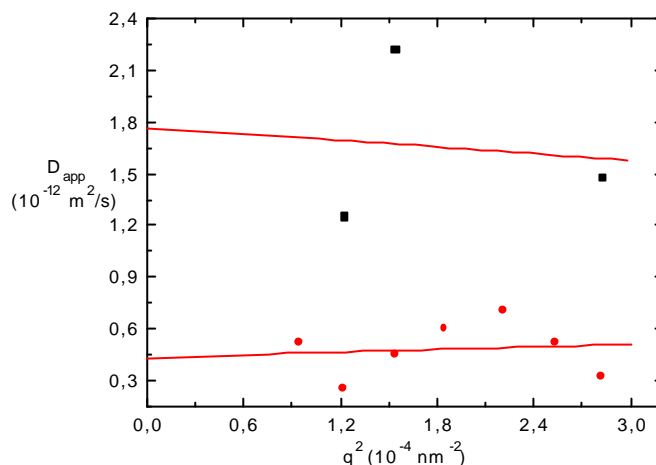

Fig.153: Diffusion profile for the sample 0.74g/l (1.89 10^{-5} M) I65MeBr in 1.056 10^{-4} M G1 aq at the charge ratio I65MeBr/G1= 1.2/1. The sample is opalescent and per 1 ionene molecule contains 6 dendrimer molecules. The slow mode is equal D_{app}= 4.35 10^{-13} (m^2/s) and the radius is ($R_{h\,app}$=734 nm). The fast mode is equal D_{app}= 1.7 10^{-12} (m^2/s) with a radius (R_h = 167 nm).

After salt addition three modes are observed for the sample 1.528 g/l (3.92 10^{-5} M) I65MeBr in 1.056 10^{-4} M G1. The concentration of salt in the system is 6.8 10^{-4} M KBr and the charge ratio of the compounds I65MeBr/G1= 2.5. Sample was opalescent and contains 1 ionene molecule per 3 dendrimer molecules. Before salt addition sample showed two diffusion modes according to DLS. After salt addition three diffusion modes are observed: 3.9 10^{-11} m^2/s (R_h= 6.19 nm), 1.97 10^{-12} m^2/s (R_h= 101 nm) and 2.3 10^{-13} m^2/s (R_h= 730.59). A comparison of the systems without and with low molecular weight salt addition is given in Fig.154 below.
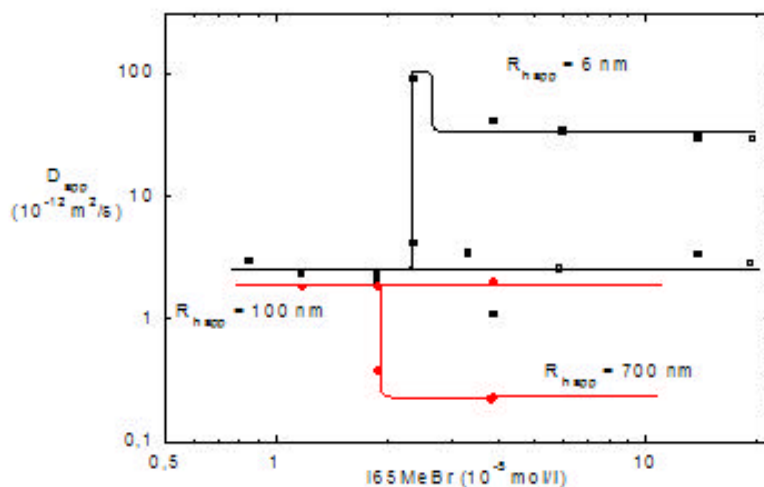
Fig.154: Comparison of the systems with and without low molecular mass salt addition. The squares indicate I65MeBr concentration range with 1.165 10^{-4} M G1 and the circles show I65MeBr concentration range with 1.165 10^{-4} M G1 and with addition of KBr (6.8 10^{-4} M in the sample).

1.1.I65/G1 systems with low molecular mass salt addition- summary

Generally addition of the low molecular mass salt to the I65/G1 system does not significantly change the diffusion profile. In the case of sample containing low concentration of ionene, e.g. 0.462g/l (1.18 10^{-5} M) I65MeBr and 1.056 10^{-4} M G1 before and after salt addition one diffusion mode is observed. It indicates aggregates which are stable under different ionic strength condition. For other samples (with increasing ionene concentration), even if the sample without salt addition was an one mode sample, after KBr addition a second mode appears. The aggregates which were observed before low molecular mass salt addition are not stable upon salt addition. Additionally the sample becomes more opalescent, which can indicate secondary aggregation and appearance of larger assemblies in the solution. Secondary aggregation after screening of the electrostatic interaction via low molecular weight salt addition can be a reason of the second (slow) mode. Upon higher salt addition, salting out and precipitation is observed. The splitting point $\lambda_{splitting}$ for the samples containing low molecular mass salt occurs for lower values than $\lambda_{splitting} = 1$. In the case of samples without salt addition $\lambda_{splitting}$ is about 1. After an experiment with low molecular mass salt addition it is clear that the two modes in the diffusion of samples containing higher concentration of the ionene are caused by the different sized aggregates, or middle-size aggregates and the single macromolecules (ionenes or dendrimers). The second mode does not disappear upon salt addition. It must thus be caused by real structures in the solution. If the two modes were caused by the polyelectrolyte effect, they disappear upon low molecular mass salt addition. Therefore different sized assemblies are expected to be a reason of the double mode profile in analogy to the ionene/PAMAM dendrimer systems.

2. SANS measurement for I65/G1 with low molecular mass salt addition systems

To investigate the structures in details it is noteworthy to consider samples with salt addition by SANS. As a first 0.34g/l (8.717 10^{-6} M) I65MeBr in 1.165 10^{-4} M G1 at 6.8 10^{-4} M KBr concentration where charge ratio I65MeBr/G1= 1/2 was investigated. Sample short name M034.

The sample was opalescent and contain 1 ionene molecule per 14 dendrimer molecules. Figure 155 shows scattering intensity as a function of scattering vector for the already mentioned sample.


Fig.155: Scattering curve for the sample I65MeBr 0.34g/l
(8.717 10^{-6} M) in 1.165 10^{-4} M G1 aq at the charge ratio
I65MeBr/G1= 1/2. The sample name is M034.The sample
is opalescent and contains 1 ionene molecule per 14 dendrimer molecules.

Zimm plot curvature indicates spherical shape of the particles formed (Fig.156).
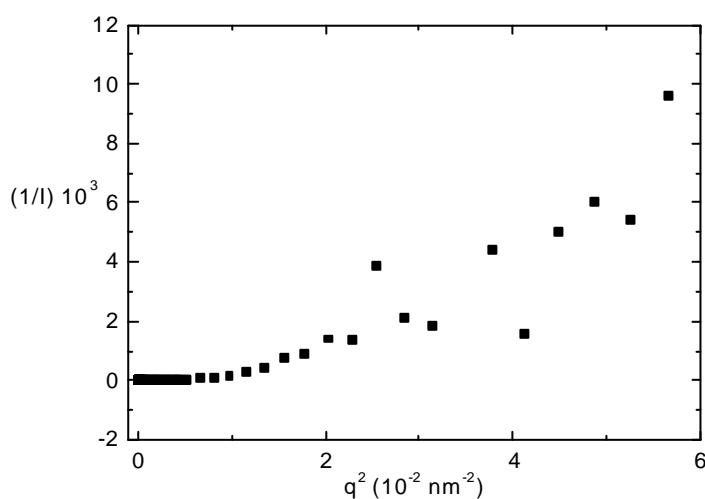
Fig.156: Zimm plot for the sample 0.34g/l (8.717 10^{-6} M)
I65MeBr in 1.165 10^{-4} M G1 aq at the charge ratio
I65MeBr/G1= 1/2. The sample name is M034. The sample
is opalescent and contains 1 ionene molecule per 14 dendrimer molecules.
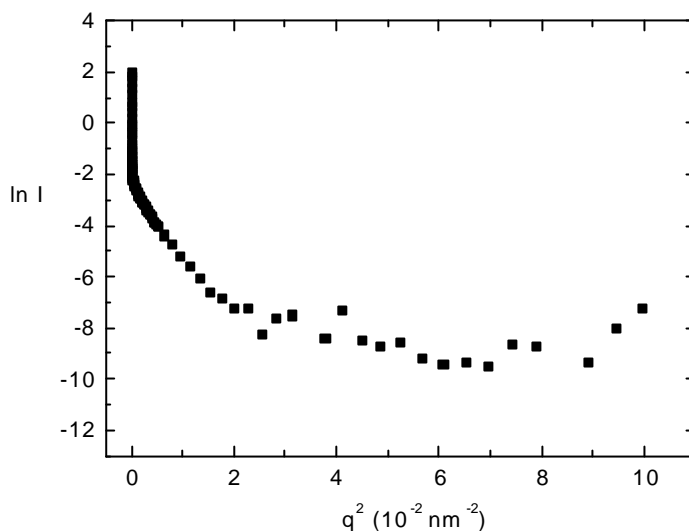
Fig.157: Guinier plot for the sample I65MeBr 0.34g/l
(8.717 10^{-6} M) in 1.165 10^{-4} M G1 aq at the charge
ratio I65MeBr/G1= 1/2. The sample name is M034.
The sample is opalescent and contains 1 ionene
molecule per 14 dendrimer molecules.
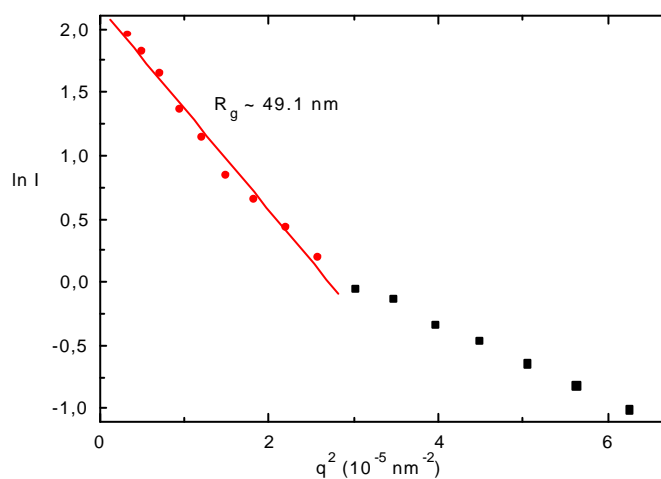
Fig.158: Guinier plot, R_g determination for I65MeBr
0.34 g/l (8.717 10^{-6} M) in 1.165 10^{-4} M G1 aq
The charge ratio I65MeBr/G1 = 1/2. The sample name is
M034. The sample condition is opalescent and per 1
ionene molecule 14 dendrimer molecules is present
in the solution.

The $R_g = 49.1$ nm was calculated from the Guinier plot (Fig.158). Initial slope of Guinier plot was taken into account. $R_g/R_h = 49.1/131 = 0.375$. Such value characterizes microgel-like condition, which was already discussed for the ionene/PAMAM case. According to experiment of Burchard et.al. $R_g/R_h = 0.3$ to 0.6 for a microgel.[123-125]

For the case where 0.75g/l ($1.897 \ 10^{-5}$ M) I65MeBr is mixed with $1.165 \ 10^{-4}$ M G1 aqueous solution and the salt concentration in the system equals $6.8 \ 10^{-4}$ M KBr the charge ratio of compounds is I65MeBr/G1 = 1.09. Sample name is M037 and the sample is opalescent. The system contains 1 ionene molecule per 7 dendrimer molecules (Fig.159). In this case the R_g calculation was not so obvious. The Zimm plot is linear, but the Gunier does not show any linearity. A final calculation concerning R_g and R_g/R_h is additionally hindered by the presence of two modes when DLS analysis has been performed. Only slight indication of the upturn in the initial part of the scattering curve is observed. In case of the PE-effect, the upturn in the initial part of the scattering curve would be much stronger.
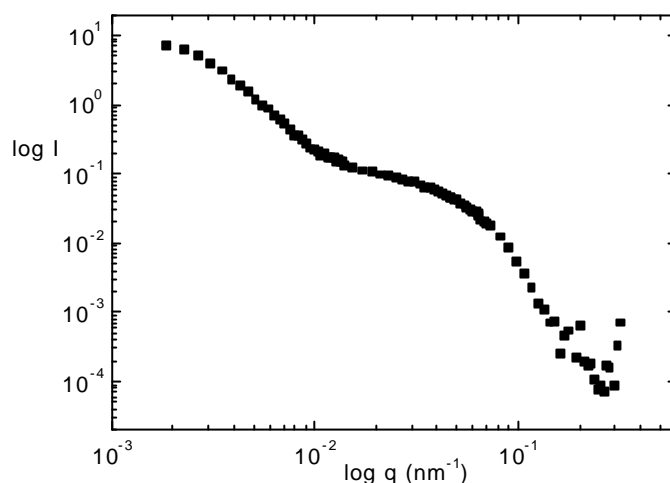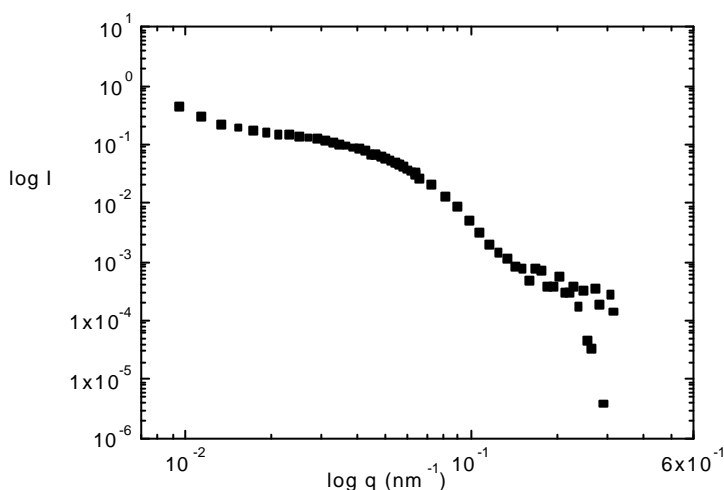

Fig.159: Scattering curve for the sample I65MeBr

0.75g/l ($1.897 \ 10^{-5}$ M) in $1.165 \ 10^{-4}$ M G1 aq. The charge

ratio I65MeBr/G1 = 1.09/1 and the sample name is M023.

The sample is opalescent and 1 ionene molecule per

7 dendrimer molecules is present in the solution.

In the case of the sample M023 one can suppose two different sized species present in the solution. A kind of microgel-like condition indicated via big differences between R_g and R_h and R_g/R_h ratio has been found for those sample. The R_g ranges from 4 to 50 nm and and R_h ranges from 100 to 150 nm. The interpretation of such sample behavior is difficult due to complications in DLS (two diffusion modes). The sample without salt addition are clear or slightly opalescent, after salt addition become opalescent, even with very small visible flocks, salting out occurs.

2.1. SANS measurement for I65/G1 with salt systems- summary

Table 20 below presents data calculated for different I65/G1 systems with and without salt addition.

Tab.20: Parameters calculated for the I65/G1 system without and with low molecular mass addition.

I65/G1 without salt				I65/G1 with salt			
Charge ratio	Rh,nm /DLS	Rg,nm/SANS	Rg/Rh	Charge ratio	Rh,nm /DLS	Rg,nm /SANS	Rg/Rh
0.5	75.3	57.2	0.759	0.769	132	49.1	0.38
1.09	60.2	69.9	1.16	1.2	two diffusion modes/difficult analysis		
2.26	two diffusion modes/difficult analysis			2.25	two diffusion modes/difficult analysis		

Structures of well defined shape i.e. hard spheres or stars are found for the systems without salt addition (see paragraph 2.b.1). Electrostatic interactions between charged objects in the system are partially screened after low molecular mass salt addition. Microgel like structures can appear. Fig.160 sketch possible structures.

AFTER SALT ADDITION

A.

B.
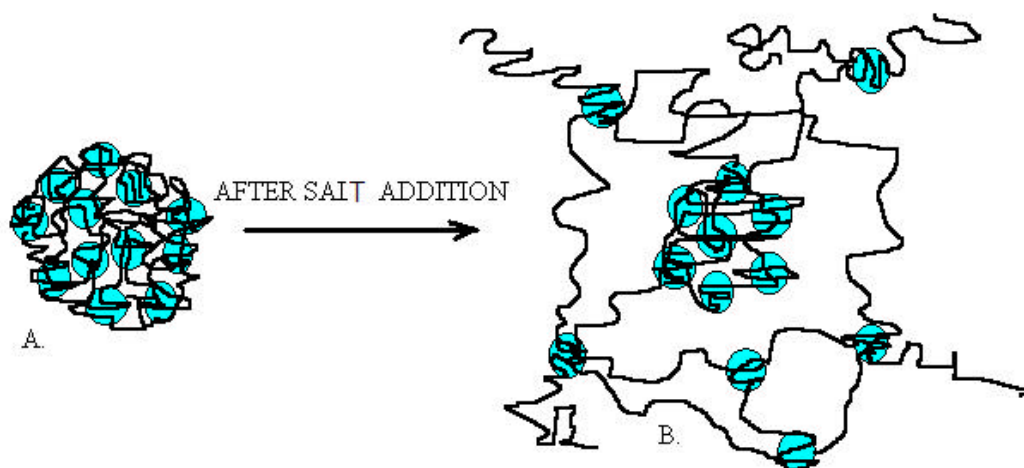
Fig.160: Sketch of the structures presented in the I65/G1 system after salt addition.

A possible explanation for the phenomenon observed in Fig.160 will be discussed here. In the case of the sample where without salt hard sphere-like objects were observed (Fig.160A) addition of salt causes loosing of the persistence of the spherical shape. The interactions between ionene molecules wrapped on the dendrimer core and this core are screened. Parts of single ionene chains stretch from the core (B).

When ionene chain are attached and already extended on the dendrimer core (star-like objects before salt addition), an addition of salt causes also a screening of the electrostatic interactions. The repulsion forces between ionene molecules and attraction forces between ionene and the dendrimer molecule are screened. The shape persistent, star-like assemblies are not observed any more. Like in the previously hard sphere-like assemblies case, parts of the single ionene molecules stretch from the assembly core. The behavior becomes more complicated due to the interactions between stretched assemblies. The influence of the salt may be a reason of the complexes destruction. The larger objects divide in smaller ones giving rise to the faster diffusion mode. However, opalescence of the samples after salt addition suggest an appearance of rather larger than smaller structures. The fast diffusion mode after salt addition can be also caused by

the movement of a part of larger core-shell assemblies. The whole assembly structures itself may cause the slow mode. However more than one mode samples are difficult for the analysis.

3. Time dependent behavior of salt containing samples. Light scattering study

Samples without salt addition in case of I65MeBr complexes with G1 remain of the same radii even after longer time (weeks). This observation is supported by the DLS measurement for selected samples. It is now of interest to measure time dependency of the systems containing low molecular mass salt addition. In order to find out how addition of salt influences equilibrium and structure stability, the following samples were investigated time dependently:

- 0.462g/l ($1.18 \cdot 10^{-5}$ M) I65MeBr in $1.056 \cdot 10^{-4}$ M G1 aq with $6.8 \cdot 10^{-4}$ M KBr addition. The charge ratio of I65MeBr/G1 = 1/1.3. The sample is slightly opalescent after salt addition. 1 ionene molecule per 9 dendrimer molecules is present in the solution.
- 0.74g/l ($1.89 \cdot 10^{-5}$ M) I65MeBr in $1.056 \cdot 10^{-4}$ M G1 aq with $6.8 \cdot 10^{-4}$ M KBr addition. The charge ratio I65MeBr/G1 = 1.2/1 and the sample is opalescent. Per 1 ionene molecule 6 dendrimer molecules is present in the system.

The sample have been investigated by means of DLS 24 h after mixing and again, two weeks after primal sample preparation.

In the early stage, after sample preparation and salt addition, two diffusion modes were observed. In both cases however, after two weeks, one diffusion mode has been found. The hydrodynamic radii measured were: 224.6 nm (for 0.462 g/l I65MeBr sample) and 447.6 nm (for 0.74g/l I65MeBr sample). The radius of gyration values calculated according to the again appropriate Guinier plot are: R_g= 180.66 nm (for 0.462 g/l I65MeBr sample) and R_g= 377 nm (for 0.74g/l I65MeBr sample). Zimm plot like in the case of SANS data indicates spherical structure. The σ coefficient values in both cases indicate homogenous hard sphere like structures: σ (for 0.462 g/l I65MeBr sample) equal 0.8 and σ (for 0.462 g/l I65MeBr sample) equal 0.789. (Literature value of σ coefficient for homogenous hard sphere: 0.778).

Conclusion based on the results of both, direct and after-two-weeks-measurements is that the structures of stable shape occur in the system with low molecular weight salt addition after longer time. Additional aggregation is expected after longer waiting time in the samples with salt addition. The microgel-like structure observed right after mixing and salt addition seems to be an "intermediate" structure before renewal formation of spherical objects occurs. Aggregates measured after two weeks are larger than those measured direct after sample preparation.

IV.I.C. Comments to the I65/G1 system analysis

Ionene chains and globular dendrimer molecules in the solution form spherical structures that are homogenous (hard) sphere-like. Up to a molecular ratio of I65MeBr to G1 of about 1/7 these are well defined. Only one kind of self-assembly species is present for the samples without salt addition. These self-assembly structures are characterized by a size of about 60-100 nm. Addition of low molecular weight salt induces self-assemblies that are similar in hydrodynamic radii as the ones appearing in without-salt system for the immediately measured samples. After 2 weeks, structures appearing in the system with salt are much larger than observed earlier. Salt-containing samples change with time leading through microgel-like phase 24 h after salt addition to the recombination into bigger complex structures ($R_h \sim$ 200-500 nm; $R_g \sim$ 180-400 nm) two weeks after salt addition. The microgel-like condition is supposed to be a transitional state in the case of samples with salt during the time when equilibrium is not yet reached. The process is understandable since screening with low-molecular mass salt decreases repulsive interaction of like-charged aggregates and supports aggregation. For higher concentrations of I65MeBr salting

out effect is observed, i.e. even macroscopic precipitation occurs as a result of secondary aggregation. Thus the addition of salt initially does not change the behavior. This indicates that the diffusion modes observed without salt correspond to "real particles" rather than polyelectrolyte (PE)-diffusion. PE-diffusion would disappear upon addition of salt when concentration of polyelectrolyte charges is equal monovalent salt concentration. Although we do not know the charges of particle aggregates, we can estimate that in our case the salt concentration is higher than the concentration of particle aggregate charges. For a salt concentration higher than $6.8 \ 10^{-4}$ M salting out effect occurs even when lower concentrated I65/G1 samples are investigated. The concentration of $6.8 \ 10^{-4}$ M was the highest salt concentration possible. This concentration is 5 times lower than the highest initial concentration of polyelectrolyte charges in the system. However assuming an aggregation process and neutralization of charges between oppositely charged ionene and the dendrimer, we can estimate that the $6.8 \ 10^{-4}$ M KBr should be sufficient to screen rest "free" charges in the system. Results also confirm that R_g –values previously obtained from SANS data (chapter 2.1 in IV.I.A and 2 in IV.I.B) are "real" R_g–values of particles present in the solution and not influenced by interaction effects. With time the assemblies present in the solution further aggregate or even precipitate when low-molecular mass salt is present in the solution. This indicates that in this case assemblies are stable as hierarchical units like classical colloids and can be "salted out".

V. Conclusion

Under certain conditions, i.e. charge ratio of ionene to the dendrimer, charge density of ionene and dendrimer also concentration of sample, the ionenes and dendrimers build complexes in solution. An appearance of such complexes in seen first "by eye": The sample becomes opalescent or even turbid after mixing ionene and dendrimer solution. Then, by dynamic light scattering measurement an agreement between the appearance of turbid samples and one diffusion mode samples is observed. Opalescent samples contain aggregates which give one diffusion mode in light scattering experiments. These aggregate species are well defined in terms of shape and mass, i.e. number of building elements involved. Based on further experiments (SLS, SANS, ξ-potential measurements) we analyzed the shape of such assembly structures as spherical of the Rh between 80 and 150 nm. In case of I65/G1 systems, objects found may have persistent shapes e.g. hard sphere-like or hairy spheres. Ionenes when complexed with PAMAM dendrimers create core-shell structures. The difference (Fig.161a, 161b) between a morphology of ionene/PAMAM and ionene/poly(phenylene) dendrimers complexes is caused by the dendrimer molecules. PAMAM dendrimers are flexible as compared to the poly(phenylene) dendrimers containing aromatic rings. This stiffness must be a reason for the formation of shape persistent, more globular, more homogeneously dense assemblies. Besides poly(phenylene) dendrimer molecules themselves tend to aggregate even at high ionic strength. They are able to build densely packed core connected by the ionene molecules. Ionene chain molecules can also wrap around these densely packed dendrimer conglomerate. Sometimes "hair-like" ionene molecules stretch from this stiff core. Compare with Fig.161a D.

The geometric charge density of G1 is the lowest as compared to the PAMAM dendrimers. An apparent surface area of the G1-sphere has been calculated based on the hydrodynamic radius equal 4 nm from the computer simulation. We expect a high dissociation degree due to the low surface charge density of the G1. The core-shell structures appear in the ionene/G1 systems upon higher ionic strength (after low molecular mass salt addition).
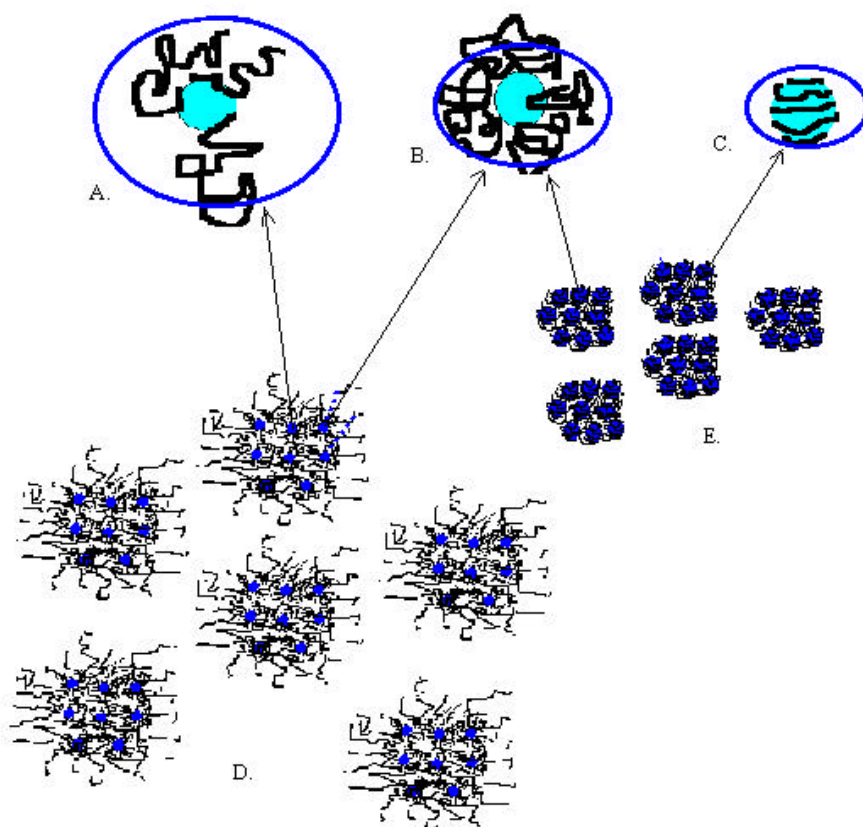
Fig.161a: Ionene with G1 dendrimers, schematic
picture of the self-assembly objects (D,E) and
enlargement of subunits(A,B,C).

In Fig.161a posible morphology of the I65/G1 assemblies is presented. The hard sphere and star-like units (D,E) may be build from the blocks sketched (A,B,C). Note, that this is a schematic representation of the kind of structure that is not quantitatively exact.

In the case of ionene/PAMAM dendrimers, core-shell structures appear after mixing the samples and even without the small molecular mass salt addition as sketched in Fig.161b. It indicates that the attractive interactions between the building blocks in these systems are weaker than those for ionene/G1 complexes i.e. electrostatic repulsion between primary aggregates is larger. Addition of the low molecular mass salt to the ionene/PAMAM dendrimer system indicates that two diffusion mode samples contain different two sizes of aggregates. On the diffusion profile for higher concentrated ionene/PAMAM dendrimer systems two transition regimes were found, always around $\lambda_{\text{splitting}} = 1$. For lower concentrated samples of ionene and PAMAM dendrimers and for I65/G1 only one transition regime is present at $\lambda_{\text{splitting}} = 1$. The fast mode is "faster" than the diffusion in one mode range. The slow mode does not change as compared to the regime of one mode. This is not typical for normal polyelectrolytes, where the slow mode is slower than the mode in the single diffusion range. Sometimes a peak appears in the fast mode as a function of ionene concentration after the splitting point. This is also not usual for the normal polyelectrolytes and (as we discussed in chapter 3 concerning scattering techniques) occurs due to the diffusion of not complexed ionene molecules.

The reason for the two modes in the ionene/PAMAM dendrimer systems are generally two different species of aggregates. Only in the concentration range where the peak in the fast mode appears, aggregates are accompanied by single ionene molecules in the solution, which cause the fast diffusion mode. Addition of salt does not remove the two modes effect from the solution. However, based on the ξ-potential measurements charged aggregates have been found which may give rise to the PE-effect and interaction as well. By-and-by the assemblies present in the solution secondary aggregate and eventually even precipitate when low-molecular mass salt is added. This confirms assemblies to be hierarchically stable moieties which can be salted out similar to classical colloids. Salting out requires less amount of salt in case of I65/G1 than in case of ionene PAMAM dendrimer complexes. This can be due to the smaller number of charges present in the system of I65/G1 as compared to the systems with PAMAM dendrimers, e.g. I65 possesses 322 charges per chain and G1 48 charges per molecule, whereas G7.5 has 1024 charges per single molecule.
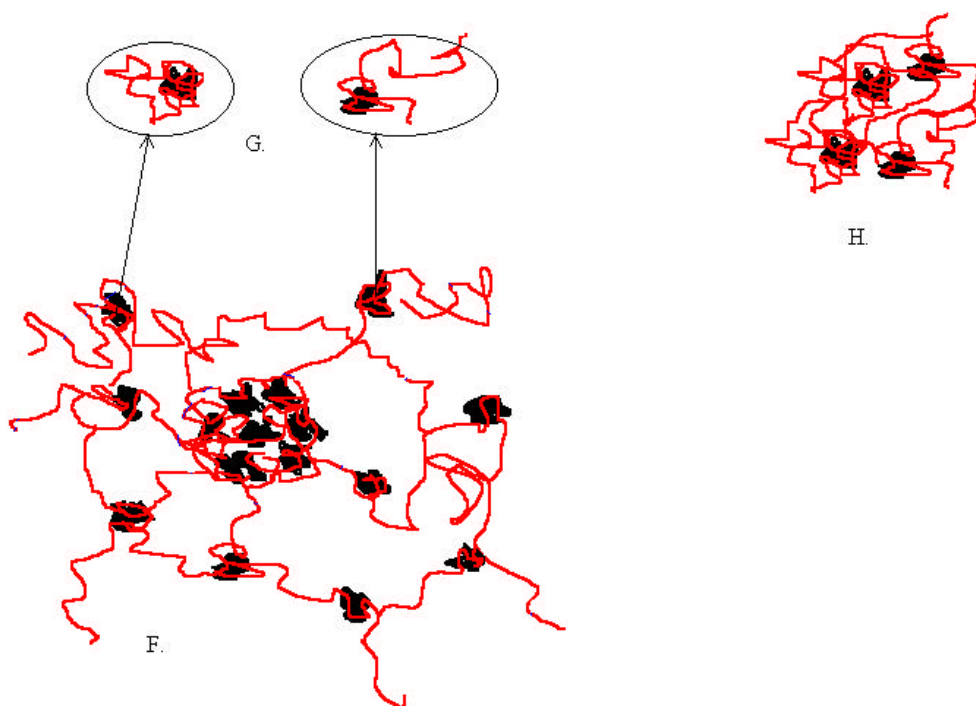
Fig.161b: Ionene with PAMAMdendrimers, schematic picture of the self-assembly objects. Core-shell structure (F) and a "zoom" of subunits (G). H shows the middle-size aggregate.

Fig.161b shows possible structures of the ionene/PAMAM dendrimer complexes (F, H). F is the core shell-structure typical for this system. H presents "middle-size aggregates" (oligoaggregates) which coexist in the system with large aggregates, and potentially with single macromolecules. The middle-size assemblies may cause the fast mode in the ionene/PAMAM diffusion behavior. Also the morphology of the single building blocks (ionene linear chains attached to the dendrimer molecule) is presented (G). Structures in Fig.161b are again a schematic representation of the kind of structure and the dendrimer/ionene ratio varies over the range of investigated charge ratio (see Tab.9).

The PAMAM complexes are influenced by the charge density of the linear compound, surface charge potential of the dendrimer, charge ratio of the compounds and their concentration. A

parameter expression describing the diffusion properties of ionene/PAMAM dendrimer complexes has been proposed.

As mentioned in the theoretical part (subchapter 5), the binding of a polyelectrolyte to the spherical particle is strictly dependent on the CAC (critical aggregation concentration) value. These findings have been described based on a computer simulation by Wallin and Linse.[78,79] In the case of the ionenes/dendrimers systems investigated here in contrast no CAC is observed in the investigated concentration range. Aggregates are always present. However, a characteristic concentration dependence of coexisting species is found. The appearance of one diffusion mode (well defined aggregates) during the DLS experiment is concentration dependent (compare paragraph III.I.A.3): for lower concentrated systems one diffusion mode is observed at low ionene concentrations, whereas for higher concentrated samples in the same ionene concentrations range two diffusion modes have been found. Additionally from the Wallin's and Lind's computer simulation one can see an influence of the flexibility of the polymer chain on the assembly formation. The more flexible the chain, the easier an assembly can be formed. We have not found any confirmation in the Imn/Gx.y systems. The I25 are densely charged and that is why stiffer. The densely packed positive charges on the chain repel and cause local rigidity. However, the I25 possesses similar complex formation ability like the I65. The length of a binding site on the polyelectrolyte chain is strongly influenced by the chain stiffness. The binding site length is comparable with the persistence length of the polymer chain. H. Zhand et. al.[72] observed that complexation occurs when the relative size of the polymer binding segment is comparable with the radius of the macroion. This hypothesis is also not in agreement with our observation. The complexation occurs even when the random coil of polyelectrolyte possesses a radius comparable with that of the macroion (dendrimer).

Odjik and Scheutjens[65,66] predicted the transition corresponding to the appearance of a bound state at some critical surface charge density or critical surface potential. The binding is only possible, if the charge density of the macroion is sufficient to overcome the elastic resistance stored in the polymer chain. The system of I65/G7.5 investigated by the potentiometric titration gave here similar results. The critical surface potential of the dendrimer molecule caused to attach an ionene molecule. Accordingly, different behavior of I25 and I65 may be ascribed to their difference in charge density. The difference is most obvious in complexes with PAMAM G2.5 where for I25 the usual two mode-one mode-two mode behavior is observed while the I65/G2.5 shows no one mode range. This could be due to the fact that the charge densities of I25 and G2.5 are comparable so that formation of aggregates by "complete" complexation becomes possible. No additional small species are present in the one mode range. Such complexation might not be possible that perfectly for the I65/G2.5 system.

Caminati et. al.[75] postulated a noncooperative nature of the linear polyelectrolyte binding to the charged dendrimer of lower generation. According to this study, the higher generations bind linear polyelectrolytes cooperatively. Caminati supports his theory by the morphology change between lower and higher dendrimer generations. The lower generations characterize "opened" morphologies, whereas the higher generations are more spherical. This hypothesis stays in an agreement with our findings. We also have found spherical shapes for G5.5 and G7.5, what means for the higher, compact generations of dendrimers. The G2.5 generation is, according to our study much more loose, rather entangled than compact.

Jonsson and Linse[80] discovered, based on computer simulations, that a relatively small, single macroion prefers to be complexed to the inner site of a large linear polyelectrolyte.

We postulate that the complexes between ionene and dendrimers one can regard as huge "polyelectrolytes". Since they are charged, they may also be described by some features of usual polyelectrolytes. In case of ionene/dendrimer aggregates the tendency discovered by Jonsson and

Linse is in analogy to the core-shell structure of our aggregates that are however much more complicated structures. Size discrepancies between relatively small ("calculable") objects used in computer simulation and large objects existing in real systems might be a reason for not direct overlapping of calculation and observation. Although our experimental observation is in accordance with Jonsson and Linse's simulations, i.e. in both cases a denser, more complexed "core" is surrounded by a looser, less complexed "shell", the explanation of this phenomenon is still open. In this context it might be useful to regard the association of a positively charge of ionene with a negatively charged group of the dendrimer as "charge neutralization". When larger aggregates form, it is likely that charges in the inside are neutralized first, leaving charge on the surface, such as in a Faraday-cage. This point of view is in accordance with the fact that around ionene/dendrimer charge ratio of 1 aggregates formed are found to be still positively charged. The ionene is always completely ionized, while the dendrimer is not totally dissociated, i.e. positive charge remain. These will preferably be located in the outer parts of the complexes. Assuming that a more complete association of charged groups causes a denser aggregated structure this may be the origin for the core-shell structure with a denser core. If the core strongly attracts macromolecules on its surface the hard sphere-like assembly arises. If the interaction between core and surface macromolecules is not so strong, star like aggregates can appear. Eventually, when the core attraction is very weak, directly microgel-like, entangled structures can be formed. The described structure of the aggregates being charged and/or having a "hairy" surface may also be responsible for their stability, i.e. their restricted growth and defined size in solution, in analogy to common colloid stabilization. However, a complete description of the complex system here is expected to be more complicated.

Not only the electrostatic interactions are responsible for the complex formation. Also the hydrophobic cluster formation, like in the case of micelle formation (mentioned in paragraph 5 in the theoretical part) may be a reason for the assembly growing,[71] especially for I65, where the hydrophobic regions are longer than those of I25. Results here seem to indicate that the difference in charge density rather than hydrophobicity plays the major role in causing slight quantitative differences between the ionenes, as described above. However, the hydrophobic/hydrophilic properties of the ionenes have not been our main focus here. A study of the ionene complex formation in different solvents might be of future interest.

V.I. Summary

New polyelectrolyte systems composed of ionenes and dendrimers have been investigated.

System compounds are typical polyelectrolytes, but structures which they build behave not the way typical polyelectrolytes do. In a one diffusion mode regime aggregates of about 100 nm hydrodynamic radius have been found. Such aggregates are core-shell or anisotropic core shell structures in the case of ionenes/PAMAM dendrimers complexes. These complexes are stable even at high ionic strength. In case of ionenes with poly(phenylene) dendrimers, hard sphere-like objects or spherical objects with hairy-like surface have been found in a one diffusion mode regime. Their stability at high ionic strength is lower. For the ionenes/poly(phenylene) dendrimers systems one transition point has been found from one to two diffusion processes, towards increasing ionene concentration, i.e. for the samples with fixed dendrimer concentration towards increasing ionic strength. For the diffusion profile of ionene/PAMAM dendrimers in most cases two transition regimes are observed. One at very low ionene concentration, the second one at high ionene concentrations, which again means for the samples with fixed dendrimer concentration, also at higher ionic strength. Both two mode regimes are separated by the one

mode regime. As confirmed experimentally, the one diffusion mode regime is caused by the motion of well defined assemblies. The two diffusion mode regimes are caused by the movement of different sized species in solution, large aggregates and middle-size aggregates (oligoaggregates). The location and also the number of transition points in the diffusion profiles is dependent on the ionene to dendrimer charge ratio, charge density of the compounds and concentration. No influence of the molecular mass of the ionene has been found. The aggregates are found to be charged on the surface; however, this surface charge does not significantly influence the diffusion properties of the system.

VI. Appendix
1.Synthesis and preparation techniques
Synthesis of ionene I65 and I25 via polycondensationreaction. 6,605g (0,0384 Mol) 1,6-Bis(Dimethylamine)Hexane and 8,7381g (0,038Mol) 1,5-Dibromopentane was solved in 38 ml (1:1) DMF:MeOH mixture. Reaction runs 4 days at room temperature under stirring. After 4 days polymer falls from the solution Polymer was precipitated in aceton and then cleaned by dissolving water and precipitating again in aceton (3x ca. 50-70 ml of aceton was used for every step). Finally aceton was evaporated in rotary evaporator. Polymer was dried 5 days in 50°C under vaccum. For I25MeBr synthesis only amount of the amine changes 0.0384M (4,45g) N,N,N',N'-Tetramethyl-ethylene diamine has been used. Rest of the procedure stays the same.

2.Complexation techniques
Compelxes were prepared 24h before the UV- and pH measurements. DLS was measure not later than 50h after mixing of the compounds.

For the pH, UV and LLS measurements 2 ml of samples were prepared. The ξ-potential measurement requires at least 4 ml volume of the sample.

Stock solutions of ionenes and dendrimers were prepared. Appropriate amounts of which were mixed and eventually filled up with mq water to the required volume. During first 24h after mixing of the compounds samples were stirred on a magnet-stirrer.

Before LLS measurements sample were filtered up (3 times, 45 μm filter pore size).

3.Description of equipment used
1. Laser Light Scattering Static and Dynamic(SLS, DLS) Equipment: ALV 5000-Korrelator, ALV-SP81-Goniometer Krypton-Ion-Laser was used of 647,1 nm wavelength with Avalanche Photodiode Module. Samples were filtrated before scattering measurement using 45 μm pore size filters. Every time around 1.5 ml of the solution was placed in the $\varnothing$10 mm couvets. The measurements was carried at room temperature. Refractive index increment was measured by Michelson scanning interferometer. All measurements were done at MPI-P in Mainz.

2. SANS measurements were done in Grenoble in Institut Laue-Langevin, D11 instrument. D11 is the archetype of a long, pinhole geometry instrument for small-angle neutron scattering (SANS), designed for the study of large scale structures in chemistry, biology and solid state physics. Possible incident wavelength range from $4.5 < [Å] < 40$. It is possible to measure at the guide-to-sample distances 1.5...40.5 m (12 possible distances). Additional collimation distance equals 1.5m, 28m, 34m. Detector type used 3He gas detector (CERCA).

The SANS scattering curve presented shows data after solvent and incoherent background (Porod slope of (-4)) correction.

We were able to measure SANS samples of I65/PAMAM up to the sample detector distance of 5.5 m. Covered scattering vector range was from around q_{min}= 0.01 [1/A°] to q_{max}= 0.3 [1/A°]. The maximal and minimal measurable objects diameter calculated based on the information of q_{min} and q_{max} is D_{max}= 63 nm and D_{min}= 2.1 nm respectively. Where

$$D_{min} = \frac{2\boldsymbol{p}}{q_{max}}, \quad D_{max} = \frac{2\boldsymbol{p}}{q_{min}}.$$ Only for three sample (M021; M040; M043) - see Tab.14 the

scattering intensity was sufficient to measure for the longest distance 26 m. Only in this case the intensity was high enough to collect the valuable data. Then maximal measurable diameter D_{max}= 314 nm.

3. For the GPC measurements PSS Suprema Max 8/300 mm column was used. As a solution for the ionene systems 9 g/l water solution of Ammoniumformiat and as a standard Pullalan has been selected.

VII. Literature

1. An interview with Professor Gero Decher, Science (1997), 277, 29 August, 1232-7

2. David S. Lawrence, Tao Jiang, Michael Levett, Chem. Rev. (1995), 95, 2229-2260

3. J.Kötz, S.Kosmella, T.Beitz, Prog. Polym. Sci, (2001), 26, 1199-1232

4. JM Lehn, Reports on progress in physics, (2004), 67, 3, 249-265

5. A.F.Thünemann, M.Müller, H.Dautzenberg, J-F. Joanny, H.Löwen, Adv. Polym. Sci. (2004), 166, 113-171

6. E.Nordmeier, Macromol. Chem. Phys. (1995) 196, 1321-13747.

7. G.S.Manning, Q. Rev. Biophys. (1978), 11, 179

8. M.Le Bret, B.H. Zimm, Biopolymers (1984), 23, 287

9. M.Le Bret, B.H. Zimm, Biopolymers (1984), 23, 271

10. M.Olmsted, C.F.Anderson, M.T.Record, Proc. Natl. Acad. Sci. U. S. A. (1989), 86, 7766

11. D.E. Draper, Biophys. Chem, (1985), 21, 91

12. R.J.Hunter, Foundations of Colloid Science; second edition; Oxford University Press 2001

13. H.Kawabe, H.Gregor, J. Colloid Interface Sci. (1966), 21, 79

14. C.G.Sinn, R.Dimova, M.Antonietti, Macromolecules (2004), 37, 3444-3450

15. S.Paula, W.Süs, J.Tuchtenhagen, A.Blume, J.Phys.Chem, (1995), 99, 11742-11751

16. C.Tanford, The hydrophobic effect: formation of Micelles in Biological Membranes, 2nd ed.; Willey: NY, (1980)

17. N.T.Southall, K.A.Dill, A.D.J.Haymet, J.Phys.Chem. B, (2002), 106, 521-533

18. I.Pochard, P.Couchot, A.Foissy, Colloid Polym. Sci. (1999), 277, 818-826

19. S.Lagerge, A.Kamyshny, S.Magdassi, S.Partyka, J.Therm.Anal.Calorim. (2003), 71, 291-310

20. J.Klos, T.Pakula, J. Chem. Phys., (2004), 120, 5, 2496-2501

21. J.Klos, T.Pakula, J. Chem. Phys., (2004), 120, 5, 2502-2506

22. B.Philipp, W.Dawydoff, K.J.Linow, Zeitschrift für Chemie, (1982), 22, 1

23. Herbert Dautzenberg, Natalia Karibyants, Macromol. Chem. Phys., (1999), 200, 118-125

24. Herbert Dautzenberg, Macromol. Symp. (2000), 162, 1-21

25. N.Carybiantis, H.Dautzenberg, H.Cölfen, Macromolecules, (1997), 307, 803

26. B.Philip, H.Dautzenberg, K.J.Linov, J.Koetz, W.Dawydoff, Progr. Polym. Sci., (1989), 14, 91

27. A.B.Zezin, V.A.Kabanov, Usp Khim, (1982), 51, 1447

28. V.A.Kabanov, A.B.Zezin, Pure Appl. Chem., (1984,)56, 343

29. V.A.Kabanov (1994) In: P.Dubin, J.Bock, R.M.Davies, D.N.Schulz, C.Thies (eds) Macromolecular Complexes in Chemistry and Biology. Springer Verlag, Berlin Heidelberg, New York, p 151

30. E.Tsuchida, Y.Osada, K.Sanada, J. Polym. Sci. A (1972), 10, 3397

31. E.Tsuchida, Y.Osada, H.Ohno, J. Macromol. Sci. B (1980), 17, 683

32. E.Tsuchida, K.Abe, Adv. Polym. Sci. (1982), 45, 1

33. V.A.Izmurudow, O.A.Kharenko, A.V.Kharenko, Z.G.Gulewa, V.A.Kasaikin, A.B.Zezin, V.A.Kabanov, Vysokomol. Soedin., (1980), 22, 692

34. D.V.Pergushov, V.A.Izmurudow, A.B.Zezin, V.A.Kabanov, J. Polym. Sci. A, (1993) 35, 844

35. K.N.Bakeev, V.A.Izmurudow, S.I.Kuchanov, A.B.Zezin, V.A.Kabanov, Doklad. Akad. Nauk SSSR, (1988), 300, 132

36. V.A.Izmurudow, T.K.Bronich, O.S.Saburowa, A.B.Zezin, V.A.Kabanov, Macromol. Chem. Rapd Comm., (1988), 9, 7

37. H.Dautzenberg, G.Rother, J.Hartmann (1994) In: K.S.Schmitz (ed), Macro-ion Characterization from Dilute Solution to Complex Fluids. ACS Symposium Series 548 ACS, Washington DC p 219

38. H.Dautzenberg, J.Hartmann, S.Grunewald, F.Brand, Ber Bunsen-Gessel, Conference Peoceedings of "Polyelectrolytes Potsdam' 95" (1995), 100, 1024

39. B.Phillip, H.Dautzenberg, K.J.Linow, J.Kötz, W.Dawydoff, Prog. Polym. Sci., (1989), 14, 91

40. H.Dautzenberg, J.Kötz, K.J.Linow, B.Phillip, G.Rother, (1994), In: P.Dubin, J.Bock, R.M.Davies, D.N.Schulz, C.Thies (eds), Macromolecular Complexes in Chemistry and Biology, Springer, Berlin Heidelberg New York, p 119

41. H.Dautzenberg, Ho Dautzenberg, Acta Polymerica, (1988), 36, 102

42. H.Dautzenberg, Macromolecules, (1997), 30, 7810

43. H.Dautzenberg, N.Karybiantis, (1999) In: I.Noda, E.Kokufuta, (eds), Proceeding of the 50th Yamada Conference and Second International Symposium on Polyelectrolytes, Inuyama, Japan, Yamada Science Foundation, Osaka, p284

44. H.Dautzenberg, N.Karybiantis, Macromol. Chem. Phys., (1999), 200, 118

45. N.Karybiantis, H.Dautzenberg, Langmuir, (1998), 14, 4427

46. *Y.Hayashi, M.Ullner, P.Linse, (2002), J. Chem. Phys., 116, 15, 6836-6845*

47. *G.A.Christos, S.L.Carnie, Chem. Phys. Lett. (1990), 172, 249*

48. *J.Stevens, K.Kremer, Phys. Rev. Lett. (1993), 71, 2228*

49. *J.Stevens, K.Kremer, Macromolecules, (1993), 26, 4717*

50. *J.Stevens, K.Kremer, J. Chem. Phys. (1995), 103, 1669*

51. *J.Stevens, K.Kremer, J. Phys. II (1996), 6, 1607*

52. *J.P.Valleau, J. Chem. Phys. (1989), 129, 163*

53. *G.A.Christos, S.L.Carnie, J. Chem. Phys. (1990), 92, 7661*

54. *C.E.Woodward, B.Jönssen, J. Chem. Phys. (1991), 155, 207*

55. *M.Ullner, C.E.Woodward, Macromolecules (2000), 33, 7144*

56. *H.Löwen, E.Allahyarow, C.N.Lykos, R.Blaak, J.Dzubiella, A.Jusufi, N.Hoffmann and H.M.Harreis, J. Phys. A : Math. Gen, (2003), 36, 5827-5834*

57. *D.S.Lawrenve,Tao Jiang, Michael Levett, Chem. Rev., (1995), 95, 2229-2260*

58. *H.Zhang, P.L.Dubin, J.Kaplan, C.N.Moorfield, G.R.Newkome, J. Phys. Chem., (1997) 101, 3494*

59. *M.Smoluchowski, Bull. Acad. Sci. Cracovie, Classe Sci. Math. Natur., (1903), 1, 182*

60. *Q.R.Huang, P.L.Dubin, C.N.Moorefield, and G.R.Newkome, J. Phys. Chem. B, (2000), 104, 898-904*

61. *E.Gonzales-Tovar, M.Lozada-Cassou, J. Phys. Chem., (1989), 93, 3761*

62. *L.Degreve, M.Lozada-Cassou, Mol. Phys., (1995), 86, 759*

63. *F.W.J.Wigiel, J. Phys A: Math. Gen (1977), 10, 299*

64. *M.Muthukumar, J. Chem. Phys., (1987), 86, 7230*

65. *O.A.Evers, G.J.Fleer, J.M.H.M.Scheutjens, J.Lyklema, J. Colloid Interface Sci., (1986), 11, 446*

66. *T.Odijk, Macromolecules, (1980), 13, 1542*

67. *P.L.Dubin, S.S.The, D.W.McQuigg, C.H.Chew, L.M.Gan, Langmuir, (1989), 5, 89*

68. *D.W.McQuigg, J.I.Kaplan, P.L.Dubin, J. Phys. Chem. (1992), 96, 1972*

69. *P.L.Dubin, M.E.Curran, J.D.Hua, Langmuir, (1990), 6, 707*

70. *H.Zhang, P.L.Dubin, R.Spindler, D.Tomalia, Ber. Bunsenges. Phys. Chem., (1996), 100, 923-928, No.6*

71. http://www.webster-dictionary.org

72. H.Zhand, P.L.Dubin, J.Ray, G.S.Manning, C.N.Moorefield, G.R.Newkome,

     J. Phys. Chem B, (1999), 103, 2347-2354

73. K.K.Kunze, R.R.Netz, Phys. Rev. Lett., (2000), 85, No.20, 4389-4392

74. T.D.Yager, C.T.McMurray, K.E. van Holde, Biochemistry, (1989), 28, 2271

75. G.Caminati, N.J.Turro, D.A.Tomalia, J. Am. Chem. Soc., (1990), 112, 8515

76. Y.Li, P.L.Dubin, Macromolecules, (1995), 28, 8426

77. N.Miura, P.L.Dubin, C.N.Moorefield, G.R.Newkome, Langmuir, (1999), 15, 4245-4250

78. T.Wallin, P.Linse, Langmuir, (1996), 12, 305-314

79. T.Wallin, P.Linse, J. Phys. Chem., (1996), 100, 17873-17880

80. M.Jonsson, P.Linse, J. Chem. Phys., (2001), 115, No.7, 3406-3418

81. D.A.Tomalia, and H.D.Durst, (1993) Genealogically directed synthesis: starburst/cascade dendrimers and hyperbranched structures. In Topics in Current Chemistry: Supramolecular Chemistry I – Directed Synthesis and Molecular Recognition (Vol. 165) (Weber, E., ed.), pp. 193–313, Springer-Verlag

82. G.R.Newkome, et al. (1996), Dendritic Molecules, VCH

83. A.W.Bosman, et al. About dendrimers: structure, physical properties and applications. Chem. Rev., (1999), 99, 1665–1688

84. D.A.Tomalia, and I.Majoros, (2000) Dendrimeric supramolecular and supramacromolecular assemblies. In Supramolecular Polymers (Ciferri, A., ed.), pp. 359–435, Marcel Dekker

85. M.Fischer, and F.Vögtle, (1999) Dendrimers: from design to application – a progress report. Angew. Chem., Int. Ed. Engl. 38, 884–905, 52

86. R.Esfand, and D.A.Tomalia, (2001), DDT. 6, 427–436

87. U.M.Wiesler, T.Weil, K.Müllen Topics in current chemistry Nanosized Polyphenylene Dendrimers, (2001), 212, 1-40

88. D.Casson, and A.Rembaum, Maromolecules, (1972), 5, 75-81,

89. A.Rembaum, W.Baumgartner, A.Eisenberg, Polymer Letters, (1968), 6, 159-171

90. H.Noguchi, A.Rembaum, Polymer Letters, (1969), 7, 383-394

91. J.Wang, W.H.Meyer, G.Wegner, On the polymerization of N,N,N',N'-tetramethyl-á,ù-alkanediamines with dibromoalkanes-an in-situ NMR study, (1994), Hüthig & Wepf Verlag, Basel

92. Atkins, *Physical Chemistry, 6th edition, (1998), New York, Freeman*

93. *J.Cohen, Z.Priel, and Y.Rabin, J. Chem. Phys., (1988), 88, 7111*

94. *E.A.Balazs and T.C.Laurent, J. Polym. Sci., (1951), 6, 633*

95. *D.Chen, X.Liu, Y.Zhou, X.Yang, L.Lu, X.Wang, J. Appl. Polym. Sci., (2000), Vol.76, 481-487*

96. *Y.Rabin, J.Cohen, Z.Priel, J. Pol. Sci. C, Polymer Letters, (1998), Vol.26, 397-399*

97. *M.Rinaudo, M.Milas, M.Joun, and R.Borsali, Polymer, (1993), 34, 17, 3710*

98. *H.Fujita and T.Homma, J. Colloid Sci., (1954), 9, 591*

99. *S.Basu, Nature, (1951), 168, 341*

100. *S.Basu, P.C. Dasgupta, and A.K.Sircar, J. Colloid Sci., (1950), 6, 539*

101. *R.M.Fuoss, and V.P.Strauss, J.Polymer Sci., (1948), 3, 602*

102. *D.F.Hodgson, and E.J.Amis, J. Chem. Phys., (1991), 94, 4581*

103. *J.Yamanaka, H.Matsuoka, H.Kitano, M.Hasegawa, and N.Ise, J. Am. Chem. Soc., (1990), 112, 587*

104. *Wayne F. Reed, J. Chem. Phys., (1994), 101, 2515*

105. *T.A.Witten, and P.Pincus, Europhys. Lett., (1987), 3, 315*

106. *H.H.Chuah, D.Lin-Vien, U.Soni, Polymer, (2001), 42, 7137-7139*

107. *Chen at all, J. Appl. Polym. Sci., (2000), 76, 481-487*

108. *P.Linder, Th.Zemb, "Neutrons, X-rays and Light: Scattering Methods Applied to Soft Condensed Matter" North-Holland Delta Series 2002.*

109. *H.Schnablegger, "Statische und Dynamische Lichtstreung", MPI für Kolloid- und Grenzlfächenforschung, Teltow; GDCh Fortbildungsprogramm Chemie, (1998)*

110. *P.Linder, Th.Zemb, Neutron, X-Ray and Light Scattering Introduction to an Investigative Tool for Colloidal and Polymer Systems, (1991), North Holland*

111.*W.Burchard, G.D.Patterson, Light Scattering From Polymers, (1983), Springer-Verlag, Berlin, Heidelberg, New York*

112. *A.Topp et al. Macromolecules, (1996), Vol.29, No.16, 5392-5397*

113. *M.Schmidt, Macromol. Chem. Rapid Commun., (1989), 10, 89-96*

114. *S.Förster, M.Schmidt, M.Antonietti, Polymer (1990), Vol.31, 781-792*

115. *S.Förster, M.Schmidt, M.Antonietti, J. Phys. Chem., (1992), 96, 4008-4014*

116. *F.Gröhn, A.Topp, L.Belkoura, D.Woermann, Ber. Bunsenges. Phys. Chem., (1995), 99, No.5, 736-740*

117. *A.Topp, L.Belkoura, D.Woermann, Ber. Bunsenges. Phys. Chem., (1995), 99, No.5, 730-735*

118. *L.H.Sperling, Introduction to Physical Polymer Science, 3rd edition, (2001), Wiley-Interscience, p. 101*

129. *M.Antonietti, A.Briel, S.Förster, J. Chem. Phys., (1996), 105, (17), 7795-7807*

120. *T.Odjik, Langmuir, (1991), Vol.7, no.10*

121. *M.Mende, G.Petzold, H-M.Buchhammer, Colloid Polymer. Sci., (2002), 280, 342-351*

122. *H.Zhang, P.L.Dubin, R.Spindler, D.Tomalia, Ber. Bunsenges. Phys. Chem., (1996), 100, No.6, 923-928.*

123. *M.Schmidt, D.Nerger, W.Burchard, Polymer, (1979), Vol.20, 582*

124. *W.Burchard, Adv. Polym. Sci., (1983), 4*

125. *W.Burchard, Adv. Polym. Sci., (1999), 143*

126. *P.K.Maiti, T.Ç aĝin, G.Wang, W.A.Goddard, Macromolecules, (2004), 37, 6236-62*

127. *P.C.Hiemenz, Principiels of colloid and surface chemistry, Marcel Dekker, Inc. New and Basel, (1986)*

128. *A.Topp, B.J.Bauer, D.A.Tomalia, E.J.Amis, Macromolecules, (1999), 32, 7232-7237*

129. *A.Topp, B.J.Bauer, J.W.Klimash, R.Spindler, D.A.Tomalia, E.J.Amis, Macromolecules, (1999), 32, 7226-7231*

130. *J.Li, L.T.Piehler, D.Qin, J.R.Baker, D.A.Tomalia, D.J.Meier, Langmuir, (2000), 16, 5613-5616*

131. *A.M.Naylor, W.A.Goddard, G.E.Keiffer, D.A.Tomalia, J. Am. Chem. Soc., (1989), 111, 2339-2341.*

132. *S.Jockusch, J.Ramirez, K.Sanghvi, R.Nociti, N.J.Turro, D.A.Tomalia, Macromolecules, (1999), 32, 4419-4423*

133. *M.Mende, G.Petzold, H.M.Buchhammer, Colloid Polym. Sci., (2002), 280, 4, 342-351*

134. *V.A.Izmurudov, P.O.Vahlund, P.E.Gustavsson, et. al. Langmuir, (2003), 19, 11, 4733-47-39*

135. *S.Danielsen, K.M.Varum, B.T.stokke, Biomacromolecules, (2004), 5, 3, 928-936*

136. *H.Dautzenberg, W.Jaeger, Macromol. Chem. Phys., (2002), 203, 2095-2102*

137. *E.Tsuhida, J.M.S.-Pure Appl. Chem., (1994), A31, 1, 1-15*

138. *George Mihov "Design, Synthesis and Application of Polyphenylene Dendrimers for Biological/Pharmaceutical Assays", Dissertation, (2004), MPI-P Mainz*